(12) INTERNATIONAL APPLICATION PUBLISHED UNDER THE PATENT COOPERATION TREATY (PCT)

(19) World Intellectual Property Organization
International Bureau

(43) International Publication Date
21 December 2023 (21.12.2023)

WIPO | PCT

(10) International Publication Number
WO 2023/244870 A1

(51) International Patent Classification:
A61P 35/02 (2006.01) *C12N 15/52* (2006.01)
A61K 38/46 (2006.01) *A61K 31/7115* (2006.01)
A61K 47/69 (2017.01) *C12N 15/85* (2006.01)
C12N 15/113 (2010.01)

(21) International Application Number:
PCT/US2023/025793

(22) International Filing Date:
20 June 2023 (20.06.2023)

(25) Filing Language: English

(26) Publication Language: English

(30) Priority Data:
63/353,521 17 June 2022 (17.06.2022) US

(71) Applicants: **INSTITUTE FOR CANCER RESEARCH d.b.a THE RESEARCH INSTITUTE OF FOX CHASE CANCER CENTER** [US/US]; 333 Cottman Avenue, Philadelphia, PA 19111-2497 (US). **THE GENERAL HOSPITAL CORPORATION** [US/US]; 55 Fruit Street, Boston, MA 02114 (US).

(72) Inventors: **WHETSTINE, Johnathan, R.**; 1190 Fairland Drive, Ambler, PA 19002 (US). **GRAY, Zach, H.**; 7820 Algon Avenue, Apt D137, Philadelphia, PA 19111 (US). **CHAKRABORTY, Damayanti**; 12 Wait Street, Apt 2R, Boston, MA 02120 (US). **DUTTWEILER, Reuben, R.**; 27 Dayton Street, Lowell, MA 01852 (US). **MURPHY, Sedona, E.**; 278 Monroe Drive, Apt 33, Mountain View, CA 94040 (US). **ALEKBAEVA, Gulnaz**; 8048 Oxford Avenue, Apt C3, Philadelphia, PA 19111 (US).

(74) Agent: **RIGAUT, Kathleen, D.** et al.; Howson & Howson LLP, 325 Sentry Parkway East, Five Sentry East, Suite 160, Blue Bell, PA 19422 (US).

(81) Designated States *(unless otherwise indicated, for every kind of national protection available)*: AE, AG, AL, AM, AO, AT, AU, AZ, BA, BB, BG, BH, BN, BR, BW, BY, BZ, CA, CH, CL, CN, CO, CR, CU, CV, CZ, DE, DJ, DK, DM, DO, DZ, EC, EE, EG, ES, FI, GB, GD, GE, GH, GM, GT, HN, HR, HU, ID, IL, IN, IQ, IR, IS, IT, JM, JO, JP, KE, KG, KH, KN, KP, KR, KW, KZ, LA, LC, LK, LR, LS, LU, LY, MA, MD, MG, MK, MN, MU, MW, MX, MY, MZ, NA, NG, NI, NO, NZ, OM, PA, PE, PG, PH, PL, PT, QA, RO, RS, RU, RW, SA, SC, SD, SE, SG, SK, SL, ST, SV, SY, TH,

(54) Title: COMPOSITIONS AND METHODS FOR CONTROL OF TRANSIENT SITE-SPECIFIC COPY GAINS, GENOMIC INSERTIONS, AND REARRANGEMENTS ASSOCIATED WITH MIXED LINEAGE LEUKEMIA

FIG. 1A

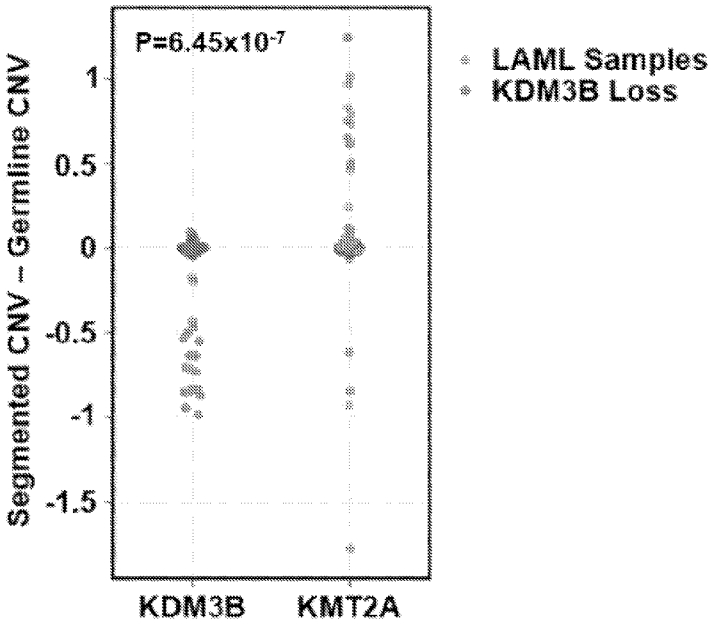

(57) Abstract: Compositions and methods for control of transient site-specific copy gains and genomic insertion associated with mixed lineage leukemia are provided.

WO 2023/244870 A1

[Continued on next page]

TJ, TM, TN, TR, TT, TZ, UA, UG, US, UZ, VC, VN, WS, ZA, ZM, ZW.

(84) **Designated States** *(unless otherwise indicated, for every kind of regional protection available)*: ARIPO (BW, CV, GH, GM, KE, LR, LS, MW, MZ, NA, RW, SC, SD, SL, ST, SZ, TZ, UG, ZM, ZW), Eurasian (AM, AZ, BY, KG, KZ, RU, TJ, TM), European (AL, AT, BE, BG, CH, CY, CZ, DE, DK, EE, ES, FI, FR, GB, GR, HR, HU, IE, IS, IT, LT, LU, LV, MC, ME, MK, MT, NL, NO, PL, PT, RO, RS, SE, SI, SK, SM, TR), OAPI (BF, BJ, CF, CG, CI, CM, GA, GN, GQ, GW, KM, ML, MR, NE, SN, TD, TG).

Published:

— *with international search report (Art. 21(3))*

— *before the expiration of the time limit for amending the claims and to be republished in the event of receipt of amendments (Rule 48.2(h))*

COMPOSITIONS AND METHODS FOR CONTROL OF TRANSIENT SITE-SPECIFIC COPY GAINS, GENOMIC INSERTIONS, AND REARRANGEMENTS ASSOCIATED WITH MIXED LINEAGE LEUKEMIA

Cross-reference to Related Application

This application claims priority to United States Provisional Patent Application No. 63/353,521 filed June 17, 2022, which is incorporated herein by reference in its entirety.

Grant Support Statement

This invention was made with government support under grant numbers GM097360 and GM144131 awarded by the National Institutes of Health. The government has certain rights in the invention.

Field of the Invention

The invention relates to compositions and methods for control of transient site-specific copy gains, amplifications, rearrangements, and genomic insertions associated with mixed lineage leukemia. More specifically, the invention provides methods for reducing MLL/KMT2A copy number, thereby minimizing amplification and formation of breakpoints causing de novo and therapy induced acute myeloid leukemia (AML) and myelodysplasia (MDS). Furthermore, the data establishes that topoisomerase inhibitors (Doxorubicin) promoted MLL/KMT2 amplification and rearrangements, providing a new strategy for treatment of chemotherapy induced leukemia and MDS.

Background of the Invention

Several publications and patent documents are cited throughout the specification in order

to describe the state of the art to which this invention pertains. Each of these citations is incorporated herein by reference as though set forth in full.

Genomic instability is hallmark of cancer. Cancer cells are often associated with copy number changes (*e.g.*, gains or losses of chromosome arms and/or whole chromosomes along, amplification/deletion of short stretches of genomic regions) and structural variation. (Mishra and Whetstine, 2016) Although these events can be genetically stable, focal DNA copy gains can also be extrachromosomal, and transiently appear and disappear (Bailey et al., 2020; Mishra and Whetstine, 2016). These events can also co-exist within a cell or population of cells (Mishra and Whetstine, 2016; Song et al., 2022). A key question remains as to whether the appearance of low or high copy extrachromosomal amplifications are associated with the integrated events that result in genomic rearrangements, and in turn, genetic heterogeneity.

In recent years, a number of epigenetic regulators have been shown to regulate transient site-specific extrachromosomal copy gains (TSSGs) of regions impacting therapeutic response and drug resistance. (Black et al., 2015; Black et al., 2013; Black et al., 2016; Clarke et al., 2020; Mishra et al., 2018; Mishra and Whetstine, 2016) The first documented enzyme shown to promote selective extrachromosomal TSSGs was the Histone 3 lysine 9/36 (H3K9/36) tri-demethylase KDM4A. (Black et al., 2013). Subsequently, a compendium of methyl-lysine modifying chromatin molecules were shown to regulate these TSSG events. (Clarke et al., 2020; Mishra et al., 2018). These studies indicate that additional chromatin modulators could be involved in fine-tuning local and global chromatin states and regulating unknown TSSGs. However, the question remained as to whether these transient extrachromosomal DNA (ecDNA) events could promote genetic diversity through rearrangement or insertions.

Acute myeloid leukemia (AML) and myelodysplasia (MDS) are characterized by genomic amplifications and translocations of the 11q23 region, which includes MLL/KMT2A and other target genes(Poppe et al., 2004; Schichman et al., 1994; Tang et al., 2015; Walter et al., 2009). Infant acute leukemias MLL/KMT2A rearrangements are a hallmark of greater than 70 percent of infant leukemias (Rice and Roy, 2020; Woo et al., 2014). MLL translocations are also found in adult primary leukemias and therapy related leukemia(Andersen et al., 2001; Meyer et al., 2018; Super et al., 1993; Winters and Bernt, 2017). A vast array of translocation events and fusion partners have been documented for MLL/KMT2A with some being more prevalent than others (Meyer et al., 2018). While 10% of acute leukemias have MLL rearrangements, other

types of leukemia have an array of translocation partners. These are also impacted by patient age. For example, in infant ALL cases, MLL-AF4 is most common in ALL, while in AML MLL-AF9 is most frequent (Winters and Bernt, 2017). In contrast to these frequent partners, others are observed such as LAF4/AFF3, an AF4 related gene, that is associated with poor outcomes (von Bergh et al., 2002). De novo AML cases with complex karyotype exhibit MLL/KMT2A copy gains, with many of the cases showing simultaneous 5q deletion and poor survival rates (Herry et al., 2006; Schoch et al., 2005).

Frequent cytogenetic loss of Chromosome 5 (whole chromosome, loss of long arm 5q, and more focal deletions) is observed in malignant myeloid disorders including MDS and AML (Bacher et al., 2015; Rea et al., 2020; Walter et al., 2009; Zahid et al., 2017). Chromosome 5 loss is observed in *de novo* AML and chemotherapy induced leukemia (Godley and Larson, 2008). Cytogenetic loss of chromosome 5 has been correlated with poor chemotherapy responses and lower survival. Studies have successfully defined minimal chromosomal locations at 5q31 observed in patients with MDS, AML, and secondary AML. (Liu et al., 2007; Stoddart et al., 2014).

Clearly, there is a major clinical need to understand the direct impact that epigenetic and genetic interplay have on amplifications and structural variations. Such information could then provide guidance for effective therapeutic strategies to control both copy number and rearrangements associated with aberrant cellular proliferation.

Summary of the Invention

In accordance with the present invention, compositions and methods for reducing MLL/KMT2A amplifications/rearrangements in a patient in need thereof are disclosed. An exemplary method entails administration of an effective amount of one or more agents including i) a first agent which increases KDM3B expression and function and, or ii) a second agent which inhibits expression or activity of H3K9 methyltransferase, wherein the agents are administered in one or more pharmaceutically acceptable carriers and reducing MLL/KMT2A amplification/rearrangements in said patient. In one embodiment, the first agent is a KDM3B agonist, and the second agent is a G9a inhibitor and both agents are administered. In certain embodiments, the MLL/KMT2A amplification can be caused by administration of a chemotherapeutic agent such as a chemotherapeutic agent that reduces KDM3B expression. In

certain embodiments, the chemotherapeutic agent is a topoisomerase inhibitor, such as a topoisomerase II inhibitor. In certain embodiments, the topoisomerase II inhibitors, include without limitation doxorubicin, daunorubin, and etoposide. In another embodiment of the invention, the patient has a genetic loss of KDM3B. In certain embodiments, the method further comprises administration of a chemotherapeutic agent. In other approaches, the administration of agents which reduce MLL/KMT2A amplification can be performed before, during or after administration of said chemotherapeutic agent. In preferred embodiments, the patient has reduced MLL/KMT2A copy numbers after treatment when compared to an untreated control. In other embodiments the patient is treated with a third agent, i.e., a proteosome inhibitor selected from bortezomib, carfilzomib, and ixazomib. UNC 0642, an inhibitor of G9a, an siRNA that targets H3K9 methyltransferase, and/or an siRNA that targets the molecules listed in Table 1 are also suitable for use in the invention.

Another aspect of the invention includes methods for treating a patient already having cancer patient with MLL/KMT2A amplification, the method comprising administration of an effective amount of the agents described above.

Yet another aspect of the invention includes methods for reducing TCF3 or AFF3 amplifications/rearrangements in a patient in need thereof, the method comprising a administration of an effective amount of one or more agents including i) a first agent which increases KDM3B expression and function and, or ii) a second agent which inhibits expression or activity of H3K9 methyltransferase, wherein the agents are administered in one or more pharmaceutically acceptable carriers and reducing MLL/KMT2A amplification/rearrangements in said patient. In one embodiment, the first agent is a KDM3B agonist, and the second agent is a G9a inhibitor and both agents are administered. In certain embodiments, the MLL/KMT2A amplification can be caused by administration of a chemotherapeutic agent such as a chemotherapeutic agent that reduces KDM3B expression. In certain embodiments, the chemotherapeutic agent is a topoisomerase inhibitor, such as a topoisomerase II inhibitor. In certain embodiments, the topoisomerase II inhibitors, include without limitation doxorubicin, daunorubin, and etoposide. In another embodiment of the invention, the patient has a genetic loss of KDM3B. In certain embodiments, the method further comprises administration of a chemotherapeutic agent. In other approaches, the administration of agents which reduce MLL/KMT2A amplification can be performed before, during or after administration of said

chemotherapeutic agent. In preferred embodiments, the patient has reduced MLL/KMT2A copy numbers after treatment when compared to an untreated control. In other embodiments the patient is treated with a third agent, i.e., a proteosome inhibitor selected from bortezomib, carfilzomib, and ixazomib. UNC 0642, an inhibitor of G9a, an siRNA that targets H3K9 methyltransferase, and/or an siRNA that targets the molecules listed in Table 1 are also suitable for use in the invention.

Brief Description of the Drawings

Figures 1A - 1L: KDM3B depletion induces *KMT2A* DNA copy gains and break aparts Fig. 1A) TCGA Acute Myeloid Leukemia (TCGA LAML) samples with >50% KDM3B loss. Plot shows most LAML samples with *KDM3B* loss also have *KMT2A* copy gain with a p-value of 6.45e-07. Statistical significance was computed by Wilcoxon rank-sum test, which provides a non-parametric hypothesis test on two independent samples**. Fig. 1B**) Representative examples with the 5qDel FISH probe (5q probe covers the *KDM3B* locus) demonstrate that KG1a (upper) and HL60 (lower) are LOH for *KDM3B* (red) (left panels). Representative examples with the clinical *KMT2A* DNA FISH break apart probe (panel C) demonstrate that there is a baseline increase in *KMT2A* copies in KG1a (upper) and HL60 (lower) (right panels). Arrowheads highlight the FISH signal. **Fig. 1C**) A schematic of DNA Fluorescent *In Situ* Hybridization (FISH) probe genomic locations that are used for *KMT2A* locus. **Fig. 1D**) Representative siCTRL (upper) and siKDM3B (lower) DNA FISH images with the *KMT2A-1* probe (orange probe location in schematic C and centromere 11 (*11C*; control probe)) in RPE cells. **Fig. 1E**) KDM3 family siRNA screen demonstrates that only KDM3B depletion generates *KMT2A* copy gains (*KMT2A-1;* orange) but not copy gains of centromere 11 (*11C*; grey) in RPE cells. **Fig. 1F**) Representative example images with the clinical *KMT2A* DNA FISH break apart probe (red and green probes in schematic C) that show no copy gain in siCTRL (top panel), DNA copy gains (middle 3 panels) and break apart events (bottom panel) upon KDM3B siRNA depletion in RPE cells. Arrowheads highlight the FISH signal. **Fig. 1G**) Quantification of DNA FISH experiments showing KDM3B siRNA knockdown results in *KMT2A* copy gains (black) and break aparts (purple). **Fig. 1H**) Quantification of DNA FISH experiments showing KMD3B siRNA knockdown did not promote copy gains of the *CD3* probe, demonstrating site-specificity of *KMT2A* copy gains in Fig, 1G. **Fig. 1I**) Representative example images with the clinical *KMT2A*

DNA FISH break apart probe (red and green probes in schematic C) that show *KMT2A* copy gains with siRNA-mediated KDM3B knockdown in U937 leukemia cells. Arrowheads highlight the FISH signal. **Fig. 1J**) Quantification of DNA FISH experiments showing KDM3B siRNA knockdown results in *KMT2A* copy gains and break aparts in U937 cells. **Fig. 1K**) Quantification of DNA FISH experiments showing KMD3B siRNA knockdown did not promote copy gains of the *CD3* probe in U937 cells demonstrating specificity. **Fig. 1L**) IGV tracks of the region containing *KMT2A* for H3K9me1-3 ChIP-seq. KDM3B Depletion increased H3K9me1 and H3K9me2 at the *KMT2A* locus. Publicly available ChIP-seq shows KDM3B binding within the BCR in HCT-116 cells which is lost upon shKDM3 treatment (49). **Fig. 1M**) Bar graphs of ChIP-seq data demonstrating increased fold enrichments of H3K9me1/2 within the *KMT2A* locus. Error bars represent the SEM. Asterisk indicates significant difference from indicated ($p < 0.05$) by two-tailed Student's t-test. Scale bar represents 5μm. A minimum of 2 replicates per experiment were conducted. For FISH in **Fig. 1E**, two independent Control and KDM3B siRNAs were used and a minimum of 100 nuclei were scored per siRNA. For FISH in **Figs, 1G-1H**, **1J-1K** a minimum of 200 nuclei were scored for each independent siRNA per experiment. BA-Break aparts.

Figures 2A – 2K. KDM3B chemical inhibition (KDM3i) promotes transient *KMT2A* copy gains and break aparts. Fig. 2A, *In vitro* KDM assay with commercial full length purified KDM3B protein incubated with histones and western blotted for KDM3B, H3K9me1 and H3K9me3. Blot demonstrates reduction in H3K9me1 levels upon incubation with KDM3B is rescued with KDM3i addition. **Fig. 2B,** Cell growth assay for KDM3i treated RPE cells. Treatment with KDM3i at 25nM does not impact cell growth, whereas 250nM and 1μM modestly but significantly suppresses growth. **Fig. 2C,** Western blot demonstrating KDM3B protein levels are not reduced with KDM3i treatment in RPE cells in Fig. 2D. **Fig. 2D,** A representative example from quantification of western blots for KDM3B in KDM3i treated RPE cells (n=3). KDM3B levels are not reduced upon treatment with KDM3i. **Fig. 2E** Cell growth assay for KDM3i treated RPE cells corresponding to Figure 3F. Cell growth is not impacted after 12hrs KDM3i treatment, or after 12hr KDM3i washout. **Fig. 2F,** Schematic (top) and quantification of DNA FISH (bottom) demonstrating that *KMT2A* amplification and break apart events occur with KDM3B inhibitor treatment at 25nM and 1μM for 72 hours but no change in copy number at the adjacent *CD3* locus in RPE cells. **Fig. 2G,** Quantification of DNA FISH

showing that KDM3B inhibition at 1μM for 72 hours results in *KMT2A* copy gains and break aparts in KG1a cells with no change in copy number at the *CD3* locus. **Fig. 2H,** Quantification of DNA FISH showing that KDM3B inhibition at 1μM for 72 hours results in *KMT2A* copy gains and break aparts in primary AML organoids with no change in copy number at the *CD3* locus. **Fig. 2I,** Quantification of DNA FISH showing that KDM3B inhibition at 1μM for 72 hours results in *KMT2A* copy gains and break aparts in primary AML cells with no change in copy number at the *CD3* locus. **Fig. 2J,** Quantification of DNA FISH showing that KDM3B inhibition at 1μM for 72 hours results in *KMT2A* copy gains and break aparts in primary Hematopoietic Stem and Progenitor Cells (HSPCs) with no change in copy number at the *CD3* locus. **Fig. 2K,** Schematic (top) and quantification of DNA FISH (bottom) showing that 12hr KDM3i treatments result in significant *KMT2A* copy gains and break aparts when compared to vehicle control. Upon KDM3i washout (12hrs Washout), copy gains and break aparts no longer occur when compared to vehicle control. No significant change occurred with the *CD3* probe.

Error bars represent the SEM. Asterisk indicates significant difference from indicated ($p < 0.05$) by two-tailed Student's t-test. A minimum of 2 replicates per experiment were conducted.

Figures 3A – 3L. KDM3B suppression leads to integration and inheritance of *KMT2A* copy gains and break aparts. Fig. 3A, KDM3i treatment schematic and associated passaging of RPE cells. Cells were initially treated for 72hrs with 25nM of KDM3i. Cells were then passaged in media without KDM3i every 3 days for sequential passages. **Fig. 3B,** Quantification of *KMT2A* and *CD3* DNA FISH at passage 0 and passage 10 after KDM3i treatment, which demonstrates *KMT2A* copy gains and break aparts are inherited in RPE cells after 10 passages (P10). No significant change occurred with the *CD3* probe. **Fig. 3C,** Example metaphase spreads for *KMT2A* FISH are shown for vehicle and KDM3i treated cells at passage 10. Arrowheads highlight the FISH signal. **Fig. 3D,** Quantification of the metaphase spreads with *KMT2A* FISH in KDM3i treated and passage 10 cells demonstrating increased copies of *KMT2A* are retained. **Fig. 3E,** A KDM3B siRNA depletion schematic and associated passaging of RPE cells (left). Western blots for KDM3B at cell passages used for DNA FISH are shown, which demonstrates KDM3B protein levels return to baseline by passage 3 (P3; right). **Fig. 3F,** Quantification of *KMT2A* and *CD3* FISH of KDM3B siRNA passaged cells, which demonstrates inheritance at

passage 3, 5 and 15. No significant change occurred with the *CD3* probe at any passage. **Fig. 3G,** Example metaphase spreads for *KMT2A* FISH are shown for siCTRL and siKDM3B cells at passage 3. Arrowheads highlight the FISH signal. **Fig. 3H,** Quantification of the metaphase spreads with *KMT2A* FISH in cells treated with siCTRL and siKDM3B from two independently propagated siCTRL and siKDM3B cells at passages 3 and 9 demonstrating increased copies of *KMT2A* are retained. Copy Number Variation analysis using Digital Droplet PCR (ddPCR) shows *KMT2A* copy number increase in later passage of the inherited *KMT2A* cell lines used in **Figures 3G-H**. **Fig. 3I,** Copy number is quantified by computing ratio of *KMT2A* to *CD3E* reference gene (4 biological replicates with 2 technical replicates). **Fig. 3J,** Quantification of DNA FISH for *TCF3/E2A* after passaging KDM3B siRNA depleted RPE cells. *TCF3/E2A* copy gain and break aparts are retained after 15 passages in KDM3B siRNA depleted cells. **Fig. 3K,** DNA FISH for *SubTel19* after passaging KDM3B siRNA depleted RPE cells. *Subtel19* copy gain does not change in KDM3B siRNA depleted cells. **Fig. 3L,** DNA FISH for *AFF3/LAF4* after passage KDM3B siRNA depleted RPE cells. *AFF3* copy gains occur at P0, but are not retained after 3 passages in KDM3B siRNA depleted cells. *NMYC* copy gain does not change.

Error bars represent the SEM. Asterisk indicates significant difference from indicated ($p < 0.05$) by two-tailed Student's t-test. Scale bar represents 5μm. A minimum of 2 replicates per experiment were conducted. For FISH, a minimum of 200 nuclei were scored per replicate per experiment. BA- Break aparts.

Figures 4A – 4H. H3K9me1 balance controls *KMT2A* copy gains and break aparts. Fig. 4A, A schematic (upper) and DNA FISH quantification (lower) for co-depletion of KDM3B with EHMT1 or EHMT2/G9a. siRNA depleted G9a but not EHMT1 prevents *KMT2A* copy gains and break aparts upon KDM3B siRNA depletion. No significant change occurred with the *CD3* probe. **Fig. 4B, A** schematic (upper) and DNA FISH quantification (lower) for KDM3i and EHMTi treatment. EHMT1/2 chemical inhibition prevents *KMT2A* copy gains and break aparts upon KDM3i treatment. No significant change occurred with the *CD3* probe. **Fig. 4C,** A schematic (upper) and DNA FISH quantification (lower) that shows G9a overexpression promotes *KMT2A* copy gains and break aparts. Halo-EV- Halo empty vector. No significant change occurred with the *11C* probe. **Fig. 4D**A schematic (upper) and DNA FISH quantification (lower) for depletion of G9a in HL60 cells (*KDM3B* LOH cell line). G9a depletion modestly but

significantly suppresses *KMT2A* copy gains in HL60 cells. No significant change occurred with the *CD3* probe. **Fig. 4E,** A schematic (upper) and DNA FISH quantification (lower) for depletion of G9a in RPE-WT or RPE-inherited *KMT2A* cells. G9a depletion does not suppress *KMT2A* copy gains or break aparts in the RPE-inherited *KMT2A* cells. No significant change occurred with the *CD3* probe. **Fig. 4F,** Genomic tracks in the vicinity of *KMT2A* gene for input-normalized ChIP-seq densities of H3K9me1/2/3 upon siKDM3B or siG9a alone or in combination in RPE cells. **Fig. 4G,** Bar graphs representing H3K9 methylation ChIP-seq fold enrichment over input in three parts of *KMT2A* gene shown in (4F). **Fig. 4H,** A model depicting interplay between KDM3B-G9a regulating H3K9me1/2 and modulating *KMT2A* amplifications/rearrangements.

Error bars represent the SEM. Asterisk indicates significant difference from indicated ($p < 0.05$) by two-tailed Student's t-test. A minimum of 2 replicates per experiment were conducted. For FISH, a minimum of 200 nuclei were scored per replicate per experiment. BA-Break aparts. NS- not significant to control.

Figures 5A – 5L. Reduced CTCF occupancy leads to *KMT2A* copy gains and break aparts. **Fig. 5A,** Genomic tracks of publicly available ENCODE input-normalized ChIP-seq densities of CTCF in multiple ENCODE cell lines or tissues at the *KMT2A* locus. CTCF binding at exon 11 of *KMT2A* is conserved in multiple cell lines and directly overlaps with KDM3B binding in HCT116 cells (Li *et al.*, 2017). **Fig. 5B,** DNA FISH quantification demonstrating single and co-siRNA depletion of KDM3B and CTCF promotes *KMT2A* copy gains and break aparts. No significant change occurred with the *CD3* probe. **Fig. 5C,** Quantification of western blots (N=8) for CTCF in KDM3B siRNA depleted RPE cells. No significant change in steady state total CTCF protein levels were observed. **Fig. 5D,** Genomic tracks of publicly available input-normalized ChIP-seq densities of KDM3B (Li *et al.*, 2017) in control and shKDM3 cells. KDM3B binds at exon 11 and is lost upon shKDM3 (green tracks). Lower tracks: input-normalized ChIP-seq densities of CTCF showing that siKDM3B reduced CTCF binding at exon 11 in RPE cells (lower tracks). **Fig. 5E,** ChIP-qPCR demonstrating suppression of CTCF occupancy at *KMT2A* exon 11 (*KMT2A ex 11*; black) or a negative control for CTCF binding (*CTCF negative site*) is shown in yellow following KDM3B siRNA depletion. **Fig. 5F,** Venn diagram of the overlap between KDM3B ChIP-seq peaks from a public dataset and CTCF ChIP-

seq peaks in this study. 6,386 of all KDM3B binding sites (41.5%) co-localize with a CTCF binding site (P-value=1.0e-07). **Fig. 5G,** A total of 17,077 CTCF sites out of 46,340 (36.9%) had reduced occupancy with KDM3B depletion. Among all 6,386 KDM3B binding sites coinciding with CTCF binding, 1,005 sites show a significant decrease in CTCF binding upon KDM3B knockdown, with an extremely significant Z-score of 143.38 corresponding to a *P*-value close to 0. **Fig. 5H,** Double KDM3B and G9a knockdown rescued the increase of H3K9me1 at the vast majority of the CTCF peaks reduced by siKDM3B. Barplot showing genome-wide number of CTCF proximal regions (+/- 5Kb from a CTCF peak) that decreased CTCF and increased H3K9me1 level upon KDM3B knockdown (points above upper red line in **I,** left scatterplot). Red, the fraction of regions where this increase was rescued by double knockdown (points moved below upper red line in **I**, right scatterplot). **Fig. 5I,** Genome-wide effects of siKDM3B, siG9a, and double knockdown on H3K9me1 levels at the subset of CTCF binding sites where CTCF binding was decreased by siKDM3B (17,077 sites). KDM3B and G9a knockdowns have opposite skews, whereas the double knockdown strongly reduces these H3K9me1 changes. Left, scatterplot comparing input-normalized H3K9me1 ChIP-seq densities in +/- 5Kb proximity of all these individual CTCF peaks across the genome in control vs siKDM3B; H3K9me1 changes are skewed towards increase (points above upper red line corresponding to > 1.5 fold increase in siKM3B cells). Middle, scatterplot for control vs siG9a cells; H3K9me1 changes are skewed towards decrease (points below lower red line corresponding to > 1.5 fold decrease in siG9a cells). Right, scatterplot for control vs siKDM3B + siG9a cells, with much fewer H3K9me1 changes in either direction. Red point, +/-5-Kb vicinity of CTCF binding site within KMT2A gene. **Fig. 5J,** DNA FISH quantification demonstrating siRNA depletion of G9a prevents *KMT2A* copy gains and break aparts upon CTCF siRNA depletion. No significant change occurred with the *CD3* probe. **Fig. 5K,** DNA FISH quantification demonstrating EHMT1/2 chemical inhibition prevents *KMT2A* copy gains and break aparts upon CTCF siRNA depletion. No significant change occurred with the *CD3* probe. **Fig. 5L,** A model depicting interplay between KDM3B-G9a-CTCF upon H3K9me1/2 modulation.

Error bars represent the SEM. Asterisk indicates significant difference from indicated ($p < 0.05$) by two-tailed Student's t-test. A minimum of 2 replicates per experiment were conducted. For FISH, a minimum of 200 nuclei were scored per replicate per experiment. BA-Break aparts. NS- not significant to control.

Figures 6A – 6M. Doxorubicin promotes *KMT2A* amplification and rearrangement as well as reduces KDM3B and CTCF protein levels. Fig. 6A, A schematic of human *KMT2A* and adjacent *CD3* DNA FISH probes (top). Graph of the DNA FISH quantification for RPE cells treated with Dox for 72hrs (bottom). Dox treatment causes significant copy gains and break aparts at the *KMT2A* locus; while the control region (*CD3*) changes were not significant. **Fig. 6B,** A schematic of human *KMT2A* and adjacent *CD3* DNA FISH probes (top). Graph of the DNA FISH quantification for Primary Hematopoietic Stem and Progenitor Cells (HSPC) treated with Dox for 72hrs (bottom). Dox treatment causes significant copy gains and break aparts at the *KMT2A* locus; while the control region (*CD3*) changes were not significant. **Fig. 6C,** A schematic of DNA FISH probe genomic locations that are used for mouse *Kmt2a/Con9* locus (top). Graph of DNA FISH quantification demonstrating that cells isolated from the Spleen of mice treated with Dox (1.5mg/kg for 3 days) have increased copy gains of *Kmt2a* but not the adjacent *Control 9* region (bottom). **Fig. 6D,** RT-qPCR analysis demonstrating that Dox significantly reduced KDM3B transcript levels relative to ß-actin after 72 hours of exposure in RPE cells. **Fig. 6E,** Representative western blot illustrating Dox reducing KDM3B protein levels after 72 hours of exposure in RPE cells. **Fig. 6F,** Quantification of western blots (n=4) showing a significant reduction in KDM3B protein levels following Dox treatment after 72 hours of exposure in RPE cells. **Fig. 6G,** RT-qPCR analysis demonstrating that Dox significantly reduced CTCF transcript levels relative to ß-actin after 72 hours of exposure in RPE cells. **Fig. 6H,** Representative western blot illustrating Dox reducing CTCF protein levels after 72 hours of exposure in RPE cells. **Fig. 6I,** Quantification of western blots (n=4) showing a significant reduction in CTCF protein levels following Dox treatment after 72 hours of exposure in RPE cells. **Fig. 6J,** Graph of the quantification of western blots in panel S6F showing a significant reduction in KDM3B (black) and CTCF (blue) protein levels following Dox treatment in KG1a cells. **Fig. 6K,** Western blot illustrating etoposide dose-dependently reducing KDM3B (upper) and CTCF (lower) protein levels after 72 hours of exposure in RPE cells. **Fig. 6L,** Western blot illustrating MG132 partially rescuing KDM3B protein levels in the presence of Dox treatment in RPE cells. **Fig. 6M,** Western blot illustrating MG132 rescuing CTCF protein levels in the presence of Dox treatment. Protein levels were quantified using ImageJ and CTCF was normalized to α-Actinin.

Error bars represent the SEM. Asterisk indicates significant difference from indicated ($p < 0.05$) by two-tailed Student's t-test. A minimum of 2 replicates per experiment were conducted. For FISH, a minimum of 200 nuclei were scored per replicate per experiment. BA- Break aparts. NS- not significant to control.

Figures 7A- 7G. KDM3B and CTCF regulation controls Doxorubicin-induced *KMT2A* amplification and rearrangement. Fig. 7A, ChIP-qPCR demonstrating increase of H3K9me1 at *KMT2A* exon 11 (*KMT2A* CTCF site) following KDM3B siRNA depletion (left; upper) and Dox treatment at 1pg/μL for 24hr (right; upper). ChIP-qPCR demonstrating suppression of CTCF occupancy at *KMT2A* exon 11 (*KMT2A ex 11*; black) or a negative control for CTCF binding (*CTCF negative site;* yellow) following Dox treatment at 1pg/μL for 24hr (lower). **Fig. 7B,** A treatment schematic (upper) and DNA FISH quantification (lower) demonstrating that Dox treatment causes *KMT2A* amplification and rearrangements. *KMT2A* amplifications generated by Dox treatment are significantly rescued with CTCF overexpression by DNA FISH. **Fig. 7C,** A treatment schematic (upper) and DNA FISH quantification (lower) demonstrating that Dox treatment causes *KMT2A* amplification and rearrangement. *KMT2A* amplifications and rearrangements generated by Dox treatment that are significantly rescued with G9a depletion by DNA FISH. **Fig. 7D,** A treatment schematic (upper) and DNA FISH quantification (lower) demonstrating that Dox treatment causes *KMT2A* amplification and rearrangements that are significantly rescued with EHMT1/2 inhibition by DNA FISH. **Fig. 7E,** A treatment schematic (upper) and DNA FISH (lower) demonstrating that Dox treatment causes *KMT2A* amplification and rearrangements that are significantly rescued with KDM3B overexpression by DNA FISH. **Fig. 7F,** A first model summarizing the data described herein. The model illustrates that KDM3B and CTCF are suppressed with Dox treatment, leading to increased H3K9 mono- and di-methylation and reducing CTCF occupancy, which in turn promotes *KMT2A* amplification and rearrangements (BA). G9a is critical in promoting the *KMT2A* copy gains and rearrangements. **Fig. 7G,** A second schematic depicting the regulation of *KMT2A* DNA copy gains and rearrangements. KDM3B and/or CTCF control *KMT2A* copy gains and break aparts, while G9a promotes these events (**I**; **Figures 1, 2, 4,** and **5**). Upon removal of transient suppression of KDM3B (<1 cell cycle), *KMT2A* extrachromosomal DNA copy gains and break aparts recover and return to baseline (**II**; **Figure 2K**). With longer suppression of KDM3B (multiple cell

cycles), *KMT2A* copy gains and rearrangement events become inherited in the genome (Bottom; **Figure 3**). Continuous depletion of KDM3B (e.g., *KDM3B* LOH) generates transient extrachromosomal and inherited *KMT2A* amplifications (**III**; **Figure 4D**). Recovery from KDM3B depletion or suppression after multiple cell cycles results in inherited *KMT2A* DNA copy gains as rearrangements, which cannot be removed or rescued (**IV**; **Figure 4E**).

Error bars represent the SEM. Asterisk indicates significant difference from indicated ($p < 0.05$) by two-tailed Student's t-test. A minimum of 2 replicates per experiment were conducted. For FISH, a minimum of 200 nuclei were scored per replicate per experiment. BA- Break aparts. NS- not significant to control.

Figure 8. A table showing the different domains and regions of the KDM3B amino acid sequence that provide therapeutic targets for the treatment of MLL. Peptide mimetics can be designed which mimic the enzymatic regions and/or the intrinsic disordered domains of the KDM3B protein. Another region of interest is the LXLL motif mimics and along with the regions containing the mutations in KDM3B correlated with cancer and de novo in individuals. A mutation at the zinc finger domain, i.e., Amino acids 1031-1056, for example at c.3095A>T; p.Asp1032Val, is linked to Hodgkins lymphoma. Another alteration, a c.277G>T; p.Glu93* change is associated with acute myeloid leukemia. In cases where KDM3B function or activity is reduced, destabilized, or lost entirely, peptide mimics of such regions could function to effectively restore or stabilize activity. In certain approaches use of KDM3B mimics or agonists are used with G9a inhibitor(s) as described herein below.

Detailed Description of the Invention

Acute myeloid leukemia (AML) and myelodysplasia (MDS) are characterized by genomic amplifications and translocations of the 11q23 region, which includes *MLL/KMT2A* and other target genes (Cox *et al.*, 2003; Dolan *et al.*, 2002; Maitta *et al.*, 2009; Poppe *et al.*, 2004; Schichman *et al.*, 1994; Sperling *et al.*, 2017; Tang *et al.*, 2015; Walter *et al.*, 2009). *MLL/KMT2A* rearrangements are a hallmark of greater than 70 percent of infant leukemias (Rice and Roy, 2020; Woo *et al.*, 2014). *MLL* translocations are also found in adult primary and therapy-related leukemias (Andersen *et al.*, 2001; Dulak *et al.*, 2012; Meyer *et al.*, 2023; Pedersen-Bjergaard *et al.*, 1998; Super *et al.*, 1993; Winters and Bernt, 2017). In fact, more than

100 known *KMT2A* rearrangement partners have been documented (Meyer *et al.*, 2023). These *KMT2A* rearrangements result in the fusion of the gene to any of the partner genes, leading to protein chimeras. *KMT2A* can also rearrange to several noncoding regions throughout the genome (Meyer *et al.*, 2023). Therefore, not all rearrangement events generate functional fusion proteins (Aplan, 2006b). Therapy-related acute myeloid leukemia (t-AML) is a clinical syndrome occurring long after chemotherapy treatment with agents such topoisomerase II (topo II) inhibitors (Campo *et al.*, 2011; Godley and Larson, 2008; Leone *et al.*, 1999). In fact, topo II inhibitors have been shown to promote non-leukemia and leukemia-associated *KMT2A* rearrangements in hematopoietic stem cells and a host of other non-hematologic cell types (Gómez-Herreros *et al.*, 2017; Gothe *et al.*, 2019; Libura *et al.*, 2005). Approximately 10% of all AML cases arise after a patient's exposure to therapy for a primary malignancy (Leone *et al.*, 1999), and t-AML patients have a significantly worse outcome than those who develop AML *de novo* (Borthakur and Estey, 2007; Godley and Larson, 2008; Leone *et al.*, 1999). To date, there is a clinically unmet need regarding the mechanistic understanding of how chemotherapy promotes undesirable DNA rearrangements.

The H3K9me1/2 lysine demethylase KDM3B, originally named 5qNCA, resides in the frequently deleted region of 5q31 associated with loss of heterozygosity (LOH) (Ebert, 2010; Hu *et al.*, 2001; Yoo *et al.*, 2020). *MLL/KMT2A* copy gains often occur with 5q LOH (Herry *et al.*, 2006; Schoch *et al.*, 2005). KDM3B has been implicated as a myeloid leukemia tumor suppressor through oncogene regulation and is shown to contribute to genome stability; however, a full appreciation for the role KDM3B plays in genome regulation is understudied (Hu *et al.*, 2001; Kim *et al.*, 2012; MacKinnon *et al.*, 2011; Saavedra *et al.*, 2020; Xu *et al.*, 2018). We previously reported that the loss of a region on chromosome 19, containing microRNA mir-23, promoted TSSGs through KDM4A stabilization (Black *et al.*, 2016). These observations prompted us to assess whether reduced KDM3B was directly promoting the *MLL/KMT2A* copy gains and associated genomic insertions.

Consistent with the documented relationship between 5q loss and *KMT2A* amplification and rearrangement (Herry *et al.*, 2006; Schoch *et al.*, 2005), we demonstrated with DNA Fluorescent In Situ Hybridization (FISH) that both KDM3B depletion and chemical inhibition was sufficient to promote transient and integrated site-specific *MLL/KMT2A* copy gains and rearrangements. These events were directly antagonized by depletion or inhibition of a specific

H3K9me1/2 lysine methyltransferase (KMT) G9a/EHMT2. This specific KMT-KDM axis controlled the H3K9me1/2 balance at *KMT2A*, especially in the region most frequently associated with genomic break aparts and rearrangements. We further demonstrated that a KDM3B-G9a balance controls CTCF occupancy in the region enriched in H3K9 methylation, and in turn, the ability of the *KMT2A/MLL* locus to undergo site-specific copy gains and genomic rearrangement. Lastly, we established that the chemotherapeutic agent Doxorubicin (Dox) reduces KDM3B and CTCF protein levels, and as a consequence, promotes *KMT2A* copy gains and rearrangements. Upon overexpression, KDM3B rescued the Dox-induced *KMT2A* changes. Furthermore, knockdown or chemical inhibition of G9a rescued the *MLL/KMT2A* amplification and break apart events in Dox-treated cells. Collectively, these data highlight a critical role for H3K9me1/2 balance through KDM3B/G9a in regulating the selective amplification, integration and rearrangement of *KMT2A*. This discovery has major clinical implications in understanding the genesis of extrachromosomal amplifications and associated chromosomal rearrangements, and elucidates new approaches to therapeutically control the emergence of treatment-induced *KMT2A* amplifications and rearrangements in cancer patients.

Definitions:

The following definitions are provided to facilitate an understanding of the present invention. Unless defined otherwise, all technical and scientific terms used herein have the same meaning as commonly understood by one of ordinary skill in the art to which this invention belongs. Generally, conventional methods of molecular biology, microbiology, recombinant DNA techniques, cell biology, and virology within the skill of the art are employed in the present invention. Such techniques are explained fully in the literature.

For purposes of the present invention, "a" or "an" entity refers to one or more of that entity; for example, "a cDNA" refers to one or more cDNA or at least one cDNA. As such, the terms "a" or "an," "one or more" and "at least one" can be used interchangeably herein. It is also noted that the terms "comprising," "including," and "having" can be used interchangeably. Furthermore, a compound "selected from the group consisting of" refers to one or more of the compounds in the list that follows, including mixtures (i.e. combinations) of two or more of the compounds.

The phrase "consisting essentially of" when referring to a particular nucleotide or amino acid means a sequence having the properties of a given SEQ ID NO. For example, when used in reference to an amino acid sequence, the phrase includes the sequence per se and molecular modifications that would not affect the functional and novel characteristics of the sequence.

A "derivative" of a polypeptide, polynucleotide or fragments thereof means a sequence modified by varying the sequence of the construct, e.g. by manipulation of the nucleic acid encoding the protein or by altering the protein itself. "Derivatives" of a gene or nucleotide sequence refers to any isolated nucleic acid molecule that contains significant sequence similarity to the gene or nucleotide sequence or a part thereof. In addition, "derivatives" include such isolated nucleic acids containing modified nucleotides or mimetics of naturally-occurring nucleotides.

The term "functional" as used herein implies that the nucleic or amino acid sequence is functional for the recited assay or purpose.

For purposes of the invention, "Nucleic acid", "nucleotide sequence" or a "nucleic acid molecule" as used herein refers to any DNA or RNA molecule, either single or double stranded and, if single stranded, the molecule of its complementary sequence in either linear or circular form. In discussing nucleic acid molecules, a sequence or structure of a particular nucleic acid molecule may be described herein according to the normal convention of providing the sequence in the 5' to 3' direction. With reference to nucleic acids of the invention, the term "isolated nucleic acid" is sometimes used. This term, when applied to DNA, refers to a DNA molecule that is separated from sequences with which it is immediately contiguous in the naturally occurring genome of the organism in which it originated. For example, an "isolated nucleic acid" may comprise a DNA molecule inserted into a vector, such as a plasmid or virus vector, or integrated into the genomic DNA of a prokaryotic or eukaryotic cell or host organism. Alternatively, this term may refer to a DNA that has been sufficiently separated from (e.g., substantially free of) other cellular components with which it would naturally be associated. "Isolated" is not meant to exclude artificial or synthetic mixtures with other compounds or materials, or the presence of impurities that do not interfere with the fundamental activity, and that may be present, for example, due to incomplete purification. When applied to RNA, the term "isolated nucleic acid" refers primarily to an RNA molecule encoded by an isolated DNA molecule as defined above. Alternatively, the term may refer to an RNA molecule that has been sufficiently separated from

other nucleic acids with which it would be associated in its natural state (i.e., in cells or tissues). An isolated nucleic acid (either DNA or RNA) may further represent a molecule produced directly by biological or synthetic means and separated from other components present during its production.

According to the present invention, an isolated or biologically pure molecule or cell is a compound that has been removed from its natural milieu. As such, "isolated" and "biologically pure" do not necessarily reflect the extent to which the compound has been purified. An isolated compound of the present invention can be obtained from its natural source, can be produced using laboratory synthetic techniques or can be produced by any such chemical synthetic route.

In certain embodiments, the method of treatment effectively suppresses symptoms associated with cancer. Symptoms of vary according to the location and type of cancer being treated. In certain embodiments, symptoms of cancer include, fatigue, weight loss, lumps, swelling, pain, coughing, wheezing, new or unusual growth, discoloration, and no symptoms at all. In certain embodiments, the treatment reduces the risk of relapse. In the context of a cancer, treatment or inhibition may be assessed by inhibition of disease progression, inhibition of tumor growth, reduction of primary tumor, relief of tumor-related symptoms, inhibition of tumor secreted factors, delayed appearance of primary or secondary tumors, slowed development of primary or secondary tumors, decreased occurrence of primary or secondary tumors, slowed or decreased severity of secondary effects of disease, arrested tumor growth and regression of tumors, increased Time To Progression (TTP), increased Progression Free Survival (PFS), increased Overall Survival (OS), among others. OS as used herein means the time from treatment onset until death from any cause. TTP as used herein means the time from treatment onset until tumor progression; TTP does not include deaths. Time to Remission (TTR) as used herein means the time from treatment onset until remisison, for example, complete or partial remission. As used herein, PFS means the time from treatment onset until tumor progression or death. In one embodiment, PFS rates will be computed using the Kaplan-Meier estimates. Event-free survival (EFS) means the time from study entry until any treatment failure, including disease progression, treatment discontinuation for any reason, or death. Relapse-free survival (RFS) means the length of time after the treatment ends that the patient survives without any signs or symptoms of that cancer. Overall response rate (ORR) means the sum of the percentage of patients who achieve complete and partial responses. Complete remission rate (CRR) refers to the percentage of

patients achieving complete remission (CR). Duration of response (DoR) is the time from achieving a response until relapse or disease progression. Duration of remission is the time from achieving remission, for example, complete or partial remission, until relapse. In the extreme, complete inhibition, is referred to herein as prevention or chemoprevention. In this context, the term "prevention" includes either preventing the onset of clinically evident cancer altogether or preventing the onset of a preclinically evident stage of a cancer. Also intended to be encompassed by this definition is the prevention of transformation into malignant cells or to arrest or reverse the progression of premalignant cells to malignant cells. This includes prophylactic treatment of those at risk of developing a cancer.

A "chromosomal translocation" is defined as a genome abnormality in which a chromosome breaks and either the whole or a portion of it reattaches to a different chromosome. Depending on the location of the breaks, translocations may lead to the formation of fusion genes, or may disrupt a gene or its regulatory sequences, and in this way cause gene misregulation.

"MLL1–4 or KMT2A-D" are histone methyltransferases that methylate lysine 4 on the histone H3 tail and regulate crucial functions of the genome by modulating the chromatin structure and DNA accessibility.

"G9a/EHMT-2" is a histone methyltransferase that specifically mono- and dimethylates 'Lys-9' of histone H3 (H3K9me1 and H3K9me2, respectively) in euchromatin. H3K9me represents a specific tag for epigenetic transcriptional repression by recruiting HP1 proteins to methylated histones. Also mediates monomethylation of 'Lys-56' of histone H3 (H3K56me1) in G1 phase, thereby promoting interaction between histone H3 and PCNA and regulating DNA replication. Also weakly methylates 'Lys-27' of histone H3 (H3K27me).

"CTCF" is an insulator protein, that along with cohesin, controls domain location by folding domains into loop structures. CTCF and cohesin co-occupy the same sites and physically interact as a complex. The cohesin complex is a multi-subunit ring-like structure composed of SMC1A, SMC3, RAD21, and STAG1 or STAG2 proteins and functions in the processes of anaphase sister chromatid exchange (mitotic checkpoint), DNA repair regulation, and transcription control. Agents which increase binding functions of CTCF and or RAD21 can be included with the other MLL/DKMTA amplification reducing agents described herein. Studies show that both CTCF and RAD21 are mutated in a variety of cancers and other diseases. See for

example, Antony et al. (2021) Int. J. Mol. Sci. 22:(13):6788;Deardorff et al. (2012) Am. J. Human Genet. 90(6):1014-1027 and Debaugny et al., Curr Opin Genet Dev. (2020) 61:44-52 each of which are incorporated herein by reference. Common mutations in CTCF associated with disease include, for example, in order of occurrence, p.R377, p.R448, p.R457, p.H284, and p.S354. Zinc finger 1 (amino acids 260-288) and zinc finger 2, (amino acids 294-316) are also frequently mutated. Peptide mimics of these regions which stabilize or restore mutated zinc finger sequences in CTCF are also within the scope of the invention.

A protein mimetic is a molecule such as a peptide, a modified peptide or any other molecule that biologically mimics the action or activity of some other protein. Protein mimetics are commonly used in drug design and discovery. Types of mimetics include without limitation, Antibody mimetics, e .g., molecules that mimic antigen binding activity of antibodies; peptidomimetics - small protein-like chains designed to mimic larger peptide and phosphomimetics - An amino acid substitution or modification which mimic the effect of protein phosphorylation. The design and generation of molecules capable of mimicking the binding and/or functional sites of proteins are used to advantage for the exploration and modulation of protein function through controlled interference with the underlying molecular interactions. Synthetic peptides are effective mimics of native protein sites because such peptides can be generated as exact copies of protein fragments and can also comprise diverse chemical modifications, which includes the incorporation of a large range of non-proteinogenic amino acids as well as the modification of the peptide backbone. Apart from extending the chemical and structural diversity presented by peptides, such modifications also increase the proteolytic stability of the molecules, enhancing their utility for biological applications. Peptide mimetics of KDM3B and CTCF could provide therapeutic benefit to subjects having or being a risk for MLL.

The phrase “break-apart or translocation probes” refer to probes which target two areas of a specific gene sequence. Usually, a green fluorescent label is used on one end of a gene sequence and a red fluorescent label is used on the other end of the gene sequence. When the gene sequences are intact (still close together), the green and red signals will usually fluoresce as a yellow signal, known as a fusion signal. The width of the green and red signals are determined. If the green and red signals are closer than the width of one signal, they are said to be intact. When a break in the gene sequence occurs, the green and red signal will not be close together anymore and will thus appear as separate green and red signals. A “break point” is where a

precise area a break occurs. The “break apart” is analyzed by the FISH technique, refers to separate areas on the gene and is typically characterized as a rearrangement.

The terms “extrachromosomal DNA” or “ecDNA” refer to any DNA that is found off the chromosomes, either inside or outside the nucleus. Multiple forms of ecDNA exist and can play an important role in diseases such as cancer. ecDNA has been identified in the nuclei of various cancer cells and has been shown to cary many copies of driver oncogenes. ecDNA is considered to be a primary mechanism of gene amplification, resulting in many copies of driver oncogenes and very aggressive cancers.

Proteasome inhibitors (PIs) induce the accumulation of unfolded and misfolded proteins, leading to apoptosis and cell death through ER stress, reactive oxygen species production, JNK and p53 activation, cyclin-dependent kinase inhibitors, and pro-apoptotic proteins induction. These PIs, together with other agonists (directed to KDM3B, CTCF, RAD21) and inhibitors (G9a) described herein, including alkylators, immunomodulatory drugs, and monoclonal antibodies can be used to advantage to inhibit cancer growth.

The terms "miRNA" and "microRNA" refer to about 10-35 nt, preferably about 15-30 nt, and more preferably about 19-26 nt, non-coding RNAs derived from endogenous genes encoded in the genomes of plants and animals. They are processed from longer hairpin-like precursors termed pre-miRNAs that are often hundreds of nucleotides in length. MicroRNAs assemble in complexes termed miRNPs and recognize their targets by antisense complementarity. These highly conserved, endogenously expressed RNAs are believed to regulate the expression of genes by binding to the 3'-untranslated regions (3'-UTR) of specific mRNAs as well as other regions on targeted mRNAs. Without being bound by theory, a possible mechanism of action assumes that if the microRNAs match 100% their target, i.e. the complementarity is complete, the target mRNA is cleaved, and the miRNA acts like a siRNA. However, if the match is incomplete, i.e. the complementarity is partial, then the translation of the target mRNA is blocked. The manner by which a miRNA base-pairs with its mRNA target correlates with its function: if the complementarity between a mRNA and its target is extensive, the RNA target is cleaved; if the complementarity is partial, the stability of the target mRNA in not affected but its translation is repressed.

The term "RNA interference" or "RNAi" refers generally to a process or system in which a RNA molecule changes the expression of a nucleic acid sequence with which RNA molecule

shares substantial or total homology. The term "RNAi agent" refers to an RNA sequence that elicits RNAi.

An "siRNA" refers to a molecule involved in the RNA interference process for a sequence-specific post-transcriptional gene silencing or gene knockdown by providing small interfering RNAs (siRNAs) that has homology with the sequence of the targeted gene. Small interfering RNAs (siRNAs) can be synthesized in vitro or generated by ribonuclease III cleavage from longer dsRNA and are the mediators of sequence-specific mRNA degradation. Preferably, the siRNA of the invention are chemically synthesized using appropriately protected ribonucleoside phosphoramidites and a conventional DNA/RNA synthesizer. The siRNA can be synthesized as two separate, complementary RNA molecules, or as a single RNA molecule with two complementary regions. Commercial suppliers of synthetic RNA molecules or synthesis reagents include Applied Biosystems (Foster City, Calif., USA), Proligo (Hamburg, Germany), Dharmacon Research (Lafayette, Colo., USA), Pierce Chemical (part of Perbio Science, Rockford, Ill., USA), Glen Research (Sterling, Va., USA), ChemGenes (Ashland, Mass., USA) and Cruachem (Glasgow, UK).

A "small nucleic acid inhibitor" refers to any sequence based nucleic acid molecule which, when introduced into a cell expressing the target nucleic acid, is capable of modulating expression of that target. siRNA, antisense, miRNA, shRNA and the like may be utilized in the methods of the invention.

The term "delivery" as used herein refers to the introduction of foreign molecule (i.e., miRNA containing nanoparticle) into cells. The term "administration" as used herein means the introduction of a foreign molecule into a cell. The term is intended to be synonymous with the term "delivery".

The terms "construct", “cassette”, "expression cassette", “plasmid”, “vector”, or “expression vector” is understood to mean a recombinant nucleic acid, generally recombinant DNA, which has been generated for the purpose of the expression or propagation of a nucleotide sequence(s) of interest or is to be used in the construction of other recombinant nucleotide sequences.

The term “promoter” or “promoter polynucleotide” is understood to mean a regulatory sequence/element or control sequence/element that is capable of binding/recruiting an RNA polymerase and initiating transcription of sequence downstream or in a 3’ direction from the

promoter. A promoter can be, for example, constitutively active, or always on, or inducible in which the promoter is active or inactive in the presence of an external stimulus. Example of promoters include T7 promoters or U6 promoters.

The term “operably linked” can mean the positioning of components in a relationship which permits them to function in their intended manner. For example, a promoter can be linked to a polynucleotide sequence to induce transcription of the polynucleotide sequence.

The terms "complementarity" or “complement” refer to the ability of a nucleic acid to form hydrogen bond(s) with another nucleic acid sequence by either traditional Watson-Crick or other non-traditional types. A percent complementarity indicates the percentage of residues in a nucleic acid molecule which can form hydrogen bonds (e.g., Watson-Crick base pairing) with a second nucleic acid sequence (e.g., 4, 5, and 6 out of 6 being 66.67%, 83.33%, and 100% complementary). "Perfectly complementary" means that all the contiguous residues of a nucleic acid sequence will hydrogen bond with the same number of contiguous residues in a second nucleic acid sequence. "Substantially complementary" as used herein refers to a degree of complementarity that is at least 40%, 50%, 60%, 62.5%, 70%, 75%, 80%, 85%, 90%, 95%, 97%, 98%, 99%, or 100%, or percentages in between over a region of 4, 5, 6, 7, and 8 nucleotides, or refers to two nucleic acids that hybridize under stringent conditions.

In some aspects, the invention provides methods comprising delivering one or more polynucleotides, such as or one or more vectors as described herein (e.g., encoding siRNA, antisense oligonucleotides or other type of inhibitory nucleic acid), to a host cell. In some aspects, the invention further provides cells produced by such methods, and organisms or cells comprising or produced from such cells. Conventional viral and non-viral based gene transfer methods can be used to introduce nucleic acids in mammalian cells or target tissues. Such methods can be used to administer nucleic acids encoding inhibitory compounds to cells in culture, or in a host organism. Non-viral vector delivery systems include DNA plasmids, RNA (e.g. a transcript of a vector described herein), naked nucleic acid, and nucleic acid complexed with a delivery vehicle, such as a liposome. Viral vector delivery systems include DNA and RNA viruses, which have either episomal or integrated genomes after delivery to the cell. For a review of gene therapy procedures, see Anderson, Science 256:808-813 (1992); Nabel & Felgner, TIBTECH 11:211-217 (1993); Mitani & Caskey, TIBTECH 11:162-166 (1993); Dillon, TIBTECH 11:167-175 (1993); Miller, Nature 357:455-460 (1992); Van Brunt, Biotechnology

6(10):1149-1154 (1988); Vigne, Restorative Neurology and Neuroscience 8:35-36 (1995); Kremer & Perricaudet, British Medical Bulletin 51(1):31-44 (1995); Haddada et al., in Current Topics in Microbiology and Immunology Doerfler and Bihm (eds) (1995); and Yu et al., Gene Therapy 1:13-26 (1994).

Methods of non-viral delivery of nucleic acids include lipofection, nucleofection, microinjection, biolistics, virosomes, liposomes, immunoliposomes, polycation or lipid:nucleic acid conjugates, naked DNA, artificial virions, and agent-enhanced uptake of DNA. Lipofection is described in e.g., U.S. Pat. Nos. 5,049,386, 4,946,787; and 4,897,355) and lipofection reagents are sold commercially (e.g., Transfectam™ and Lipofectin™). Cationic and neutral lipids that are suitable for efficient receptor-recognition lipofection of polynucleotides include those of Feigner, WO 91/17424; WO 91/16024. Delivery can be to cells (e.g. in vitro or ex vivo administration) or target tissues (e.g. in vivo administration).

The preparation of lipid:nucleic acid complexes, including targeted liposomes such as immunolipid complexes, is well known to one of skill in the art (see, e.g., Crystal, Science 270:404-410 (1995); Blaese et al., Cancer Gene Ther. 2:291-297 (1995); Behr et al., Bioconjugate Chem. 5:382-389 (1994); Remy et al., Bioconjugate Chem. 5:647-654 (1994); Gao et al., Gene Therapy 2:710-722 (1995); Ahmad et al., Cancer Res. 52:4817-4820 (1992); U.S. Pat. Nos. 4,186,183, 4,217,344, 4,235,871, 4,261,975, 4,485,054, 4,501,728, 4,774,085, 4,837,028, and 4,946,787).

The use of RNA or DNA viral based systems for the delivery of nucleic acids take advantage of highly evolved processes for targeting a virus to specific cells in the body and trafficking the viral payload to the nucleus. Viral vectors can be administered directly to patients (*in vivo*) or they can be used to treat cells *in vitro*, and the modified cells may optionally be administered to patients (*ex vivo*). Conventional viral based systems could include retroviral, lentivirus, adenoviral, adeno-associated and herpes simplex virus vectors for gene transfer. Integration in the host genome is possible with the retrovirus, lentivirus, and adeno-associated virus gene transfer methods, often resulting in long term expression of the inserted transgene. Additionally, high transduction efficiencies have been observed in many different cell types and target tissues.

The tropism of a retrovirus can be altered by incorporating foreign envelope proteins, expanding the potential target population of target cells. Lentiviral vectors are retroviral vectors

that are able to transduce or infect non-dividing cells and typically produce high viral titers. Selection of a retroviral gene transfer system would therefore depend on the target tissue. Retroviral vectors are comprised of cis-acting long terminal repeats with packaging capacity for up to 6-10 kb of foreign sequence. The minimum cis-acting LTRs are sufficient for replication and packaging of the vectors, which are then used to integrate the therapeutic gene into the target cell to provide permanent transgene expression. Widely used retroviral vectors include those based upon murine leukemia virus (MuLV), gibbon ape leukemia virus (GaLV), Simian Immuno deficiency virus (SIV), human immuno deficiency virus (HIV), and combinations thereof (see, e.g., Buchscher et al., J. Virol. 66:2731-2739 (1992); Johann et al., J. Virol. 66:1635-1640 (1992); Sommnerfelt et al., Virol. 176:58-59 (1990); Wilson et al., J. Virol. 63:2374-2378 (1989); Miller et al., J. Virol. 65:2220-2224 (1991); PCT/US94/05700). In applications where transient expression is preferred, adenoviral based systems may be used. Adenoviral based vectors are capable of very high transduction efficiency in many cell types and do not require cell division. With such vectors, high titer and levels of expression have been obtained. This vector can be produced in large quantities in a relatively simple system. Adeno-associated virus ("AAV") vectors may also be used to transduce cells with target nucleic acids, e.g., in the in vitro production of nucleic acids and peptides, and for in vivo and ex vivo gene therapy procedures (see, e.g., West et al., Virology 160:38-47 (1987); U.S. Pat. No. 4,797,368; WO 93/24641; Kotin, Human Gene Therapy 5:793-801 (1994); Muzyczka, J. Clin. Invest. 94:1351 (1994). Construction of recombinant AAV vectors are described in a number of publications, including U.S. Pat. No. 5,173,414; Tratschin et al., Mol. Cell. Biol. 5:3251-3260 (1985); Tratschin, et al., Mol. Cell. Biol. 4:2072-2081 (1984); Hermonat & Muzyczka, PNAS 81:6466-6470 (1984); and Samulski et al., J. Virol. 63:03822-3828 (1989).

Packaging cells are typically used to form virus particles that are capable of infecting a host cell. Such cells include 293 cells, which package adenovirus, and ψ2 cells or PA317 cells, which package retrovirus. Viral vectors used in gene therapy are usually generated by producing a cell line that packages a nucleic acid vector into a viral particle. The vectors typically contain the minimal viral sequences required for packaging and subsequent integration into a host, other viral sequences being replaced by an expression cassette for the polynucleotide(s) to be expressed. The missing viral functions are typically supplied in trans by the packaging cell line. For example, AAV vectors used in gene therapy typically only possess ITR sequences from the

AAV genome which are required for packaging and integration into the host genome. Viral DNA is packaged in a cell line, which contains a helper plasmid encoding the other AAV genes, namely rep and cap, but lacking ITR sequences. The cell line may also be infected with adenovirus as a helper. The helper virus promotes replication of the AAV vector and expression of AAV genes from the helper plasmid. The helper plasmid is not packaged in significant amounts due to a lack of ITR sequences. Contamination with adenovirus can be reduced by, e.g., heat treatment to which adenovirus is more sensitive than AAV.

As used herein, the phrase "effective amount" of a compound or pharmaceutical composition refers to an amount sufficient to modulate tumor growth or metastasis in an animal, especially a human, including without limitation decreasing tumor growth or size or preventing formation of tumor growth in an animal lacking any tumor formation prior to administration, i.e., prophylactic administration.

Preferably, as used herein, the term "pharmaceutically acceptable" means approved by a regulatory agency of the Federal or a state government or listed in the U.S. Pharmacopeia or other generally recognized pharmacopeia for use in animals, and more particularly in humans.

The term "carrier" refers, for example to a diluent, adjuvant, excipient, auxiliary agent or vehicle with which an active agent of the present invention is administered. Such pharmaceutical carriers can be sterile liquids, such as water and oils, including those of petroleum, animal, vegetable or synthetic origin, such as peanut oil, soybean oil, mineral oil, sesame oil and the like. Water or aqueous saline solutions and aqueous dextrose and glycerol solutions are preferably employed as carriers, particularly for injectable solutions. Suitable pharmaceutical carriers are described in "Remington's Pharmaceutical Sciences" by E. W. Martin.

A pharmaceutical composition of the present invention can be administered by any suitable route, for example, by injection, by oral, pulmonary, nasal or other forms of administration. In general, pharmaceutical compositions contemplated to be within the scope of the invention, comprise, inter alia, pharmaceutically acceptable diluents, preservatives, solubilizers, emulsifiers, adjuvants and/or carriers. Such compositions can include diluents of various buffer content (e.g., Tris HCl, acetate, phosphate), pH and ionic strength; additives such as detergents and solubilizing agents (e.g., Tween 80, Polysorbate 80), anti oxidants (e.g., ascorbic acid, sodium metabisulfite), preservatives (e.g., Thimersol, benzyl alcohol) and bulking substances (e.g., lactose, mannitol); incorporation of the material into particulate preparations of

polymeric compounds such as polylactic acid, polyglycolic acid, etc., or into liposomes. Such compositions may influence the physical state, stability, rate of in vivo release, and rate of in vivo clearance of components of a pharmaceutical composition of the present invention. See, e.g., Remington's Pharmaceutical Sciences, 18th Ed. (1990, Mack Publishing Co., Easton, Pa. 18042) pages 1435 1712 which are herein incorporated by reference. A pharmaceutical composition of the present invention can be prepared, for example, in liquid form, or can be in dried powder, such as lyophilized form. Particular methods of administering such compositions are described infra.

In yet another embodiment, a pharmaceutical composition of the present invention can be delivered in a controlled release system, such as using an intravenous infusion, an implantable osmotic pump, a transdermal patch, liposomes, or other modes of administration. In a particular embodiment, a pump may be used [see Langer, supra; Sefton, CRC Crit. Ref. Biomed. Eng. 14:201 (1987); Buchwald et al., Surgery 88:507 (1980); Saudek et al., N. Engl. J. Med. 321:574 (1989)]. In another embodiment, polymeric materials can be used [see Medical Applications of Controlled Release, Langer and Wise (eds.), CRC Press: Boca Raton, Fla. (1974); Controlled Drug Bioavailability, Drug Product Design and Performance, Smolen and Ball (eds.), Wiley: New York (1984); Ranger and Peppas, J. Macromol. Sci. Rev. Macromol. Chem. 23:61 (1983); see also Levy et al., Science 228:190 (1985); During et al., Ann. Neurol. 25:351 (1989); Howard et al., J. Neurosurg. 71:105 (1989)]. In yet another embodiment, a controlled release system can be placed in proximity of the target tissues of the animal, thus requiring only a fraction of the systemic dose [see, e.g., Goodson, in Medical Applications of Controlled Release, supra, vol. 2, pp. 115 138 (1984)]. In particular, a controlled release device can be introduced into an animal in proximity of the site of inappropriate immune activation or a tumor. Other controlled release systems are discussed in the review by Langer [Science 249:1527 1533 (1990)].

As used herein the term "biomarker" refers to a characteristic that is objectively measured and evaluated as an indicator of normal biologic processes, pathogenic processes, or pharmacologic responses to a therapeutic intervention.

As used herein, the terms "modulate", "modulating" or "modulation" refer to changing the rate at which a particular process occurs, inhibiting or promoting a particular process, reversing a particular process, and/or preventing the initiation of a particular process. Accordingly, if the particular process is tumor growth or metastasis, the term "modulation"

includes, without limitation, decreasing the rate at which tumor growth and/or metastasis occurs; inhibiting tumor growth and/or metastasis; reversing tumor growth and/or metastasis (including tumor shrinkage and/or eradication) and/or preventing tumor growth and/or metastasis. A compound that increases a known activity, e.g., tumor growth or metastasis, is an “agonist”. One that decreases, or prevents, an undesirable malignant phenotype is an “antagonist” or “inhibitor”.

As used herein, the terms "tumor", "tumor growth" or "tumor tissue" can be used interchangeably, and refer to an abnormal growth of tissue resulting from uncontrolled progressive multiplication of cells and serving no physiological function. A solid tumor can be malignant, e.g. tending to metastasize and being life threatening, or benign. Examples of solid tumors that can be treated or prevented according to a method of the present invention include sarcomas and carcinomas such as, but not limited to: fibrosarcoma, myxosarcoma, liposarcoma, chondrosarcoma, osteogenic sarcoma, chordoma, angiosarcoma, endotheliosarcoma, lymphangiosarcoma, lymphangioendotheliosarcoma, synovioma, mesothelioma, Ewing's tumor, leiomyosarcoma, rhabdomyosarcoma, colon carcinoma, colorectal cancer, gastic cancer, pancreatic cancer, breast cancer, ovarian cancer, prostate cancer, squamous cell carcinoma, basal cell carcinoma, adenocarcinoma, sweat gland carcinoma, sebaceous gland carcinoma, papillary carcinoma, papillary adenocarcinomas, cystadenocarcinoma, medullary carcinoma, bronchogenic carcinoma, renal cell carcinoma, hepatoma, liver metastases, bile duct carcinoma, choriocarcinoma, seminoma, embryonal carcinoma, thyroid carcinoma such as anaplastic thyroid cancer, Wilms' tumor, cervical cancer, testicular tumor, lung carcinoma such as small cell lung carcinoma and non-small cell lung carcinoma, bladder carcinoma, epithelial carcinoma, glioma, astrocytoma, medulloblastoma, craniopharyngioma, ependymoma, pinealoma, hemangioblastoma, acoustic neuroma, oligodendroglioma, meningioma, melanoma, neuroblastoma, glioblastoma, and retinoblastoma.

The phrase “treatment induced cancer” refers to a new cancer or tumor in a patient with a preexisting cancer that is developed in response to treatment of the preexisting cancer. “Chemo-induced cancer” or “chemotherapy induced cancer” refers to a treatment induced cancer that was developed in response to chemotherapy treatment.

As used herein, the phrase “chromosomal instability” refers to a higher than normal rate of mis-segregation of chromosomes or parts of chromosomes during mitosis due to defective cell cycle quality control mechanisms, resulting in copy number alterations (CNAs) or aneuploidy.

The phrase “gene amplification” or “copy number amplification” or “DNA copy gain” refers to an increase in the number of copies of a gene sequence. In certain embodiments, these phrases refer to any number of copies greater than diploid. There may also be an increase in the RNA and protein made from that gene. Gene amplification is common in cancer cells, and some amplified genes may cause cancer cells to grow or become resistant to anticancer drugs. Gene amplification of oncogenes on ecDNA is a frequent event in cancer.

Epigenetic state or Epigenetic phenomena, as used herein, means changes produced in gene expression or other DNA-dependent processes caused by mechanisms other than changes in the underlying DNA sequence. For example, methylation of cytosines (Cs) or histone modifications can affect expression of a gene. These molecular modifications of the DNA are often called "epigenetic marks." For example, increased or decreased methylation of Cs in a genome are part of normal biology but can also be associated with disease. In a similar fashion, post translational modifications (PTMs) occur on histones and impact DNA-dependent processes. As used herein, "epigenetic state" refers to a gene or region in a genome that reflects particular epigenetic phenomena. For example, in a particular disease cohort, a gene can be found that causes disease through multiple mechanisms, including, but not limited to, impairment of protein function by a SNV, deletion of the gene via a CNV, little or no expression of the gene due to a change in the epigenetic state of the gene itself and/or regulatory region(s) in the genome controlling expression of the gene.

An "inhibitor" (interchangeably termed "antagonist") of a polypeptide of interest is an agent that interferes with activation or function of the polypeptide of interest, e.g., partially or fully blocks, inhibits, or neutralizes a biological activity mediated by a polypeptide of interest. For example, an antagonist of G9a may refers to any molecule that partially or fully blocks, inhibits, or neutralizes a biological activity mediated by G9a. Examples of inhibitors include antibodies; ligand antibodies; small molecule antagonists; antisense and inhibitory RNA (e.g., siRNA) molecules.

siRNAs described above “modified nucleotides”. These are nucleotides comprising non-naturally occurring moieties that confer increased nuclease resistance or thermodynamic stability during hybridization as compared with a polynucleotide or polyribonucleotide that differs from the inhibitory nucleic acid only by having a natural nucleotide in place of the modified nucleotide. In certain embodiments, the ribose moiety of a nucleotide is modified with an extra

bridge connecting the 2′ oxygen and 4′ carbon. Numerous chemical modifications are commonly used for the synthesis of oligonucleotides for a variety of reasons. For example, to increase the phosphate backbone's stability, adjust duplex stability, change the oligonucleotide's conformation, or increase its ability to penetrate a lipid bilayer. Modified sugar moieties are also being incorporated into therapeutic oligonucleotides. Changing the sugar moiety generally increases nuclease resistance and binding affinity to a complementary target.

"Bridged nucleic acid" ("BNA") refers to 2′-O,4′-C-methylene-modified nucleic acids. In preferred embodiments, BNA, where the 2′ oxygen and 4′ carbon are bridged by a methylene group are used. In other approaches, 2′-O,4′-C-ethylene-bridged nucleic acids (ENA), the 2′ oxygen and 4′ carbon are bridged by an ethylene group. Other examples of BNA can include, but are not limited to, 2′,4′-BNA^{NC}[NH], 2′,4′-BNA^{NC}[NMe], and 2′,4′-BNA^{NC}[NBn], (s)-cEt (S-constrained Ethyl). tcDNA (tricycloDNA) modifications can also be used to constrain nucleotides.

"Locked nucleic acid nucleotide" ("LNA nucleotide") as used herein, refers to a modified RNA nucleotide that provides the polynucleotide with greater thermodynamic stability during hybridization as compared with a polynucleotide that differs from the LNA only by having a natural ribonucleotide in place of the modified RNA nucleotide. In certain embodiments, the ribose moiety of a modified RNA nucleotide is modified with an extra bridge connecting the 2′ oxygen and 4′ carbon. LNA nucleotides can comprise any type of extra bridge between the 2′-O and 4′-C of the RNA that increases the thermodynamic stability of the duplex between the LNA and its complement.

Other 2′-O-modified nucleotides, such as 2′-O-Me, demonstrate greater stability, as well.

Oligonucleotide backbone configurations that demonstrate particularly high binding affinities to the target (measured by melting temperature or Tm) are preferred for implementing the steric hindrance mechanism. BNA, LNA, FANA, 2′-fluoro, 2'-O-methoxyethyl (2'-MOE), 2'-NH_2, 2'-F-RNA, morpholino and piperazine containing backbones are particularly well suited for this purpose.

Other modifications on the oligonucleotide ribose include, are not limited to, FHNA (Fluoro Hexitol Nucleic Acid), (s)-5'-C-methyl, UNA (Unlocked Nucleic Acid), 4'-thio-RNA, cyclohexene nucleic acid.

Modified backbone linkages are sometimes used instead of phosphodiester linkage to minimize oligonucleotide degradation by nucleases. Some examples include, are not limited to, phosphorothioate, boranophosphonate, phosphoramidate, methyl phosphonate, (SC5' Rp)-α,β-CNA (Dioxaphosphorinane-Constrained Nucleic Acid), PNA (Peptide Nucleic Acid), PMO (Phosphorodiamidate Morpholino Oligonucleotide), phosphoryl guanidine. 5' modifications to increase phosphate stability include, are not limited to, E-VP ((E)-VinylPhosphonate), 5' methyl phosphonate, 5'-phosphorothioate, (s)-5'-methyl with phosphate, 5'-methoxy. 3' modifications to increase phosphate stability include, are not limited to, 2-hydroxyethylphosphate AND, 3'-ddc (dideoxyCytosine), 3'-amino. Base modifications to improve 3' stability include, are not limited to, 2'-thio-dT.

The generation of oligonucleotides with mixed linkages such as boranophosphate and phosphate linkages has been accomplished by several solid phase methods including one involving the use of bis(trimethylsiloxy)cyclododecyloxysilyl as the 5′-0-protecting group (Brummel and Caruthers, Tetrahedron Lett 43: 749, 2002). In another example the 5′-hydroxyl is initially protected with a benzhydroxybis-(trimethylsilyloxy)silyl group and then deblocked by Et_3N:HF before the next cycle (McCuen et al., J Am Chem Soc 128: 8138, 2006). This method can result in a 99% coupling yield and can be applied to the synthesis of oligos with pure boranophosphate linkages or boranophosphate mixed with phosphodiester, phosphorothioate, phosphorodithioate or methyl phosphonate linkages.

The boranophosphorylating reagent 2-(4-nitrophenyl)ethyl ester of boranophosphoramidate can be used to produce boranophosphate linked oligoribonucleotides This reagent readily reacts with a hydroxyl group on the nucleosides in the presence of 1H-tetrazole as a catalyst. The 2-(4-nitrophenyl)ethyl group can be removed by 1,4-diazabicyclo[5.4.0]undec-7-ene (DBU) through beta-elimination, producing the corresponding nucleoside boranomonophosphates (NMPB) in good yield.

Nucleobase modifications to increase binding affinity include, are not limited to, 5'-methylcytidine, 5-methyluridine (ribothymidine), and abasic RNA.

The phrase "MLL inhibitor", "KMT2A inhibitor", "MLL/KMT2A inhibitor" "Mixed Lineage Leukemia inhibitor" or "lysine methyltransferase 2A inhibitor" refers to any compound naturally occurring or synthesized, having the ability of inhibiting MLL/KMT2A amplification.

Agents that reduce MLL/KMT2A break aparts, and amplifications include, without limitation, a G9a inhibitor or KDM3B agonist.

The phrase "G9a inhibitor" refers to any compound natural occurring or synthesized, having the ability of inhibiting G9a activity, stability or expression. A G9a inhibitor is for example UNC0642, available on the world wide web at apexbt.com/unc-0642.html?gclid=EAIaIQobChMI-4Ku0tW1-AIVIxTUAR3f_gpZEAAYASAAEgKST_D_BwE. Additional G9a inhibitors are known to those skilled in the art. Also see Vedadi et al. (2011) Nat. Chem. Biol.7(8):566-574.

The phrase "KDM3B agonist" refers to any compound natural occurring or synthesized, having the ability of promoting KDM3B expression or overexpression. A KDM3B agonist is for example any molecule that can increase activity or stabilize the protein such as an RNA aptamer.

The term "drug response" as used herein, means any biological response in an organism that is the result of exposure to the drug. Drug responses can be favorable, such as when a patient's disease is eradicated by treatment with the drug, or unfavorable, such as when a patient enters a coma upon treatment with a drug.

The following materials and methods are provided to facilitate the practice of the present invention.

Cell Culture:

Retinal pigment epithelial (RPE) cells were cultured in DMEM-high glucose (Sigma) media supplemented with 10% heat-inactivated fetal bovine serum (FBS), 100U/ml penicillin, 100µg/ml streptomycin, and 2mM L-glutamine. U937 cells were cultured in RPMI 1640 media supplemented with 10% heat-inactivated FBS, 100U/ml penicillin, 100µg/ml streptomycin and 2mM L-glutamine. HL60 and KG1a cells were cultured in RPMI 1640 media supplemented with 20% heat-inactivated FBS, 100U/ml penicillin, 100µg/ml streptomycin and 2mM L-glutamine. Cell line identities were authenticated by short tandem repeat analysis and Mycoplasma tested using the MycoAlert Detection Kit (Lonza, LT07-218).

Human primary patient-derived AML cells were obtained and generated as described previously (Duy et al., 2019). Primary patient-derived AML cells were maintained on 30 Gy-irradiated OP9 feeder layer cells in complete in Iscove's modified Dulbecco's medium (IMDM; Thermo Fisher Scientific, Waltham, MA) containing 20% fetal bovine serum (Corning Premium

FBS), 100 IU/ml penicillin, 100 µg/ml streptomycin, 50 µM 2-mercaptoethanol and supplemented with AML-maintaining cytokines (50 ng/ml SCF, 20 ng/ml GM-CSF, 50 ng/ml FLT3 ligand, 20 ng/ml IL-3, 20 ng/ml IL-6, and 20 ng/ml G-CSF).

Isolation of HSPCs:

Cryopreserved CD34+ hematopoietic stem and progenitor cells (HSPCs) were derived from human umbilical cord blood cells and propagated using an ex vivo co-culture model as previously described (Duy et al., 2019).

Transfection Procedure for RPE cells:

Cells were plated in 10 cm cell culture dishes and allowed to adhere for 16-20 hours. Cell culture medium was removed, cells were rinsed with phosphate buffered saline (PBS) and then replaced with OPTI-MEM medium (Life Technologies) prior to siRNA transfections (5nM-10nM/transfection). Transfections were changed to complete cell culture media after 4 hr of transfection, and cells were collected 72 hr post transfection. Transient overexpression transfections were performed using Lipofectamine 3000 transfection reagent and P3000 reagent (Life Technologies) in OPTI-MEM medium for 4 hrs, followed by changing to complete DMEM media. Silencer select negative controls and siRNAs were purchased from Life Technologies. Their sequences and unique identification numbers are tabulated in the tables below.

TABLE 1: siRNA Oligos		
siRNA Name	**siRNA Sequence**	**Unique Identifier**
KDM3A	GAAGAUCGGAAAUAUGGAAtt	s224392
KDM3A	GUCAGAUACAUGAACCAGAtt	s224394
KDM3B	GGUUCACAAUCUAUACAGUtt	s28658
KDM3B	GAAGAGUUGGUACAACAAAtt	s224243
KDM3B	UAUGCAACUGUAUAGAUUGTg	s28657
KDM3B	UAAACUUCCGGUACCGCUCca	s224244
KDM3C	CCCAAUCAAGUGUUACAAAtt	s47941
KDM3C	GGAAGUCUGUUGACACUCAtt	s47942
G9A	GCUCUAACUGAACAACUAAtt	s21469
G9A	CGCUGAUUUUCGAGUGUAAtt	s21470
EHMT1	CAGCUGCAGUAUCUCGGAAtt	s36390
EHMT1	CUCUCACCGUUUCCACAAAtt	s36391
Suv39H1	AGAACAGCUUCGUCAUGGAtt	s13658
Suv39H1	CAAAUCGUGUGGUACAGAAtt	s13660
Suv39H2	GAAUGAGUUUUGUCAUGGAtt	s36183
Suv39H2	GUAUUCGCUUUGCAUCUUUtt	s36184
CTCF	GGACGAUACCCAGAUUAUAtt	s20967
CTCF	GCUUUGCAGUUACACGUGUtt	s20968

Table 2. Oligos for qRT-PCR, qPCR and ddPCR

Primer Identifier	Primer Sequence
KDM3A Forward	5'-CCACCTAACCTTGGAGCAAA-3'
KDM3A Reverse	5'-GCTTCAGACTTTGTATTTAGACAGGA-3'
KDM3B Forward	5'-TTATCGTGCTTCTGCTGGAA-3'
KDM3B Reverse	5'-CATTGTGCAATGGAGACTCG-3'
KDM3C Forward	5'-CCTACAATGAATGGTGTATCTCAATC-3'
KDM3C Reverse	5'-TGTTATCTGTGCCTACATCACTCTC-3'
G9a Forward	5'-TGGGAAAGGTGACCTCAGAT-3'
G9a Reverse	5'-GGGCAGAACCTAACTCCTCTG-3'
EHMT1 Forward	5'-GCCAAAGAGGTGACGATAGC-3'
EHMT1 Reverse	5'-ACTGCCCGTTGTGGTGTC-3'
Actin Forward	5'-AGGCCAACCGCGAGAAG-3'
Actin Reverse	5'-ACAGCCTGGATAGCAACGTACAT-3'

CTCF Forward	5'-ATGTGCGATTACGCCAGTGTA-3'
CTCF Reverse	5'-TGAAACGGACGCTCTCCAGTA-3'
KMT2A Ex11 CTCF site Forward	5'-TCTGTCACGTTTGTGGAAG-3'
KMT2A Ex11 CTCF site Reverse	5'-GCCCAGCTGTAGTTCTATTAC-3'
CTCF negative site Forward	5'-GAATCAGACTGAGACCCTAAAC-3'
CTCF negative site Reverse	5'-GCCAATCCAGTCTTCTCATAC-3'
KMT2A CTCF flanking site Forward	5'-CAGCCAGAATCCCAGTAGA-3'
KMT2A CTCF flanking site Reverse	5'-CTTTCAGAGGAGGCTACAGA-3'
KMT2A Ex11 ddPCR Forward	5'-GTGTTGTCGTCGTTGCAAAT-3'
Reverse	5'-AGGCCCAGCTGTAGTTCTAT-3'
Probe – FAM	5'-TGTGGAAGGCAACATCAGGCTACA-3'
CD3E ddPCR Forward	5' AGGCTAAGCATGAACCTCAC-3'
Reverse	5'- TGGAATTAGACACTGCCCAC-3'
Probe - HEX	5'- TGGATGAGACCCTCTTTGGGAAGTC-3'

Tables 3A- H. Reagents and Materials

Table3A		
Reagent or Resource	**Source**	**Identifier**
miRNeasy Mini Kit	Qiagen	Cat# 217004
Superscript IV 1st Strand System	Life Technologies	Cat# 18091050
CL-XPosure™ Film	Thermo Scientific	Cat# 34091
Lumi-Light Western Blotting Substrate	Roche	Cat# 12015200001
Pierce BCA Protein Assay	Thermo Scientific	Cat# 23223 and 23224
Protein A Dynabeads	Thermo Scientific	Cat# 10002D
Protein G Dynabeads	Thermo Scientific	Cat# 10004D
TruSeq ChIP Sample Prep Kit Set A (48 samples)	Illumina	Cat# 10748010

NextSeq® 500/550 High Output Kit v2 (75 cycles)	Illumina	Cat# FC-404-2005
Dead Cell Apoptosis Kits with Annexin V	Life Technologies	Cat# V13241
Pierce Protease Inhibitor Tablets	Thermo Scientific	Cat# A32953
Pierce Phosphatase Inhibitor Tablets	Thermo Scientific	Cat# A32957

Table 3B.

Antibodies	Source	Identifier
Anti-KDM3B, clone C69G2	Cell Signaling	Cat# 3314 RRID:AB_1264294
Anti-JMJD1B	Invitrogen	Cat# PA5-53459
Anti-G9a	Sigma	Cat# Cat# G6919, RRID:AB_262007
Anti-beta Actin	Millipore	Cat# MAB1501; RRID:AB626633
Anti-Actinin	Santa Cruz	Cat# sc-17829; RRID:AB_626633
Goat anti-mouse HRP	Biorad	Cat# 170-6516; RRID: AB11125547
Goat anti-rabbit HRP	GenScript	Cat# A00167
Anti-H3K9me1	Abcam	Cat# ab8896
Anti-H3K9me2	Abcam	Cat# ab1220
Anti-H3K9me3	Abcam	Cat# ab8898
Anti-CTCF, clone D31H2	Cell Signaling	Cat# 3418

Table 3C.

Recombinant DNA	Source	Identifier
Halo-CTCF	Promega	N/A
Halo-KDM3B	Promega	N/A

Halo-Tag Alone	Promega	Cat# G6591
MLL-1 Probe	Oxford Gene Technology	Cat# LPH 506-A
MLL breakapart	Oxford Gene Technology	Cat# LPH 013-A
AML1 breakapart	Oxford Gene Technology	Cat# LPH 027-SA
BCL6 breakapart	Oxford Gene Technology	Cat# LPH 035-SA
EVL1 breakapart	Oxford Gene Technology	Cat# LPH 036-SA
TCRB breakapart	Oxford Gene Technology	Cat# LPH 048-SA
MLLT1	Oxford Gene Technology	Cat# LPH 508-A
MLLT3	Oxford Gene Technology	Cat# LPH 509-A
Chromosome 11 Alpha Satellite Red	Oxford Gene Technology	Cat# LPE 011R-A
E2A breakapart	Oxford Gene Technology	Cat# LPH 019-SA
5q del probe	Oxford Gene Technology	Cat# LPH 024
19p probe	Oxford Gene Technology	Cat# LPT19 PR-A
NMYC/LAF4 probe	Oxford Gene Technology	Cat# LPS-009A
MLL adjacent probe (*CD3*)	Empire Genomics	RPCI-11 215H18
Kmt2a/Chr9 Mouse	Empire Genomics	Mouse KMT2A-Chr09

Table 3D. Experimental Models: Cell Lines		
RPE-hTERT1	Nick Dyson	N/A
U937	FCCC Cell Culture Facility	CRL-1593.2
HL60	ATCC	CCL-240
KG1a	ATCC	CCL-246.1
HSPC	Cihan Duy	N/A
Primary AML	Cihan Duy	N/A
AML Organoid	Cihan Duy	N/A

Table 3E. Experimental Models: Organisms		
Mouse: C57BL/6 / 129/Sv	Tomasz Skorski	

Table 3F.

Chemicals, Peptides and Recombinant Proteins	Source	Identifier
Propidium Iodide Solution	Sigma Aldrich	Cat# P4864
Doxorubicin	Sigma Aldrich	ab142052
Doxorubicin (Mouse study)	Selleckchem	Cat# E2516
Dulbecco's Modified Eagles Medium – High Glucose	Sigma Aldrich	Cat# D5648
Roswell Park Memorial Institute Medium (RPMI)1640	Sigma Aldrich	Cat# R6504
Iscove's Modified Dulbecco Medium (IMDM)	Thermofisher	Cat# 12440053
Opti-Mem	Life Technologies	Cat# 31985070
Trypsin (0.25%) EDTA	Life Technologies	Cat# 2520056
L-Glutamine	Life Technologies	Cat# 25030-081
Penicillin and Streptomycin	Life Technologies	Cat# 15140122
Fetal Bovine Serum (FBS)	Gibco	Cat# 26140-079
Lipofectamine 3000	Life Technologies	Cat# L30000015
EHMTi	Jian Jin	UNC0642
KDM3i/JDI12	Cynthia Myers/Jian Jin	PMID: 31271662

Table 3G.

Software and Algorithms	Source	
Scaffold 6.0	3i-intelligent imaging Innovations	https://www.intelligent-imaging.com/slidebook

Table 3H.

Resource	Source	Identifier
Raw sequencing: ChIP-seq	This paper	GEO: GSE210480
KDM3B ChIP-seq	Public data	PMID: 28440295

For co-transfection experiments, both the siRNAs were transfected at the same time and collected at 72 hr from transfection (FIG. 9B-9C, 10A-10D). For Figures 8A and 7A-7F, cells were first transfected with siEHTM1/EHMT2 siRNA's for 24 hr followed by KDM3B siRNA transfection for 48hr.

Transfection procedure for U937 cells:

U937 were transfected using Neon System (Invitrogen) following manufacturer's instructions. Cells were mixed with siRNA constructs in 10µl of supplied buffer. Cell mixture was loaded in Neon syringe and submerged in electrode buffer. For U937 cells, 3 pulses of 1400V with a width of 10ms was applied for 500,000 cells. Cells were immediately transferred into fresh media in 6 well plates.

Long term passage of siRNA transfected cells:

Control siRNA transfected and KDM3B siRNA transfected cells were considered as passage 0 (P=0) 72 hours post transfection. After 72 hours post transfection, the $2.5X10^5$ cells were plated and cultured for 72 hours as passage P=1. The cells were subsequently plated, passaged and harvested at indicated passage numbers.

RNA extraction and quantitative real-time PCR:

Cells were washed and collected by trypsinization after two PBS washes. Cell pellet was resuspended in Qiazol reagent (QIAGEN) for lysis and stored at -80°C before further processing. Total RNA was extracted using miRNAeasy Mini Kit (QIAGEN) with an on-column DNase digestion according to the manufacturer's instructions. RNA was quantified using NanoDrop 2000 or One (Thermo Scientific). Single strand cDNA was prepared using Super Script IV first strand synthesis kit (Invitrogen) using random hexamers. Expression levels were analysed using FastStart Universal SYBR Green Master (ROX) (Roche) according to the manufacturer's instructions on a LightCycler 480 PCR machine (Roche) or QuantStudio 5 Real-time PCR machine (Applied Biosystems). Samples were normalized to β-actin. Primer sequences are provided in the tables above.

Protein purification

Human full length of KDM3A, KDM3B and KDM5A were cloned into pFastbac1 with flag tag at N-terminal, then Bacmid were made to produce baculovirus in insect cells(sf9), after infection of sf9 cells, proteins were purified and eluted from Flag-M2 agarose beads with 3Xflag peptide (0.15mg/ml).

Immunoblotting:

Cells were trypsinized and washed two times with PBS before resuspending in RIPA lysis buffer [50mM Tris pH 7.4, 150mM NaCl, 0.25% Sodium Deoxycholate, 1% NP40, 1mM EDTA, 10% Glycerol] freshly supplemented with protease inhibitor and PhosSTOP phosphatase inhibitor cocktails (Roche). Cells were lysed on ice for 15 min and stored at 80°C until further processing. Lysates were sonicated for 15 min (30sec ON and 30sec OFF cycle) at 70% amplitude in QSonica Q700 sonicator (Qsonica) followed by centrifugation at 12,000rpm for 15min. Cell lysate was transferred to a fresh tube and protein quantification was performed with Pierce BCA reagent (Thermo Scientific). Equal amounts of proteins were separated by SDS gel electrophoresis and transferred on nitrocellulose membrane (BioTrace NT, Pall Life Sciences) for at least 3 hr at a constant current. The membranes were blocked for at least 1 hr in 5% BSA-PBST (1X PBS with 0.5% Tween-20) or 5% milk-PBST and probed over night with specific antibodies as follows at the following dilutions: anti-KDM3B (Cell Signaling) (1:1000); anti-β-Actin (1:10,000); anti-G9A (Sigma) (1:1000); anti-Actinin (Santacruz) (1:1000). Catalog numbers for all antibodies used in this study can be found in the tables above.

Membranes were washed three times in PBST the next day, incubated with goat anti-mouse IgG peroxidase conjugated secondary antibody (170-6516, Biorad) or goat anti-rabbit peroxidase conjugated secondary antibody (A00167, GenScript) at 1:2500 in 5% milk-PBST for at least 1hr at room temperature, washed 3 times with PBST and incubated in Lumi-Light western blotting substrate (12015200001, Roche) 1min. Membranes were developed with Lumi-Film Chemiluminiscent detection film (11666657001, Roche). The western blot images displayed in the figures have been cropped and auto-contrasted.

Cell Cycle Analysis:

Samples were washed with PBS, centrifuged at 1400rpm for 5 min, and permeabilized with 500mL PBS containing 0.5% Triton X-100 for 30 min. After this incubation, cells were

washed with PBS and centrifuged at 1400rpm for 5 min. Samples were then stained with 1:100 dilutions of 1mg/mL PI solution and 0.5M EDTA with 100 mg RNase A, overnight at 4°C. Cell cycle distribution was analyzed by flow cytometry using the LSRII flow cytometry system (BD Biosciences).

DNA Fluorescent *In Situ* Hybridization (FISH):

The FISH protocol was performed as described previously in Black et al. (2013). Briefly, cell suspensions were fixed in ice-cold methanol:glacial acetic acid (3:1) solution for a minimum of four hours, before being centrifuged onto 8 Chamber Polystyrene vessel tissue culture treated glass slides (Falcon, Fisher Scientific) at 900rpm. The slides were air-dried and incubated in 2X SSC buffer for 2 min, followed by serial ethanol dilution (70%, 85% and 100%) incubations for 2 min each, for a total of 6 min. Air-dried slides were hybridized with probes that were diluted in appropriate buffer overnight at 37°C. The slides were washed the next day for 3 to 4 mins in appropriate wash buffers at 69°C with 0.4X SSC for Cytocell probes or Agilent Buffer1 for Agilent probes, followed by washing in 2X SSC with 0.05% Tween-20 (Cytocell probes) or Agilent Buffer 2 for Agilent probes. The slides were incubated in 1mg/mL DAPI solution made in 1% BSA-PBS, followed by a final 1X PBS wash. After the wash, the slides were mounted with ProLong Gold antifade reagent (Invitrogen).

FISH images were acquired using an Olympus IX81 or Olympus IX83 spinning disk microscope at 40X magnification and analyzed using Slidebook 6.0 softwares. A minimum of 20 z-planes with 0.5um step size was acquired for each field. Copy number gains for MLL1,11C, NMYC/LAF4 were scored in RPE cells as three or more foci. For MLL breakapart probe, copy gains were scored as 3 or more foci for the N terminus flanking probe (green) and C terminus flanking probe (red). Complete separation of red and green probe with no overlap was called breakapart for the MLL locus, TCF3 locus and any other locus FISHed with dual breakapart probe. A minimum of 100 nuclei are scored for each independent experiment. Extended list of probes used are provided in the tables above.

Metaphase Spreads:

RPE cells were transfected with siRNAs and passed 3 times. Cells were seeded for 48 hours. The cells were treated with KaryoMAX colcemid solution (Gibco) at a final concentration of 2μg/mL for 4 hour and were collected by mitotic shake off, washed with 1X PBS followed by

0.59% KCl (w/v) hypotonic solution for 1 hour 30 minute for expansion and swelling. The reaction was terminated by addition of 3:1 solution of cold methanol:acetic acid, followed by 4 washes. The cells were then resuspended in fixative solution. The cells were pipetted and dropped on a glass slide from a height of 12-15 inches to make the metaphase spread. FISH was performed for the indicated probes post drying of the slides. The images were taken with 25 z-planes with 0.5 µm step size using the Olympus IX83 microscope. The images were analyzed for FISH using Slidebook 6.0 software.

Drug Treatment Condition:

Doxorubicin treatment: RPE cells were plated in 10 cm tissue culture plates at a density of $2.5x10^5$. Cells were allowed to adhere for approximately 16 hours before Doxorubicin (Sigma) (dissolved in DMSO) was supplemented to media in different concentrations. Final concentrations used were 5, 2.5 and 1pg/µl. Cells were cultured in Doxorubicin for a total of 72 hours before harvesting. For Figures 12D and 14F-14G, cells were transfected with KDM3B plasmid for 4 hr. After removal of transfection mixture, cells were supplemented with 1 pg/µl Doxorubicin supplemented media and cultured for 20 hours before harvesting. For Figures 12C and 14C-14D, Doxorubicin supplemented media was added after removal of EHMT2 siRNA transfection mix and cultured for 72 hours before harvesting.

JDI12/KDM3i treatment:

RPE cells were plated in 10cm tissue culture plates at a density of $3x10^5$ cells. Cells were allowed to adhere to the plate for a minimum of 24h before JDI12/KDM3i (dissolved in DMSO) was supplemented to media at 25nM unless specified differently. Cells were cultured for a total of 72 hours before harvesting. For washout experiment (Fig. 4C), cells were allowed to adhere for 48h or 60h before treatment with JDI12/KDM3i. Cells were treated for 12h before media was removed, plates were washed with 1x PBS, and cells were either harvested or fresh complete media was added back to the plate without JDI12. For passage experiments, RPE cells were plated at $1.5x10^5$ cells. Cells were allowed to adhere to the plate for 24h before JDI12/KDM3i was supplemented to media at 25nM. Cells were cultured in JDI12/KDM3i for 72h further before being harvested and passaged at $3x10^5$ per 10cm plate. Cells were passaged every 3 days and seeded at the same amount each passage.

EHMTi (UNC0642) treatment:

For JDI12 + EHMTi (UNC0642) experiments, cells were seeded at $3x10^5$ in 10cm tissue culture plates and allowed to adhere for 60h before media was supplemented with JDI12 (25nM) and G9ai (2.5μM). Cells were harvested 12 hours post treatment. For siCTCF + G9ai experiments, cells were seeded in 10cm tissue culture plates at $2.1x10^5$ and allowed to adhere for 24h before following the transfection procedure described above. 24h post-transfection, media was supplemented with 1.5uM G9ai. Cells were cultured for a further 48h (72h total transfection) before being harvested. For Dox+EHMTi experiments, cells were plated at $1.5x10^5$ and allowed to adhere for 24h. EHMTi was supplemented to media at a final concentration of 1.5uM. 48h later DOX was supplemented to the media at 1pg/ul. 24h after Dox supplement (72h total EHMTi, 24h total Dox), cells were harvested.

Histone demethylase reactions

400ng KDM3A, KDM3B and KDM5A were incubated with 1μg bulk histones(Histone from calf thymus) or 3.3μM H3K9me2 peptide in 30μl reaction system at 27 degree, 5 hours. Reaction buffer: Hepes(PH7.5) 50mM, 2-OG 50μM, Fe(NH4)2(SO4)2 50μM, Sodium L-Acorbate 400μM, TCEP 1mM.

Recombinant human KDM3B/JMJD1B protein (abcam ab271569) was incubated with 1μM KDM3i, 1M Tris, 5M NaCl, 10mM Asorbic Acid, 10mM α-Ketoglutarate, 10mM Fe(NH4)2(SO4)2(H2O)6 at 27 C, 30 minutes. 1μL Histone from Calf Thymus (1mg/mL) in H2O was added to make reaction 100μL then incubated at 27 C for 5 hrs. 4X Laemmli Loading buffer with 5% β-Mercaptoethanol was added to reaction and then heated 95 C for 10 mins. Samples were snap frozen and then used for western blots.

Digital Droplet PCR:

The Digital Droplet PCR (ddPCR) was performed using 10 μL of 2 × ddPCR Supermix for Probes (no dUTP) (Bio-Rad), 900 nM of each primer, 250 nM probe, 50 ng of digested DNA template using HindIII restriction enzyme (NEB) and r2.1 Buffer (NEB), and nuclease free water to a total volume of 20 μL. The QX200 droplet generator (Bio-Rad) was used to generate the droplet mixture. The droplet mixture was then transferred to a PCR reaction plate and amplified with the following conditions: denaturation of 95 °C for 10 min, followed by 40 cycles of a two-

step thermal profile consisting of 95 °C for 15 s and 60 °C for 60 s, then incubated at 98 °C for 10 min and cooled to 8°C until the droplets were read. Once complete, the plate was transferred to the QX200 droplet reader (Bio-Rad) and analyzed for copy number variation (CNV). The number of positive (high level of fluorescence) and negative (low and constant level of fluorescence) droplets obtained were analyzed using QuantaSoft software (Bio-Rad, Pleasanton, CA, USA). Ratios of *KMT2A* to *CD3E* gene were used to determine copy number. Primer and probe sequences are provided in **Table 2**.

Annexin V Staining:

$3x10^5$ control or *KMT2A* inherited cells were seeded in a 10 cm plate and grown asynchronously for 72 hours. Cells were treated with 25nM of KDM3i for 12, 6, or 3 hours before prior to harvesting. Collected cells were processed using ALEXA FLUOR 488 conjugated Annexin V and PI staining following the manufacturer's instructions (Life Technologies). Data was collected on a BD Biosciences Symphony A5 flow cytometer and analyzed using FACSDiva software.

ChIP and ChIP sequencing:

Chromatin was prepared and ChIP were performed as described in Mishra et al 2018 and Black et al 2013. Sonication of chromatin was done with the Qsonica Q800R2 system (Qsonica). For H3K9Me3, H3K36Me3 and H3K27Me3 ChIP, $0.3x10^6$ RPE cells were seeded in 10cm plates. Cross linking of the cells were done by adding 1% formaldehyde to the media for 13 min at 37°C and stopped with 0.125M glycine, pH2.6. Plates were washed with ice cold PBS and scraped off, followed by centrifugation at 800 rpm for 5 min at 4°C. The pellet was resuspended in cellular lysis buffer (5mM PIPES pH8.00, 85mM KCl, 0.5% NP40) supplemented with protease and phosphatase inhibitors, incubated 5min on ice and centrifuged at 800 rpm, 5 min at 4°C. The pellet was resuspended in nuclear lysis buffer (NLB, 50mM Tris, pH 8.0, 1.0% SDS).

Chromatin was sonicated at 70% amplitude 15 s on 45sec off setting for 35 min. 4 µL of chromatin was reverse cross-linked overnight at 65°C in presence of proteinase K. After RNase treatment, DNA was isolated with phenol:chloroform extraction and checked on 1% agarose gel for a smear below 300bp. 1-10 µg of chromatin was precleared by centrifugation at 14,000rpm

for 10min at 4°C. For each IP, chromatin was immunoprecipitated with 0.2-2µg of antibody in dilution IP buffer (16.7mM Tris pH 8.0, 1.2mM EDTA pH 8.0, 167mM NaCl, 0.2% SDS, 0.24% or 1.84% Triston-X-100) at 4°C overnight. Chromatin was precleared for 2 hr each with protein A agarose and magnetic protein A or protein G beads (Invitrogen; to match antibody isotype) before immunoprecipitation. The immunoprecipitated material was washed 2 times in dilution IP buffer, 1 time in TSE buffer (20mM Tris pH 8.0, 2mM EDTA pH8.0, 500mM NaCl, 1% Triton X-100, 0.1% SDS), 1 time in LiCl buffer (100mM Tris pH 8.0, 500mM LiCl, 1% deoxycholic acid, 1% NP40) and 2 times in TE (10mM Tris pH 8.0, 1mM EDTA pH8.0) before elution in elution buffer (50mM $NaHCO_3$, 140mM NaCl, 1% SDS) with 10ug proteinase K at 1 hr 55°C 1000 rpm. The samples were removed from beads and reverse cross-linked at 65°C for 4 hr. Immunoprecipitated DNA was purified using either PCR purification columns (Promega) or AMPureXP beads. All the ChIPs were performed with at least two independent chromatin preparations from two independent siRNAs or two independent RPE cell lines. Antibodies used for ChIP are as follows: H3K9me1 Abcam ab8896-100, H3K9me2 Abcam ab1220, H3K9me3 Abcam ab8898.

ChIP sequencing libraries were prepped using the TruSeq ChIP Sample Preparation kit (Illumina). Libraries were single-end sequenced (75 cycles) using a NextSeq500 (Illumina).

ChIP-seq analysis:

ChIP-seq analysis was performed as previously described (Clarke et al., 2020; Van Rechem et al., 2021; Van Rechem et al., 2020). Sequencing reads were aligned against the human hg19 reference genome using BWA (Li and Durbin, 2010). Alignments were filtered for uniquely mapped reads and duplicates were removed. Input-normalized ratio coverage tracks were generated using Deeptools (Ramirez et al., 2016).

Statistical Analysis:

All pairwise comparisons were done using two-tailed Student's t test unless otherwise stated. Significance was determined if the p value was ≤ 0.05. All FISH experiments were carried out with at least two independent siRNAs unless otherwise stated and at least 100 nuclei per replicate per experiment were counted for all the FISH studies conducted. All error bars represent the SEM.

The following examples are provided to illustrate certain embodiments of the invention. They are not intended to limit the invention in any way.

EXAMPLE I

Loss of KDM3B causes site-specific copy gains of *MLL/KMT2A* locus.

KDM3B is a H3K9me1/2 demethylase located in the 5q31.1 region that is associated with *KMT2A* copy gains and rearrangements (Herry *et al.*, 2006; Hu *et al.*, 2001; Xu *et al.*, 2018; Zatkova *et al.*, 2009). To further confirm this relationship, TCGA Acute Myeloid Leukemia (LAML) samples containing >50% *KDM3B* loss were assessed for *KMT2A* copy number gains. Most samples with >50% *KDM3B* loss have positive *KMT2A* gains, with some showing >50% copy gain (p = 6.45e-07; **Fig. 1A**, green dots). We further confirmed this relationship by conducting DNA in situ hybridization (DNA FISH) for *KDM3B* and *KMT2A* on leukemic cell lines that have *KDM3B* allelic loss (loss of heterozygosity; LOH) (KG1a and HL60; **Fig. 1B**). We leveraged a clinically relevant DNA FISH probe covering *KMT2A* and the flanking regions (green: 5'-end of *KMT2A* and red: 3'-end of *KMT2A*; **Fig. 1C**), which allows both locus rearrangement (referred to as break apart, BA) and DNA copy gains to be identified. Consistent with the literature and the TCGA analysis (**Fig. 1A**), both HL60 and KG1a had cells within the population that had an increased baseline copy number of *KMT2A* (**Fig. 1B**).

These data prompted us to directly test whether depletion of KDM3B and/or other KDM3 family members generate *KMT2A* copy gains and genomic structural changes. Specifically, immortalized retinal pigment epithelial cells (RPEs) were siRNA depleted with at least two independent siRNAs for each KDM3 family member (Black *et al.*, 2013; Jiang *et al.*, 1999; Mishra *et al.*, 2018). These cells are ideal for assessing DNA amplification and rearrangement mechanisms because they have a stable genome, do not harbor cancer mutations and are near diploid (Black *et al.*, 2013; Janssen *et al.*, 2011; Jiang *et al.*, 1999; Maciejowski *et al.*, 2015; Mardin *et al.*, 2015; Mishra *et al.*, 2018; Zhang *et al.*, 2015). Each independent set of siRNAs was validated and assessed for major cell cycle defects by flow cytometry analysis before being assayed by DNA FISH (data not shown). A DNA FISH probe against the *KMT2A* gene (**Fig. 1C**; noted in orange) and a centromeric region at chromosome 11 (*11C*) were used to evaluate site-specific DNA copy gains. Copy number gain evaluation for each FISH probe was measured in

percentages as previously described (Black *et al.*, 2015a; Black *et al.*, 2013; Black *et al.*, 2016; Clarke *et al.*, 2020; Mishra *et al.*, 2018).

While KDM3 family members have comparable H3K9me1/2 activity *in vitro*, only KDM3B siRNA depletion caused a significant increase in *KMT2A* copy gains with no significant changes to the *11C* control region (**Figs. 1D-1E**). We then leveraged the clinically relevant DNA FISH probe covering *KMT2A* and further tested the site-specific alterations promoted by KDM3B depletion by leveraging an adjacent and partially overlapping FISH probe (called *CD3*; **Figure 1C**). KDM3B knockdown caused a significant increase in *KMT2A* gains (black bars) as well as break apart (BA; purple bars) events (**Figs. 1F-1G**). The copy gains did not appear to have N-terminal (green) or C-terminal (red) bias for the *KMT2A* gene, including the whole locus of the *KMT2A* gene (both probes- pseudo-colored yellow) (**Fig. 1F**). These events are focal as the adjacent FISH probe *CD3* (**Fig. 1C;** grey) did not significantly change upon KDM3B depletion (**Fig. 1H**), emphasizing the site-specific control of KDM3B depletion.

To further explore the specificity of KDM3B depletion in generating copy gains of leukemia-associated amplifications and/or rearrangements, we conducted FISH on a panel of leukemia-associated amplified and/or rearranged genes upon transient siRNA-mediated depletion of KDM3B, which included some of the fusion regions associated with *KMT2A* (*e.g.*, ENL/MLLT1, AF9/MLLT3). Most regions did not change in their basal DNA copy number, with the exception of *TCF3/E2A* and *AFF3/LAF4* (data not shown). We also observed *KMT2A* site-specific copy gains and rearrangements in the U937 leukemia cell line (de Necochea-Campion *et al.*, 2015; Sánchez-Reyes *et al.*, 2019) with KDM3B depletion, but not *TCF3/E2A* or *AFF3/LAF4*. These data suggest that, unlike the *KMT2A* locus, these other regions are not consistently regulated by KDM3B across cell lines.

KDM3B depletion alters H3K9me1/2 across the *KMT2A* genomic locus

Our *in vitro* and other published results indicate that KDM3B is an H3K9me1/2 demethylase (Kim *et al.*, 2012; Wang *et al.*, 2019). Therefore, we performed chromatin immunoprecipitation (ChIP) sequencing for H3K9me1/2/3 methylation marks in control and KDM3B siRNA transfected RPE cells. KDM3B depletion produced genome-wide H3K9me1 and H3K9me2 changes that were preferentially skewed towards an increase of these markers. As Scatterplots were generating comparing H3K9me1 levels across the whole genome at 10 Kb

resolution and the data showed that H3K9me1 was preferentially increased in KDM3B depleted cells compared to the control (showing a >1.5-fold increase). In fact, the magnitude of H3K9me1 increase across the middle of the *KMT2A* gene was one of the strongest events across the genome. The list of all 10 Kb genomic bins that had increased H3K9me1 and their nearest associated genes was also generated. A similar genome-wide increase of H3K9me2 was observed (data not shown).

Both H3K9me1/2 increased upon KDM3B depletion across the *KMT2A* gene body, particularly H3K9me1 within the 8.3kb breakpoint cluster region (BCR) spanning exons 8-14, which is enriched for the *KMT2A* rearrangements (data not shown) (Broeker *et al.*, 1996). In the control cells, H3K9me1 at BCR was lower than in the adjacent regions, corresponding to the trough of H3K9me1 density. KDM3B knockdown led to a strong increase of H3K9me1, so that this trough was reduced and H3K9me1 density became more uniform across the whole BCR vicinity. H3K9me2 was also increased on the flank to the BCR. We also observed altered H3K9me1/2 at other amplified and rearranged targets *TCF3* and *AFF3* regulated by KDM3B depletion. Consistent with a direct effect of KDM3B, analysis of published KDM3B ChIP-seq data (Li *et al.*, 2017) demonstrated that KDM3B binds across *KMT2A,* with a strong peak within the BCR that was lost upon shRNA-mediated KDM3B depletion. Furthermore, KDM3B also binds across *TCF3* and *AFF3*. Collectively, our data establish that KDM3B depletion alters H3K9me1/2 methylation landscape of the *KMT2A* locus, especially H3K9me1 at the BCR region, and contributes to the *KMT2A* copy gains and break apart events, which is consistent with other regulated regions.

Inhibition or depletion of KDM3B causes inherited *KMT2A* copy gains and genomic alterations

Using a recently identified KDM3 family inhibitor (JDI-12, referred to as KDM3i (Xu *et al.*, 2020), we were able to inhibit KDM3B enzyme activity *in vitro* (**Fig. 2A**) and noted a modest suppression of growth at 1μM with no impact at 25nM in RPE cells (**Fig. 2B**). These doses were also sufficient to promote significant *KMT2A* DNA copy gains and genomic rearrangements without altering KDM3B protein levels (**Fig. 2F** and **Figs. 2C-2D**). We further tested the impact of KDM3B inhibition on a panel of primary and cancer cell lines, which included KG1a cells, a primary AML derived cell line and a primary AML organoid model as

well as primary Hematopoietic Stem and Progenitor Cells (HSPC). KDM3i treatment significantly increased *KMT2A* copy gains and genomic rearrangements in all lines tested (**Figs. 2F-2J**). This demonstrates that KDM3B inhibition promotes conserved *KMT2A* DNA amplification and rearrangements across cancer and non-cancer cells as well as primary human cells.

KMT2A amplifications occur as both extrachromosomal and integrated events (Herry *et al.*, 006; Streubel *et al.*, 2000). By adding and removing KDM3i, we can assess the transient or permanent behavior of the *KMT2A* copy gains and genomic alterations. Should they disappear upon drug removal, these events would likely be transient site-specific extrachromosomal copy gains (TSSGs; (Clarke *et al.*, 2020; Mishra *et al.*, 2018)). In fact, *KMT2A* DNA copy gains and break apart events occur as soon as 12 hours after KDM3i treatment (**Fig. 2K,** KDM3i 12hrs), but are no longer observed upon KDM3i removal from the cells (**Fig. 2K,** KDM3i 12hrs washout). The total cell number was not reduced under these conditions (**Fig. 2E**). These data suggest that KDM3B inhibition promotes transient *KMT2A* amplifications and altered genomic rearrangement in a short timeframe, which raises the question as to whether longer treatment with KDM3i could result in inherited DNA copy gains through insertion/rearrangement. Therefore, we treated cells for 72 hours (approximately 3 cell divisions) and then passaged the cells into fresh media (wash-off) for additional passages to ensure that no active drug was present, before assessing *KMT2A* copy gains and genomic rearrangements (**Fig. 3A**). The longer suppression resulted in both *KMT2A* copy gains and genomic rearrangements being inherited through passages (**Fig. 3B**), which were confirmed with DNA FISH on mitotic chromosomes (**Figs. 3C-3D**).

siRNA inhibition does not result in a permanent genetic depletion (Bartlett and Davis, 2006). In fact, KDM3B protein levels return to baseline levels by the third passage (P3) (**Fig. 3E**). Therefore, we tested whether *KMT2A* copy gains and rearrangements were still present in P3 and later passages following siRNA-mediated KDM3B depletion. Inherited copy gains and genomic structure changes were observed at *KMT2A* and on mitotic chromosomes, but not in the adjacent control region, which highlights the selectivity (**Figs. 3F-3H**). The increased inherited copies were confirmed with *KMT2A* Digital Droplet PCR, using the adjacent *CD3E* gene as a control (**Fig. 3I**). While *TCF3* copy gains were inherited, *AFF3* copy gains did not occur in later passages (**Figs. 3J-3L**). Taken together, these data demonstrate that KDM3B inhibition and

depletion promote transient copy gains and rearrangements, as well as integrated events with extended suppression.

G9a and KDM3B cross-talk controls *KMT2A* copy gains and rearrangements

We previously demonstrated that co-depletion of specific H3K4 KMTs with the KDM5A enzyme prevents the KDM5A-driven TSSGs (Clarke *et al.*, 2020; Mishra *et al.*, 2018). Our results suggest that proper balance of H3K9me1/2 is critical in regulating site-specific copy gains and genomic rearrangements at *KMT2A* (**Figure 1**). Therefore, we co-depleted either of the two H3K9me1/2 KMTs, G9a/EHMT2 and EHMT1 (Black *et al.*, 2012), with KDM3B before assessing *KMT2A* DNA copy gains or rearrangements (data not shown).

Pre-depletion of G9a, but not EHMT1, exclusively rescued/prevented the *KMT2A* amplification and genomic alterations caused by KDM3B depletion (**Fig. 4A**). We also observed a rescue of *TCF3* and *AFF3* copy gains. Consistent with our observation, G9a is a euchromatic H3K9me1/2 KMT that regulates replication and is loaded in a ternary complex with PCNA (Esteve *et al.*, 2006). We further tested this relationship by co-treating RPE cells with the KDM3B inhibitor and/or a dual inhibitor for G9a/EHMT2 and EHMT1 (EHMTi) (Liu *et al.*, 2013). Consistent with the genetic rescue, there was a complete rescue with no impact on cell growth when compared to KDM3i alone (**Fig. 4B**). We used a short treatment time (12 hours) to generate *KMT2A* copy gains and structural changes in order to assess rescue and bypass secondary selection that could happen over time with EHMTi treatment. To strengthen the relationship between G9a and *KMT2A* amplification regulation, we transiently overexpressed G9a for 24 hours, which is the approximate cell doubling time for RPE cells and assessed *KMT2A* genomic alterations. G9a overexpression was sufficient to promote *KMT2A* copy gains and genomic alterations (**Fig. 4C**), which further emphasized the role of H3K9me1/2 methylation balance in regulating focal amplification of *KMT2A*.

Based on these data, we hypothesized that G9a depletion could rescue the extrachromosomal amplifications caused by constant reduction of KDM3B levels. To assess this possibility, we siRNA depleted G9a in the KDM3B LOH leukemia cell line HL60 and evaluated whether the higher copy gain baseline observed in these cells would be reduced or completely reset. While *KMT2A* copy gains were significantly suppressed (**Fig. 4D**), the levels were still higher than the baseline in RPE cells, which suggests that HL60 cells contain both transient

extrachromosomal and inherited forms. To further explore this relationship, we siRNA depleted G9a in the *KMT2A*-inherited RPE cell lines after their level of KDM3B had returned to baseline (**Figs. 3F-3G**) and assessed whether depletion of G9a could rescue the inherited *KMT2A* gains. G9a depletion did not impact the inherited *KMT2A* copy gains (**Fig. 4E**), which further suggests that inherited extra copies are stable and unable to be rescued once established. Collectively, these data demonstrate that KDM3B/G9a coordinate *KMT2A* amplification and rearrangements.

Since G9a depletion rescued *KMT2A* amplifications and genomic alterations caused by KDM3B suppression (**Figs. 4A-4B**), we hypothesized that co-depletion of G9a with KDM3B would reset the H3K9me1/2 patterns at *KMT2A*, which would strengthen the importance of H3K9me1/2 balance in regulating the *KMT2A* locus. Consistent with the rescue experiments, the preferential genome-wide increase of H3K9me1 and H3K9me2 caused by siKDM3B was mostly rescued by double KDM3B and G9a knockdown. The magnitude of this rescue by determined by comparing the total genomic length of the regions with > 1.5-fold H3K9me1 and H3K9me2 increase upon KDM3B knockdown to the fraction of these regions where the increase was no longer observed in the double knockdown compared to control. H3K9me1 increase was rescued across 81% of regions genome-wide (88 Mb out of total 109 Mb), whereas H3K9me2 increase was rescued across 75% of regions genome-wide (219 Mb out of total 292 Mb), suggesting that maintaining a KDM3B-G9a balance is critical for controlling H3K9me1/2 levels genome-wide.

G9a depletion was able to completely reset the H3K9me1 patterns at the BCR (exon 8-14) in *KMT2A* (**Figs. 4F-4G**). Consistent with *KMT2A*, we also observed similar rescue at *TCF3* and *AFF3* . KDM3B and G9a knockdowns produced genome-wide H3K9me1 changes with opposite preferential patterns, whereas the double knockdown rescued these skews. KDM3B knockdown resulted in a preferential increase of H3K9me1. By contrast, G9a knockdown resulted in a decrease of H3K9me1. In the double knockdown, H3K9me1 changes were strongly reduced, with smaller extent of differences from control in either direction. Similar scatterplot results for G9a rescue of H3K9me2 across the genome, including *KMT2A, TCF3, and AFF3* were observed (data not shown). These data suggest that KDM3B-G9a balance controls H3K9me1/2 levels, and in turn, site-specific DNA copy gains and genomic rearrangements (**Fig. 4H**).

Reduced CTCF occupancy promotes *KMT2A* copy gains and rearrangements

Experiments were designed to further elucidate H3K9me1/2 imbalance induced promotion of *KMT2A* amplification and rearrangement. Prior studies suggest that CTCF binding could impact genome integrity, rearrangement, or duplication, especially at the *KMT2A* locus (Atkin *et al.*, 2021; Gothe *et al.*, 2019); however, the direct role of CTCF in controlling amplification and rearrangement has not been thoroughly resolved. Upon evaluating multiple cell lines and tissues from ENCODE, we observed a highly conserved occupancy for CTCF at exon 11 within the BCR of *KMT2A*, which directly overlaps with KDM3B binding data (**Fig. 5A**). HL60 cells have a 5q allelic loss (Hejlik and Nagarajan, 2005) and appeared to have lower CTCF occupancy when compared to the other cells that were assessed. Therefore, we hypothesized that KDM3B depletion could disrupt CTCF binding and promote *KMT2A* amplification and genomic rearrangement. To address the hypothesis, we depleted KDM3B and CTCF individually or in combination before assessing *KMT2A* by DNA FISH (data not shown). CTCF depletion alone was sufficient to promote significant *KMT2A* site-specific copy gains and genomic rearrangements that were not enhanced by KDM3B depletion (**Fig. 5B**). Since the CTCF peak within exon 11 of *KMT2A* directly overlapped with the KDM3B peak (**Fig. 5A**), we hypothesized that KDM3B depletion may be disrupting CTCF binding. We tested this possibility by assessing CTCF occupancy at the *KMT2A* CTCF site in cells when KDM3B was depleted. While we did not observe a global change in CTCF steady-state protein levels, we did observe a significant reduction in CTCF binding at *KMT2A* exon 11 within the BCR by ChIP-Seq and ChIP-qPCR (**Figs. 5C-5E**).

Upon analyzing KDM3B and CTCF occupancy patterns genome-wide from public data (Li *et al.*, 2017) and our RPE ChIP-seq respectively, we observed that 6,386 KDM3B peaks in the public data (41.5% of all strong KDM3B peaks) directly overlapped with the 46,340 CTCF peaks in RPE cells (P-value=1.0e-07; **Fig. 5F**). Furthermore, 17,077 CTCF peaks reduced their intensity upon KDM3B depletion. As much as 16% of these CTCF binding sites with reduced occupancy overlapped with KDM3B binding (1,005 peaks out of 6,386 total co-occupied sites; *P*-value < 1.0e-216; Z-Score=143.38) (**Fig. 5G**). Despite the public KDM3B binding data being from a different cell line, the association between KDM3B and CTCF binding suggest a functional interplay between KDM3B and CTCF genome-wide.

To understand the genome-wide behavior of H3K9me1 at the 17,077 CTCF binding sites with reduced occupancy upon KDM3B depletion, we analyzed the impact of siKDM3B, siG9a, and double knockdown on the levels of H3K9me1 in the vicinity of all CTCF peaks (±5kb flanks from the peak center). Similar to the general effects observed across the whole genome length for H3K9me1, KDM3B and G9a knockdowns produced opposite changes in H3K9me1 at the CTCF proximal regions, whereas the double knockdown rescued these changes. Upon KDM3B knockdown, H3K9me1 levels increased at least 1.5-fold in the 5 Kb proximity of approximately 1,000 CTCF peaks genome-wide (**Figure 5H**). Upon the double knockdown of KDM3B and G9a, this increase was rescued at the majority (~80%) of these peaks, where H3K9me1 no longer showed this increase (**Figure 5H**). For example, the scatterplots in **Figure 5I** show comparisons of H3K9me1 levels for the proximal regions of the 17,077 CTCF sites after KDM3B knockdown (left), G9a knockdown (middle), and the double knockdown of KDM3B and G9a (right). KDM3B knockdown (**Figure 5I**, left plot) resulted in a preferential increase of H3K9me1 (the part above the upper red line corresponding to > 1.5-fold increase). The H3K9me1 increase at the CTCF binding site within BCR of the *KMT2A* gene (red point) was among the strongest changes of all CTCF sites genome-wide. G9a knockdown (**Figure 5I**, middle plot) resulted in decreased H3K9me1 (the part below the upper red line corresponding to > 1.5-fold decrease). However, in the double KDM3B/G9a knockdown (**Figure 5I**, right plot), H3K9me1 changes were strongly reduced, with smaller extent of differences from control in either direction (above and below red lines). The level of H3K9me1 at CTCF binding site within BCR of the KMT2A gene (red point) was close to control in the double depletion. These data indicate that KDM3B and G9a control H3K9me1/2 at CTCF peaks genome-wide, but the methylation control surrounding the *KMT2A* BCR CTCF is a strong outlier among all sites.

Since CTCF is known to regulate gene expression (Phillips and Corces, 2009), we assessed whether CTCF depletion regulated KDM3B expression levels. While depletion of CTCF modestly suppressed KDM3B transcript levels, both KDM3B and G9a protein levels were not significantly reduced, suggesting that CTCF is likely a downstream effector of KDM3B loss and H3K9me1/2 disruption. We tested this by depleting or chemically inhibiting G9a in combination with CTCF depletion. In fact, G9a depletion/inhibition was sufficient to block CTCF-induced amplifications (**Figs. 5J-5K**). Consistent with this data, the CTCF site in the *KMT2A* BCR had increased K9me1 upon KDM3B depletion that was completely rescued upon

G9a co-depletion (**Figs. 4F-4G**). Taken together, these data suggest that KDM3B and G9a coordinate H3K9me1/2 levels at and around the CTCF site, and in turn, impact CTCF occupancy and the predilection of *KMT2A* to undergo amplification and genomic rearrangement (**Fig. 5L**).

Doxorubicin promotes *KMT2A* amplification and rearrangement as well as reduces KDM3B and CTCF protein levels

KMT2A amplification and a host of genomic rearrangements are observed in pediatric leukemia and therapy-induced leukemia when conventional chemotherapy is used to treat several cancer types (Felix, 1998; Pedersen-Bjergaard *et al.*, 1998; Sanjuan-Pla *et al.*, 2015). For example, *KMT2A* amplified and rearranged MDS and AML are generated after topoisomerase II (topo II) inhibitor treatment (*e.g.*, Doxorubicin, Dox)(Godley and Larson, 2008). For other topoisomerase inhibitors, see *J. Med. Chem.* 2020, 63, 3, 884–904 and Nitiss JL. Nat Rev Cancer. 2009 May;9(5):338-50. Consistent with these clinical observations, Dox treatment promoted *KMT2A, AFF3* and *TCF3* copy gains and genomic alterations in RPE cells with no significant impact on control regions as determined by DNA FISH (**Fig. 6A**). To reduce pleiotropic defects in RPE cells, lower doses of Dox (1pg/μl and 5pg/μl) were used. Dox treatment also promoted *KMT2A* copy gains and rearrangements in primary HSPCs (**Fig. 6B**). These observations are consistent with prior reports showing that the topo II inhibitor etoposide induces heterogeneous rearrangements of *KMT2A* in a variety of primary and non-primary human cells (Gothe *et al.*, 2019; Libura *et al.*, 2005). We further tested the relationship between Dox treatment and *KMT2A* DNA copy gains by treating mixed C57BL/6-129/Sv mice with Dox (1.5mg/kg by i.v. for 3 consecutive days) before isolating their spleen and assessing *Kmt2a* copy number by DNA FISH. Consistent with the human primary HSPCs (**Fig. 6B**), cells isolated from the spleen of mice treated with Dox had increased *Kmt2a* copy gains compared to control mice. Meanwhile, there was no increase in DNA copy gain of the adjacent *Control 9* probe (**Fig. 6C**), demonstrating the site-specificity of the Dox-induced *Kmt2a* copy gain events occurring in the mice.

Since reduction of KDM3B or CTCF levels promote *KMT2A* copy gains and rearrangement (**Figures 1-4**), we assessed whether KDM3B or CTCF expression is altered upon Dox treatment. Both 1pg/μl and 5pg/μl resulted in a significant reduction in KDM3B transcript and protein levels in RPE cells (**Figs. 6D-6F**); however, no change was observed with G9a

transcripts (data not shown). In a similar fashion to KDM3B, Dox reduced CTCF transcript and protein levels (**Figs. 6G-6I**). We detected the same trend in KG1a cells, where Dox significantly reduced both KDM3B and CTCF transcript and protein levels (**Fig. 6J**). Our observations are consistent with a prior report noting a loss of CTCF protein in Dox-treated patient-derived mammary epithelial cells (Lehman *et al.*, 2021). To assess whether this was specific to Dox, we treated RPEs with another topo II inhibitor, etoposide. Consistent with Dox, etoposide significantly reduced the protein levels of KDM3B and CTCF (**Fig. 6K**), suggesting that these effects are a result of topo II inhibition.

Previous studies have shown that Dox treatment can activate the ubiquitin-proteasome system (UPS), leading to increased protein degradation (Kumarapeli *et al.*, 2005). Therefore, we hypothesized that one mechanism by which Dox could suppress KDM3B and CTCF levels is through activation of the UPS. To address this, we treated cells with Dox followed by the proteasome inhibitor MG132 and assessed the levels of KDM3B and CTCF (**Figs. 6L-6M**). While Dox treatment alone reduced the protein levels of KDM3B (**Fig. 6L**) and CTCF (**Fig. 6M**), treatment with MG132 partially rescued the levels of both KDM3B (**Fig. 6L**) and CTCF (**Fig. 6M**). Taken together, these data emphasize that Dox regulates KDM3B and CTCF levels through both transcriptional and post-transcriptional mechanisms.

KDM3B and CTCF regulation controls Doxorubicin-induced *KMT2A* amplification and rearrangement

Since KDM3B and CTCF are reduced upon Dox treatment, the imbalance in H3K9me1/2 and CTCF occupancy at *KMT2A* could be a key driver in promoting Dox-induced *KMT2A* amplification and genomic alterations. Consistent with this relationship, Dox treatment resulted in similar increase in H3K9me1 at the *KMT2A* CTCF site (**Fig. 7A**; upper graph comparing siKDM3B to Dox treatment) and H3K9me2 at the flanking region when compared to KDM3B depletion. The increased H3K9me1/2 was accompanied by reduced CTCF occupancy upon Dox treatment (**Fig. 7A**, lower bar graph). Furthermore, overexpression of CTCF was sufficient to prevent the *KMT2A* copy gains upon Dox treatment (**Fig. 7B**). CTCF overexpression alone does not cause copy gains. However, CTCF overexpression appears to alter local chromosomal organization at the locus.

Since Dox reduced KDM3B levels (**Figure 6**) and increased H3K9me1/2 in *KMT2A* (**Fig. 7A**), we tested whether G9a depletion would prevent the Dox-induced *KMT2A* changes. *KMT2A* copy gains and genomic alterations caused by Dox were completely rescued upon G9a depletion (**Fig. 7C**). We further demonstrated that chemical inhibition of G9a/EHMT1 prevented *KMT2A* copy gains and genomic alterations (EHMTi; **Fig. 7D**). Therefore, we hypothesized that increasing the expression of KDM3B would prevent the *KMT2A* copy gains and genomic structure changes. Upon Dox treatment, *KMT2A* copy gains and rearrangements were significantly upregulated; however, transient overexpression of KDM3B completely blocked *KMT2A* copy gains and rearrangements induced by Dox treatment (**Fig. 7E**). Consistent with our genetic and chemical inhibitor experiments (**Fig. 1-5**), these results suggest that Dox suppresses KDM3B and CTCF protein levels, which drives the copy gains and rearrangements driven through H3K9me1/2 methylation (**Figs. 7F, 7G**). Taken together, these data highlight an essential role for KDM3B/G9a balance and regulation of CTCF occupancy at *KMT2A* in order to prevent *KMT2A* genomic alterations, which establishes a potential mechanism to therapeutically target chemotherapy induced *KMT2A* rearrangements.

Discussion

The causal regulators for *KMT2A* amplification and rearrangements are not known but these events are observed in infant leukemias, AML and MDS, as well as in chemotherapy-induced leukemia. The data described in the examples above, demonstrate that KDM3B-G9a balance controls CTCF occupancy, and in turn, the ability of the *KMT2A* locus to undergo site-specific copy gains and genomic rearrangement. We showed that KDM3B depletion or inhibition as well as G9a overexpression, promotes the amplification of specific sites, suggesting these proteins are maintaining the methylation balance and capacity for amplification of the affected region. These observations are in alignment with G9a being part of the replication machinery and controlling H3K9me1/2 during replication (Esteve *et al.*, 2006). In the case of *KMT2A* gene locus, G9a is facilitating the amplification and rearrangement, while KDM3B and CTCF are counterbalancing these genomic alterations, illustrating the critical requirement for histone methylation regulation and the control of the transient amplification events (**Figure 7F**). Furthermore, Doxorubicin treatment reduced KDM3B and CTCF protein levels, at least in part through activation of the UPS, which resulted in *KMT2A* DNA copy gains and rearrangement.

These results revealed a molecular basis for the therapy-induced amplification and

rearrangement of *KMT2A*. Similar observations were also noted for *TCF3/E2A*, which is another rearranged loci in leukemia (Andersen *et al.*, 2011; Kager *et al.*, 2007; Mullighan, 2012). The findings reported have broad implications because they: 1) establish that epigenetic regulation controls amplification and rearrangements; 2) set the stage to discover the secondary hit(s) required for the generation of oncogenic *KMT2A* fusions; and 3) identify potential biomarkers and therapeutic targets to consider during treatments with chemotherapy and to monitor in patients post treatment.

KDM3B depletion in relationship to _KMT2A_ rearrangements and fusion partners

There are currently more than 100 known *KMT2A* rearrangement partners documented (Meyer *et al.*, 2023). These *KMT2A* rearrangements result in the fusion of the gene to any of the partner genes, leading to protein chimeras. *KMT2A* can also rearrange to several noncoding regions throughout the genome (Meyer *et al.*, 2023). Therefore, not all rearrangement events generate functional fusion proteins (Aplan, 2006b). These data suggest that the molecular mechanism(s) leading to the generation of *KMT2A* rearrangements, including those that do not generate translatable products, could be key to understanding tumors containing amplifications and rearrangements.

The data in Figures 1 – 7 demonstrate that depletion or inhibition of KDM3B is sufficient to promote amplification and inherited insertions/rearrangements of *KMT2A* and *TCF3/E2A*. Furthermore, after inheritance, the percentage of *KMT2A* or *TCF3/E2A*-rearranged cells does not increase within the population as seen by the consistent percent of cells with amplification and break apart events over time (unpublished observation across multiple cell types). Therefore, it is unlikely that loss of KDM3B alone is providing a major cellular fitness advantage for the various inherited rearrangements over the non-rearranged cells. This observation may be of no surprise since therapy-related AML has a latency period of up to 15 years after initial treatment with therapies such as Doxorubicin (Godley and Larson, 2008). These data suggest that while KDM3B suppression or loss alone generates inheritable rearrangements of *KMT2A*, it is likely just the first step necessary to promote or allow the selection of the rearrangement events resulting in functional fusion proteins that provide a cellular growth advantage. Mouse knock-in studies of the major *KMT2A* fusion genes (*i.e.*, *KMT2A-AF4, -AF9, -ENL*) demonstrate that even

the most common oncogenic associated fusions have a varying range of latency before developing into leukemia [reviewed in (Liu *et al.*, 2009)]. Therefore, the resulting fusion proteins generated clearly provide differential levels of cellular fitness advantage before developing into homogenous rearrangements and promoting leukemia. Furthermore, studies show that non-homologous end-joining is required for topo II inhibitor driven leukemia-associated *KMT2A* rearrangements (Gómez-Herreros *et al.*, 2017; Gothe *et al.*, 2019), suggesting that mis-regulated DNA damage responses are likely another factor involved in generating/selecting for the oncogenic fusion events observed in leukemia. However, additional influences could also potentiate the driver fusion events to emerge, including without limitation, cellular ageing, stress exposures, and/or acquired mutations.

KDM3B, 5q and *KMT2A* amplification and rearrangements

Not all del(5q) regions contain *KDM3B* (Eisenmann *et al.*, 2009). However, patients with del(5q) alone have a better prognosis compared to those presenting with del(5q) as well as other mutations or abnormalities (Giagounidis *et al.*, 2004). Since KDM3B loss was not responsible for gains or rearrangements of a panel of other *KMT2A* fusion partners (data not shown), we suspect that additional gene mutations and/or the dysregulation of additional epigenetic regulators are likely required to promote copy gains and rearrangements of the oncogenic fusion partners, providing the secondary hit(s) necessary. Furthermore, a number of other candidate tumor suppressor genes have been identified within the del(5q) region who may also play an oncogenic role that is independent of generating *KMT2A* amplifications and rearrangements (Ebert, 2010; Ebert *et al.*, 2008; Starczynowski *et al.*, 2010). The present study provided insight into the collection of mutated genes and/or epigenetic modulators which promote copy gains and rearrangement events of fusion partners associated with *KMT2A*. These insights allow for the systematic testing of the ability to promote the oncogenic fusions driving leukemia, thereby opening up the opportunity for new targeted therapeutic approaches to reduce occurrence of such events in the future.

Epigenetics, amplification, and in turn, rearrangements

When KDM3B was inhibited for short time intervals, the expected amplifications and break aparts at *KMT2A* locus were observed but resolved quickly with drug removal,

highlighting their transient extrachromosomal nature. However, upon longer treatment, these genomic events become inherited and are observed on the same chromosome or other chromosomes (**Fig. 3**). In fact, these events were not suppressed with G9a depletion, whereas KDM3B LOH cells had a reduction of *KMT2A* copy gains. These data illustrate that the aberrant regulation of the epigenome promotes transient DNA amplifications that can be inherited when the stimuli is maintained through multiple cell divisions. Therefore, we speculate that sustained amplification and break aparts are likely being incorporated into the genome through DNA damage repair pathways. Our data is consistent with prior proposed mechanisms (Aplan, 2006a). This study has now generated the roadmap to investigate these inherited genomic events. This information facilitates determination of the exact integration sites for building complete sequence map while also identifying the molecular features and pathways affiliated with the inherited amplifications.

Longer inhibition of KDM3B did not further increase the percent of cells within the population containing *KMT2A* copy gains or rearrangements compared to short treatment (**Figs. 2-3,** data not shown). Yet when inherited-*KMT2A* cell lines were exposed to KDM3i for a short time (3h, 6h), we observed a significant increase in *KMT2A* copy gains compared to the inherited baseline. However, upon longer treatment (12h), *KMT2A* copy gains returned to baseline, suggesting that those cells containing genomic aberrations of *KMT2A* are being negatively selected for, while a new population of cells with these aberrations emerge. This is supported by increased Annexin V in the inherited-*KMT2A* cell lines treated with KDM3i at the later time points (6h and 12h; data not shown). Consistent with a prior study (Xu *et al.*, 2020), these data suggest that *KMT2A*-rearranged cells have increased susceptibility to KDM3B inhibition. This observed sensitivity provides evidence of a promising therapeutic window in *KMT2A*-rearranged cancers.

KDM3B and CTCF as a bridge to Dox-induced *KMT2A* amplification and rearrangement

Upon topo II inhibitor treatment (*e.g.*, Doxorubicin, Dox), MDS and AML occur and are accompanied by amplification and rearrangement of the *KMT2A* locus (Godley and Larson, 2008). Prior studies demonstrate that topo II inhibitors promote non-leukemia and leukemia associated *KMT2A* rearrangements in various cell types (Gothe *et al.*, 2019; Libura *et al.*, 2005), which suggest a more universal regulatory mechanism controlling *KMT2A* alterations. A

population-based study demonstrated that younger individuals developing secondary leukemia have a significantly worse prognosis compared to *de novo* (Hulegardh *et al.*, 2015). Therefore, preventing the emergence of secondary cancer caused by chemotherapy such as Dox would have a profound clinical impact. This study demonstrates that epigenetic therapies could provide a much-needed tool to combat these cancers. We demonstrated that KDM3B and CTCF, the key suppressors of *KMT2A* amplification and rearrangements, are depleted with topo II inhibitor treatment, which associates with *KMT2A* genomic alterations. We also demonstrated that genetic or chemical depletion of G9a, a driver of *KMT2A* amplification and rearrangement, prevents the Dox-induced *KMT2A* genomic changes, while overexpression of KDM3B was also sufficient to block them. Lastly, CTCF occupancy in *KMT2A* was reduced with Dox treatment, while overexpression of CTCF prevented the Dox-induced *KMT2A* copy gain events. These data highlight the possibility of controlling Dox or other chemo-induced *KMT2A* amplification and rearrangements by pretreating or co-treating patients receiving these therapies with a G9a inhibitor or CTCF/KDM3B agonist. Collectively, these observations provide a molecular basis to develop treatment protocols to prevent therapy-associated *KMT2A* rearrangements by targeting epigenetic regulators.

Our findings establish that epigenetic mechanisms control the amplification and genomic rearrangements of *KMT2A*. We demonstrate that these events are directly promoted by Dox through suppression of KDM3B and CTCF protein levels, and can be blocked by co-depletion or inhibition of G9a/EHMT2. We also show that Dox suppresses KDM3B and CTCF protein levels through transcriptional and post-transcriptional mechanisms.

Appendix I - Sequences encoding the genes and proteins useful for practicing the invention and regions of interest for peptide mimetic binding and siRNA targeting.

Q7LBC6-1 KDM3B_Human (Isoform 1) Also see Gene ID: 51780

MADAAASPVGKRLLLLFADTAASASASAPAAAAAASGDPGPALRTRAWRAGTVRAMSGAVPQDLAIFVEF
DGCNWKQHSWVKVHAEEVIVLLLEGSLVWAPREDPVLLQGIRVSIAQWPALTFTPLVDKLGLGSVVPVEY
LLDRELRFLSDANGLHLFQMGTDSQNQILLEHAALRETVNALISDQKLQEIFSRGPYSVQGHRVKIYQPEGE
EGWLYGVVSHQDSITRLMEVSVTESGEIKSVDPRLIHVMLMDNSAPQSEGGTLKAVKSSKGKKKRESIEGK
DGRRRKSASDSGCDPASKKLKGDRGEVDSNGSDGGEASRGPWKGGNASGEPGLDQRAKQPPSTFVPQINR
NIRFATYTKENGRTLVVQDEPVGGDTPASFTPYSTATGQTPLAPEVGGAENKEAGKTLEQVGQGIVASAAV
VTTASSTPNTVRISDTGLAAGTVPEKQKGSRSQASGENSRNSILASSGFGAPLPSSSQPLTFGSGRSQSNGVL
ATENKPLGFSFGCSSAQEAQKDTDLSKNLFFQCMSQTLPTSNYFTTVSESLADDSSSRDSFKQSLESLSSGLC

KGRSVLGTDTKPGSKAGSSVDRKVPAESMPTLTPAFPRSLLNARTPENHENLFLQPPKLSREEPSNPFLAFV
EKVEHSPFSSFASQASGSSSSATTVTSKVAPSWPESHSSADSASLAKKKPLFITTDSSKLVSGVLGSALTSGG
PSLSAMGNGRSSSPTSSLTQPIEMPTLSSSPTEERPTVGPGQQDNPLLKTFSNVFGRHSGGFLSSPADFSQENK
APFEAVKRFSLDERSLACRQDSDSSTNSDLSDLSDSEEQLQAKTGLKGIPEHLMGKLGPNGERSAELLLGKS
KGKQAPKGRPRTAPLKVGQSVLKDVSKVKKLKQSGEPFLQDGSCINVAPHLHKCRECRLERYRKFKEQEQ
DDSTVACRFFHFRRLIFTRKGVLRVEGFLSPQQSDPDAMNLWIPSSSLAEGIDLETSKYILANVGDQFCQLV
MSEKEAMMMVEPHQKVAWKRAVRGVREMCDVCETTLFNIHWVCRKCGFGVCLDCYRLRKSRPRSETEE
MGDEEVFSWLKCAKGQSHEPENLMPTQIIPGTALYNIGDMVHAARGKWGIKANCPCISRQNKSVLRPAVT
NGMSQLPSINPSASSGNETTFSGGGGPAPVTTPEPDHVPKADSTDIRSEEPLKTDSSASNSNSELKAIRPPCPD
TAPPSSALHWLADLATQKAKEETKEAGSLRSVLNKESHSPFGLDSFNSTAKVSPLTPKLFNSLLLGPTASNN
KTEGSSLRDLLHSGPGKLPQTPLDTGIPFPPVFSTSSAGVKSKASLPNFLDHIIASVVENKKTSDASKRACNL
TDTQKEVKEMVMGLNVLDPHTSHSWLCDGRLLCLHDPSNKNNWKIFRECWKQGQPVLVSGVHKKLKSE
LWKPEAFSQEFGDQDVDLVNCRNCAIISDVKVRDFWDGFEIICKRLRSEDGQPMVLKLKDWPPGEDFRDM
MPTRFEDLMENLPLPEYTKRDGRLNLASRLPSYFVRPDLGPKMYNAYGLITAEDRRVGTTNLHLDVSDAV
NVMVYVGIPIGEGAHDEEVLKTIDEGDADEVTKQRIHDGKEKPGALWHIYAAKDAEKIRELLRKVGEEQG
QENPPDHDPIHDQSWYLDQTLRKRLYEEYGVQGWAIVQFLGDAVFIPAGAPHQVHNLYSCIKVAEDFVSPE
HVKHCFRLTQEFRHLSNTHTNHEDKLQVKNIIYHAVKDAVGTLKAHESKLARS

Q7LBC6-2 KDM3B_Human (Isoform 2)

MGAMEINRNIRFATYTKENGRTLVVQDEPVGGDTPASFTPYSTATGQTPLAPEVGGAENKEAGKTLEQVG
QGIVASAAVVTTASSTPNTVRISDTGLAAGTVPEKQKGSRSQASGENSRNSILASSGFGAPLPSSSQPLTFGS
GRSQSNGVLATENKPLGFSFGCSSAQEAQKDTDLSKNLFFQCMSQTLPTSNYFTTVSESLADDSSSRDSFKQ
SLESLSSGLCKGRSVLGTDTKPGSKAGSSVDRKVPAESMPTLTPAFPRSLLNARTPENHENLFLQPPKLSREE
PSNPFLAFVEKVEHSPFSSFASQASGSSSSATTVTSKVAPSWPESHSSADSASLAKKKPLFITTDSSKLVSGVL
GSALTSGGPSLSAMGNGRSSSPTSSLTQPIEMPTLSSSPTEERPTVGPGQQDNPLLKTFSNVFGRHSGGFLSSP
ADFSQENKAPFEAVKRFSLDERSLACRQDSDSSTNSDLSDLSDSEEQLQAKTGLKGIPEHLMGKLGPNGERS
AELLLGKSKGKQAPKGRPRTAPLKVGQSVLKDVSKVKKLKQSGEPFLQDGSCINVAPHLHKCRECRLERY
RKFKEQEQDDSTVACRFFHFRRLIFTRKGVLRVEGFLSPQQSDPDAMNLWIPSSSLAEGIDLETSKYILANV
GDQFCQLVMSEKEAMMMVEPHQKVAWKRAVRGVREMCDVCETTLFNIHWVCRKCGFGVCLDCYRLRK
SRPRSETEEMGDEEVFSWLKCAKGQSHEPENLMPTQIIPGTALYNIGDMVHAARGKWGIKANCPCISRQNK
SVLRPAVTNGMSQLPSINPSASSGNETTFSGGGGPAPVTTPEPDHVPKADSTDIRSEEPLKTDSSASNSNSEL
KAIRPPCPDTAPPSSALHWLADLATQKAKEETKEAGSLRSVLNKESHSPFGLDSFNSTAKVSPLTPKLFNSLL
LGPTASNNKTEGSSLRDLLHSGPGKLPQTPLDTGIPFPPVFSTSSAGVKSKASLPNFLDHIIASVVENKKTSDA
SKRACNLTDTQKEVKEMVMGLNVLDPHTSHSWLCDGRLLCLHDPSNKNNWKIFRECWKQGQPVLVSGV
HKKLKSELWKPEAFSQEFGDQDVDLVNCRNCAIISDVKVRDFWDGFEIICKRLRSEDGQPMVLKLKDWPP
GEDFRDMMPTRFEDLMENLPLPEYTKRDGRLNLASRLPSYFVRPDLGPKMYNAYGLITAEDRRVGTTNLH
LDVSDAVNVMVYVGIPIGEGAHDEEVLKTIDEGDADEVTKQRIHDGKEKPGALWHIYAAKDAEKIRELLR
KVGEEQGQENPPDHDPIHDQSWYLDQTLRKRLYEEYGVQGWAIVQFLGDAVFIPAGAPHQVHNLYSCIKV
AEDFVSPEHVKHCFRLTQEFRHLSNTHTNHEDKLQVKNIIYHAVKDAVGTLKAHESKLARS

Q7LBC6-3 KDM3B_Human (Isoform 3)

MSEKEAMMMVEPHQKVAWKRAVRGVREMCDVCETTLFNIHWVCRKCGFGVCLDCYRLRKSRPRSETEE
MGDEEVFSWLKCAKGQSHEPENLMPTQIIPGTALYNIGDMVHAARGKWGIKANCPCISRQNKSVLRPAVT
NGMSQLPSINPSASSGNETTFSGGGGPAPVTTPEPDHVPKADSTDIRSEEPLKTDSSASNSNSELKAIRPPCPD
TAPPSSALHWLADLATQKAKEETKEAGSLRSVLNKESHSPFGLDSFNSTAKVSPLTPKLFNSLLLGPTASNN
KTEGSSLRDLLHSGPGKLPQTPLDTGIPFPPVFSTSSAGVKSKASLPNFLDHIIASVVENKKTSDASKRACNL
TDTQKEVKEMVMGLNVLDPHTSHSWLCDGRLLCLHDPSNKNNWKIFRECWKQGQPVLVSGVHKKLKSE
LWKPEAFSQEFGDQDVDLVNCRNCAIISDVKVRDFWDGFEIICKRLRSEDGQPMVLKLKDWPPGEDFRDM
MPTRFEDLMENLPLPEYTKRDGRLNLASRLPSYFVRPDLGPKMYNAYGLITAEDRRVGTTNLHLDVSDAV

NVMVYVGIPIGEGAHDEEVLKTIDEGDADEVTKQRIHDGKEKPGALWHIYAAKDAEKIRELLRKVGEEQG
QENPPDHDPIHDQSWYLDQTLRKRLYEEYGVQGWAIVQFLGDAVFIPAGAPHQVHNLYSCIKVAEDFVSPE
HVKHCFRLTQEFRHLSNTHTNHEDKLQVKNIIYHAVKDAVGTLKAHESKLARS

Q96KQ7-1 · G9a/EHMT2_HUMAN Human (Isoform 1)

MAAAAGAAAAAAAAEGEAPAEMGALLLEKETRGATERVHGSLGDTPRSEETLPKATPDSLEPAGPSSPASV
TVTVGDEGADTPVGATPLIGDESENLEGDGDLRGGRILLGHATKSFPSSPSKGGSCPSRAKMSMTGAGKSP
PSVQSLAMRLLSMPGAQGAAAAGSEPPPATTSPEGQPKVHRARKTMSKPGNGQPPVPEKRPPEIQHFRMSD
DVHSLGKVTSDLAKRRKLNSGGGLSEELGSARRSGEVTLTKGDPGSLEEWETVVGDDFSLYYDSYSVDER
VDSDSKSEVEALTEQLSEEEEEEEEEEEEEEEEEEEEEEEDEESGNQSDRSGSSGRRKAKKKWRKDSPWV
KPSRKRRKREPPRAKEPRGVNGVGSSGPSEYMEVPLGSLELPSEGTLSPNHAGVSNDTSSLETERGFEELPL
CSCRMEAPKIDRISERAGHKCMATESVDGELSGCNAAILKRETMRPSSRVALMVLCETHRARMVKHHCCP
GCGYFCTAGTFLECHPDFRVAHRFHKACVSQLNGMVFCPHCGEDASEAQEVTIPRGDGVTPPAGTAAPAP
PPLSQDVPGRADTSQPSARMRGHGEPRRPPCDPLADTIDSSGPSLTLPNGGCLSAVGLPLGPGREALEKALV
IQESERRKKLRFHPRQLYLSVKQGELQKVILMLLDNLDPNFQSDQQSKRTPLHAAAQKGSVEICHVLLQAG
ANINAVDKQQRTPLMEAVVNNHLEVARYMVQRGGCVYSKEEDGSTCLHHAAKIGNLEMVSLLLSTGQVD
VNAQDSGGWTPIIWAAEHKHIEVIRMLLTRGADVTLTDNEENICLHWASFTGSAAIAEVLLNARCDLHAVN
YHGDTPLHIAARESYHDCVLLFLSRGANPELRNKEGDTAWDLTPERSDVWFALQLNRKLRLGVGNRAIRT
EKIICRDVARGYENVPIPCVNGVDGEPCPEDYKYISENCETSTMNIDRNITHLQHCTCVDDCSSSNCLCGQLS
IRCWYDKDGRLLQEFNKIEPPLIFECNQACSCWRNCKNRVVQSGIKVRLQLYRTAKMGWGVRALQTIPQG
TFICEYVGELISDAEADVREDDSYLFDLDNKDGEVYCIDARYYGNISRFINHLCDPNIIPVRVFMLHQDLRFP
RIAFFSSRDIRTGEELGFDYGDRFWDIKSKYFTCQCGSEKCKHSAEAIALEQSRLARLDPHPELLPELGSLPP
VNT

Q96KQ7-2 · EHMT2_HUMAN Human (Isoform 2)

MAAAAGAAAAAAAAEGEAPAEMGALLLEKETRGATERVHGSLGDTPRSEETLPKATPDSLEPAGPSSPASV
TVTVGDEGADTPVGATPLIGDESENLEGDGDLRGGRILLGHATKSFPSSPSKGGSCPSRAKMSMTGAGKSP
PSVQSLAMRLLSMPGAQGAAAAGSEPPPATTSPEGQPKVHRARKTMSKPGNGQPPVPEKRPPEIQHFRMSD
DVHSLGKVTSDLAKRRKLNSGGGLSEELGSARRSGEVTLTKGDPGSLEEWETVVGDDFSLYYDSYSVDER
VDSDSKSEVEALTEQLSEEEEEEEEEEEEEEEEEEEEEEEDEESGNQSDRSGSSGRRKAKKKWRKDSPWV
KPSRKRRKREPPRAKEPRGVSNDTSSLETERGFEELPLCSCRMEAPKIDRISERAGHKCMATESVDGELSGC
NAAILKRETMRPSSRVALMVLCETHRARMVKHHCCPGCGYFCTAGTFLECHPDFRVAHRFHKACVSQLN
GMVFCPHCGEDASEAQEVTIPRGDGVTPPAGTAAPAPPPLSQDVPGRADTSQPSARMRGHGEPRRPPCDPL
ADTIDSSGPSLTLPNGGCLSAVGLPLGPGREALEKALVIQESERRKKLRFHPRQLYLSVKQGELQKVILMLL
DNLDPNFQSDQQSKRTPLHAAAQKGSVEICHVLLQAGANINAVDKQQRTPLMEAVVNNHLEVARYMVQR
GGCVYSKEEDGSTCLHHAAKIGNLEMVSLLLSTGQVDVNAQDSGGWTPIIWAAEHKHIEVIRMLLTRGAD
VTLTDNEENICLHWASFTGSAAIAEVLLNARCDLHAVNYHGDTPLHIAARESYHDCVLLFLSRGANPELRN
KEGDTAWDLTPERSDVWFALQLNRKLRLGVGNRAIRTEKIICRDVARGYENVPIPCVNGVDGEPCPEDYK
YISENCETSTMNIDRNITHLQHCTCVDDCSSSNCLCGQLSIRCWYDKDGRLLQEFNKIEPPLIFECNQACSCW
RNCKNRVVQSGIKVRLQLYRTAKMGWGVRALQTIPQGTFICEYVGELISDAEADVREDDSYLFDLDNKDG
EVYCIDARYYGNISRFINHLCDPNIIPVRVFMLHQDLRFPRIAFFSSRDIRTGEELGFDYGDRFWDIKSKYFTC
QCGSEKCKHSAEAIALEQSRLARLDPHPELLPELGSLPPVNT

EHMT2/G9A encoding mRNA (human)

```
   1 atggcggcgg cggcgggagc tgcagcggcg gcggccgccg aggggaggc ccccgctgag
  61 atgggggcgc tgctgctgga gaaggaaacc agaggagcca ccgagagagt tcatggctct
 121 ttgggggaca cccctcgtag tgaagaaacc ctgcccaagg ccaaccccga ctccctggag
 181 cctgctggcc cctcatctcc agcctctgtc actgtcactg ttggtgatga gggggctgac
 241 acccctgtag gggctacacc actcattggg gatgaatctg agaatcttga gggagatggg
 301 gacctccgtg ggggccggat cctgctgggc catgccacaa agtcattccc ctcttccccc
```

```
 361 agcaaggggg gttcctgtcc tagccgggcc aagatgtcaa tgacaggggc gggaaaatca
 421 cctccatctg tccagagttt ggctatgagg ctactgagta tgccaggagc ccagggagct
 481 gcagcagcag ggtctgaacc ccctccagcc accacgagcc cagagggaca gtccaaggtc
 541 caccgagccc gcaaaaccat gtccaaacca ggaaatggac agcccccggt ccctgagaag
 601 cggcccccctg aaatacagca tttccgcatg agtgatgatg tccactcact gggaaaggtg
 661 acctcagatc tggccaaaag gaggaagctg aactcaggag gtggcctgtc ggaggagtta
 721 ggttctgccc ggcgttcagg agaagtgacc ctgacgaaag gggaccccgg gtccctggag
 781 gagtgggaga cggtggtggg tgatgacttc agtctctact atgattccta ctctgtggat
 841 gagcgcgtgg actccgacag caagtctgaa gttgaagctc taactgaaca actaagtgaa
 901 gaggaggagg aggaagagga ggaagaagaa gaagaggaag aggaggagga agaggaagaa
 961 gaagaggaag atgaggagtc agggaatcag tcagatagga gtggttccag tggccggcgc
1021 aaggccaaga agaaatggcg aaaagacagc ccatgggtga agccgtctcg gaaacggcgc
1081 aagcgggagc ctccgcgggc caaggagcca cgaggagtga atggtgtggg ctcctcaggc
1141 cccagtgagt acatggaggt ccctctgggg tccctggagc tgcccagcga ggggaccctc
1201 tcccccaacc acgctggggt gtccaatgac acatcttcgc tggagacaga gcgagggttt
1261 gaggagttgc ccctgtgcag ctgccgcatg gaggcaccca agattgaccg catcagcgag
1321 agggcggggc acaagtgcat ggccactgag agtgtggacg gagagctgtc aggctgcaat
1381 gccgccatcc tcaagcggga gaccatgagg ccatccagcc gtgtggccct gatggtgctc
1441 tgtgagaccc accgcgcccg catggtcaaa caccactgct gcccgggctg cggctacttc
1501 tgcacggcgg gcaccttcct ggagtgccac cctgacttcc gtgtggccca ccgcttccac
1561 aaggcctgtg tgtctcagct gaatgggatg gtcttctgtc cccactgtgg ggaggatgct
1621 tctgaagctc aagaggtgac catcccccgg ggtgacgggg tgaccccacc ggccggcact
1681 gcagctcctg cacccccacc cctgtcccag gatgtccccg ggagagcaga cacttctcag
1741 cccagtgccc ggatgcgagg gcatggggaa ccccggcgcc cgccctgcga tcccctggct
1801 gacaccattg acagctcagg gccctccctg accctgccca atgggggctg cctttcagcc
1861 gtggggctgc cactggggcc aggccgggag gccctggaaa aggccctggt catccaggag
1921 tcagagaggc ggaagaagct ccgtttccac cctcggcagt tgtacctgtc cgtgaagcag
1981 ggcgagctgc agaaggtgat cctgatgctg ttggacaacc tggaccccaa cttccagagc
2041 gaccagcaga gcaagcgcac gcccctgcat gcagccgccc agaagggctc cgtggagatc
2101 tgccatgtgc tgctgcaggc tggagccaac ataaatgcag tggacaaaca gcagcggacg
2161 ccactgatgg aggccgtggt gaacaaccac ctggaggtag cccgttacat ggtgcagcgt
2221 ggtggctgtg tctatagcaa ggaggaggac ggttccacct gcctccacca cgcagccaaa
2281 atcgggaact tggagatggt cagcctgctg ctgagcacag gacaggtgga cgtcaacgcc
2341 caggacagtg gggggtggac gcccatcatc tgggctgcag agcacaagca catcgaggtg
2401 atccgcatgc tactgacgcg gggcgccgac gtcaccctca ctgacaacga ggagaacatc
2461 tgcctgcact gggcctcctt cacgggcagc gccgccatcg ccgaagtcct tctgaatgcg
2521 cgctgtgacc tccatgctgt caactaccat ggggacaccc ccctgcacat cgcagctcgg
2581 gagagctacc atgactgcgt gctgttattc ctgtcacgtg gggccaaccc tgagctgcgg
2641 aacaaagagg gggacacagc atgggacctg actcccgagc gctccgacgt gtggtttgcg
2701 cttcaactca accgcaagct ccgacttggg gtgggaaatc gggccatccg cacagagaag
2761 atcatctgcc gggacgtggc tcggggctat gagaacgtgc ccattccctg tgtcaacggt
2821 gtggatgggg agccctgccc tgaggattac aagtacatct cagagaactg cgagacgtcc
2881 accatgaaca tcgatcgcaa catcacccac ctgcagcact gcacgtgtgt ggacgactgc
2941 tctagctcca accgcctgtg cggccagctc agcatccggt gctggtatga caaggatggg
3001 cgattgctcc aggaatttaa caagattgag cctccgctga ttttcgagtg taaccaggcg
3061 tgctcatgct ggagaaactg caagaaccgg gtcgtacaga gtggcatcaa ggtgcggcta
3121 cagctctacc gaacagccaa gatgggctgg ggggtccgcg ccctgcagac catcccacag
3181 gggaccttca tctgcgagta tgtcggggag ctgatctctg atgctgaggc tgatgtgaga
3241 gaggatgatt cttacctctt cgacttagac aacaaggatg gagaggtgta ctgcatagat
3301 gcccgttact atggcaacat cagccgcttc atcaaccacc tgtgtgaccc caacatcatt
3361 cccgtccggg tcttcatgct gcaccaagac ctgcgatttc cacgcatcgc cttcttcagt
3421 tcccgagaca tccggactgg ggaggagcta gggtttgact atggcgaccg cttctgggac
3481 atcaaaagca aatatttcac ctgccaatgt ggctctgaga agtgcaagca ctcagccgaa
3541 gccattgccc tggagcagag ccgtctggcc cgcctggacc cacaccctga gctgctgccc
3601 gagctcggct ccctgccccc tgtcaacaca tga
//
```

P49711-1 CTCF_Human (Isoform 1)

MEGDAVEAIVEESETFIKGKERKTYQRRREGGQEEDACHLPQNQTDGGEVVQDVNSSVQMVMMEQLDPT
LLQMKTEVMEGTVAPEAEAAVDDTQIITLQVVNMEEQPINIGELQLVQVPVPVTVPVATTSVEELQGAYEN
EVSKEGLAESEPMICHTLPLPEGFQVVKVGANGEVETLEQGELPPQEDPSWQKDPDYQPPAKKTKKTKKSK
LRYTEEGKDVDVSVYDFEEEQQEGLLSEVNAEKVVGNMKPPKPTKIKKKGVKKTFQCELCSYTCPRRSNL
DRHMKSHTDERPHKCHLCGRAFRTVTLLRNHLNTHTGTRPHKCPDCDMAFVTSGELVRHRRYKHTHEKP
FKCSMCDYASVEVSKLKRHIRSHTGERPFQCSLCSYASRDTYKLKRHMRTHSGEKPYECYICHARFTQSGT
MKMHILQKHTENVAKFHCPHCDTVIARKSDLGVHLRKQHSYIEQGKKCRYCDAVFHERYALIQHQKSHK
NEKRFKCDQCDYACRQERHMIMHKRTHTGEKPYACSHCDKTFRQKQLLDMHFKRYHDPNFVPAAFVCSK
CGKTFTRRNTMARHADNCAGPDGVEGENGGETKKSKRGRKRKMRSKKEDSSDSENAEPDLDDNEDEEEP
AVEIEPEPEPQPVTPAPPPAKKRRGRPPGRTNQPKQNQPTAIIQVEDQNTGAIENIIVEVKKEPDAEPAEGEEE
EAQPAATDAPNGDLTPEMILSMMDR

P49711-2 CTCF_Human (Isoform 2)

MAFVTSGELVRHRRYKHTHEKPFKCSMCDYASVEVSKLKRHIRSHTGERPFQCSLCSYASRDTYKLKRHM
RTHSGEKPYECYICHARFTQSGTMKMHILQKHTENVAKFHCPHCDTVIARKSDLGVHLRKQHSYIEQGKK
CRYCDAVFHERYALIQHQKSHKNEKRFKCDQCDYACRQERHMIMHKRTHTGEKPYACSHCDKTFRQKQL
LDMHFKRYHDPNFVPAAFVCSKCGKTFTRRNTMARHADNCAGPDGVEGENGGETKKSKRGRKRKMRSK
KEDSSDSENAEPDLDDNEDEEEPAVEIEPEPEPQPVTPAPPPAKKRRGRPPGRTNQPKQNQPTAIIQVEDQNT
GAIENIIVEVKKEPDAEPAEGEEEEAQPAATDAPNGDLTPEMILSMMDR

REFERENCES

Andersen, M.K., Autio, K., Barbany, G., Borgstrom, G., Cavelier, L., Golovleva, I., Heim, S., Heinonen, K., Hovland, R., Johannsson, J.H., et al. (2011). Paediatric B-cell precursor acute lymphoblastic leukaemia with t(1;19)(q23;p13): clinical and cytogenetic characteristics of 47 cases from the Nordic countries treated according to NOPHO protocols. Br J Haematol 155, 235-243. 10.1111/j.1365-2141.2011.08824.x.

Andersen, M.K., Christiansen, D.H., Jensen, B.A., Ernst, P., Hauge, G., and Pedersen-Bjergaard, J. (2001). Therapy-related acute lymphoblastic leukaemia with MLL rearrangements following DNA topoisomerase II inhibitors, an increasing problem: report on two new cases and review of the literature since 1992. Br J Haematol 114, 539-543.

Aplan, P.D. (2006a). Causes of oncogenic chromosomal translocation. Trends Genet 22, 46-55. 10.1016/j.tig.2005.10.002.

Aplan, P.D. (2006b). Chromosomal translocations involving the MLL gene: molecular mechanisms. DNA Repair (Amst) 5, 1265-1272. 10.1016/j.dnarep.2006.05.034.

Atkin, N.D., Raimer, H.M., Wang, Z., Zang, C., and Wang, Y.H. (2021). Assessing acute myeloid leukemia susceptibility in rearrangement-driven patients by DNA breakage at topoisomerase II and CCCTC-binding factor/cohesin binding sites. Genes Chromosomes Cancer 60, 808-821. 10.1002/gcc.22993.

Bailey, C., Shoura, M.J., Mischel, P.S., and Swanton, C. (2020). Extrachromosomal DNA-relieving heredity constraints, accelerating tumour evolution. Ann Oncol 31, 884-893. 10.1016/j.annonc.2020.03.303.

Bartlett, D.W., and Davis, M.E. (2006). Insights into the kinetics of siRNA-mediated gene silencing from live-cell and live-animal bioluminescent imaging. Nucleic Acids Res 34, 322-333. 10.1093/nar/gkj439.

Black, J.C., Atabakhsh, E., Kim, J., Biette, K.M., Van Rechem, C., Ladd, B., Burrowes, P.D., Donado, C., Mattoo, H., Kleinstiver, B.P., et al. (2015a). Hypoxia drives transient site-specific copy gain and drug-resistant gene expression. Genes Dev 29, 1018-1031. 10.1101/gad.259796.115.

Black, J.C., Atabakhsh, E., Kim, J., Biette, K.M., Van Rechem, C., Ladd, B., Burrowes, P.D., Donado, C., Mattoo, H., Kleinstiver, B.P., et al. (2015b). Hypoxia drives transient site-specific copy gain and drug-resistant gene expression. Genes & development 29, 1018-1031. 10.1101/gad.259796.115.

Black, J.C., Manning, A.L., Van Rechem, C., Kim, J., Ladd, B., Cho, J., Pineda, C.M., Murphy, N., Daniels, D.L., Montagna, C., et al. (2013). KDM4A lysine demethylase induces site-specific copy gain and rereplication of regions amplified in tumors. Cell 154, 541-555. 10.1016/j.cell.2013.06.051.

Black, J.C., Van Rechem, C., and Whetstine, J.R. (2012). Histone lysine methylation dynamics: establishment, regulation, and biological impact. Mol Cell 48, 491-507. 10.1016/j.molcel.2012.11.006.

Black, J.C., Zhang, H., Kim, J., Getz, G., and Whetstine, J.R. (2016). Regulation of Transient Site-specific Copy Gain by MicroRNA. J Biol Chem 291, 4862-4871. 10.1074/jbc.M115.711648.

Borthakur, G., and Estey, A.E. (2007). Therapy-related acute myelogenous leukemia and myelodysplastic syndrome. Curr Oncol Rep 9, 373-377. 10.1007/s11912-007-0050-z.

Broeker, P.L., Super, H.G., Thirman, M.J., Pomykala, H., Yonebayashi, Y., Tanabe, S., Zeleznik-Le, N., and Rowley, J.D. (1996). Distribution of 11q23 breakpoints within the MLL breakpoint cluster region in de novo acute leukemia and in treatment-related acute myeloid leukemia: correlation with scaffold attachment regions and topoisomerase II consensus binding sites. Blood 87, 1912-1922.

Campo, E., Swerdlow, S.H., Harris, N.L., Pileri, S., Stein, H., and Jaffe, E.S. (2011). The 2008 WHO classification of lymphoid neoplasms and beyond: evolving concepts and practical applications. Blood 117, 5019-5032. 10.1182/blood-2011-01-293050.

Clarke, T.L., Tang, R., Chakraborty, D., Van Rechem, C., Ji, F., Mishra, S., Ma, A., Kaniskan, H.U., Jin, J., Lawrence, M.S., et al. (2020). Histone Lysine Methylation Dynamics Control EGFR DNA Copy-Number Amplification. Cancer Discov 10, 306-325. 10.1158/2159-8290.CD-19-0463.

Cox, M.C., Panetta, P., Venditti, A., Del Poeta, G., Maurillo, L., Tamburini, A., Del Principe, M.I., and Amadori, S. (2003). Fluorescence in situ hybridization and conventional cytogenetics for the diagnosis of 11q23+/MLL+ translocation in leukaemia. Br J Haematol 121, 953-955.

de Necochea-Campion, R., Diaz Osterman, C.J., Hsu, H.W., Fan, J., Mirshahidi, S., Wall, N.R., and Chen, C.S. (2015). AML sensitivity to YM155 is modulated through AKT and Mcl-1. Cancer Lett 366, 44-51. 10.1016/j.canlet.2015.05.034.

Dolan, M., McGlennen, R.C., and Hirsch, B. (2002). MLL amplification in myeloid malignancies: clinical, molecular, and cytogenetic findings. Cancer Genet Cytogenet 134, 93-101.

Dulak, A.M., Schumacher, S.E., van Lieshout, J., Imamura, Y., Fox, C., Shim, B., Ramos, A.H., Saksena, G., Baca, S.C., Baselga, J., et al. (2012). Gastrointestinal adenocarcinomas of the esophagus, stomach, and colon exhibit distinct patterns of genome instability and oncogenesis. Cancer Res 72, 4383-4393. 10.1158/0008-5472.Can-11-3893.

Duy, C., Teater, M., Garrett-Bakelman, F.E., Lee, T.C., Meydan, C., Glass, J.L., Li, M., Hellmuth, J.C., Mohammad, H.P., Smitheman, K.N., et al. (2019). Rational Targeting of Cooperating Layers of the Epigenome Yields Enhanced Therapeutic Efficacy against AML. Cancer discovery 9, 872-889. 10.1158/2159-8290.CD-19-0106.

Ebert, B.L. (2010). Genetic deletions in AML and MDS. Best Pract Res Clin Haematol 23, 457-461. 10.1016/j.beha.2010.09.006.

Ebert, B.L., Pretz, J., Bosco, J., Chang, C.Y., Tamayo, P., Galili, N., Raza, A., Root, D.E., Attar, E., Ellis, S.R., and Golub, T.R. (2008). Identification of RPS14 as a 5q- syndrome gene by RNA interference screen. Nature 451, 335-339. 10.1038/nature06494.

Eisenmann, K.M., Dykema, K.J., Matheson, S.F., Kent, N.F., DeWard, A.D., West, R.A., Tibes, R., Furge, K.A., and Alberts, A.S. (2009). 5q- myelodysplastic syndromes: chromosome 5q genes direct a tumor-suppression network sensing actin dynamics. Oncogene 28, 3429-3441. 10.1038/onc.2009.207.

Esteve, P.O., Chin, H.G., Smallwood, A., Feehery, G.R., Gangisetty, O., Karpf, A.R., Carey, M.F., and Pradhan, S. (2006). Direct interaction between DNMT1 and G9a coordinates DNA and histone methylation during replication. Genes Dev 20, 3089-3103. 10.1101/gad.1463706.

Felix, C.A. (1998). Secondary leukemias induced by topoisomerase-targeted drugs. Biochim Biophys Acta 1400, 233-255. 10.1016/s0167-4781(98)00139-0.

Giagounidis, A.A., Germing, U., Wainscoat, J.S., Boultwood, J., and Aul, C. (2004). The 5q- syndrome. Hematology 9, 271-277. 10.1080/10245330410001723824.

Godley, L.A., and Larson, R.A. (2008). Therapy-related myeloid leukemia. Semin Oncol 35, 418-429. 10.1053/j.seminoncol.2008.04.012.

Gómez-Herreros, F., Zagnoli-Vieira, G., Ntai, I., Martínez-Macías, M.I., Anderson, R.M., Herrero-Ruíz, A., and Caldecott, K.W. (2017). TDP2 suppresses chromosomal translocations induced by DNA topoisomerase II during gene transcription. Nat Commun 8, 233. 10.1038/s41467-017-00307-y.

Gothe, H.J., Bouwman, B.A.M., Gusmao, E.G., Piccinno, R., Petrosino, G., Sayols, S., Drechsel, O., Minneker, V., Josipovic, N., Mizi, A., et al. (2019). Spatial Chromosome Folding and Active Transcription Drive DNA Fragility and Formation of Oncogenic MLL Translocations. Mol Cell 75, 267-283 e212. 10.1016/j.molcel.2019.05.015.

Hanahan, D. (2022). Hallmarks of Cancer: New Dimensions. Cancer Discov 12, 31-46. 10.1158/2159-8290.Cd-21-1059.

Hanahan, D., and Weinberg, R.A. (2011). Hallmarks of cancer: the next generation. Cell 144, 646-674. 10.1016/j.cell.2011.02.013.

Heinz, S., Benner, C., Spann, N., Bertolino, E., Lin, Y.C., Laslo, P., Cheng, J.X., Murre, C., Singh, H., and Glass, C.K. (2010). Simple combinations of lineage-determining transcription factors prime cis-regulatory elements required for macrophage and B cell identities. Mol Cell 38, 576-589. 10.1016/j.molcel.2010.05.004.

Hejlik, D.P., and Nagarajan, L. (2005). Deletion of 5q in myeloid leukemia cells HL-60: an L1 element-mediated instability. Cancer Genet Cytogenet 156, 97-103. 10.1016/j.cancergencyto.2004.05.011.

Herry, A., Douet-Guilbert, N., Guéganic, N., Morel, F., Le Bris, M.J., Berthou, C., and De Braekeleer, M. (2006). Del(5q) and MLL amplification in homogeneously staining region in acute myeloblastic leukemia: a recurrent cytogenetic association. Ann Hematol 85, 244-249. 10.1007/s00277-005-0059-z.

Hu, Z., Gomes, I., Horrigan, S.K., Kravarusic, J., Mar, B., Arbieva, Z., Chyna, B., Fulton, N., Edassery, S., Raza, A., and Westbrook, C.A. (2001). A novel nuclear protein, 5qNCA (LOC51780) is a candidate for the myeloid leukemia tumor suppressor gene on chromosome 5 band q31. Oncogene 20, 6946-6954. 10.1038/sj.onc.1204850.

Hulegardh, E., Nilsson, C., Lazarevic, V., Garelius, H., Antunovic, P., Rangert Derolf, A., Mollgard, L., Uggla, B., Wennstrom, L., Wahlin, A., et al. (2015). Characterization and prognostic features of secondary acute myeloid leukemia in a population-based setting: a report from the Swedish Acute Leukemia Registry. Am J Hematol 90, 208-214. 10.1002/ajh.23908.

Janssen, A., van der Burg, M., Szuhai, K., Kops, G.J., and Medema, R.H. (2011). Chromosome segregation errors as a cause of DNA damage and structural chromosome aberrations. Science 333, 1895-1898. 10.1126/science.1210214.

Jiang, X.R., Jimenez, G., Chang, E., Frolkis, M., Kusler, B., Sage, M., Beeche, M., Bodnar, A.G., Wahl, G.M., Tlsty, T.D., and Chiu, C.P. (1999). Telomerase expression in human somatic cells does not induce changes associated with a transformed phenotype. Nat Genet 21, 111-114. 10.1038/5056.

Kager, L., Lion, T., Attarbaschi, A., Koenig, M., Strehl, S., Haas, O.A., Dworzak, M.N., Schrappe, M., Gadner, H., Mann, G., and Austrian, B.F.M.S.G. (2007). Incidence and outcome of TCF3-PBX1-positive acute lymphoblastic leukemia in Austrian children. Haematologica 92, 1561-1564. 10.3324/haematol.11239.

Kim, J.Y., Kim, K.B., Eom, G.H., Choe, N., Kee, H.J., Son, H.J., Oh, S.T., Kim, D.W., Pak, J.H., Baek, H.J., et al. (2012). KDM3B is the H3K9 demethylase involved in transcriptional activation of lmo2 in leukemia. Mol Cell Biol 32, 2917-2933. 10.1128/mcb.00133-12.

Kumarapeli, A.R., Horak, K.M., Glasford, J.W., Li, J., Chen, Q., Liu, J., Zheng, H., and Wang, X. (2005). A novel transgenic mouse model reveals deregulation of the ubiquitin-proteasome system in the heart by doxorubicin. Faseb j 19, 2051-2053. 10.1096/fj.05-3973fje.

Lehman, B.J., Lopez-Diaz, F.J., Santisakultarm, T.P., Fang, L., Shokhirev, M.N., Diffenderfer, K.E., Manor, U., and Emerson, B.M. (2021). Dynamic regulation of CTCF stability and sub-nuclear localization in response to stress. PLoS Genet 17, e1009277. 10.1371/journal.pgen.1009277.

Leone, G., Mele, L., Pulsoni, A., Equitani, F., and Pagano, L. (1999). The incidence of secondary leukemias. Haematologica 84, 937-945.

Li, H., and Durbin, R. (2010). Fast and accurate long-read alignment with Burrows-Wheeler transform. Bioinformatics 26, 589-595. 10.1093/bioinformatics/btp698.

Li, J., Yu, B., Deng, P., Cheng, Y., Yu, Y., Kevork, K., Ramadoss, S., Ding, X., Li, X., and Wang, C.-Y. (2017). KDM3 epigenetically controls tumorigenic potentials of human colorectal cancer stem cells through Wnt/β-catenin signalling. Nature Communications 8, 15146. 10.1038/ncomms15146.

Libura, J., Slater, D.J., Felix, C.A., and Richardson, C. (2005). Therapy-related acute myeloid leukemia-like MLL rearrangements are induced by etoposide in primary human CD34+ cells and remain stable after clonal expansion. Blood 105, 2124-2131. 10.1182/blood-2004-07-2683.

Liu, F., Barsyte-Lovejoy, D., Li, F., Xiong, Y., Korboukh, V., Huang, X.P., Allali-Hassani, A., Janzen, W.P., Roth, B.L., Frye, S.V., et al. (2013). Discovery of an in vivo chemical probe of the lysine methyltransferases G9a and GLP. J Med Chem 56, 8931-8942. 10.1021/jm401480r.

Liu, H., Cheng, E.H., and Hsieh, J.J. (2009). MLL fusions: pathways to leukemia. Cancer Biol Ther 8, 1204-1211. 10.4161/cbt.8.13.8924.

Maciejowski, J., Li, Y., Bosco, N., Campbell, P.J., and de Lange, T. (2015). Chromothripsis and Kataegis Induced by Telomere Crisis. Cell 163, 1641-1654. 10.1016/j.cell.2015.11.054.

MacKinnon, R.N., Kannourakis, G., Wall, M., and Campbell, L.J. (2011). A cryptic deletion in 5q31.2 provides further evidence for a minimally deleted region in myelodysplastic syndromes. Cancer Genet 204, 187-194. 10.1016/j.cancergen.2011.02.001.

Maitta, R.W., Cannizzaro, L.A., and Ramesh, K.H. (2009). Association of MLL amplification with poor outcome in acute myeloid leukemia. Cancer Genet Cytogenet 192, 40-43. 10.1016/j.cancergencyto.2009.02.018.

Mardin, B.R., Drainas, A.P., Waszak, S.M., Weischenfeldt, J., Isokane, M., Stutz, A.M., Raeder, B., Efthymiopoulos, T., Buccitelli, C., Segura-Wang, M., et al. (2015). A cell-based model system links chromothripsis with hyperploidy. Mol Syst Biol 11, 828. 10.15252/msb.20156505.

Meyer, C., Larghero, P., Almeida Lopes, B., Burmeister, T., Gröger, D., Sutton, R., Venn, N.C., Cazzaniga, G., Corral Abascal, L., Tsaur, G., et al. (2023). The KMT2A recombinome of acute leukemias in 2023. Leukemia. 10.1038/s41375-023-01877-1.

Mishra, S., Van Rechem, C., Pal, S., Clarke, T.L., Chakraborty, D., Mahan, S.D., Black, J.C., Murphy, S.E., Lawrence, M.S., Daniels, D.L., and Whetstine, J.R. (2018). Cross-talk between Lysine-Modifying Enzymes Controls Site-Specific DNA Amplifications. Cell 174, 803-817 e816. 10.1016/j.cell.2018.06.018.

Mishra, S., and Whetstine, J.R. (2016). Different Facets of Copy Number Changes: Permanent, Transient, and Adaptive. Mol Cell Biol. 10.1128/MCB.00652-15.

Mullighan, C.G. (2012). Molecular genetics of B-precursor acute lymphoblastic leukemia. J Clin Invest 122, 3407-3415. 10.1172/JCI61203.

Pedersen-Bjergaard, J., Andersen, M.K., and Johansson, B. (1998). Balanced chromosome aberrations in leukemias following chemotherapy with DNA-topoisomerase II inhibitors. J Clin Oncol 16, 1897-1898. 10.1200/JCO.1998.16.5.1897.

Phillips, J.E., and Corces, V.G. (2009). CTCF: master weaver of the genome. Cell 137, 1194-1211. 10.1016/j.cell.2009.06.001.

Poppe, B., Vandesompele, J., Schoch, C., Lindvall, C., Mrozek, K., Bloomfield, C.D., Beverloo, H.B., Michaux, L., Dastugue, N., Herens, C., et al. (2004). Expression analyses identify MLL as a prominent target of 11q23 amplification and support an etiologic role for MLL gain of function in myeloid malignancies. Blood 103, 229-235. 10.1182/blood-2003-06-2163.

Ramirez, F., Ryan, D.P., Gruning, B., Bhardwaj, V., Kilpert, F., Richter, A.S., Heyne, S., Dundar, F., and Manke, T. (2016). deepTools2: a next generation web server for deep-sequencing data analysis. Nucleic Acids Res 44, W160-165. 10.1093/nar/gkw257.

Rice, S., and Roy, A. (2020). MLL-rearranged infant leukaemia: A 'thorn in the side' of a remarkable success story. Biochim Biophys Acta Gene Regul Mech 1863, 194564. 10.1016/j.bbagrm.2020.194564.

Ross-Innes, C.S., Stark, R., Teschendorff, A.E., Holmes, K.A., Ali, H.R., Dunning, M.J., Brown, G.D., Gojis, O., Ellis, I.O., Green, A.R., et al. (2012). Differential oestrogen receptor binding is associated with clinical outcome in breast cancer. Nature 481, 389-393. 10.1038/nature10730.

Saavedra, F., Gurard-Levin, Z.A., Rojas-Villalobos, C., Vassias, I., Quatrini, R., Almouzni, G., and Loyola, A. (2020). JMJD1B, a novel player in histone H3 and H4 processing to ensure genome stability. Epigenetics Chromatin 13, 6. 10.1186/s13072-020-00331-1.

Sánchez-Reyes, K., Pedraza-Brindis, E.J., Hernández-Flores, G., Bravo-Cuellar, A., López-López, B.A., Rosas-González, V.C., and Ortiz-Lazareno, P.C. (2019). The supernatant of cervical carcinoma cells lines induces a decrease in phosphorylation of STAT-1 and NF-κB transcription factors associated with changes in profiles of cytokines and growth factors in macrophages derived from U937 cells. Innate Immun 25, 344-355. 10.1177/1753425919848841.

Sanjuan-Pla, A., Bueno, C., Prieto, C., Acha, P., Stam, R.W., Marschalek, R., and Menendez, P. (2015). Revisiting the biology of infant t(4;11)/MLL-AF4+ B-cell acute lymphoblastic leukemia. Blood 126, 2676-2685. 10.1182/blood-2015-09-667378.

Schichman, S.A., Caligiuri, M.A., Gu, Y., Strout, M.P., Canaani, E., Bloomfield, C.D., and Croce, C.M. (1994). ALL-1 partial duplication in acute leukemia. Proc Natl Acad Sci U S A 91, 6236-6239.

Schoch, C., Kern, W., Kohlmann, A., Hiddemann, W., Schnittger, S., and Haferlach, T. (2005). Acute myeloid leukemia with a complex aberrant karyotype is a distinct biological entity characterized by genomic imbalances and a specific gene expression profile. Genes Chromosomes Cancer 43, 227-238. 10.1002/gcc.20193.

Song, K., Minami, J.K., Huang, A., Dehkordi, S.R., Lomeli, S.H., Luebeck, J., Goodman, M.H., Moriceau, G., Krijgsman, O., Dharanipragada, P., et al. (2022). Plasticity of

Extrachromosomal and Intrachromosomal BRAF Amplifications in Overcoming Targeted Therapy Dosage Challenges. Cancer Discov 12, 1046-1069. 10.1158/2159-8290.CD-20-0936.

Sperling, A.S., Gibson, C.J., and Ebert, B.L. (2017). The genetics of myelodysplastic syndrome: from clonal haematopoiesis to secondary leukaemia. Nat Rev Cancer 17, 5-19. 10.1038/nrc.2016.112.

Starczynowski, D.T., Kuchenbauer, F., Argiropoulos, B., Sung, S., Morin, R., Muranyi, A., Hirst, M., Hogge, D., Marra, M., Wells, R.A., et al. (2010). Identification of miR-145 and miR-146a as mediators of the 5q- syndrome phenotype. Nat Med 16, 49-58. 10.1038/nm.2054.

Streubel, B., Valent, P., Jäger, U., Edelhäuser, M., Wandt, H., Wagner, T., Büchner, T., Lechner, K., and Fonatsch, C. (2000). Amplification of the MLL gene on double minutes, a homogeneously staining region, and ring chromosomes in five patients with acute myeloid leukemia or myelodysplastic syndrome. Genes Chromosomes Cancer 27, 380-386.

Super, H.J., McCabe, N.R., Thirman, M.J., Larson, R.A., Le Beau, M.M., Pedersen-Bjergaard, J., Philip, P., Diaz, M.O., and Rowley, J.D. (1993). Rearrangements of the MLL gene in therapy-related acute myeloid leukemia in patients previously treated with agents targeting DNA-topoisomerase II. Blood 82, 3705-3711.

Tang, G., DiNardo, C., Zhang, L., Ravandi, F., Khoury, J.D., Huh, Y.O., Muzzafar, T., Medeiros, L.J., Wang, S.A., and Bueso-Ramos, C.E. (2015). MLL gene amplification in acute myeloid leukemia and myelodysplastic syndromes is associated with characteristic clinicopathological findings and TP53 gene mutation. Hum Pathol 46, 65-73. 10.1016/j.humpath.2014.09.008.

Van Rechem, C., Ji, F., Chakraborty, D., Black, J.C., Sadreyev, R.I., and Whetstine, J.R. (2021). Collective regulation of chromatin modifications predicts replication timing during cell cycle. Cell Rep 37, 109799. 10.1016/j.celrep.2021.109799.

Van Rechem, C., Ji, F., Mishra, S., Chakraborty, D., Murphy, S.E., Dillingham, M.E., Sadreyev, R.I., and Whetstine, J.R. (2020). The lysine demethylase KDM4A controls the cell-cycle expression of replicative canonical histone genes. Biochim Biophys Acta Gene Regul Mech 1863, 194624. 10.1016/j.bbagrm.2020.194624.

Walter, M.J., Payton, J.E., Ries, R.E., Shannon, W.D., Deshmukh, H., Zhao, Y., Baty, J., Heath, S., Westervelt, P., Watson, M.A., et al. (2009). Acquired copy number alterations in adult

acute myeloid leukemia genomes. Proc Natl Acad Sci U S A 106, 12950-12955. 10.1073/pnas.0903091106.

Wang, X., Fan, H., Xu, C., Jiang, G., Wang, H., and Zhang, J. (2019). KDM3B suppresses APL progression by restricting chromatin accessibility and facilitating the ATRA-mediated degradation of PML/RARalpha. Cancer Cell Int 19, 256. 10.1186/s12935-019-0979-7.

Winters, A.C., and Bernt, K.M. (2017). MLL-Rearranged Leukemias-An Update on Science and Clinical Approaches. Front Pediatr 5, 4. 10.3389/fped.2017.00004.

Woo, J.S., Alberti, M.O., and Tirado, C.A. (2014). Childhood B-acute lymphoblastic leukemia: a genetic update. Exp Hematol Oncol 3, 16. 10.1186/2162-3619-3-16.

Xu, X., Nagel, S., Quentmeier, H., Wang, Z., Pommerenke, C., Dirks, W.G., Macleod, R.A.F., Drexler, H.G., and Hu, Z. (2018). KDM3B shows tumor-suppressive activity and transcriptionally regulates HOXA1 through retinoic acid response elements in acute myeloid leukemia. Leuk Lymphoma 59, 204-213. 10.1080/10428194.2017.1324156.

Xu, X., Wang, L., Hu, L., Dirks, W.G., Zhao, Y., Wei, Z., Chen, D., Li, Z., Wang, Z., Han, Y., et al. (2020). Small molecular modulators of JMJD1C preferentially inhibit growth of leukemia cells. Int J Cancer 146, 400-412. 10.1002/ijc.32552.

Yoo, J., Jeon, Y.H., Cho, H.Y., Lee, S.W., Kim, G.W., Lee, D.H., and Kwon, S.H. (2020). Advances in Histone Demethylase KDM3A as a Cancer Therapeutic Target. Cancers (Basel) 12. 10.3390/cancers12051098.

Zatkova, A., Merk, S., Wendehack, M., Bilban, M., Muzik, E.M., Muradyan, A., Haferlach, C., Haferlach, T., Wimmer, K., Fonatsch, C., and Ullmann, R. (2009). AML/MDS with 11q/MLL amplification show characteristic gene expression signature and interplay of DNA copy number changes. Genes Chromosomes Cancer 48, 510-520. 10.1002/gcc.20658.

Zhang, C.Z., Spektor, A., Cornils, H., Francis, J.M., Jackson, E.K., Liu, S., Meyerson, M., and Pellman, D. (2015). Chromothripsis from DNA damage in micronuclei. Nature 522, 179-184. 10.1038/nature14493.

While certain features of the invention have been described herein, many modifications, substitutions, changes, and equivalents will now occur to those of ordinary skill in the art. It is, therefore, to be understood that the appended claims are intended to cover all such modifications and changes as fall within the true spirit of the invention.

What is claimed is:

1. A method for reducing MLL/KMT2A amplification in a patient in need thereof, the method comprising administration of an effective amount of one or more agents including

i) a first agent which increases KDM3B expression and function and, or

ii) a second agent which inhibits expression or activity of H3K9 methyltransferase, said one or more agents being administered in one or more pharmaceutically acceptable carriers and reducing MLL/KMT2A amplification in said patient.

2. The method of claim 1, wherein said first agent is a KDM3B agonist and said second agent is a G9a inhibitor and both agents are administered.

3. The method of claim 1, wherein the MLL/KMT2A amplification is caused by administration of a chemotherapeutic agent.

4. The method of any one of claims 1, 2, or 3, wherein a chemotherapeutic agent reduces KDM3B expression.

5. The method of any one of claims 1 to 4, wherein the chemotherapeutic agent is a topoisomerase II inhibitor.

6. The method one of claims 1 to 5, wherein the topoisomerase II inhibitor is doxorubicin, daunorubicin, etoposide or Topoisomerase II alpha or beta.

7. The method of any one of claims 1 to 6, wherein the patient has a genetic loss of KDM3B.

8. The method of any one of claims 3 to 7, wherein said administration of MLL/ KMT2A reducing agents is performed before, during or after administration of said chemotherapeutic agent.

9. The method of any one of the preceding claims, further comprising administration of a proteosome inhibitor.

10. The method of claim 9, wherein said proteosome inhibitor is selected from bortezomib, carfilzomib, and ixazomib.

11. The method of any one of the preceding claims, wherein said agent which increases KDM3B expression, function or activity is a KDM3B protein mimetic, a KDM3B agonist or an expression vector encoding KDM3B.

12. The method of any one of the preceding claims, wherein said patient has a mutation in a CTCF encoding nucleic acid associated with reduced binding to KMT2A, and said method further comprises administration of an agent which stabilizes CTCF binding functions.

13. The method of claim 12, wherein said agent which stabilizes CTCF binding functions is a a CTCF protein mimetic, a CTCF agonist or an expression vector encoding CTCF.

14. The method of claim 12 or claim 13, comprising administration of a rad21 protein mimetic, a rad21 agonist or an expression vector encoding rad21.

15. The method of any one of the preceding claims, wherein said G9a inhibitor is an inhibitory nucleic acid selected from an siRNA, an antisense oligonucleotide, an shRNA, and a ribozyme having sufficient sequence homology to said G9a encoding nucleic acid to reduce expression of thereof in a target cell.

16. The method of claim 15, wherein said inhibitory nucleic acid comprises one or more modified nucleotides or nucleosides.

17. The method of any one of claims 11 to 16, wherein said expression vector or said inhibitory nucleic acid is affixed to a biocompatible lipid nanoparticle.

18. A method for treating a cancer patient having chemotherapy induced MLL/KMT2A amplifications, the method comprising administration of an effective amount of at least one agent present in at least one pharmaceutically acceptable carrier, which increases KDM3B expression or inhibits expression of H3K9 methyltransferase, thereby reducing MLL/KMT2A in said cancer patient.

19. The method of claim 18, wherein both a KDM3B agonist and a G9a inhibitor are administered.

20. The method of any one of the preceding claims, wherein said treatment reduces MLL/KMT2A copy numbers when compared to untreated control patients.

21. A method for reducing TCF3 amplification or AFF3 amplification in a patient in need thereof, the method comprising administration of an effective amount of at least one agent which increases KDM3B activity or expression or inhibits activity or expression of H3K9 methyltransferase.

22. The method of claim 21, wherein said first agent is a KDM3B agonist and said second agent is a G9a inhibitor and both agents are administered.

23. The method of claim 21, wherein the MLL/KMT2A amplification is caused by administration of a chemotherapeutic agent.

24. The method of any one of claims 21, 22, or 23, wherein a chemotherapeutic agent reduces KDM3B expression.

25. The method of any one of claims 21 to 24, wherein the chemotherapeutic agent is a topoisomerase II inhibitor.

26. The method one of claims 21 to 25, wherein the topoisomerase II inhibitor is doxorubicin, daunorubicin, etoposide or Topoisomerase II alpha or beta.

27. The method of any one of claims 21 to 26, wherein the patient has a genetic loss of KDM3B.

28. The method of any one of claims 23 to 27, wherein said administration of MLL/ KMT2A reducing agents is performed before, during or after administration of said chemotherapeutic agent.

29. The method of any one of claims 21 to 28, further comprising administration of a proteosome inhibitor.

30. The method of claim 29, wherein said proteosome inhibitor is selected from bortezomib, carfilzomib, and ixazomib.

31. The method of any one claims 21 to 29 wherein said agent which increases KDM3B expression, function or activity is a KDM3B protein mimetic, a KDM3B agonist or an expression vector encoding KDM3B.

32. The method of any one of claims 29 to 31, wherein said patient has a mutation in a CTCF encoding nucleic acid associated with reduced binding to KMD2A, and said method further comprises administration of an agent which stabilizes CTCF binding functions.

33. The method of claim 32, wherein said agent which stabilizes CTCF binding functions is a a CTCF protein mimetic, a CTCF agonist or an expression vector encoding CTCF.

34. The method of claim 12 or claim 13, comprising administration of a rad21 protein mimetic, a rad21 agonist or an expression vector encoding rad21.

35. The method of any one of claims 21 to 34 wherein said G9a inhibitor is an inhibitory nucleic acid selected from an siRNA, an antisense oligonucleotide, an shRNA, and a ribozyme having sufficient sequence homology to said G9a encoding nucleic acid to reduce expression of thereof in a target cell.

36. The method of claim 35, wherein said inhibitory nucleic acid comprises one or more modified nucleotides or nucleosides.

37. The method of any one of claims 21 to 26, wherein said expression vector or said inhibitory nucleic acid is affixed to a biocompatible lipid nanoparticle.

38. A method for reducing AFF3 amplification in a patient in need thereof, the method comprising administration of an effective amount of at least one agent which increases KDM3B expression or inhibits expression of H3K9 methyltransferase.

39. The method of claim 21, wherein the method reduces TCF3 copy numbers when compared to an untreated control patients.

40. The method of claim 21, wherein the patient has reduced AFF3 copy numbers when compared to an untreated control.

41. The method of any of the preceding claims, wherein the G9a inhibiting agent is UNC 0642.

42. The method of any of the preceding claims, wherein the agent is an siRNA that targets the molecules listed in Table 1.

FIG. 1A

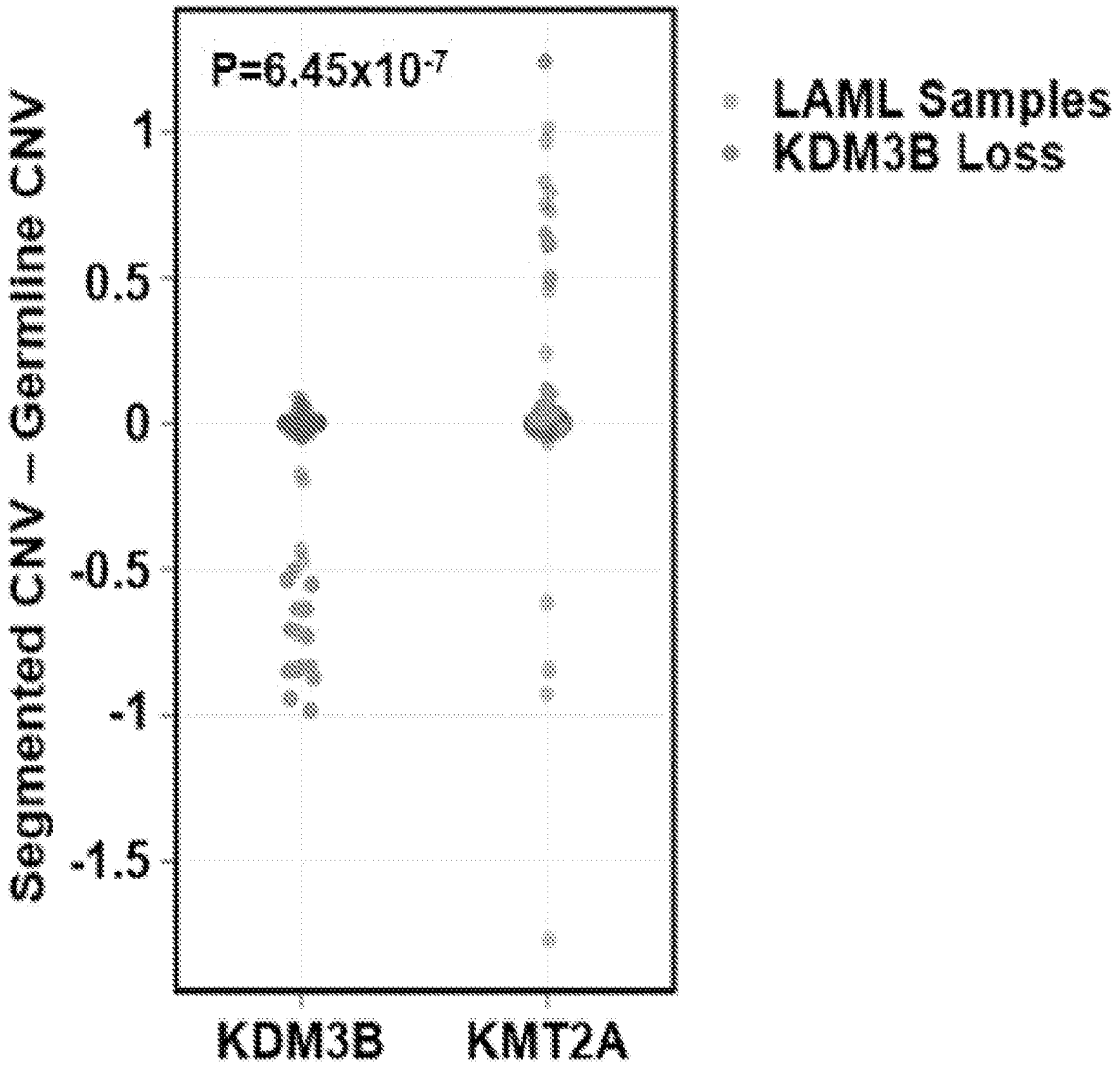
P=6.45x10-7
Segmented CNV – Germline CNV
1
0.5
0
-0.5
-1
-1.5
KDM3B
KMT2A
LAML Samples
KDM3B Loss

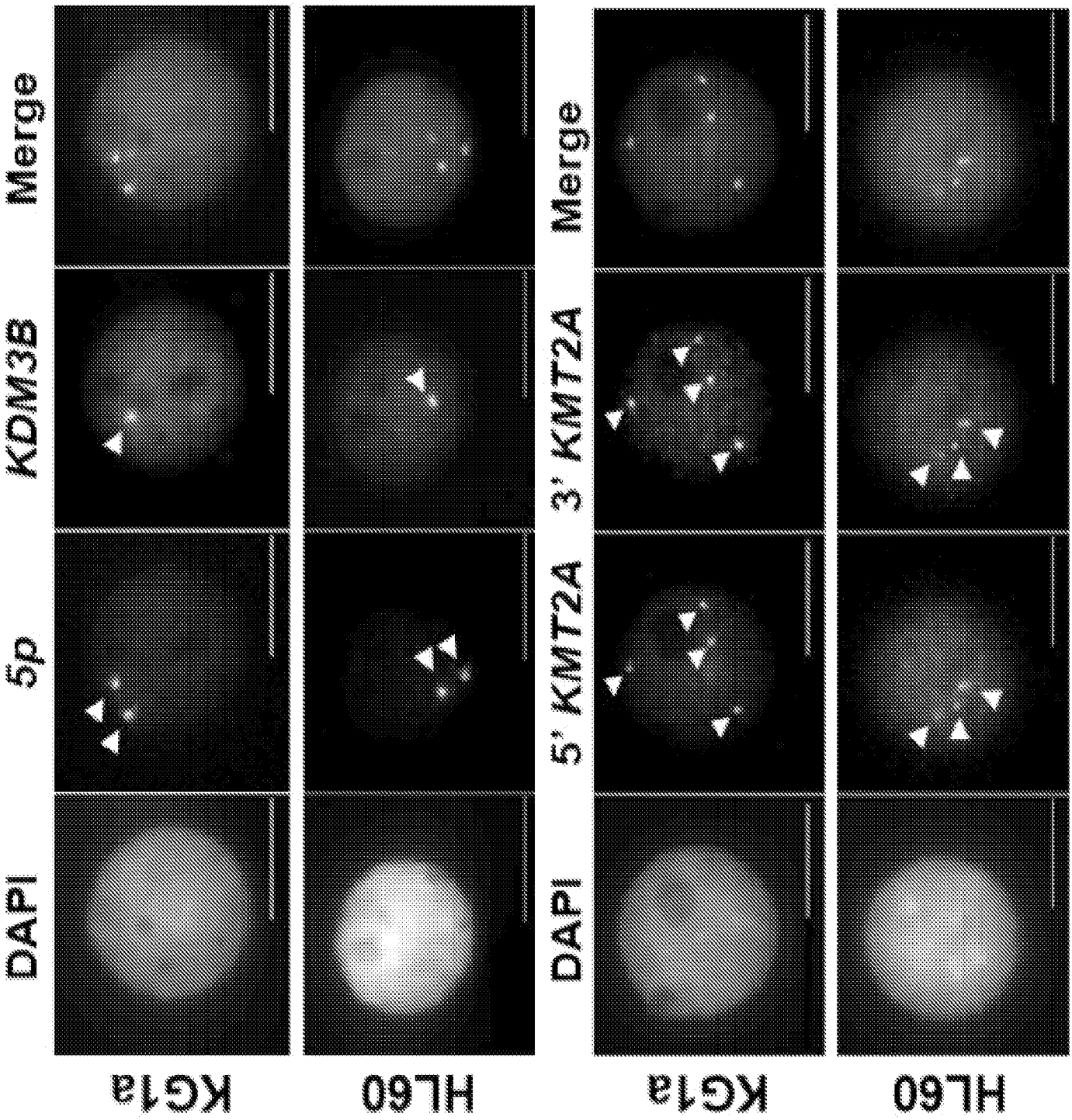

FIG. 1B

FIG. 1C

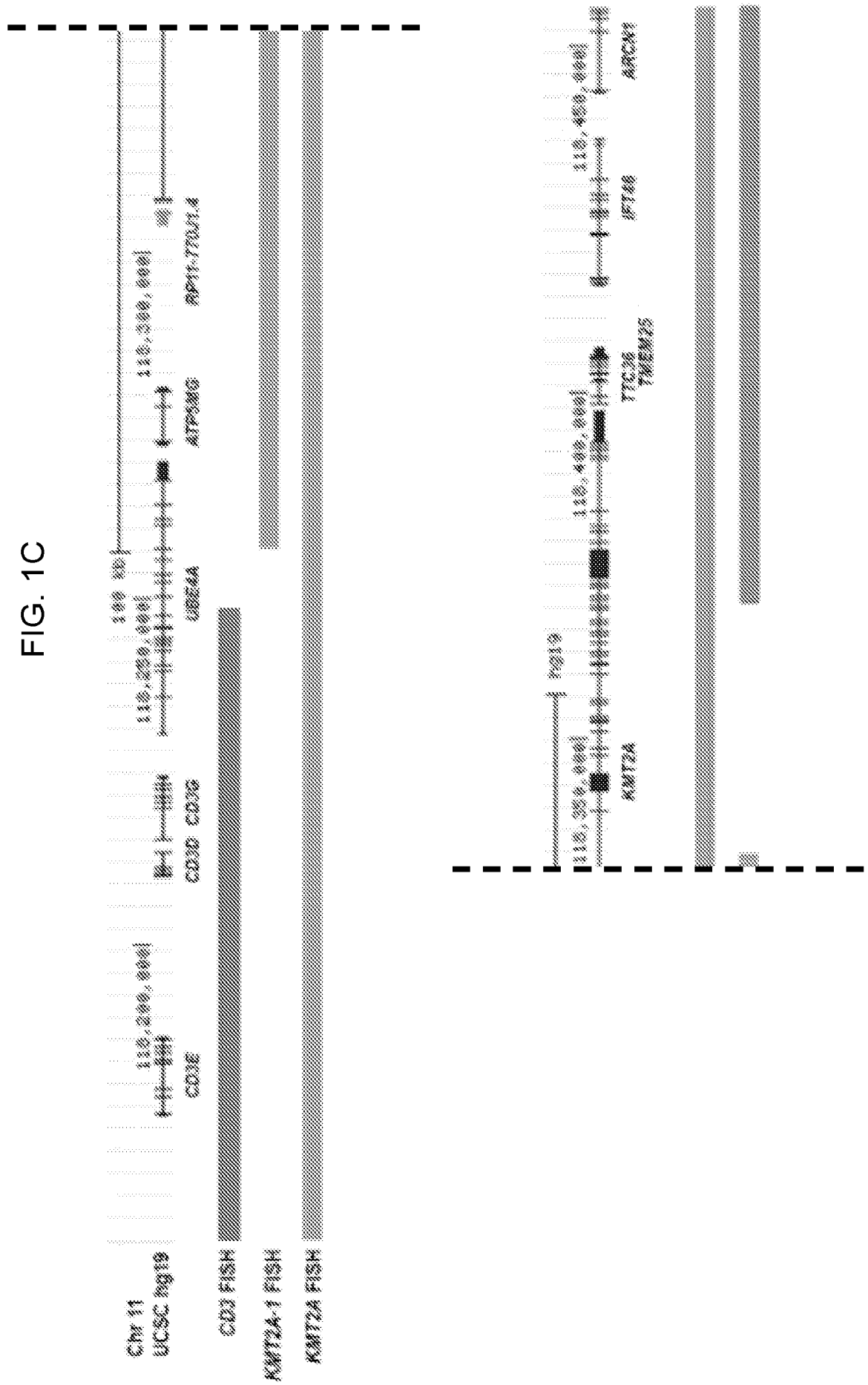
Chr 11
UCSC hg19
CD3E
CD3D
CD3G
UBE4A
ATP5MG
RP11-770J1.4
KMT2A-1 FISH
CD3 FISH
KMT2A FISH
KMT2A
hg19
TTC12
TMEM25
IFT46
ARCN1

FIG. 1D

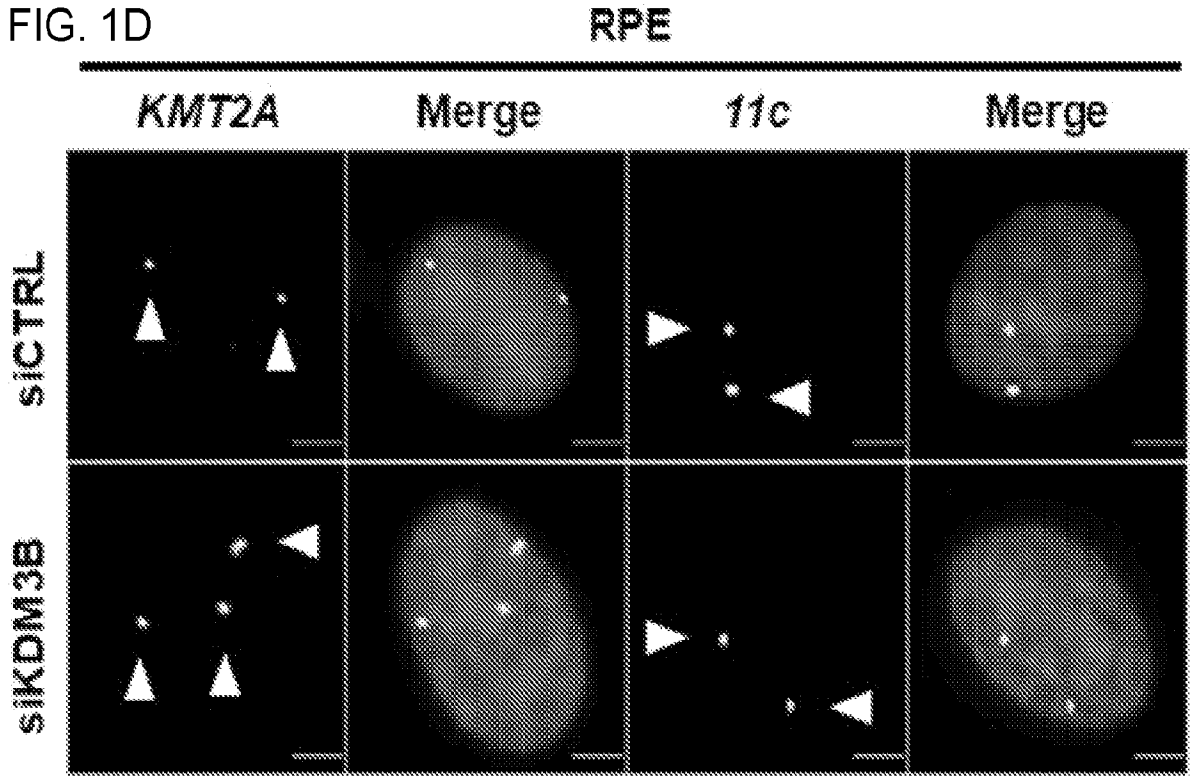
RPE
KMT2A
Merge
11c
Merge
siCTRL
siKDM3B

FIG. 1E

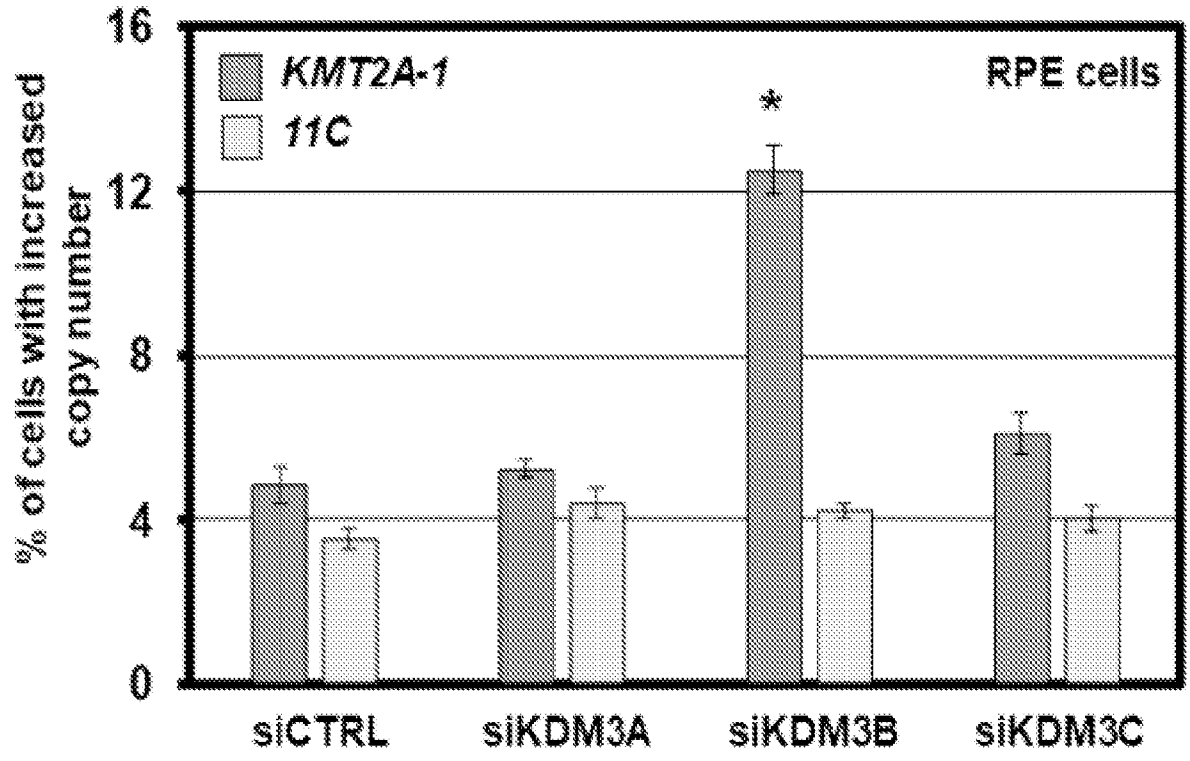
KMT2A-1
11C
RPE cells
% of cells with increased copy number
16
12
8
4
0
*
siCTRL
siKDM3A
siKDM3B
siKDM3C

FIG. 1F

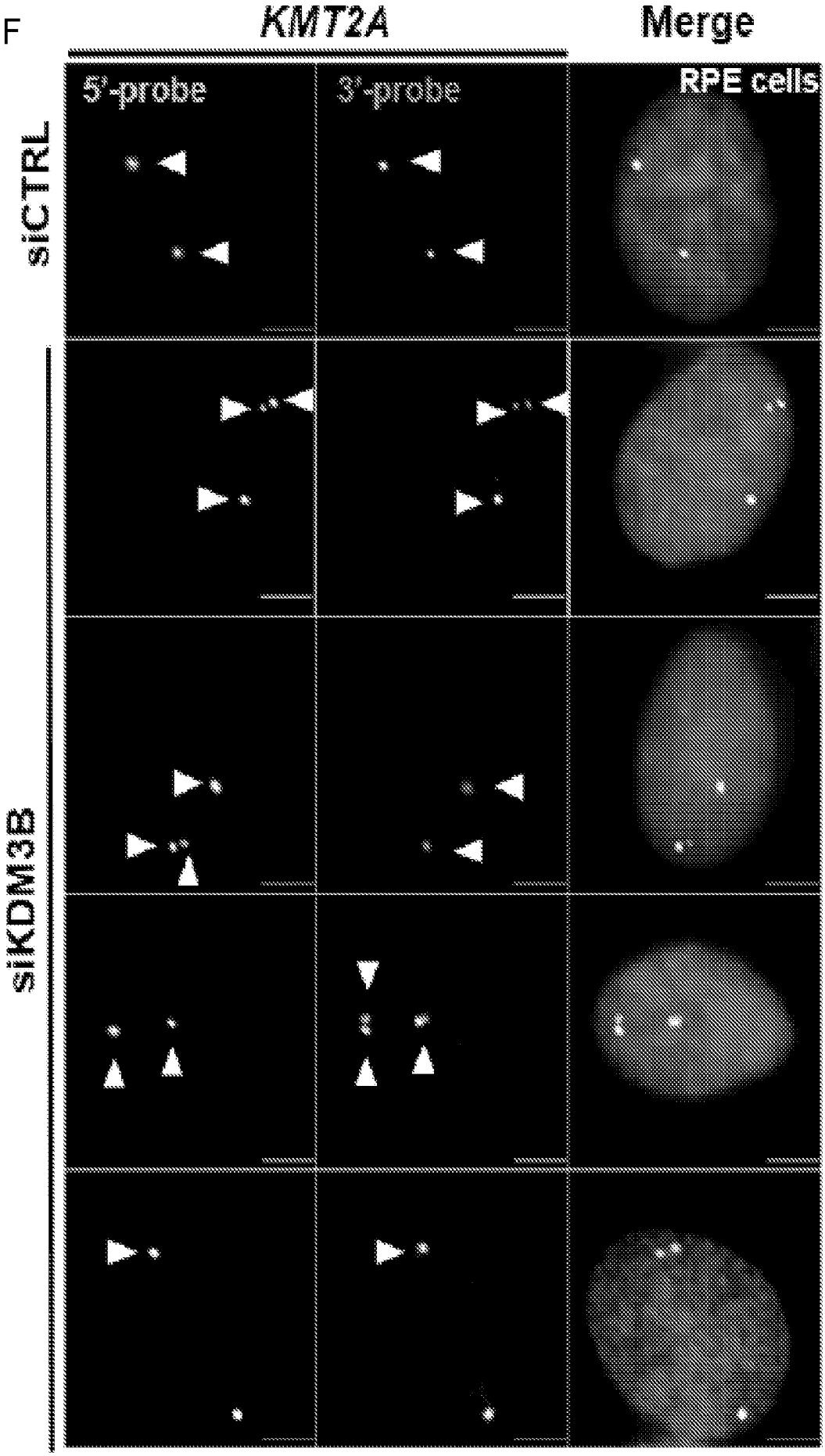

FIG. 1G

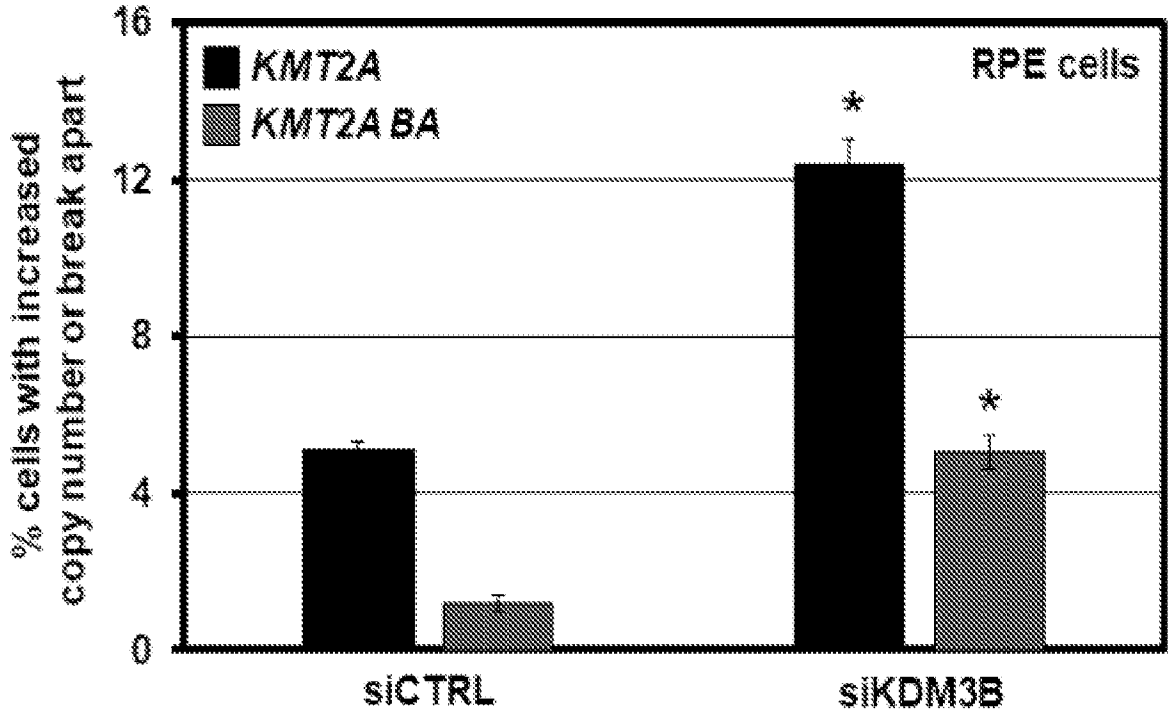
KMT2A
KMT2A BA
RPE cells
% cells with increased copy number or break apart
16
12
8
4
0
*
*
siCTRL
siKDM3B

FIG. 1H

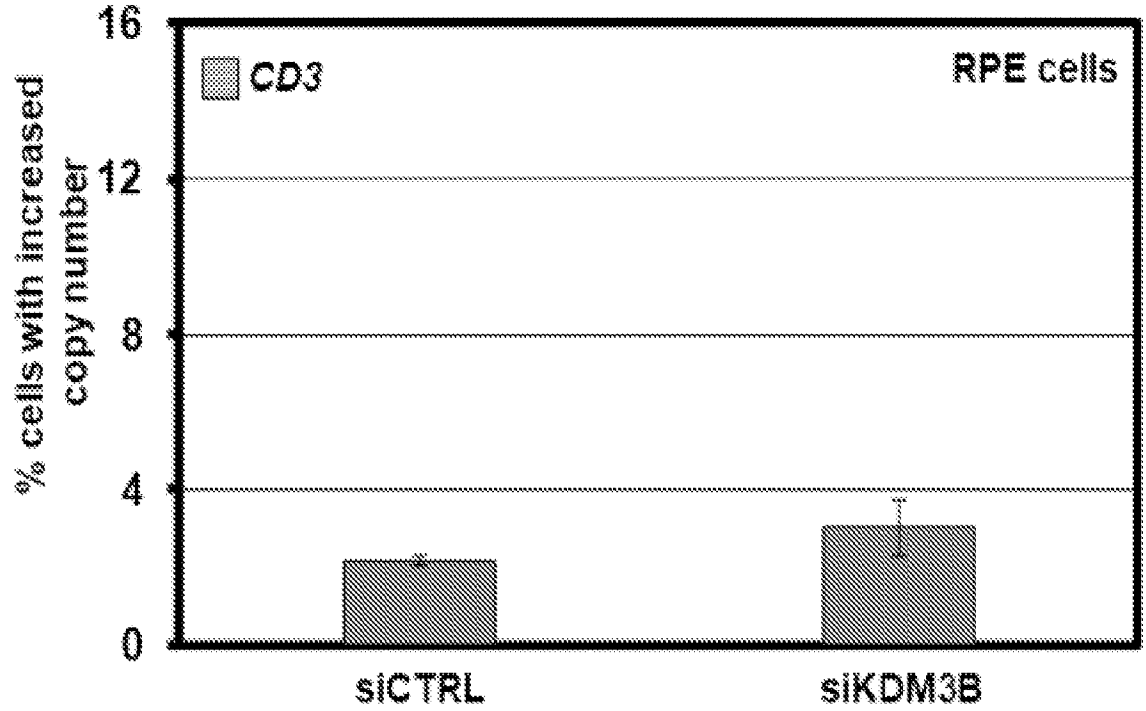
CD3
RPE cells
% cells with increased copy number
16
12
8
4
0
siCTRL
siKDM3B

FIG. 1I

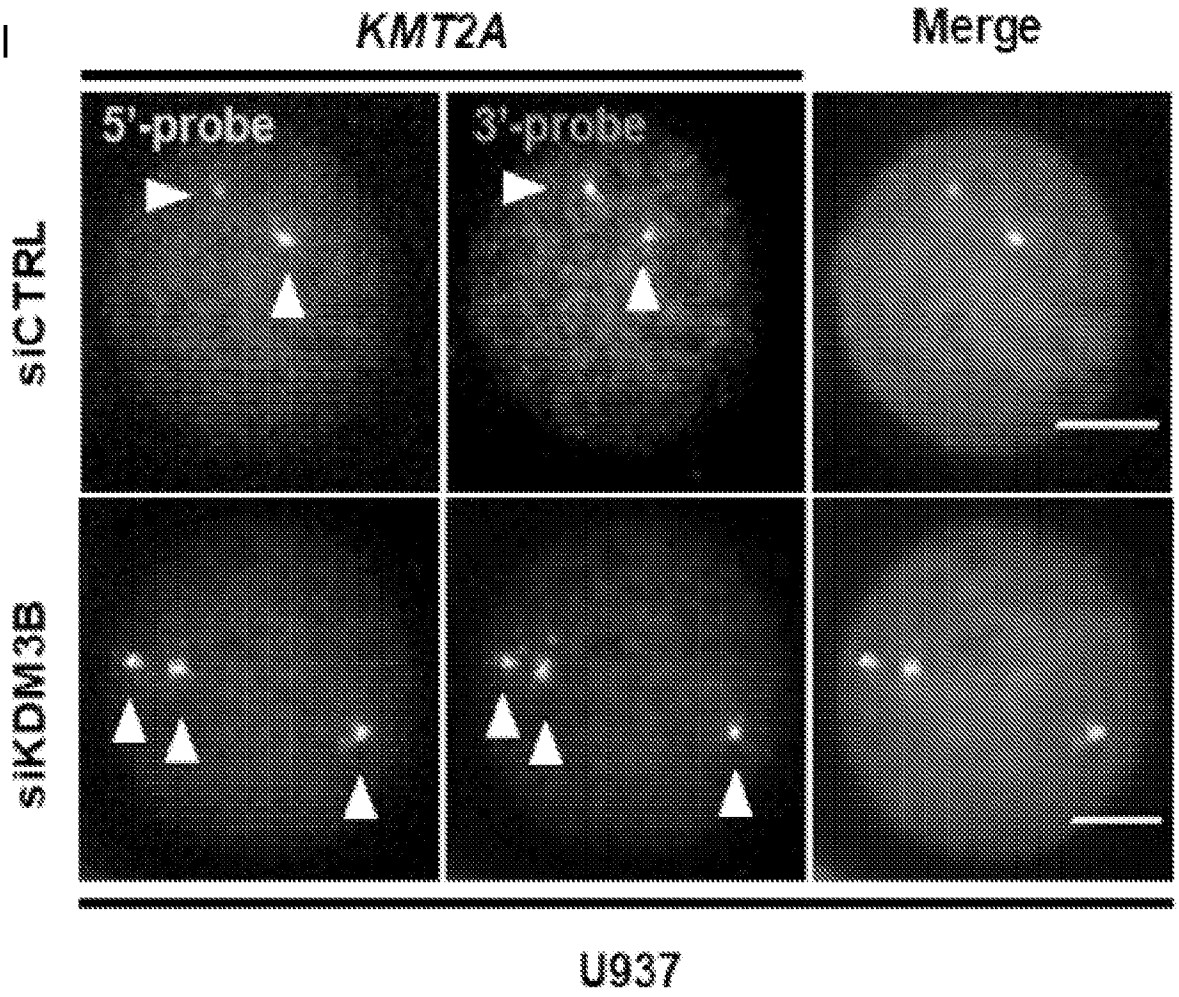
KMT2A
Merge
5'-probe
3'-probe
siCTRL
siKDM3B
U937

FIG. 1J

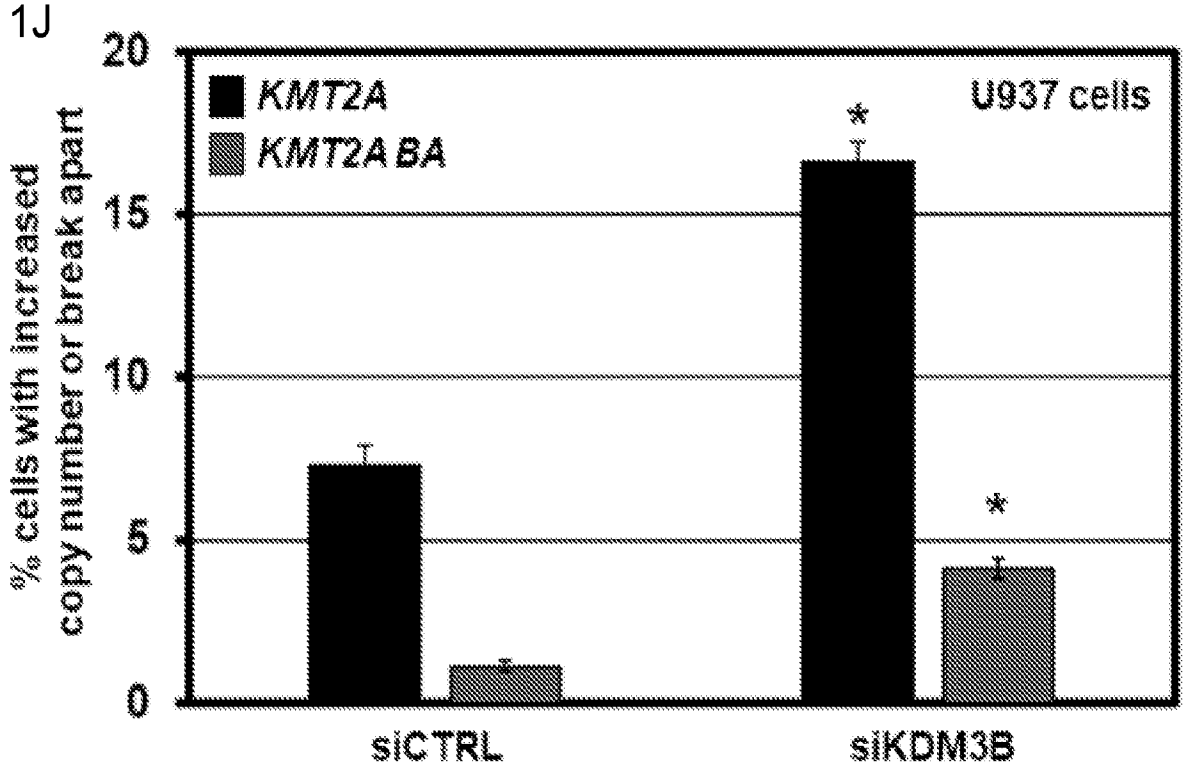
KMT2A
KMT2A BA
U937 cells
% cells with increased copy number or break apart
20
15
10
5
0
*
*
siCTRL
siKDM3B

FIG. 1K

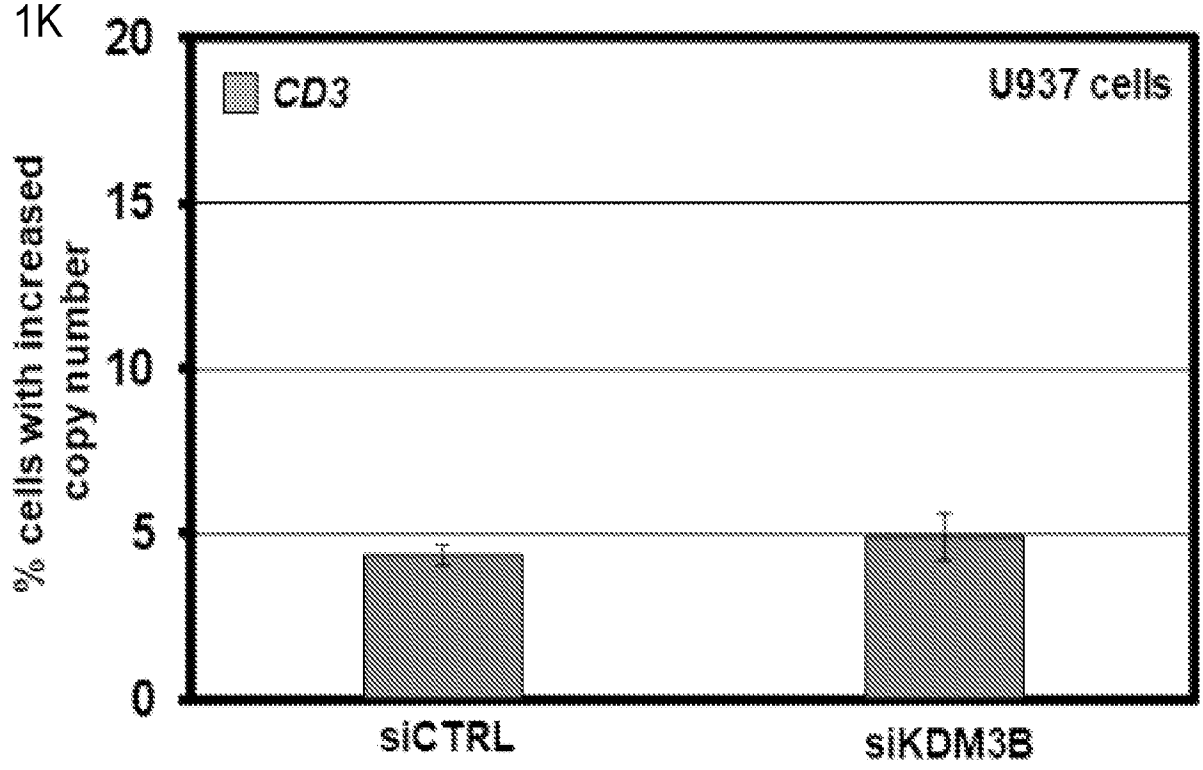
20
15
10
5
0
% cells with increased copy number
CD3
U937 cells
siCTRL
siKDM3B

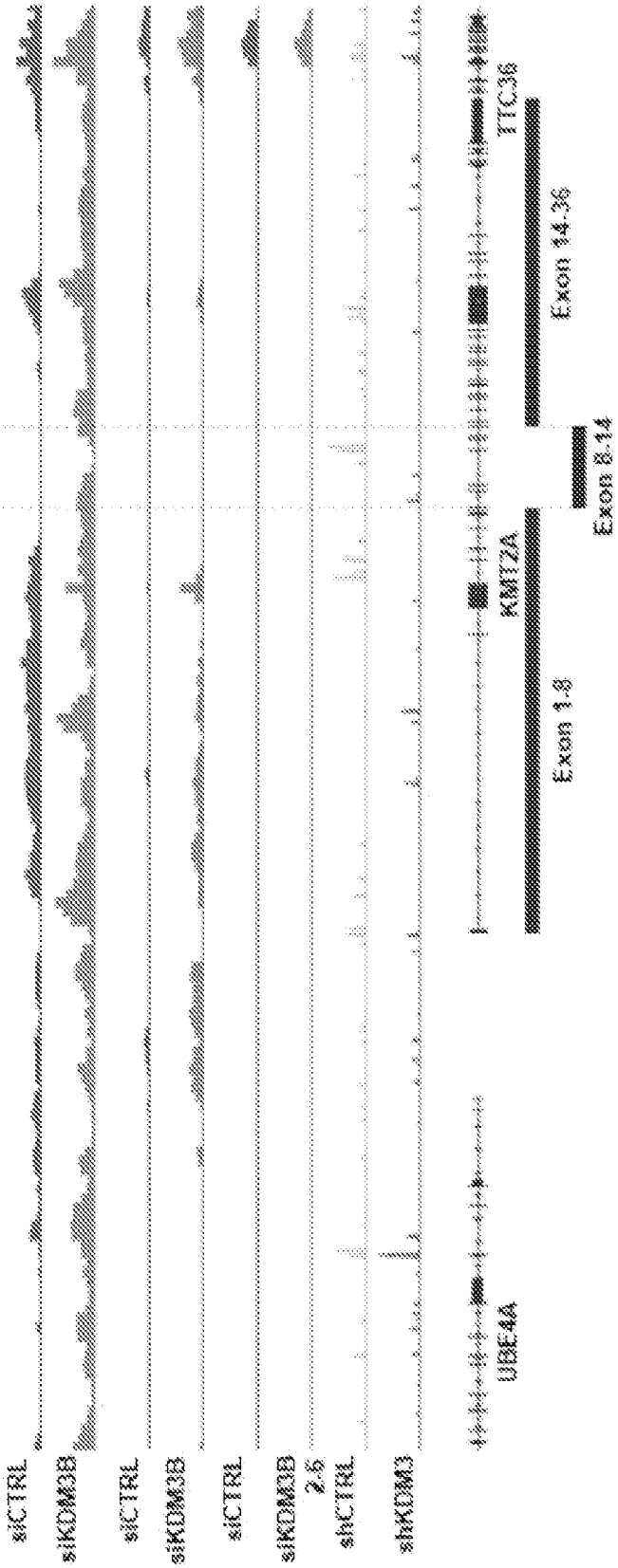
118.26
118.32
118.4
1-4
siCTRL
siKDM3B
siCTRL
siKDM3B
siCTRL
siKDM3B
2-5
shCTRL
shKDM3
H3K9me1
H3K9me2
H3K9me3
KDM3B
UBE4A
KMT2A
Exon 1-8
Exon 8-14
Exon 14-36
TTC36

FIG. 1L

FIG. 2A

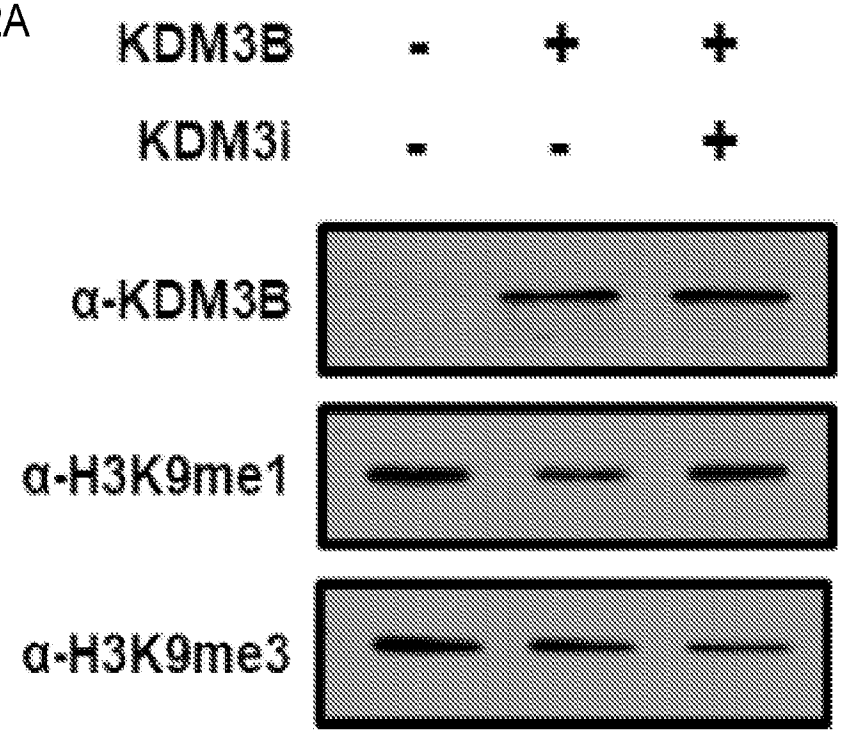
KDM3B - + +
KDM3i - - +
α-KDM3B
α-H3K9me1
α-H3K9me3

FIG. 2B

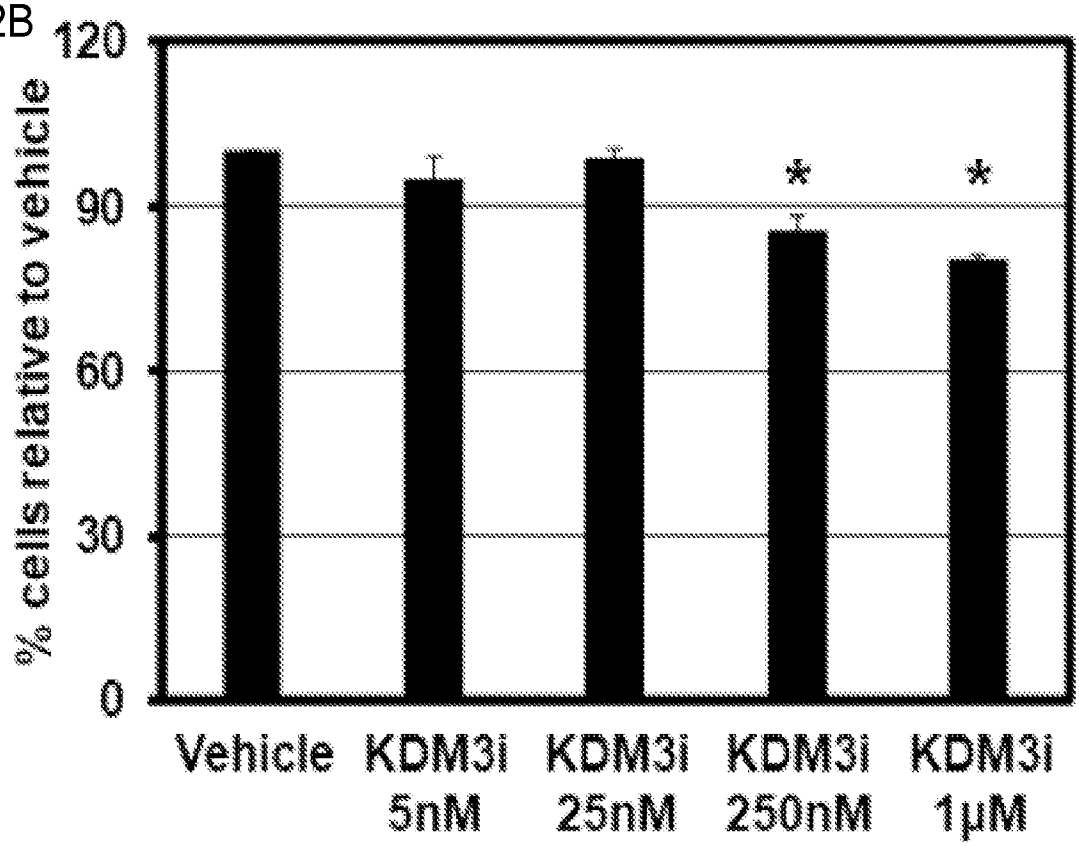
% cells relative to vehicle
120
90
60
30
0
*
*
Vehicle
KDM3i 5nM
KDM3i 25nM
KDM3i 250nM
KDM3i 1μM

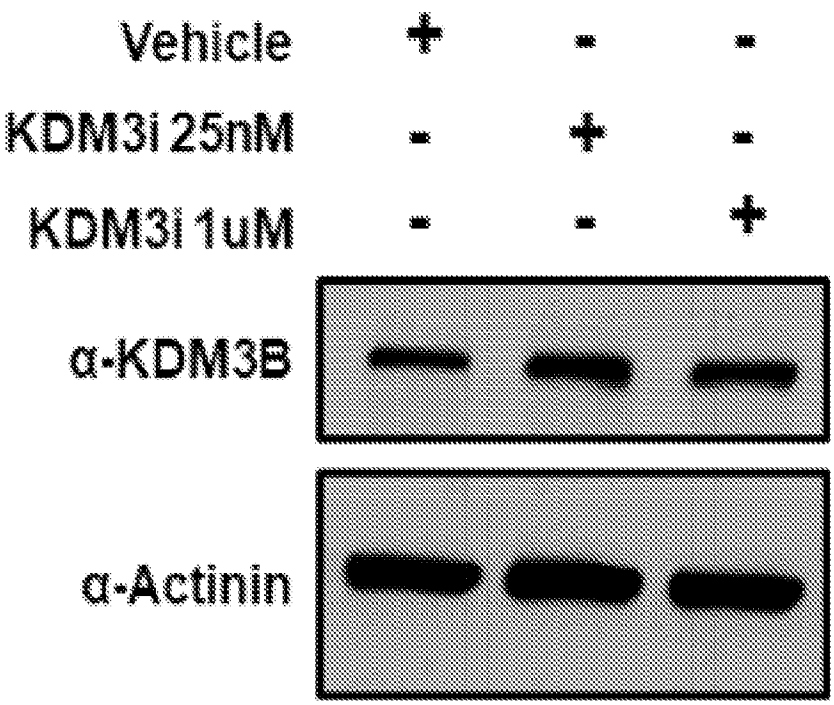
Vehicle + - -
KDM3i 25nM - + -
KDM3i 1uM - - +
α-KDM3B
α-Actinin

FIG. 2C

FIG. 2D

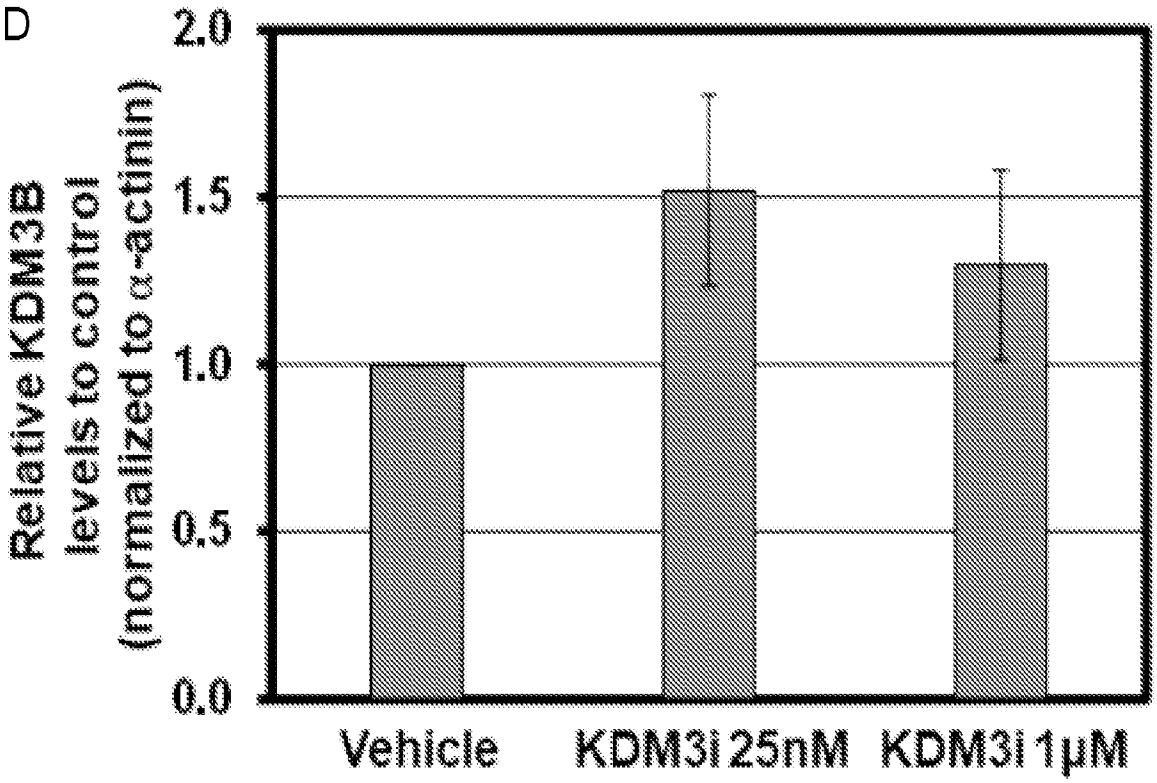
Relative KDM3B levels to control (normalized to α-actinin)
2.0
1.5
1.0
0.5
0.0
Vehicle
KDM3i 25nM
KDM3i 1μM

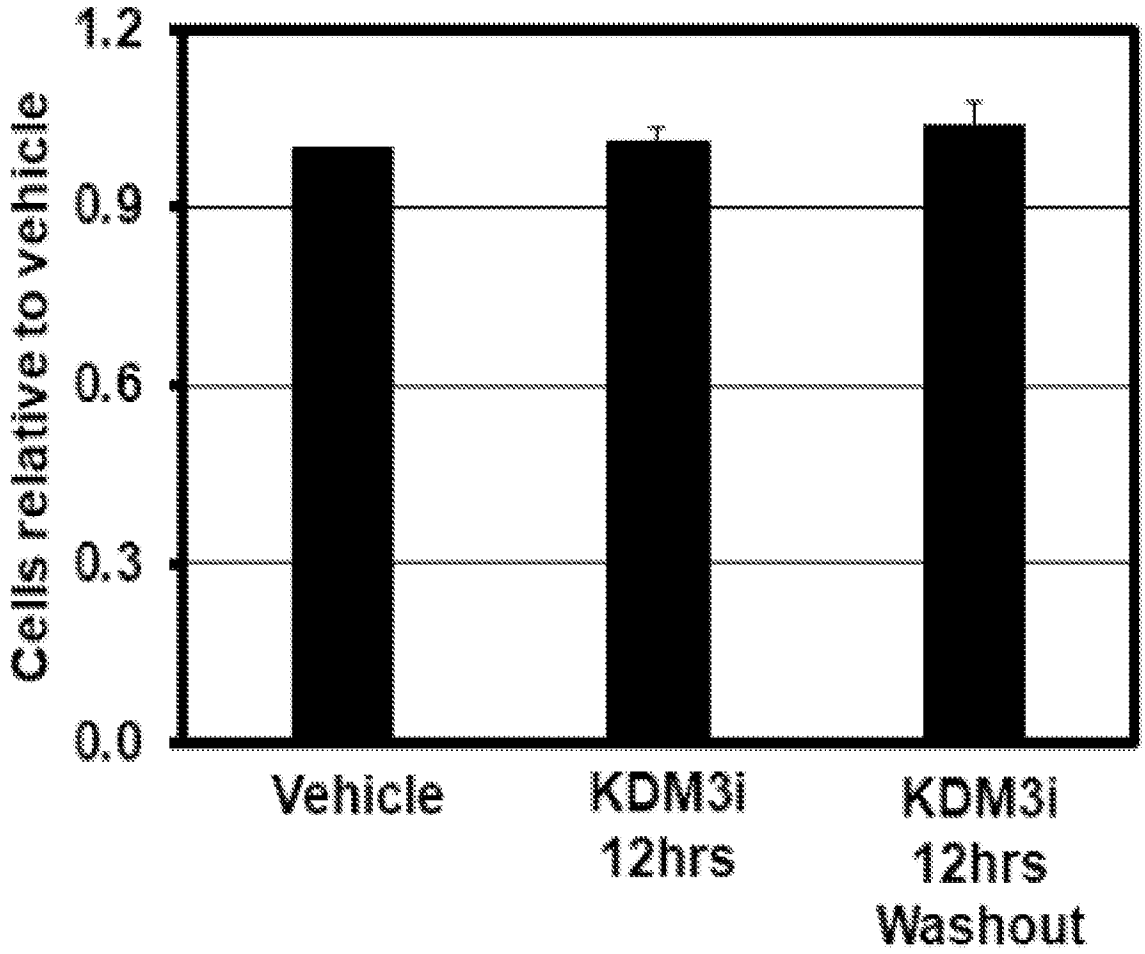
Cells relative to vehicle
1.2
0.9
0.6
0.3
0.0
Vehicle
KDM3i 12hrs
KDM3i 12hrs Washout

FIG. 2E

FIG. 2F

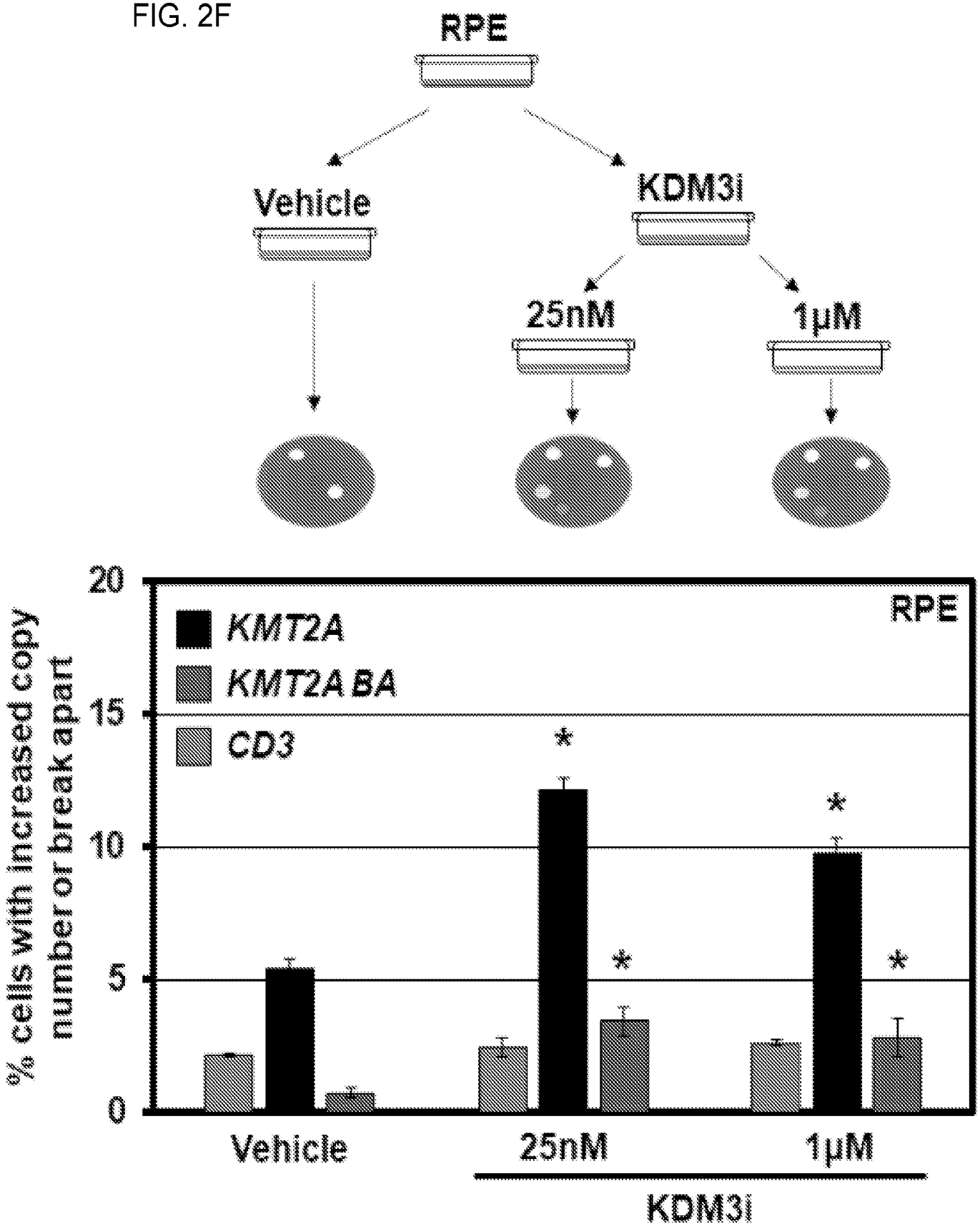
RPE
Vehicle
KDM3i
25nM
1μM
RPE
KMT2A
KMT2A BA
CD3
% cells with increased copy number or break apart
20
15
10
5
0
*
Vehicle
25nM
1μM
KDM3i

FIG. 2G

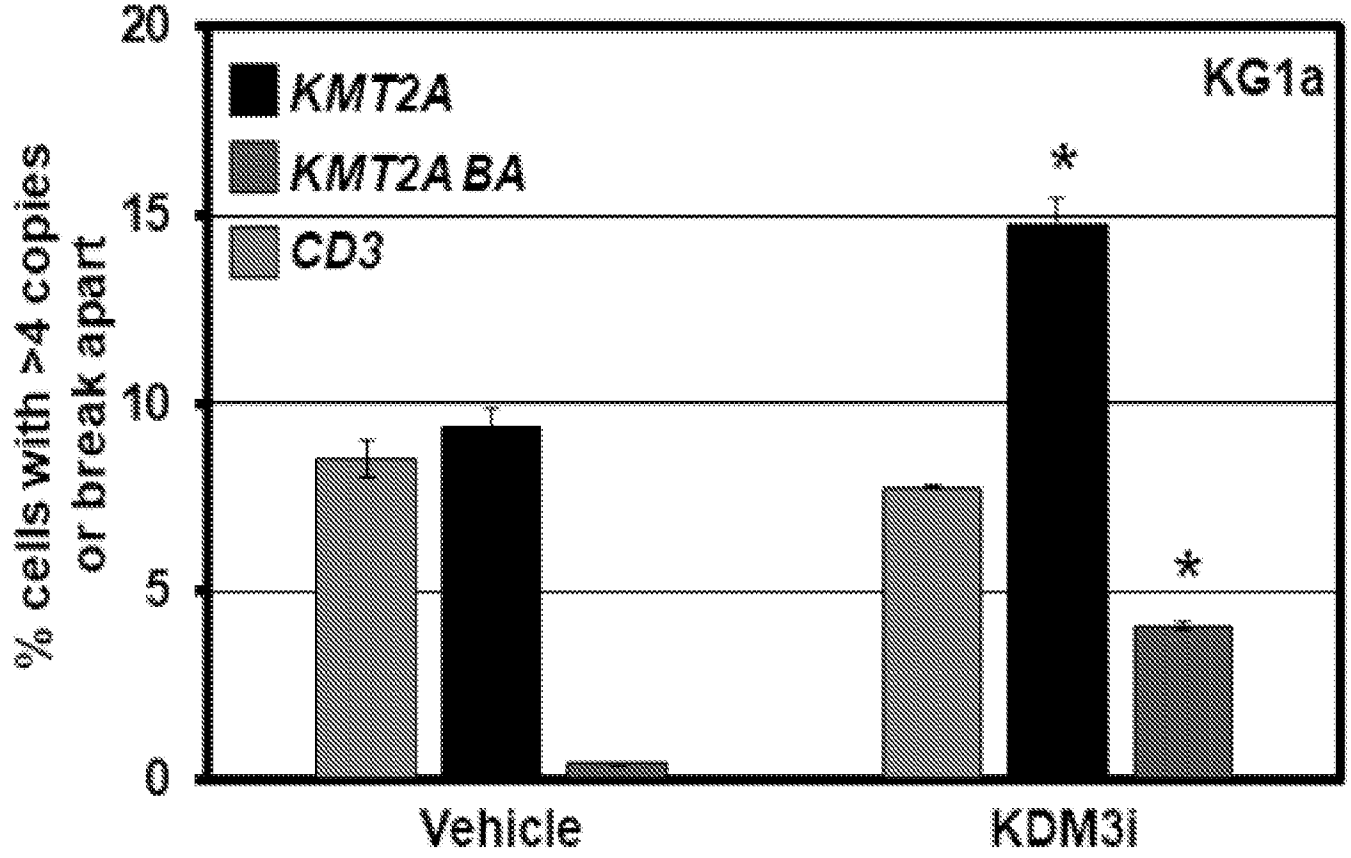
KMT2A
KMT2A BA
CD3
KG1a
% cells with >4 copies or break apart
20
15
10
5
0
*
*
Vehicle
KDM3i

FIG. 2H

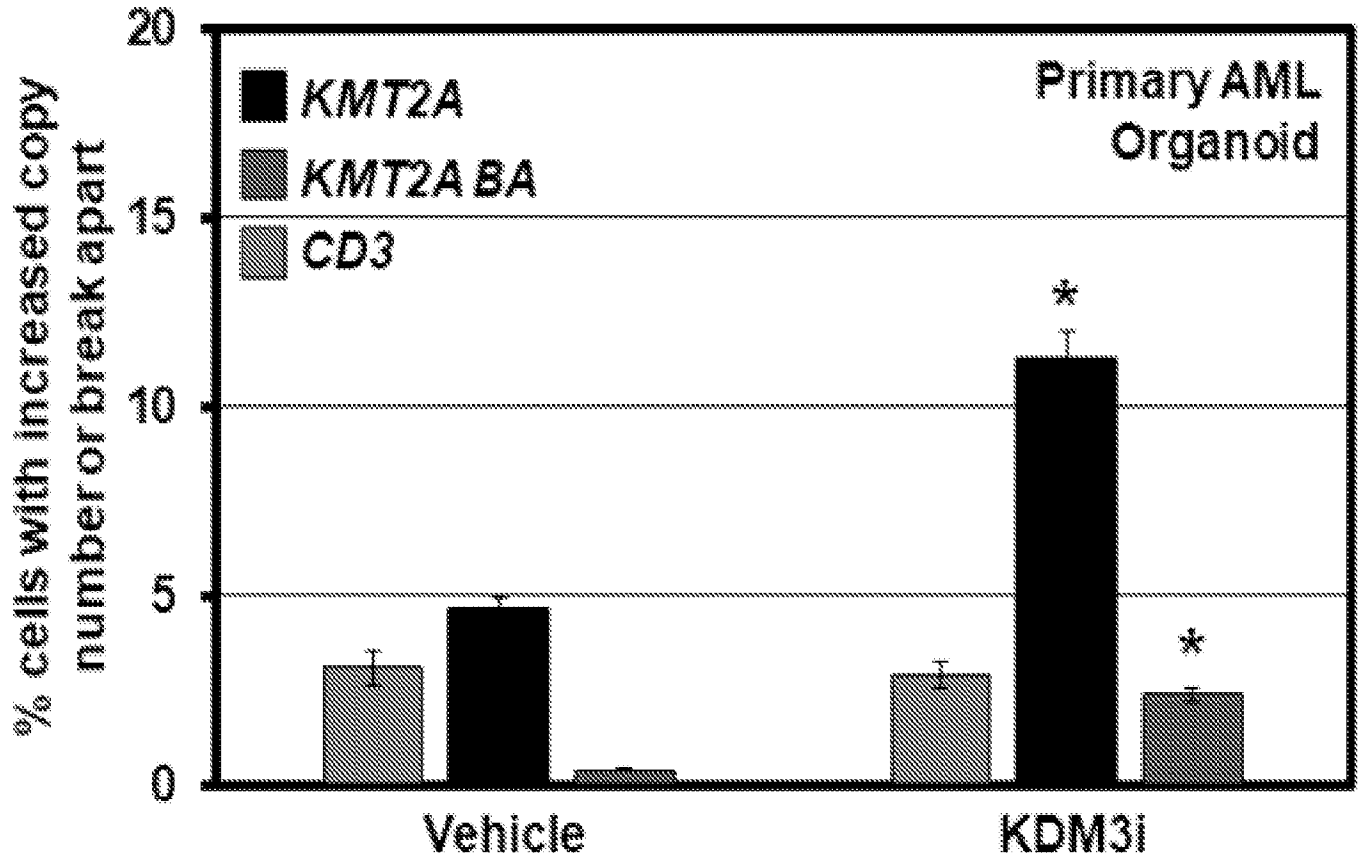
KMT2A
KMT2A BA
CD3
Primary AML Organoid
% cells with increased copy number or break apart
20
15
10
5
0
*
*
Vehicle
KDM3i

FIG. 2I

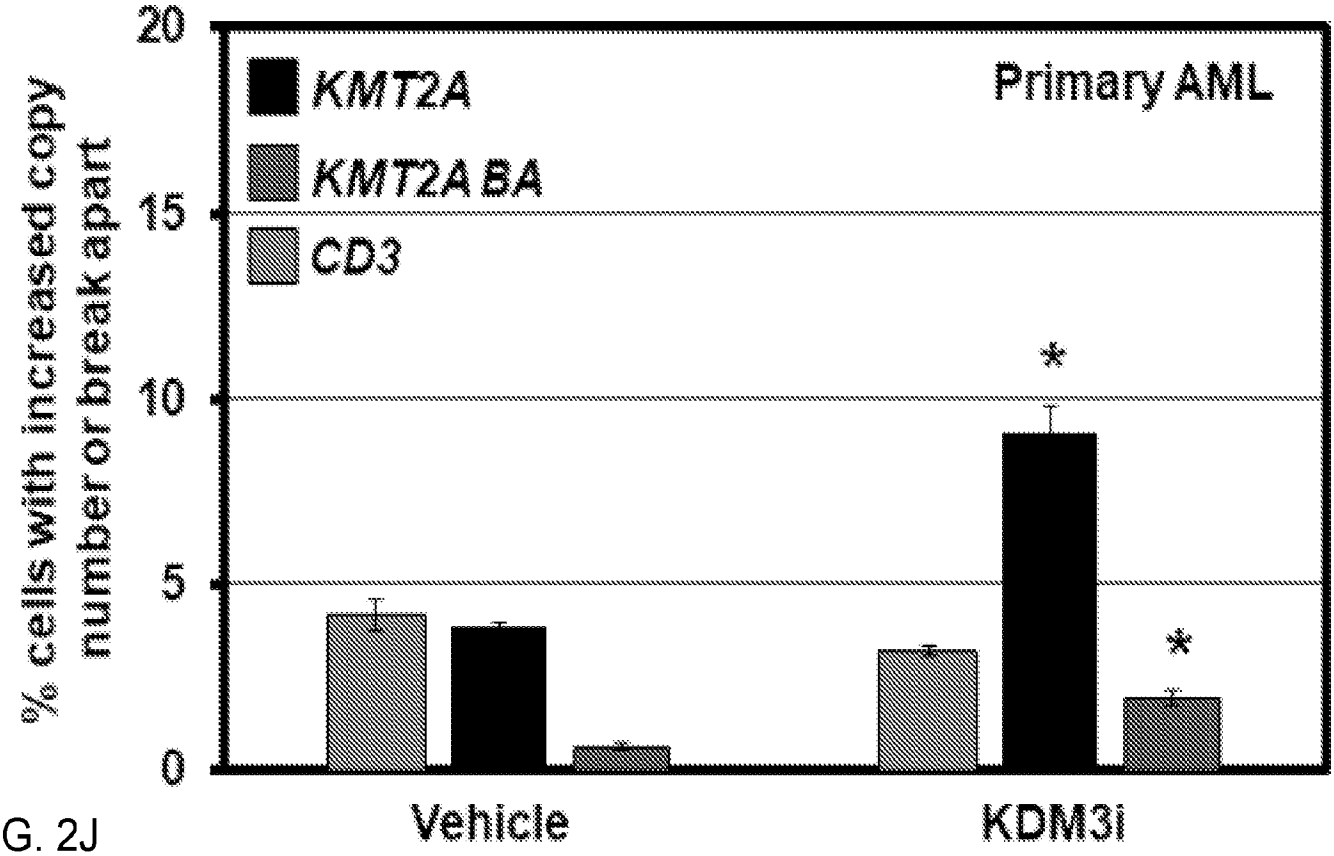
20
15
10
5
0
% cells with increased copy number or break apart
KMT2A
KMT2A BA
CD3
Primary AML
*
*
Vehicle
KDM3i

FIG. 2J

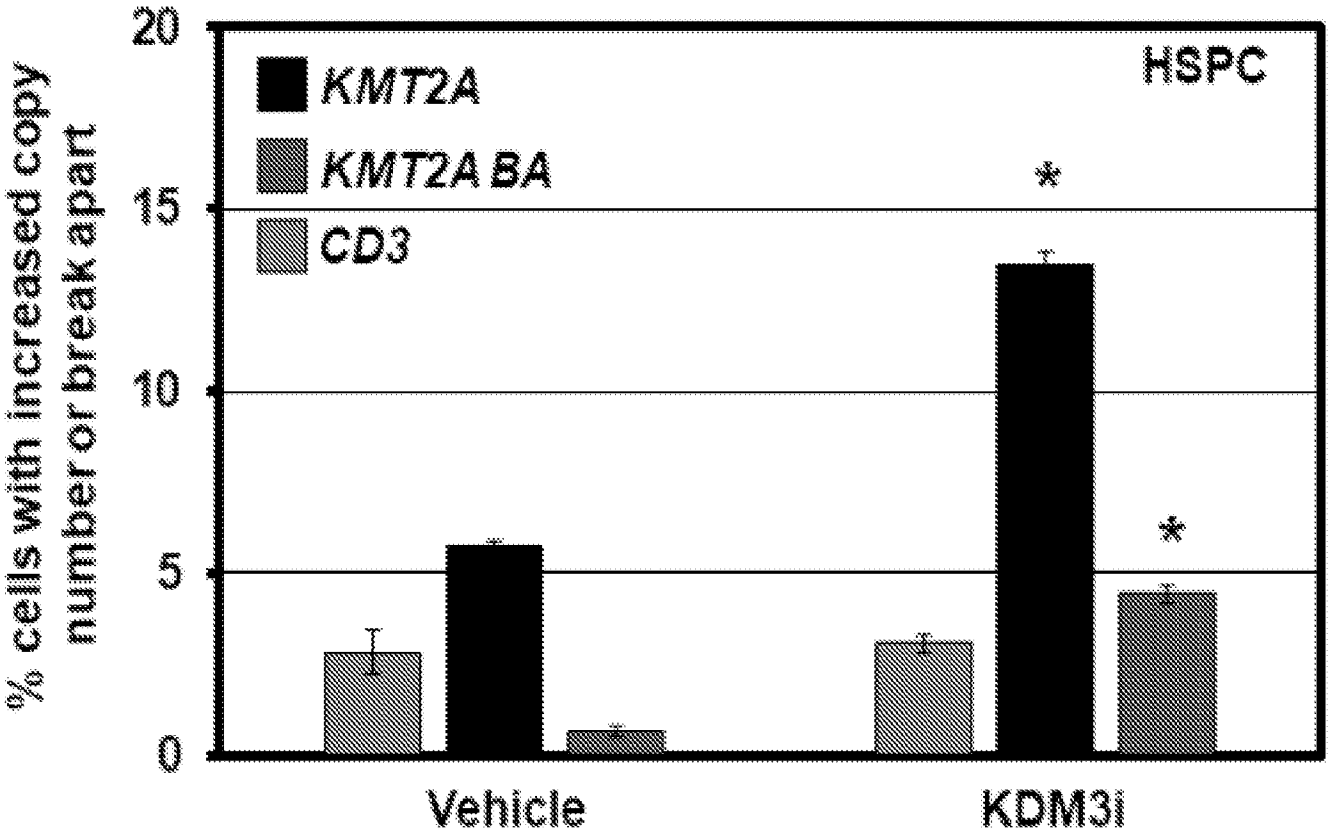
20
15
10
5
0
% cells with increased copy number or break apart
KMT2A
KMT2A BA
CD3
HSPC
*
*
Vehicle
KDM3i

FIG. 2K

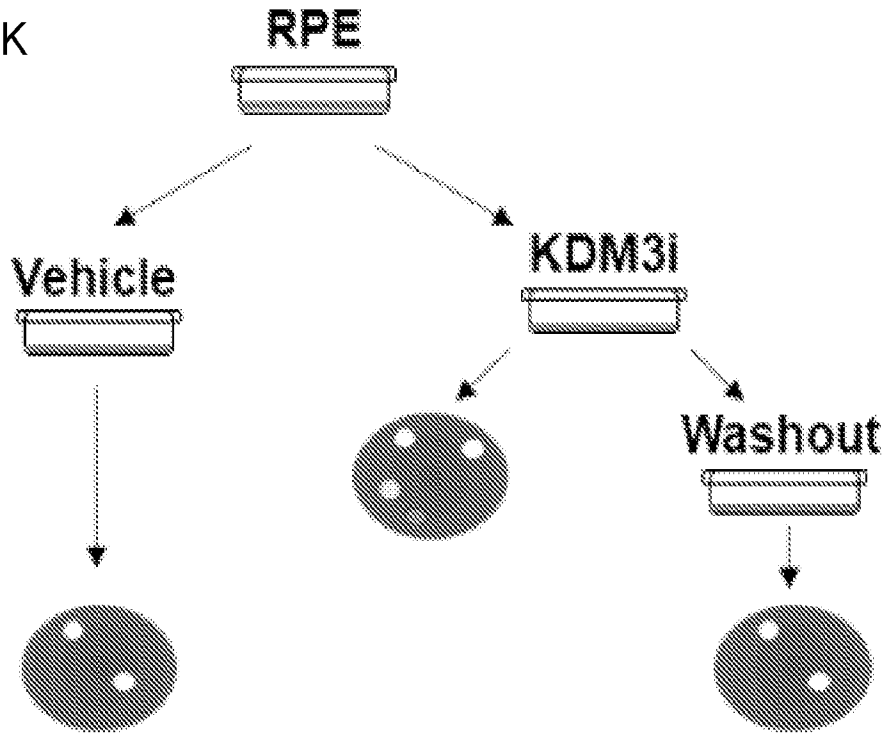
RPE
Vehicle
KDM3i
Washout

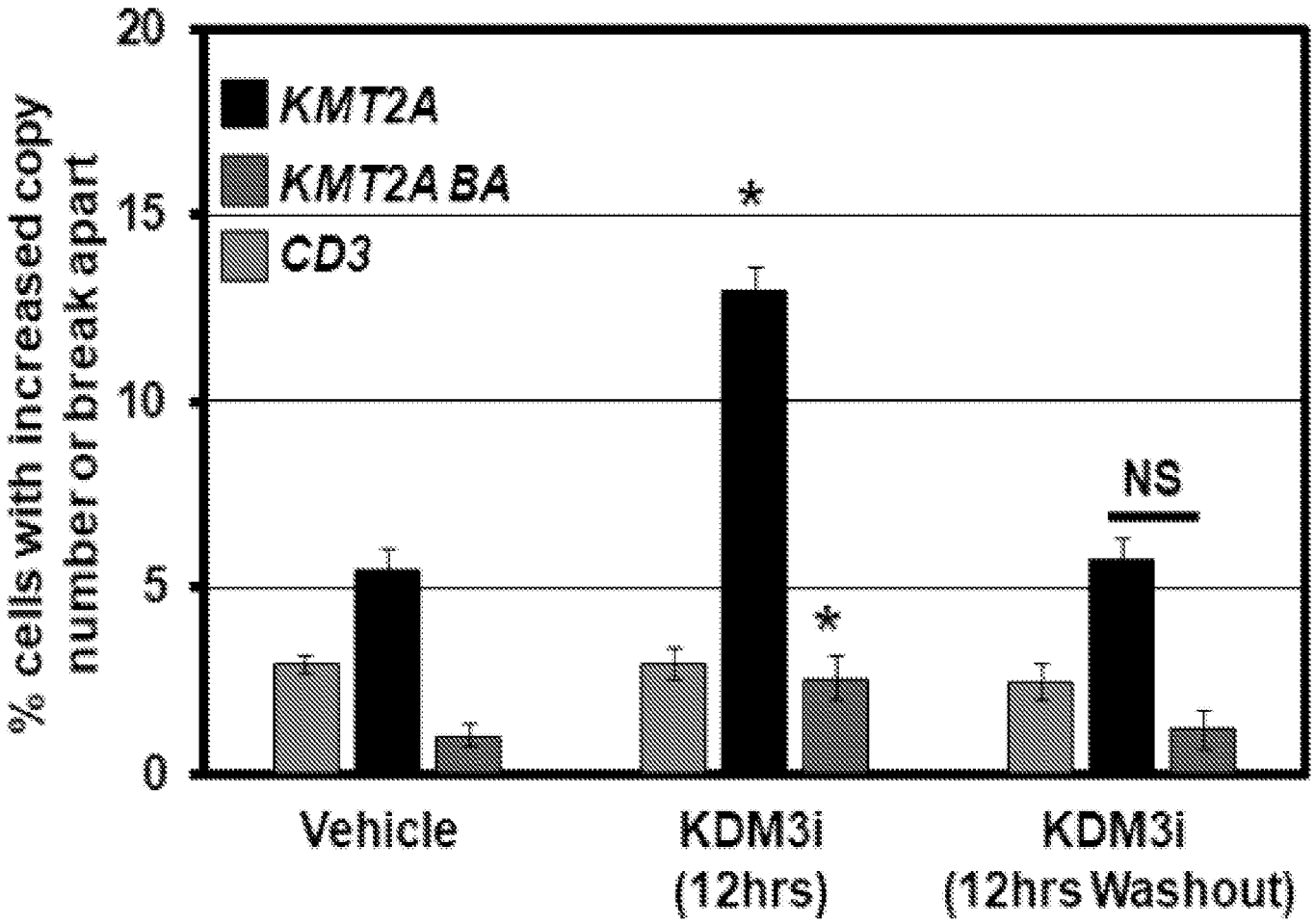
20
15
10
5
0
KMT2A
KMT2A BA
CD3
% cells with increased copy number or break apart
*
*
NS
Vehicle
KDM3i (12hrs)
KDM3i (12hrs Washout)

FIG. 3A

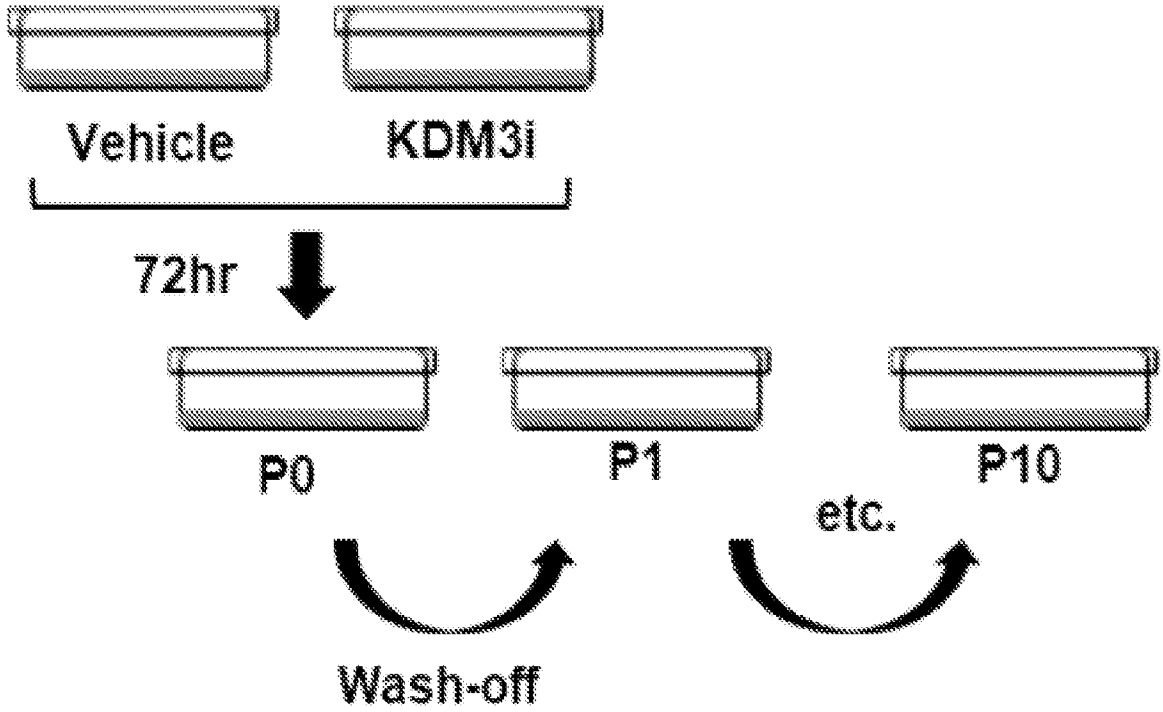

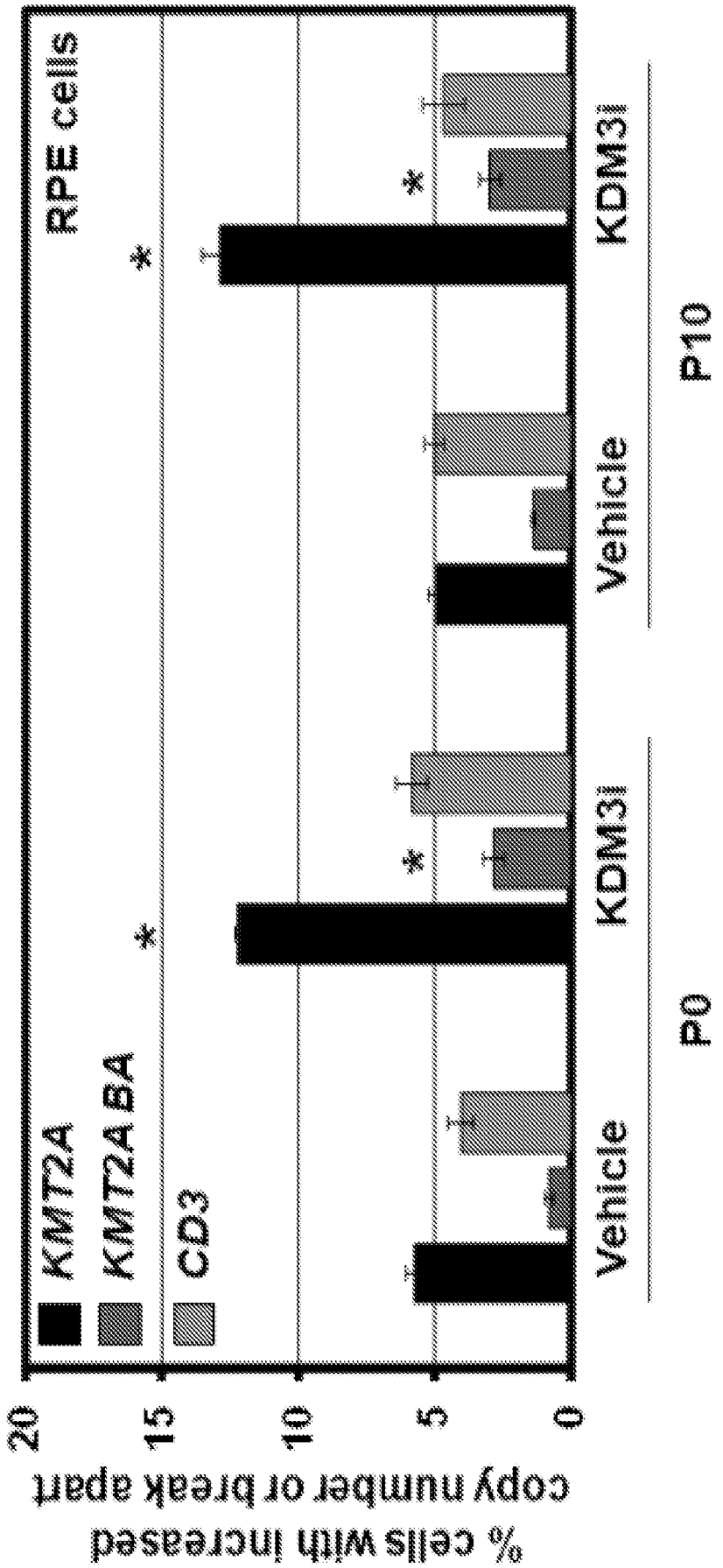
RPE cells
KMT2A
KMT2A BA
CD3
% cells with increased copy number or break apart
20
15
10
5
0
*
*
*
*
Vehicle
KDM3i
Vehicle
KDM3i
P0
P10

FIG. 3B

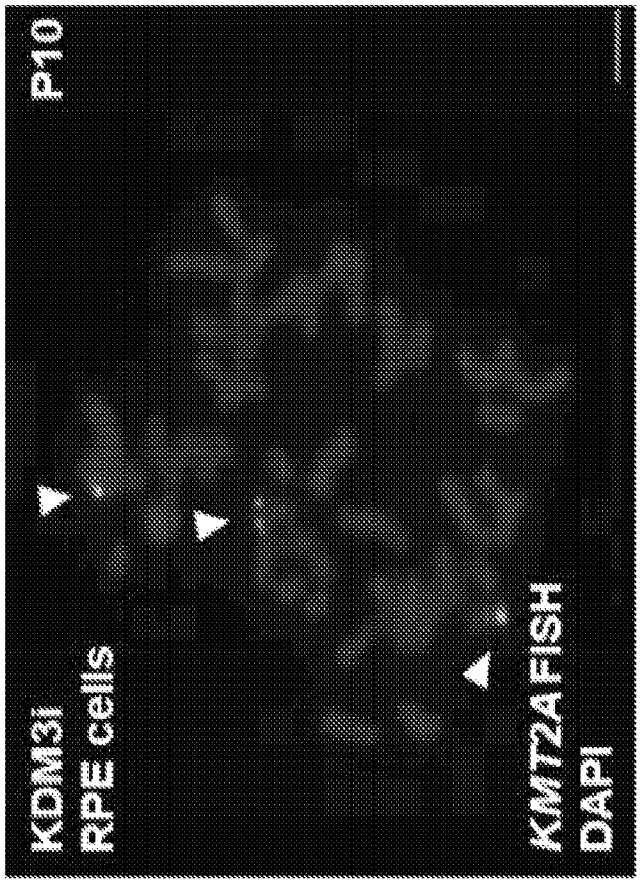
P10
KDM3i
RPE cells
KMT2A FISH
DAPI

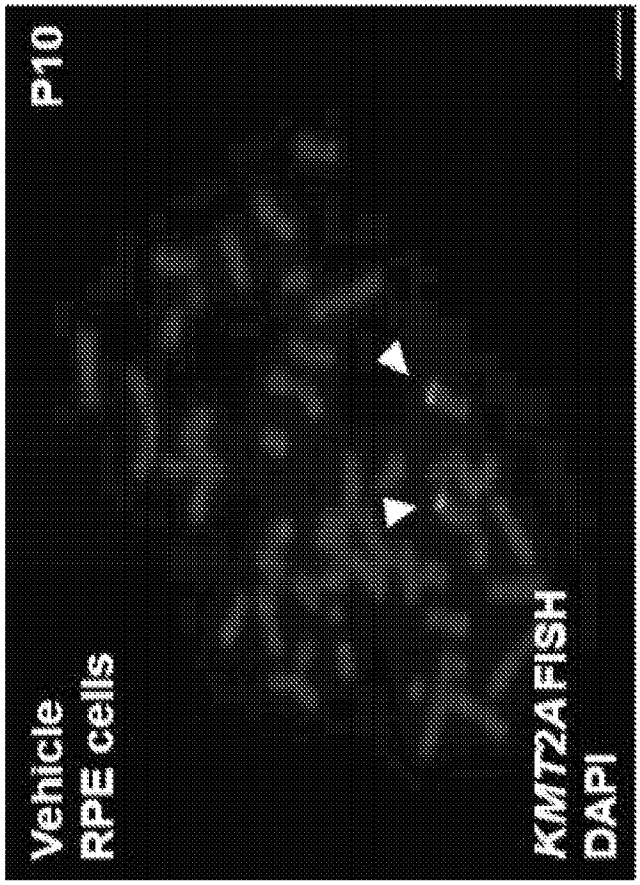
P10
Vehicle
RPE cells
KMT2A FISH
DAPI

FIG. 3C

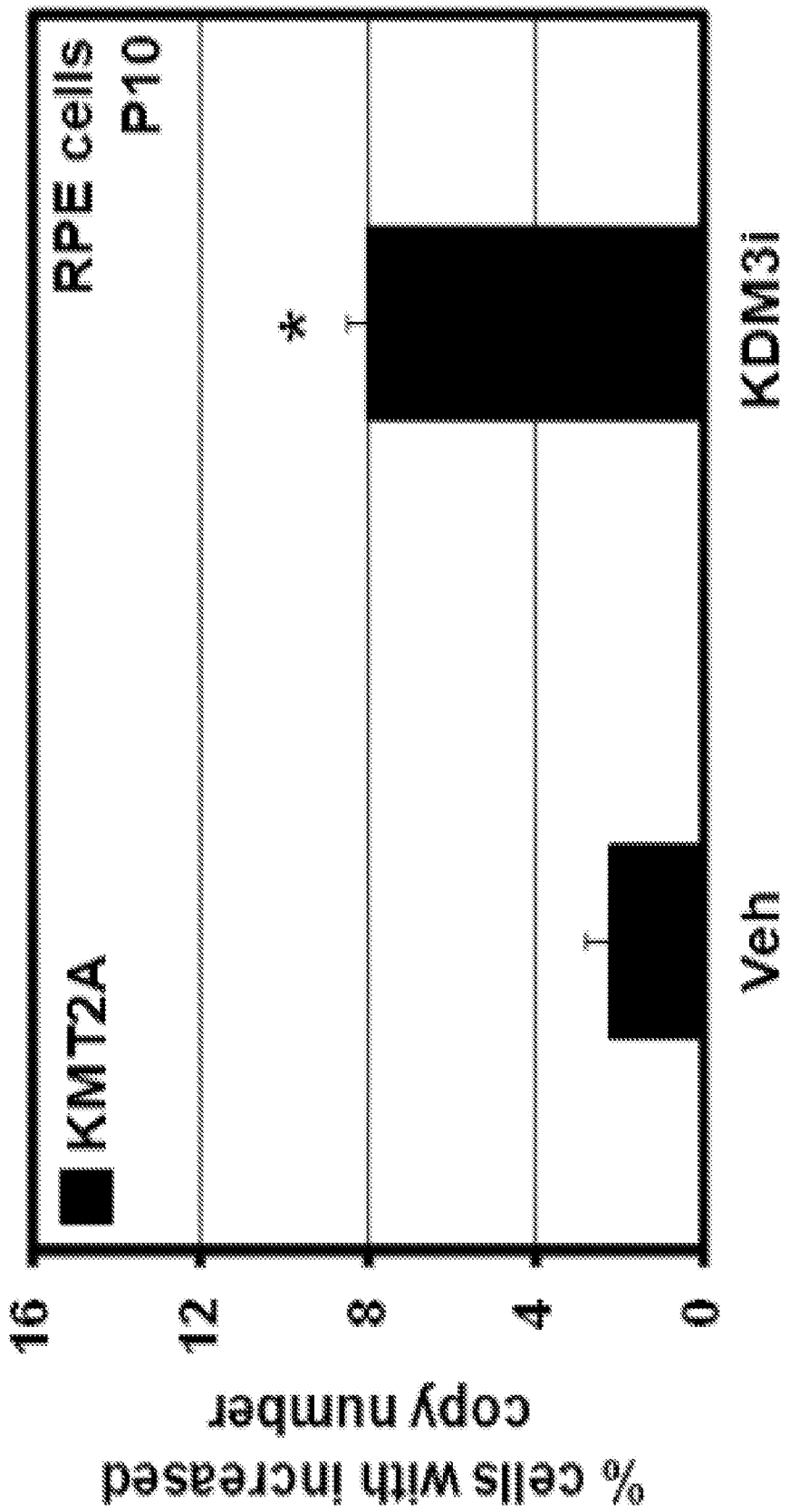
RPE cells
P10
KMT2A
KDM3i
Veh
*
16
12
8
4
0
% cells with increased copy number

FIG. 3D

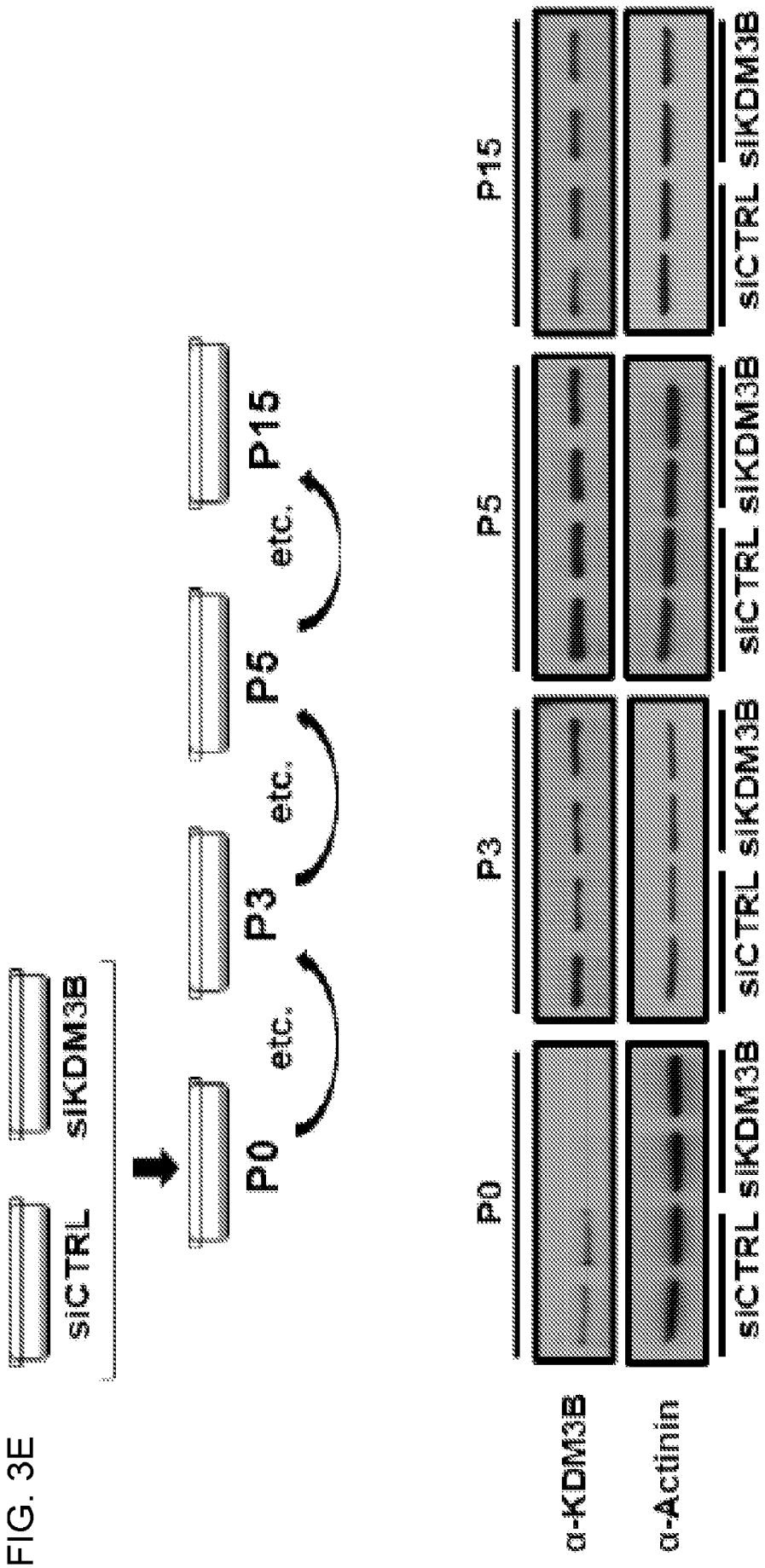
siCTRL
siKDM3B
P0
etc.
P3
etc.
P5
etc.
P15
P0
P3
P5
P15
siCTRL siKDM3B
siCTRL siKDM3B
siCTRL siKDM3B
siCTRL siKDM3B
α-KDM3B
α-Actinin

FIG. 3E

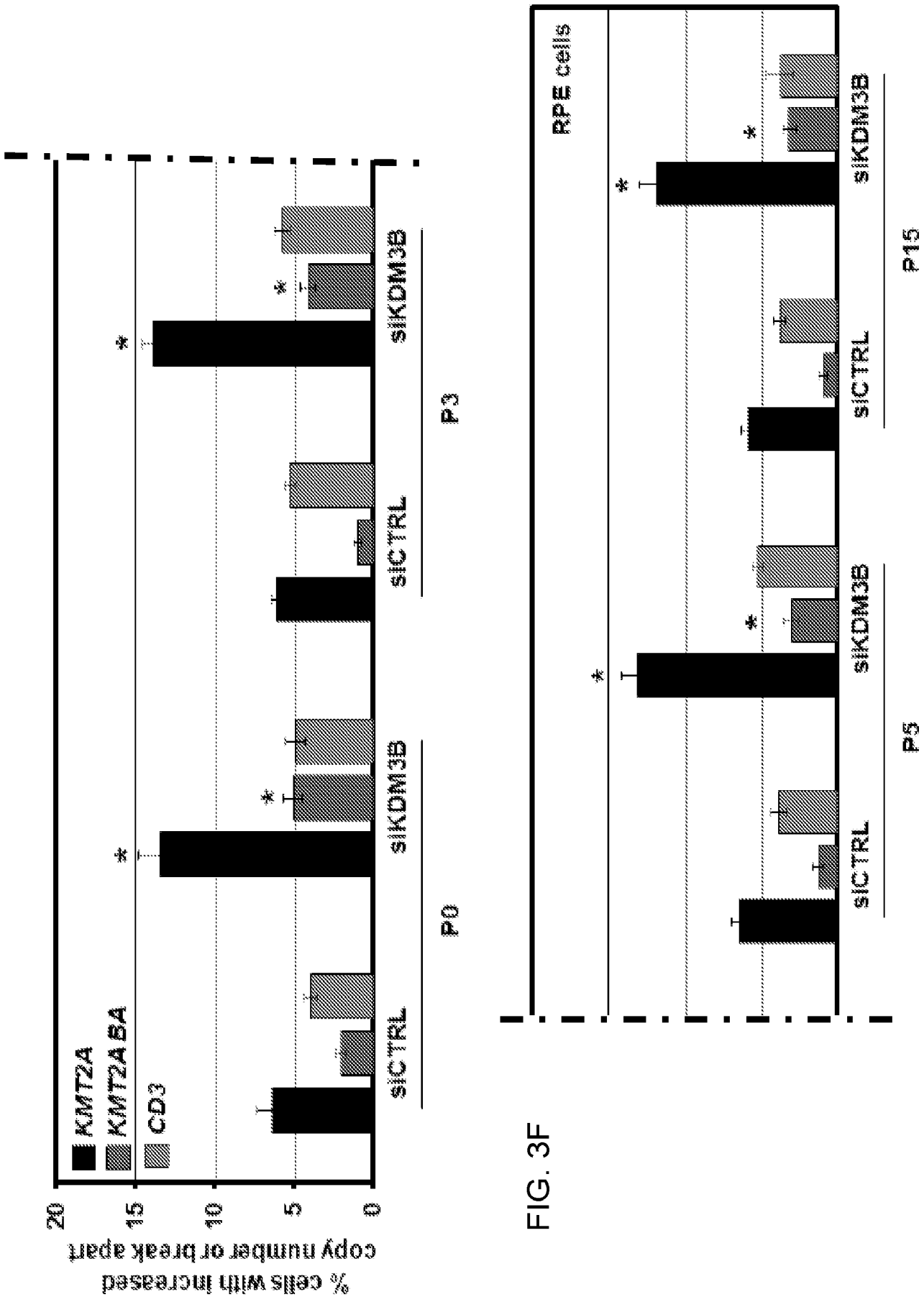
RPE cells
% cells with increased copy number or break apart
20
15
10
5
0
KMT2A
KMT2A BA
CD3
siCTRL
siKDM3B
P0
P3
P5
P15

FIG. 3F

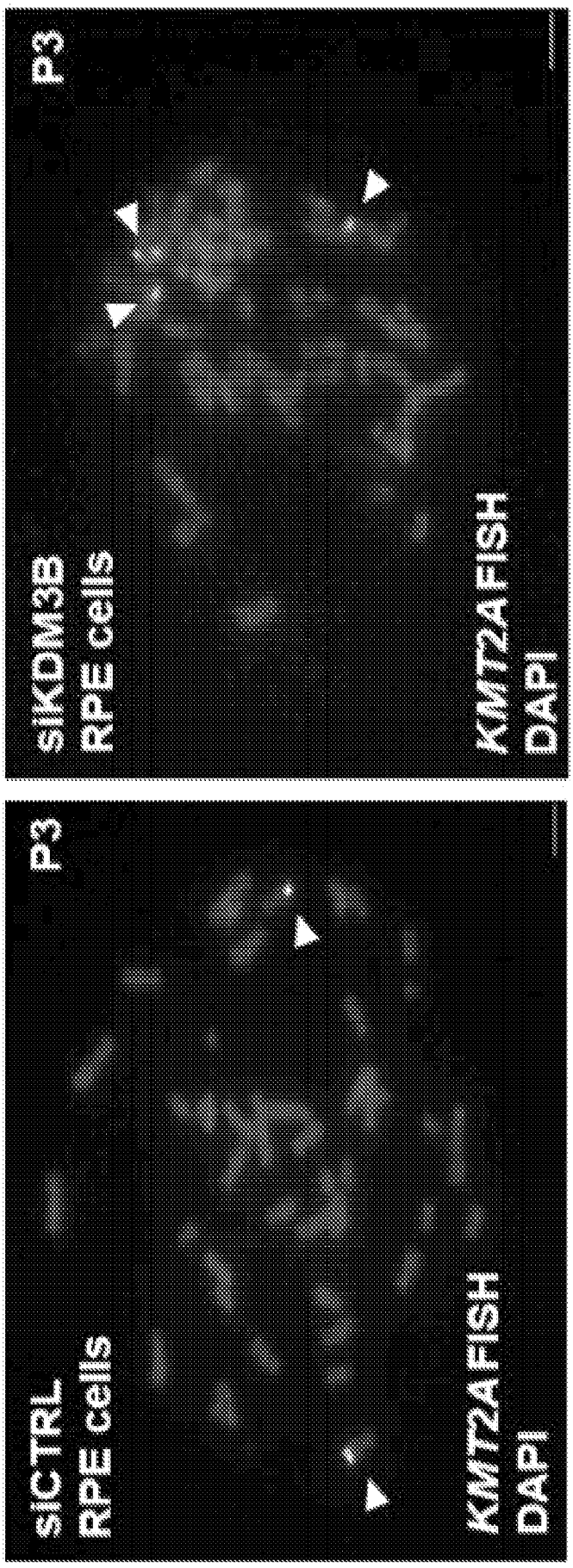
siCTRL
RPE cells
P3
KMT2A FISH
DAPI
siKDM3B
RPE cells
P3
KMT2A FISH
DAPI

FIG. 3G

FIG. 3H

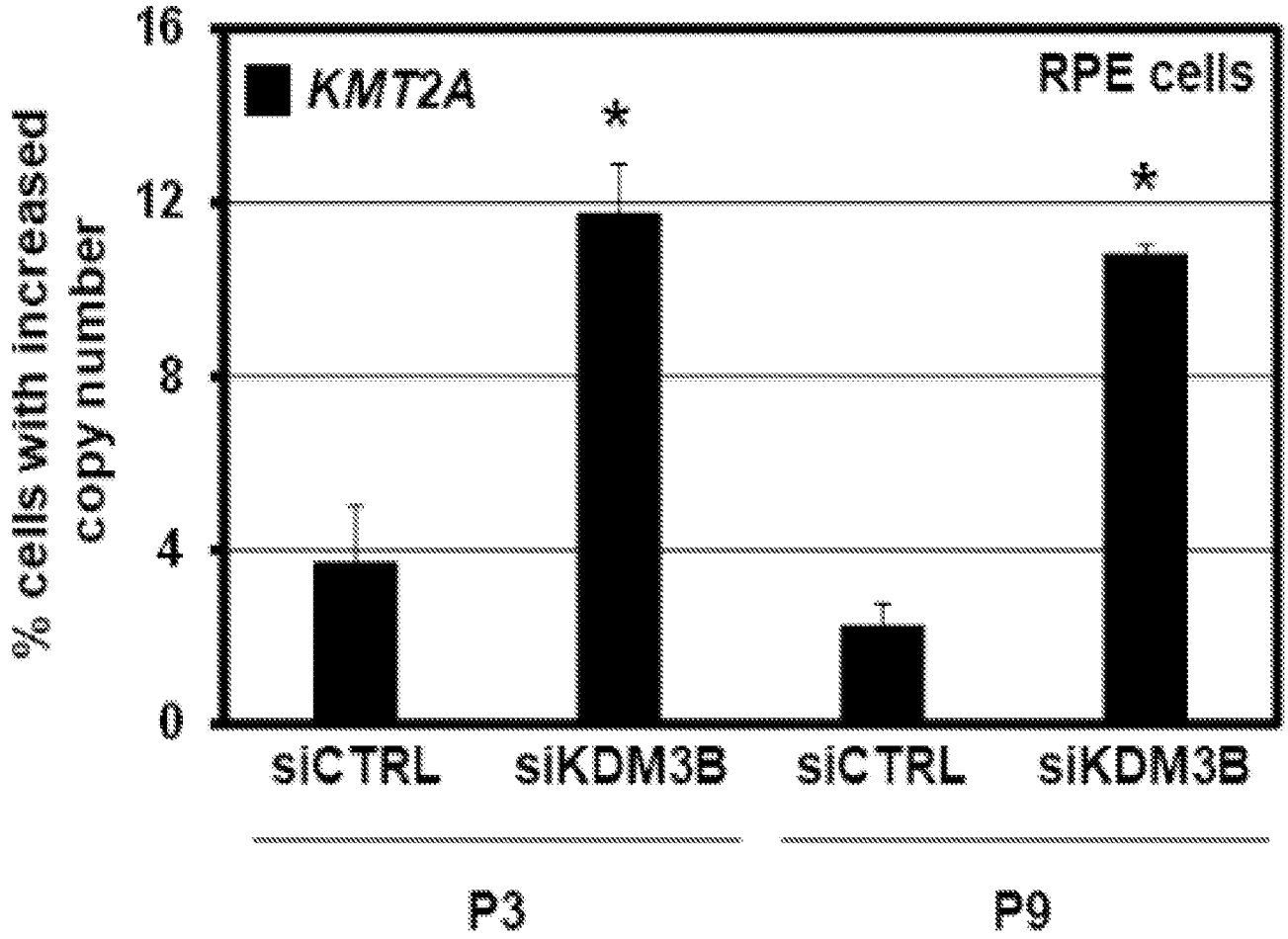
KMT2A
RPE cells
% cells with increased copy number
16
12
8
4
0
*
*
siCTRL
siKDM3B
siCTRL
siKDM3B
P3
P9

FIG. 3I

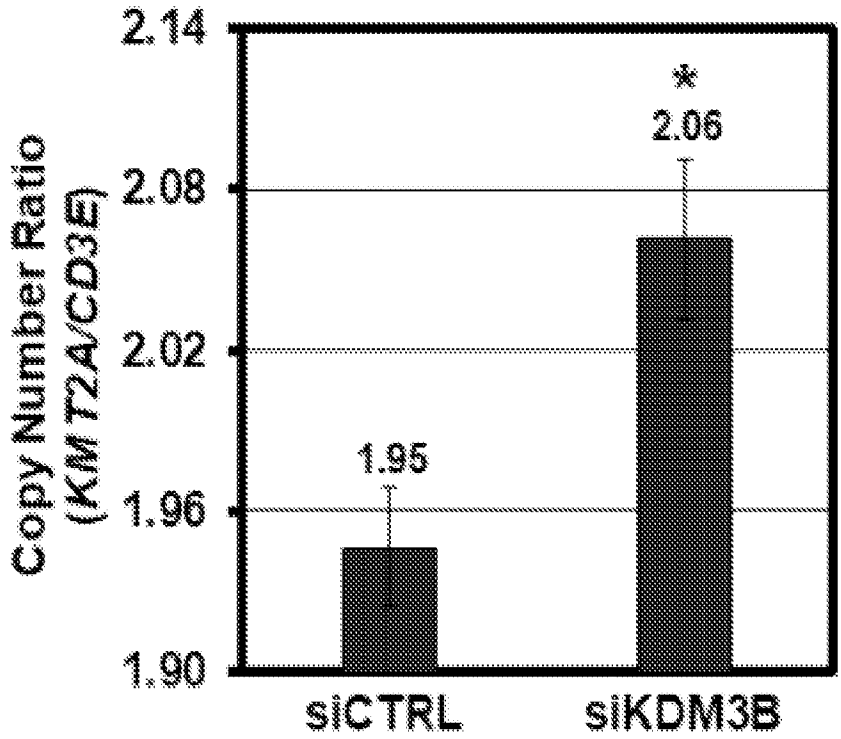
Copy Number Ratio
(KMT2A/CD3E)
2.14
2.08
2.02
1.96
1.90
1.95
2.06
*
siCTRL
siKDM3B

FIG. 3J

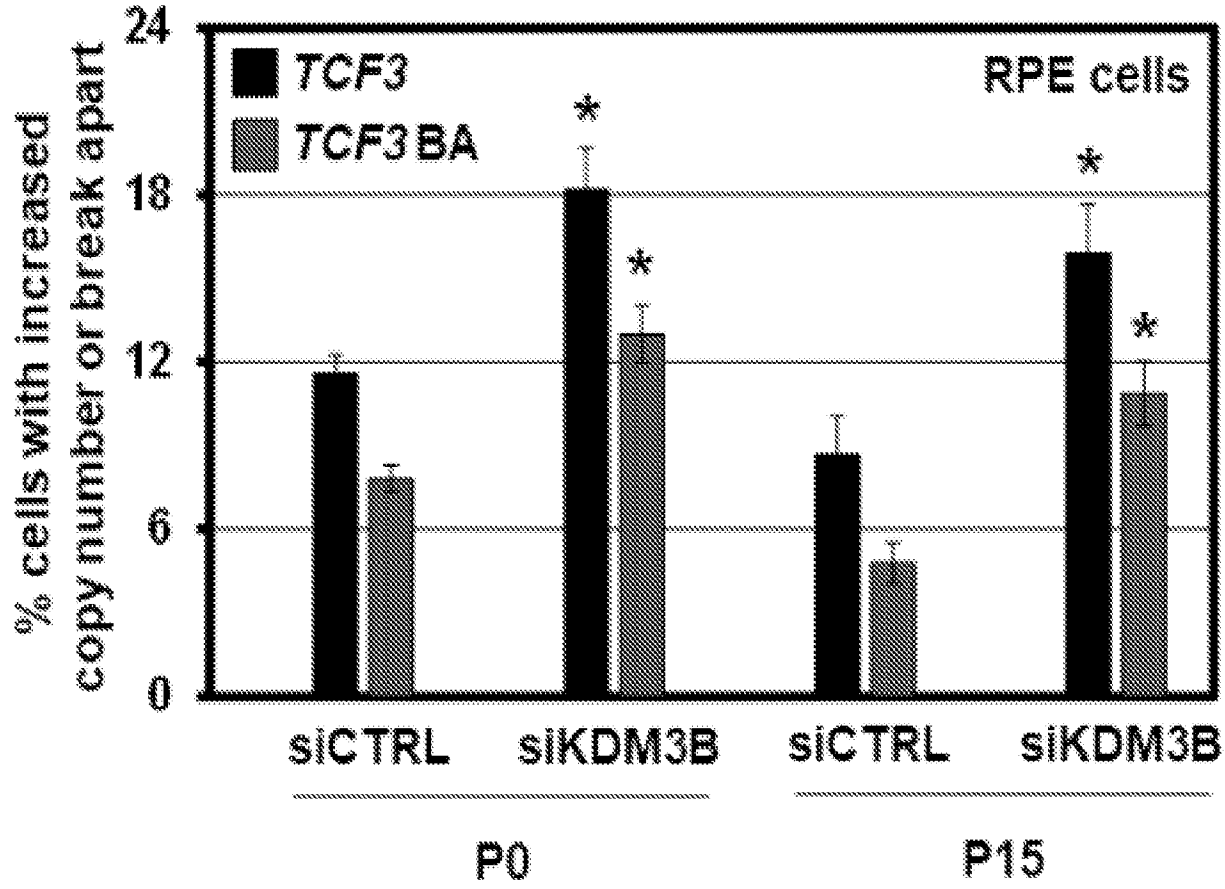
% cells with increased copy number or break apart
24
18
12
6
0
TCF3
TCF3 BA
RPE cells
*
siCTRL
siKDM3B
siCTRL
siKDM3B
P0
P15

FIG. 3K

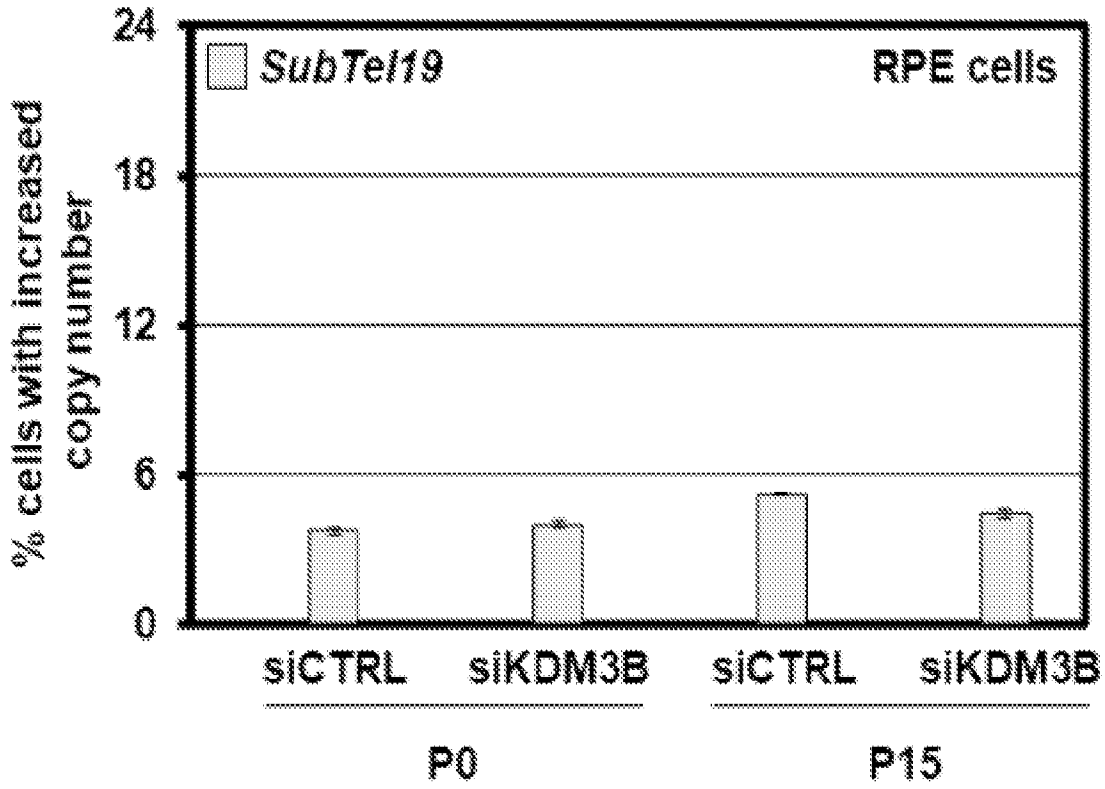
SubTel19
RPE cells
% cells with increased copy number
24
18
12
6
0
siCTRL
siKDM3B
siCTRL
siKDM3B
P0
P15

FIG. 3L

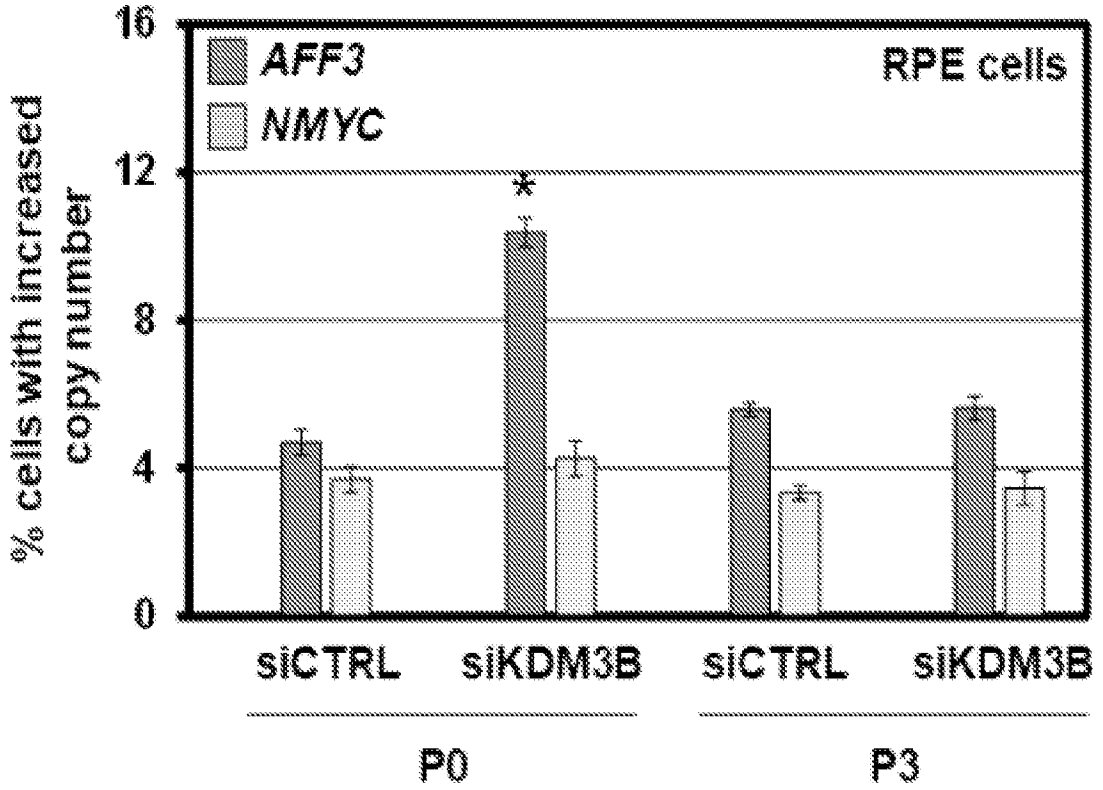
AFF3
NMYC
RPE cells
% cells with increased copy number
16
12
8
4
0
*
siCTRL
siKDM3B
siCTRL
siKDM3B
P0
P3

FIG. 4A

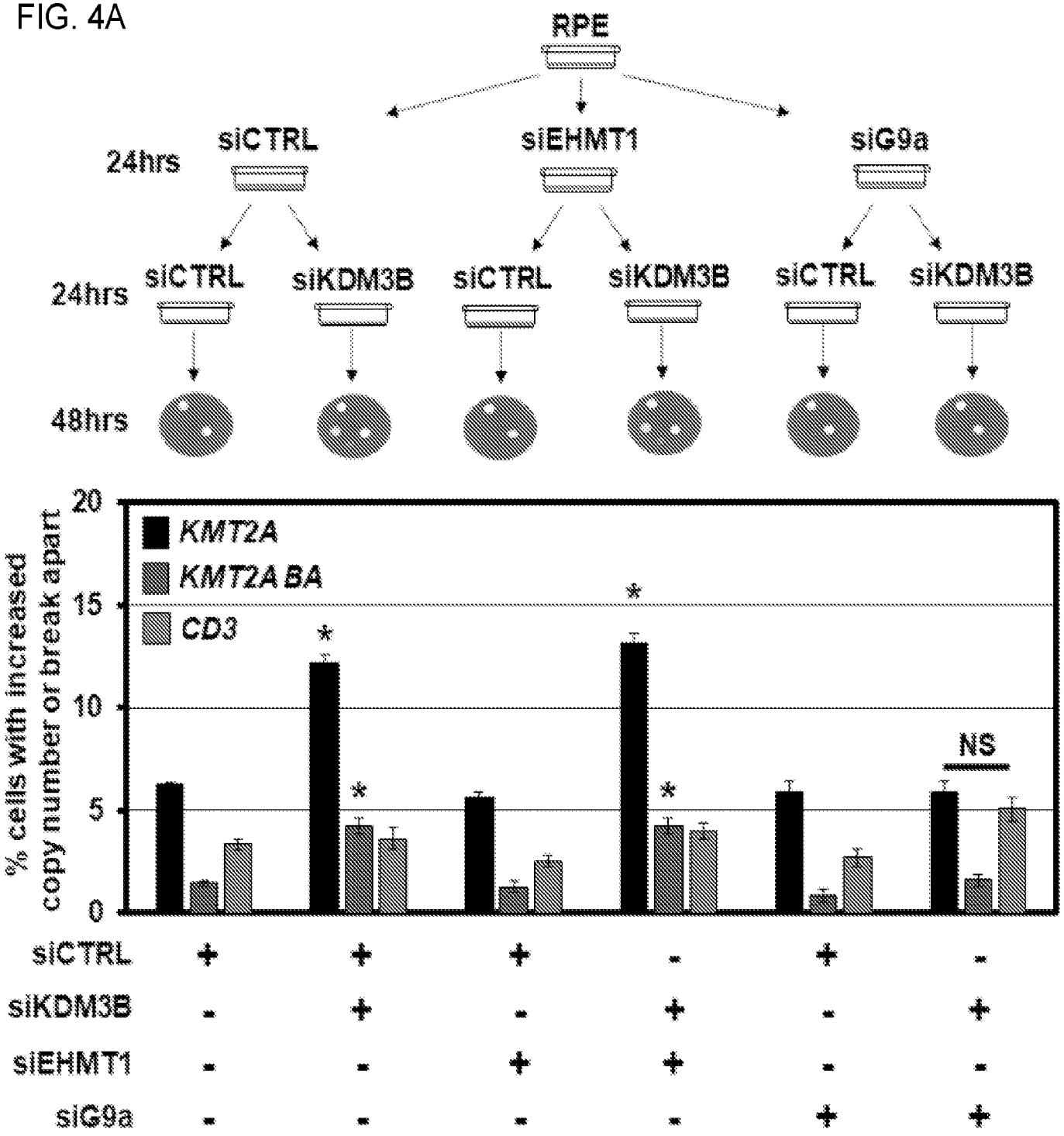
RPE
24hrs
siCTRL
siEHMT1
siG9a
24hrs
siCTRL
siKDM3B
siCTRL
siKDM3B
siCTRL
siKDM3B
48hrs
% cells with increased copy number or break apart
KMT2A
KMT2A BA
CD3
20
15
10
5
0
*
*
*
*
NS
siCTRL + + + - + -
siKDM3B - + - + - +
siEHMT1 - - + + - -
siG9a - - - - + +

FIG. 4B

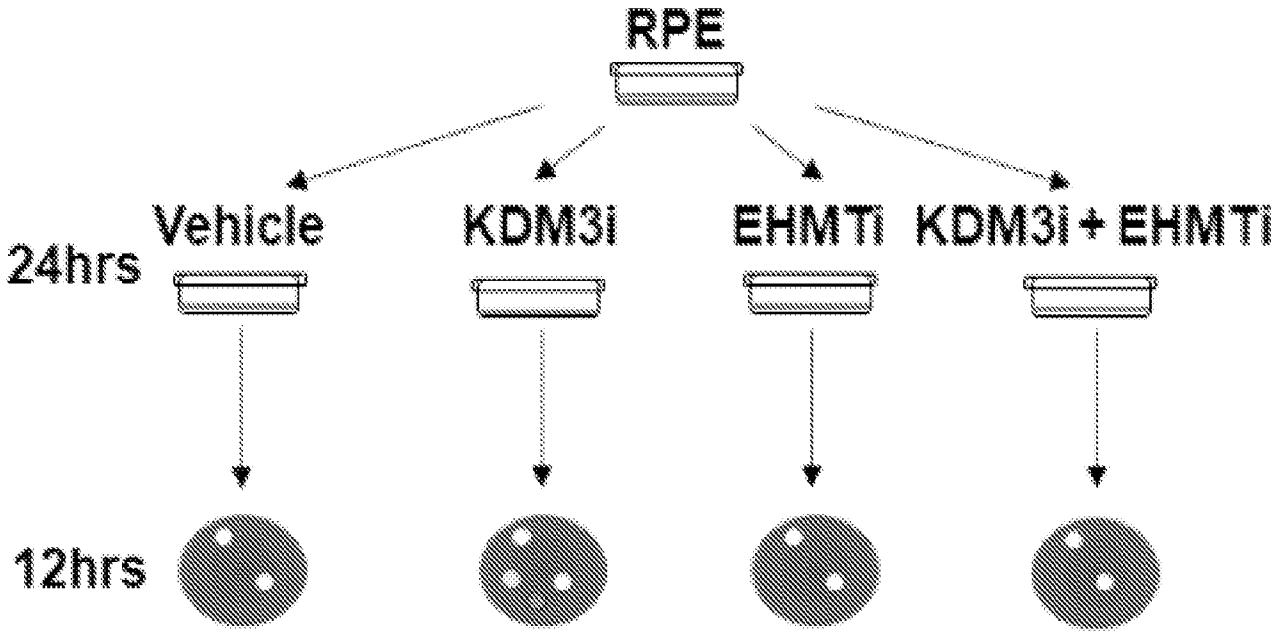
RPE
Vehicle
KDM3i
EHMTi
KDM3i + EHMTi
24hrs
12hrs

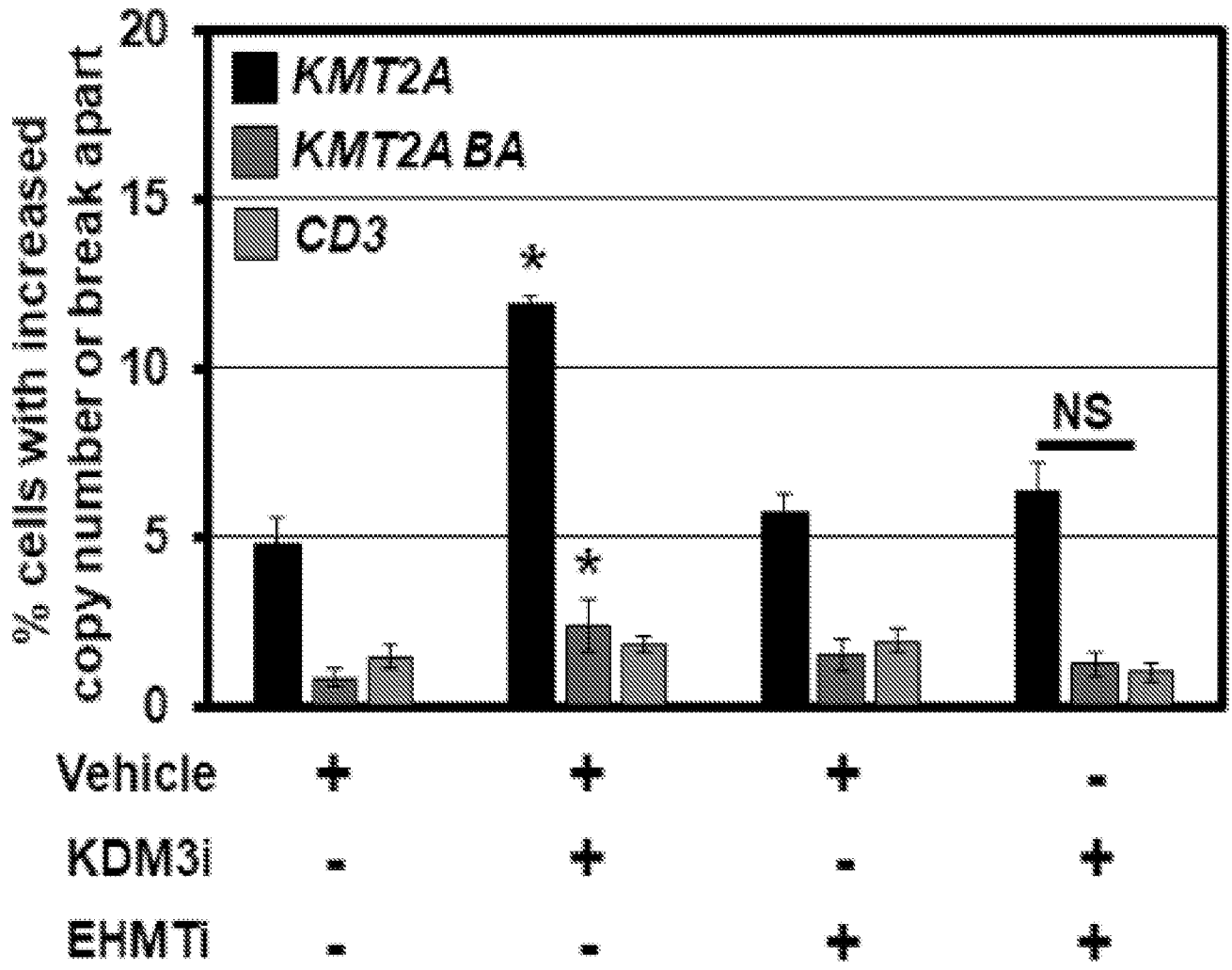
% cells with increased copy number or break apart
20
15
10
5
0
KMT2A
KMT2A BA
CD3
*
*
NS
Vehicle + + + -
KDM3i - + - +
EHMTi - - + +

FIG. 4C

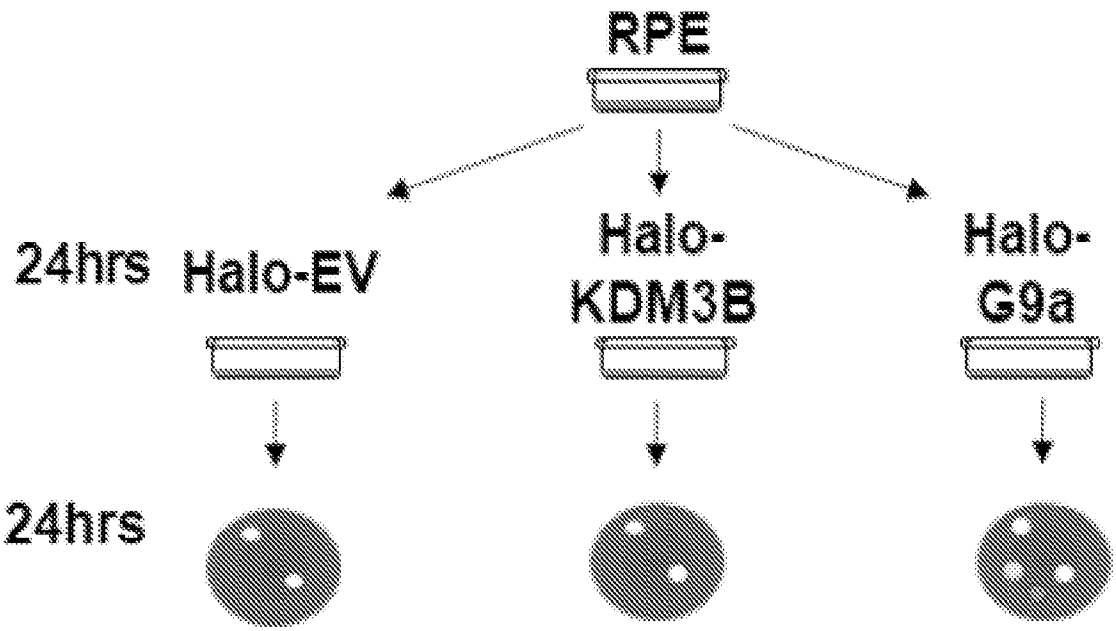
RPE
24hrs
Halo-EV
Halo-KDM3B
Halo-G9a
24hrs

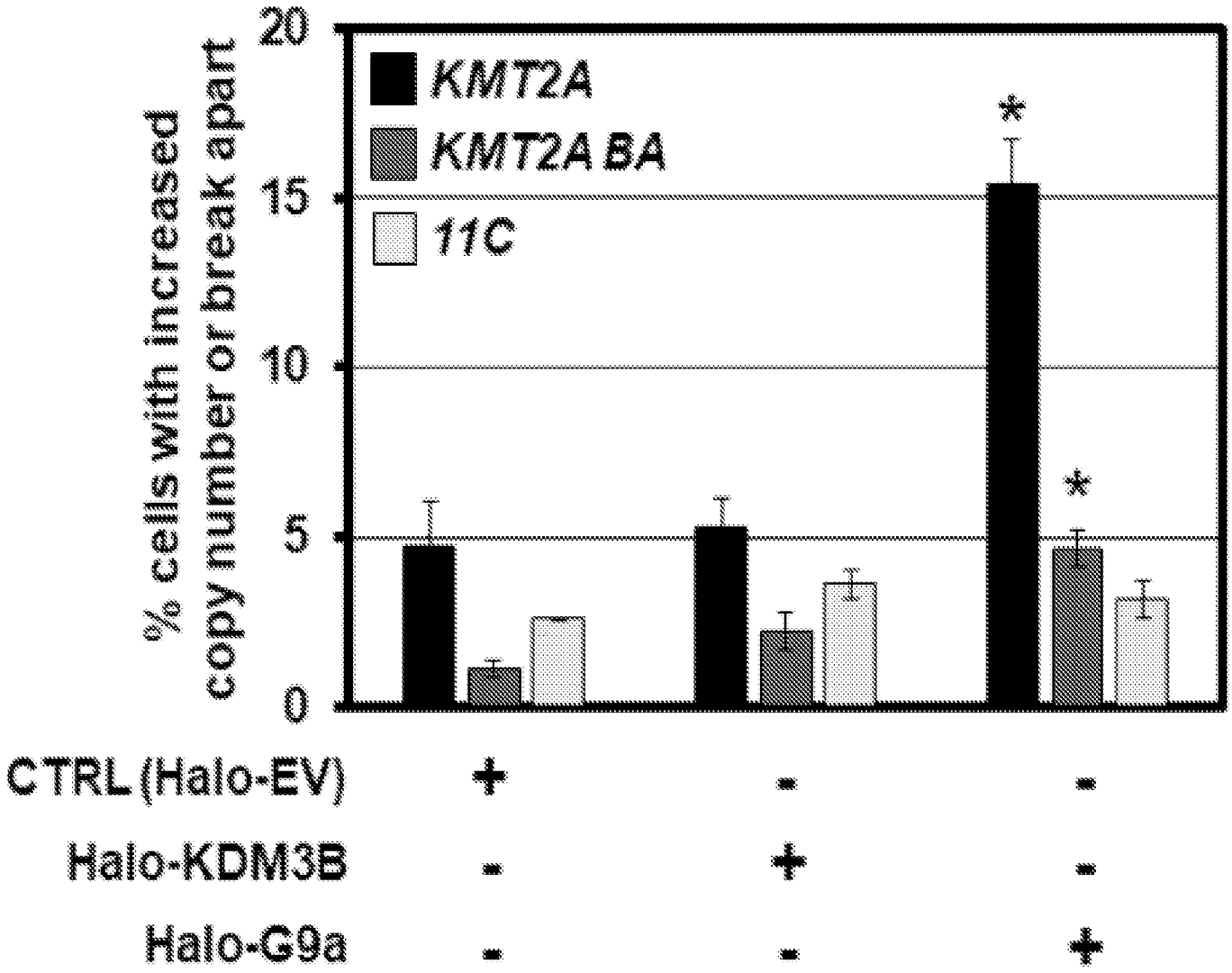
% cells with increased copy number or break apart
20
15
10
5
0
KMT2A
KMT2A BA
11C
*
*
CTRL (Halo-EV) + - -
Halo-KDM3B - + -
Halo-G9a - - +

FIG. 4D

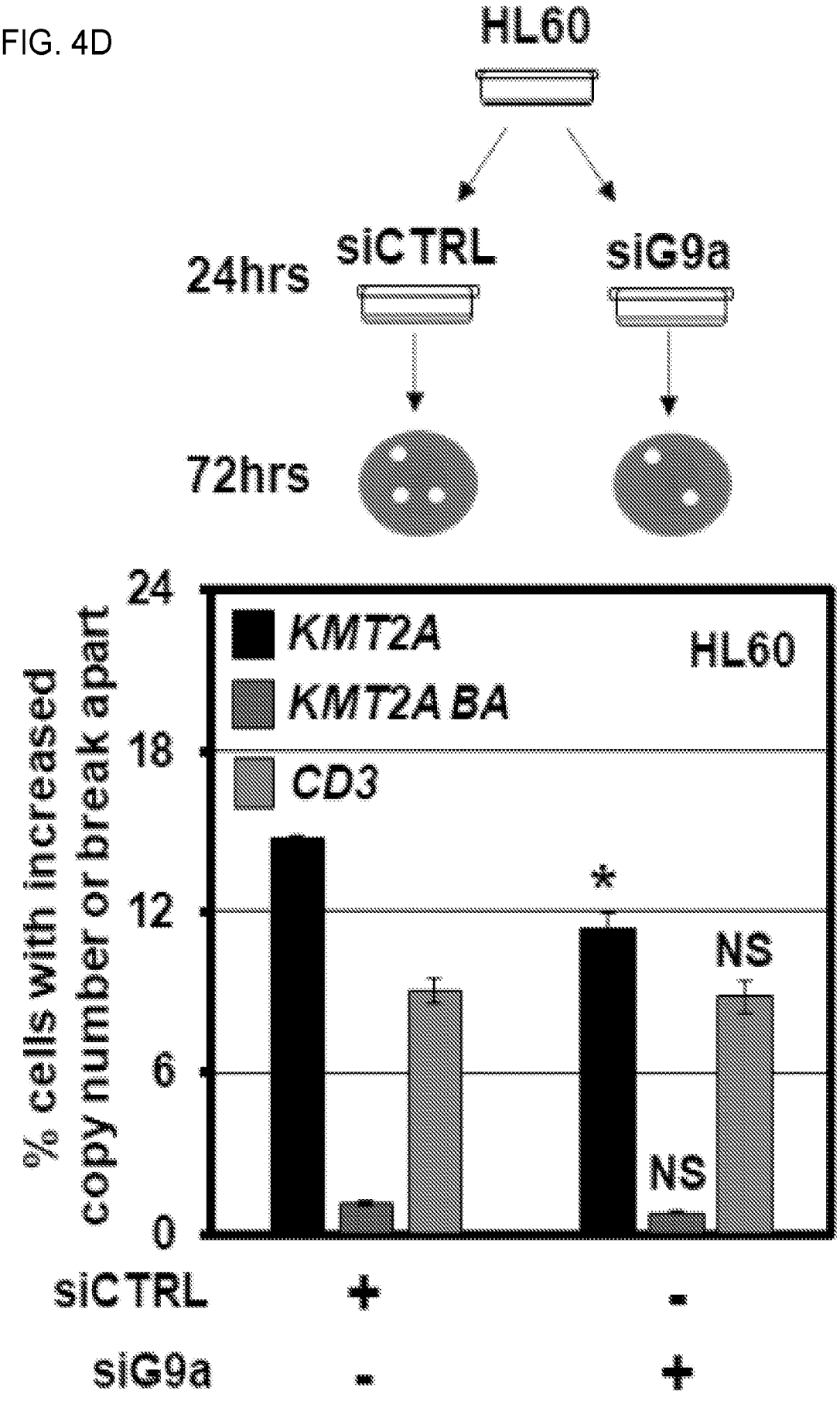
HL60
24hrs
siCTRL
siG9a
72hrs
% cells with increased copy number or break apart
24
18
12
6
0
KMT2A
KMT2A BA
CD3
HL60
*
NS
NS
siCTRL + -
siG9a - +

FIG. 4E

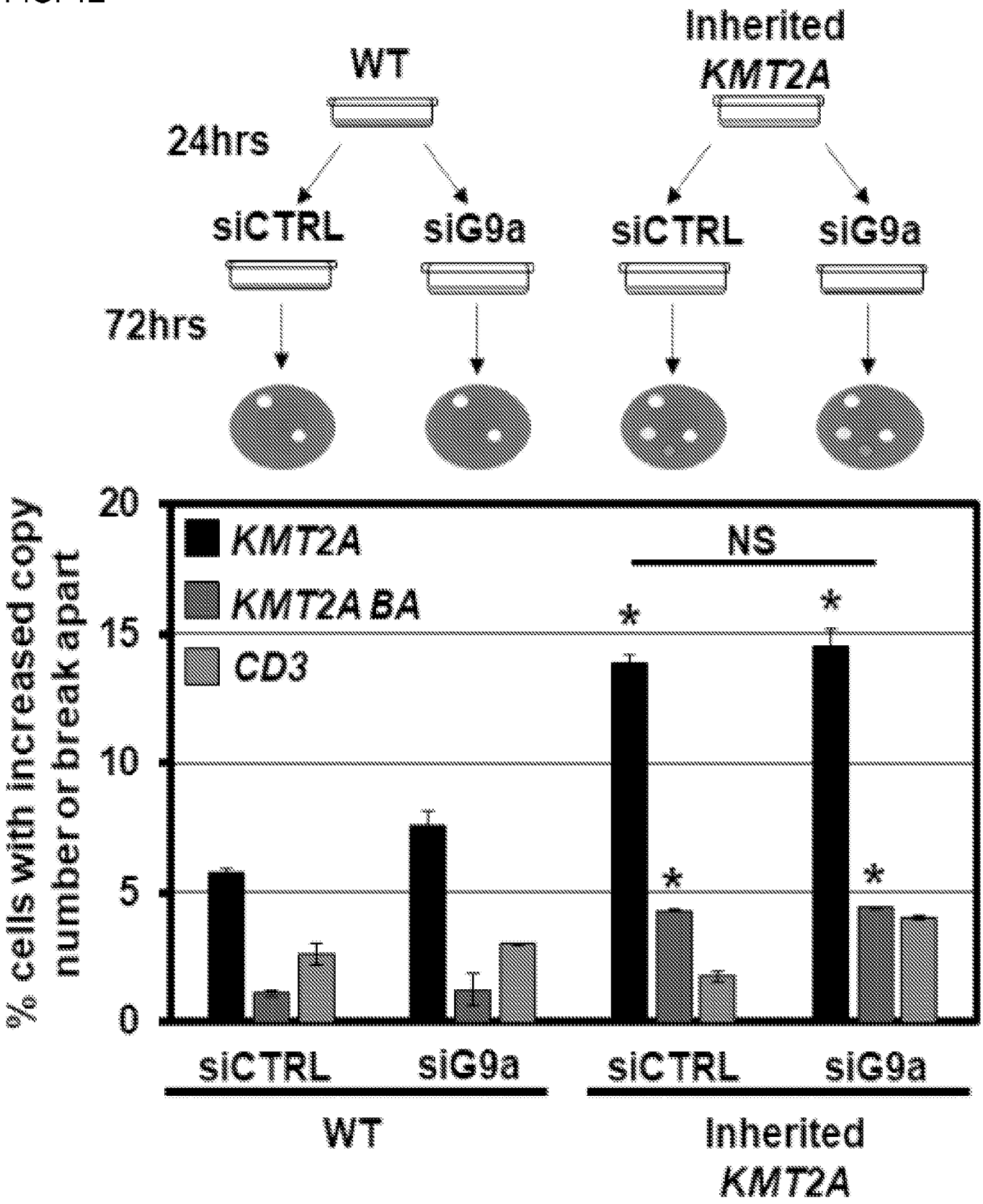
WT
Inherited
KMT2A
24hrs
siCTRL
siG9a
siCTRL
siG9a
72hrs
% cells with increased copy number or break apart
20
15
10
5
0
KMT2A
KMT2A BA
CD3
NS
*
*
*
*
siCTRL
siG9a
siCTRL
siG9a
WT
Inherited
KMT2A

FIG. 4F

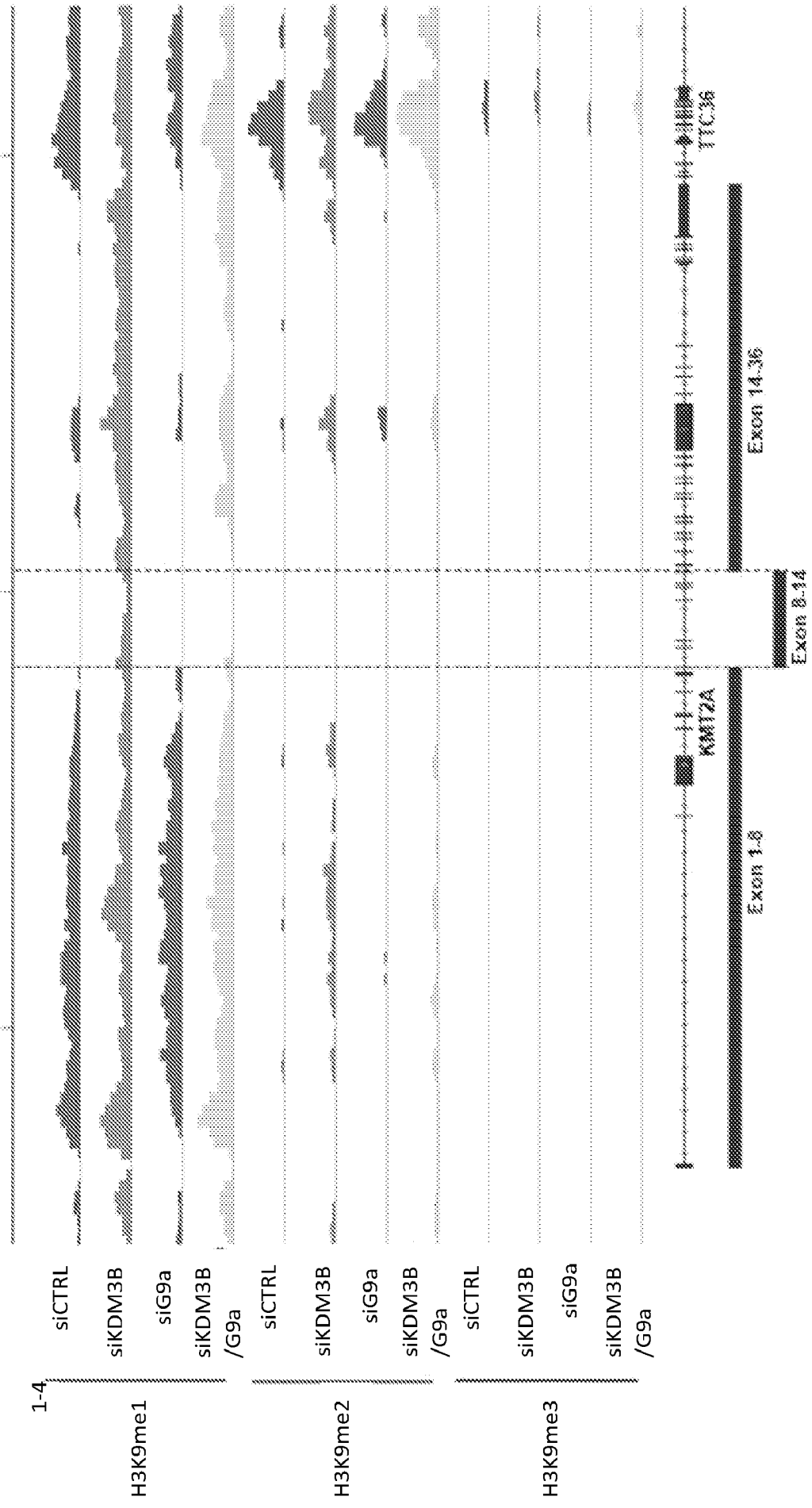
118.32
118.36
118.4
1-4
H3K9me1
H3K9me2
H3K9me3
siCTRL
siKDM3B
siG9a
siKDM3B /G9a
siCTRL
siKDM3B
siG9a
siKDM3B /G9a
siCTRL
siKDM3B
siG9a
siKDM3B /G9a
KMT2A
Exon 1-8
Exon 8-14
Exon 14-36
TTC36

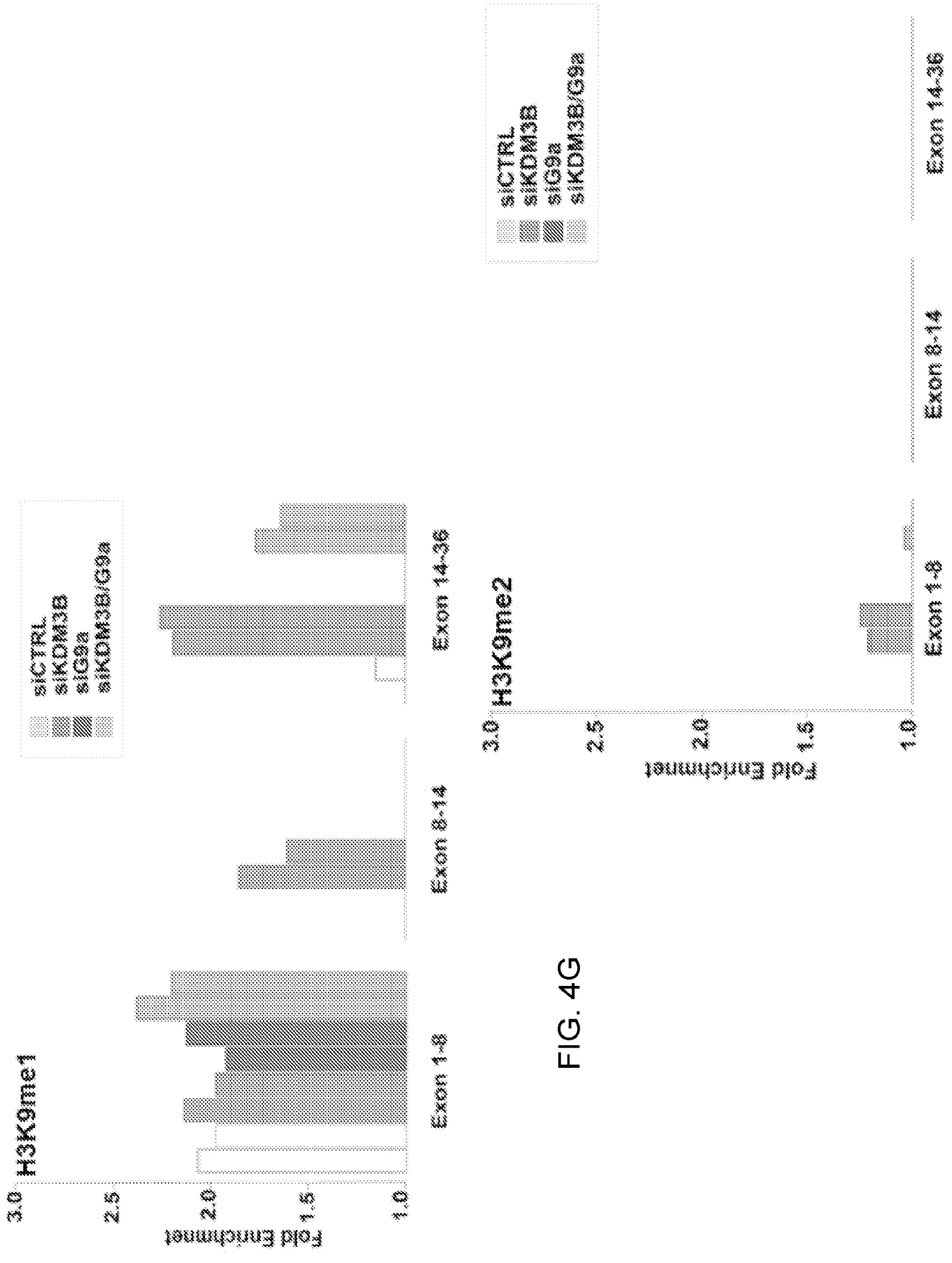
H3K9me1
H3K9me2
siCTRL
siKDM3B
siG9a
siKDM3B/G9a
Fold Enrichment
3.0
2.5
2.0
1.5
1.0
Exon 1-8
Exon 8-14
Exon 14-36

FIG. 4G

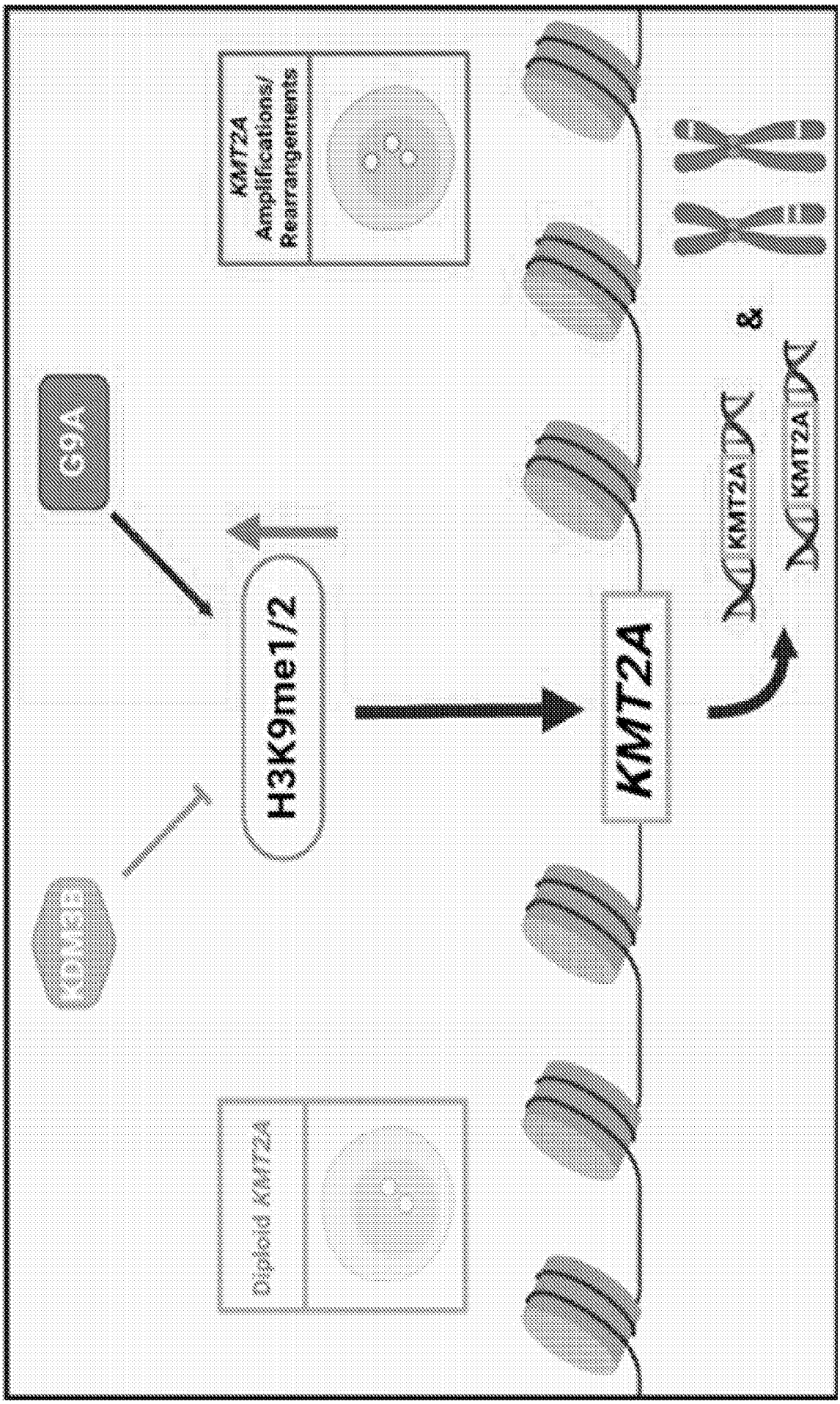
KMT2A Amplifications/ Rearrangements
G9A
H3K9me1/2
KMT2A
KMT2A
&
KMT2A
Diploid KMT2A

FIG. 4H

FIG. 5A

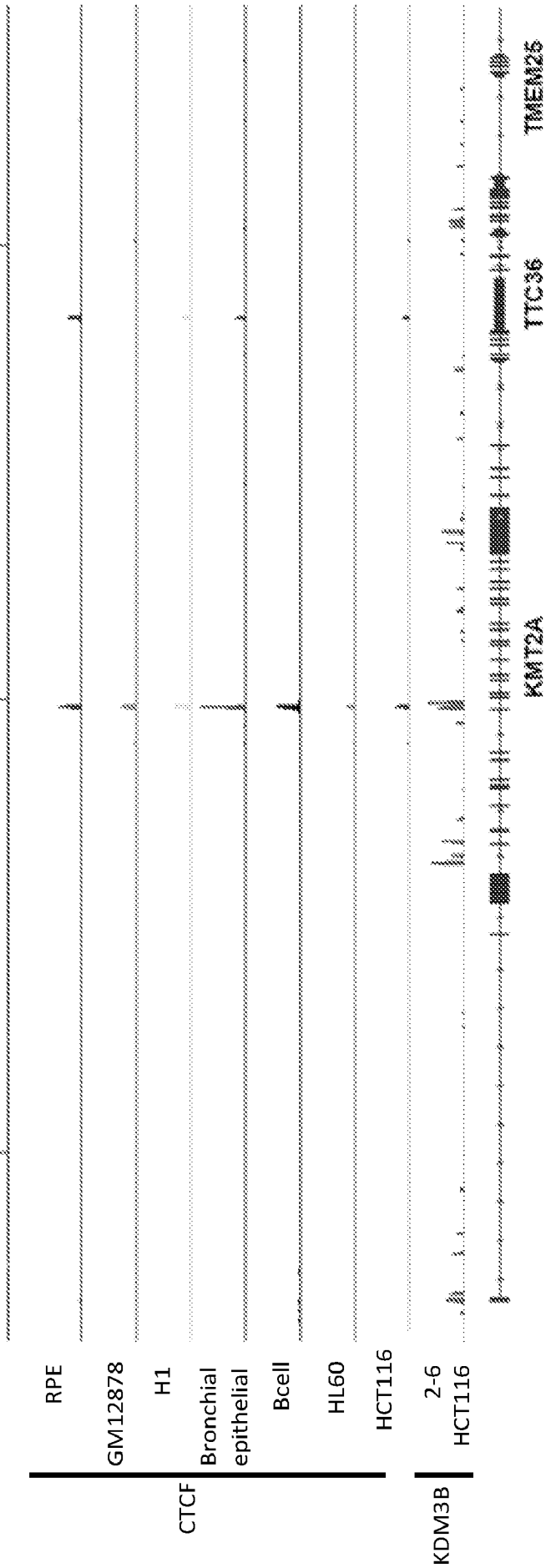
118.32
118.36
118.4
0-196
RPE
GM12878
H1
Bronchial epithelial
Bcell
HL60
HCT116
CTCF
2-6
HCT116
KDM3B
KMT2A
TTC36
TMEM25

FIG. 5B

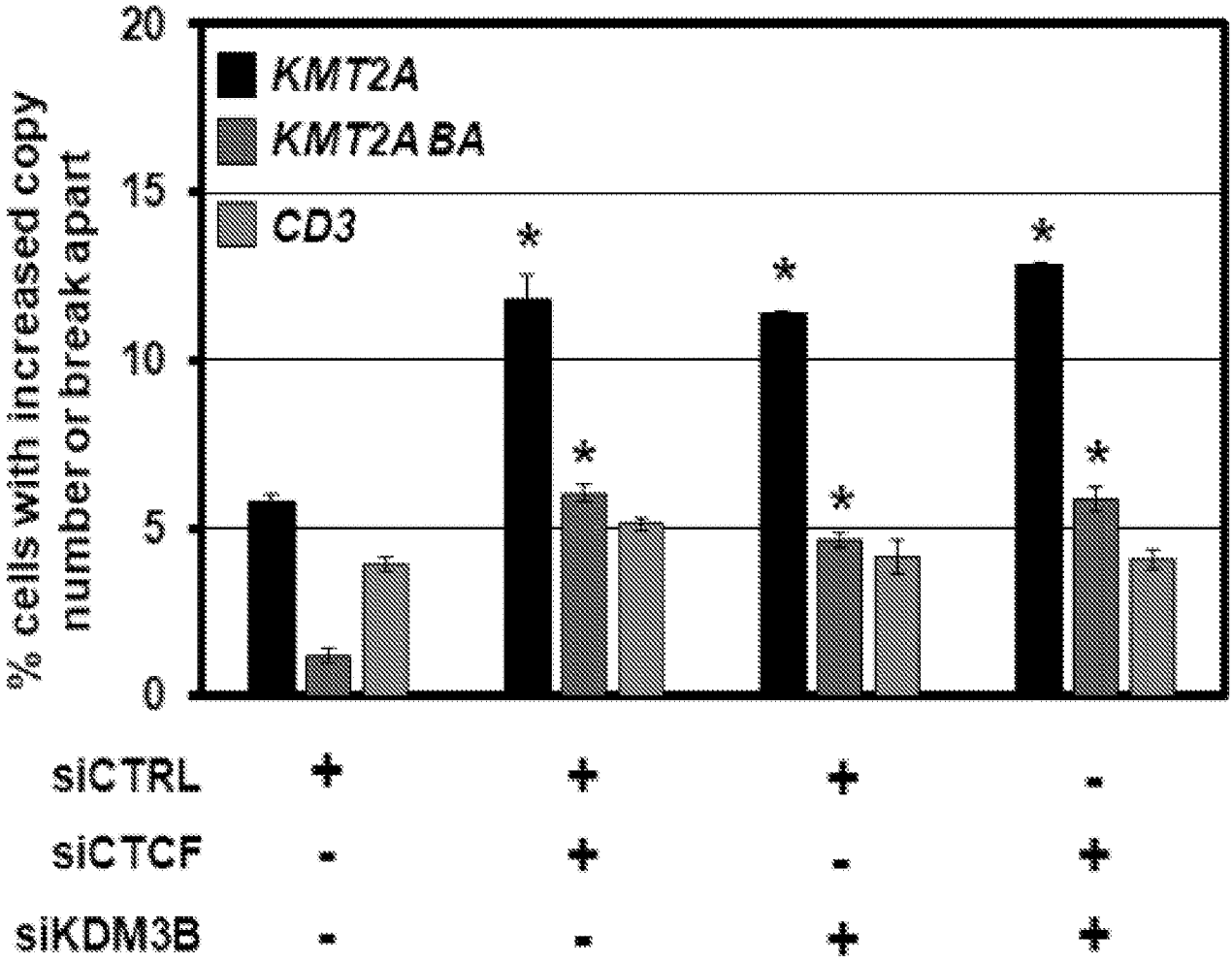
20
15
10
5
0
% cells with increased copy number or break apart
KMT2A
KMT2A BA
CD3
*
siCTRL + + + -
siCTCF - + - +
siKDM3B - - + +

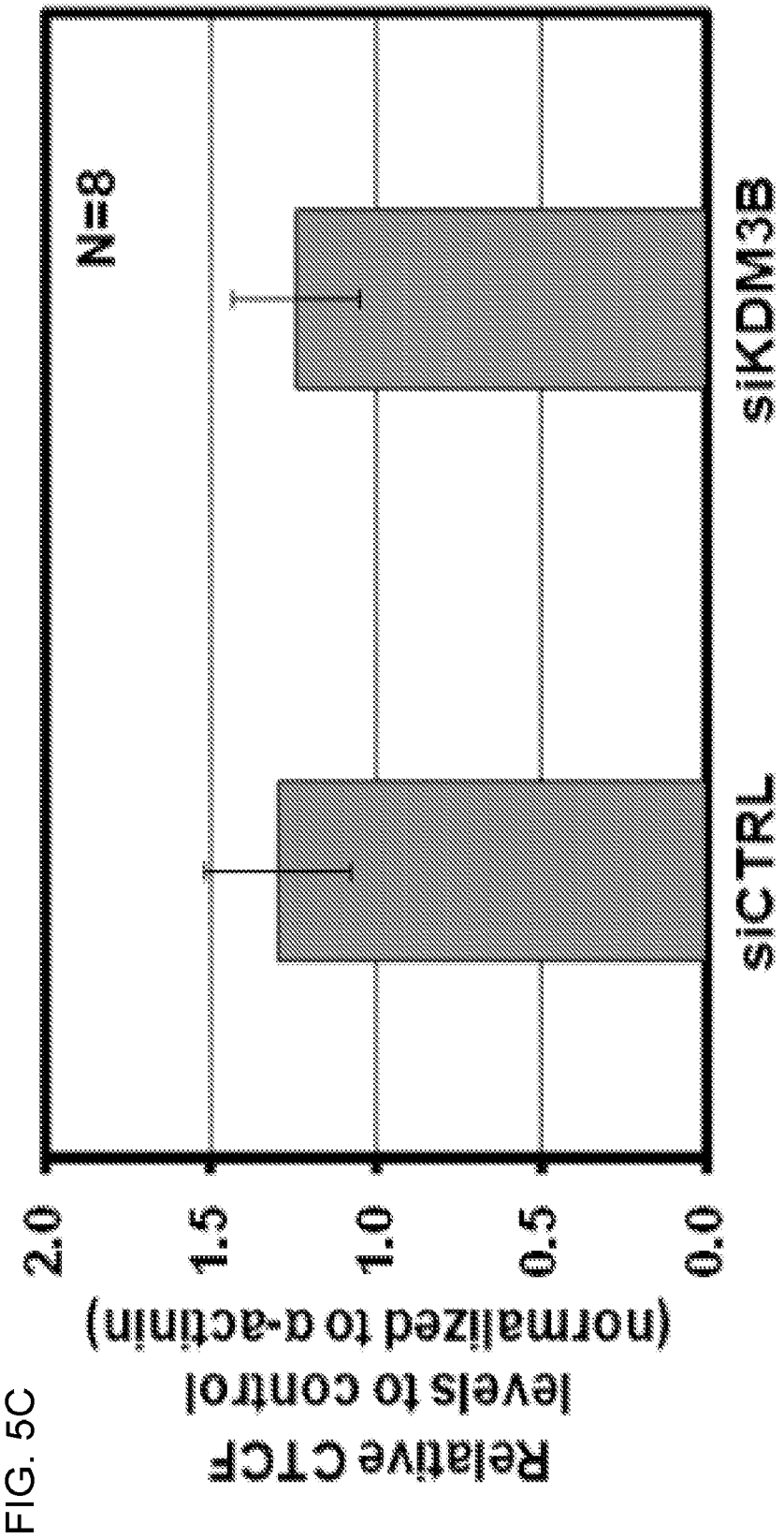
Relative CTCF
levels to control
(normalized to a-actinin)
2.0
1.5
1.0
0.5
0.0
siCTRL
siKDM3B
N=8

FIG. 5C

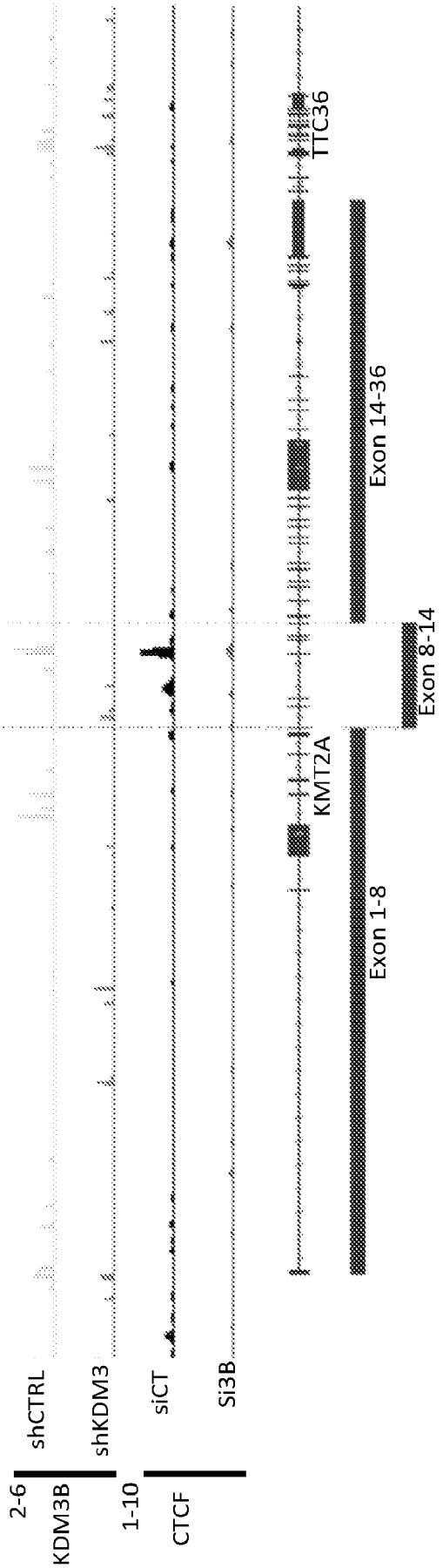
118.32
118.36
118.4
shCTRL
shKDM3
siCT
Si3B
2-6
KDM3B
1-10
CTCF
KMT2A
Exon 1-8
Exon 8-14
Exon 14-36
TTC36

FIG. 5D

FIG. 5E

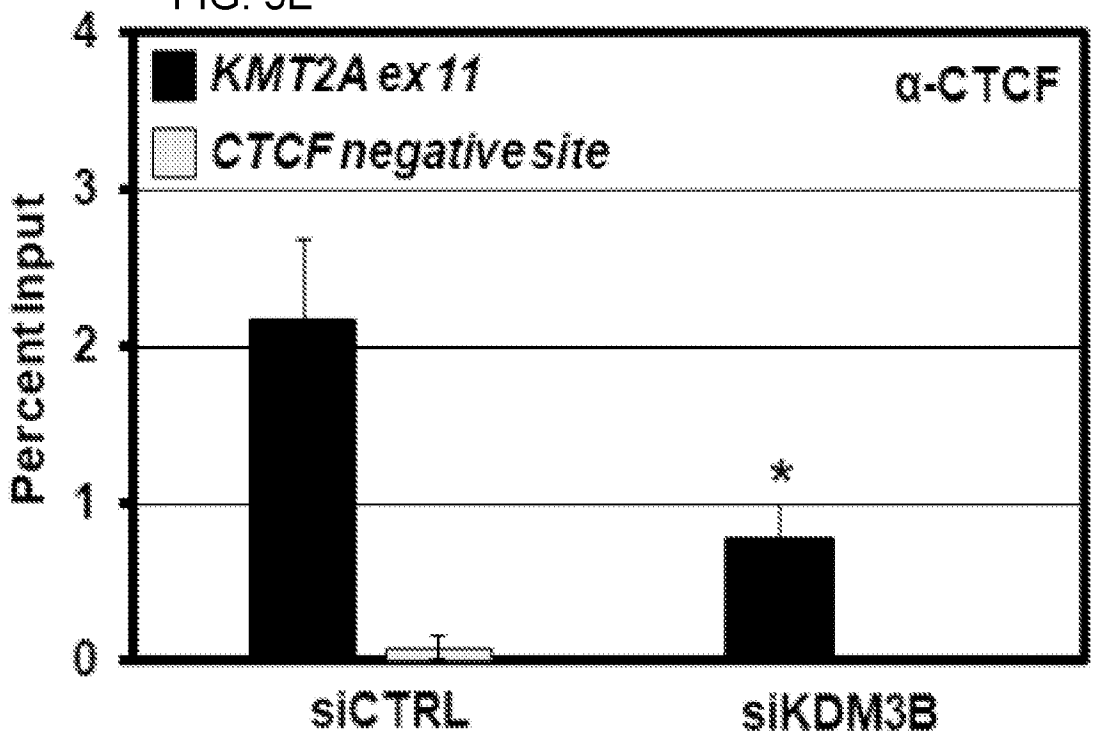
KMT2A ex11
CTCF negative site
α-CTCF
Percent Input
4
3
2
1
0
*
siCTRL
siKDM3B

FIG. 5F

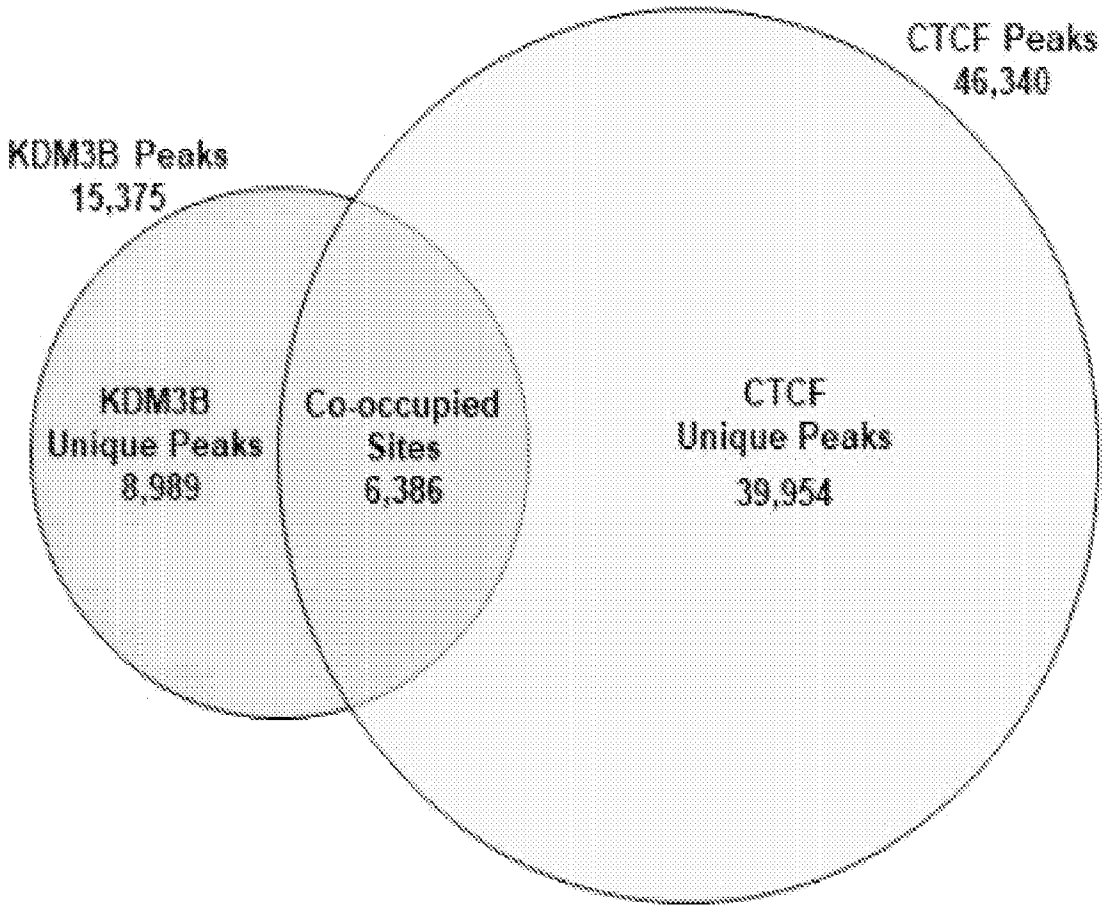
CTCF Peaks
46,340
KDM3B Peaks
15,375
KDM3B
Unique Peaks
8,989
Co-occupied
Sites
6,386
CTCF
Unique Peaks
39,954

FIG. 5G

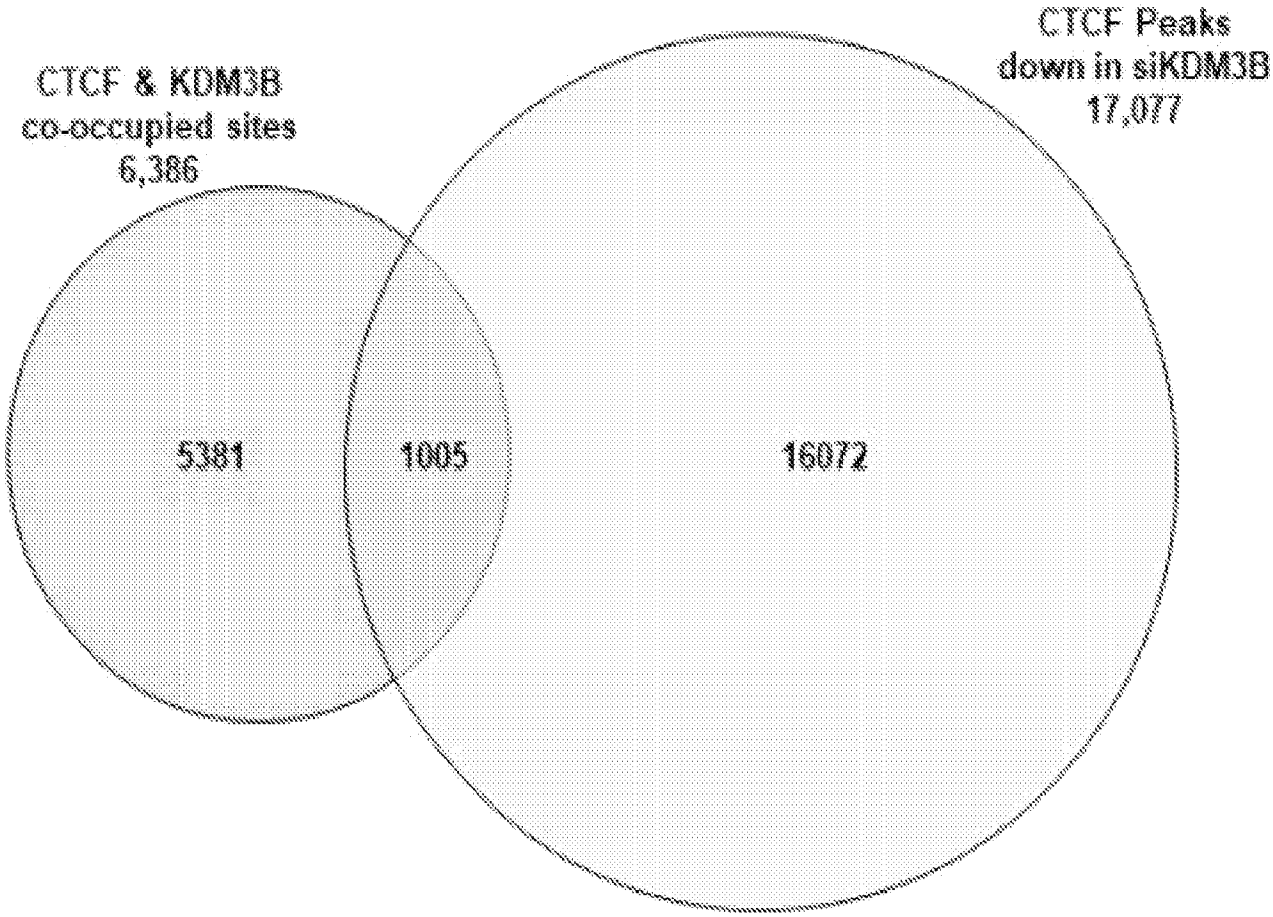
CTCF & KDM3B
co-occupied sites
6,386
CTCF Peaks
down in siKDM3B
17,077
5381
1005
16072

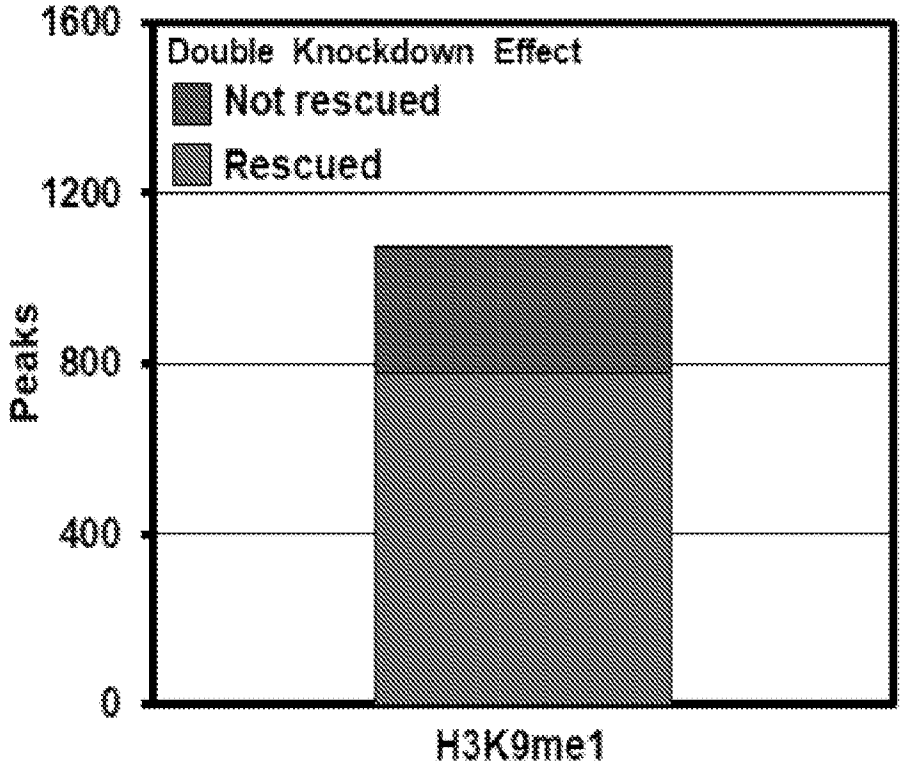
Double Knockdown Effect
Not rescued
Rescued
1600
1200
800
400
0
Peaks
H3K9me1

FIG. 5H

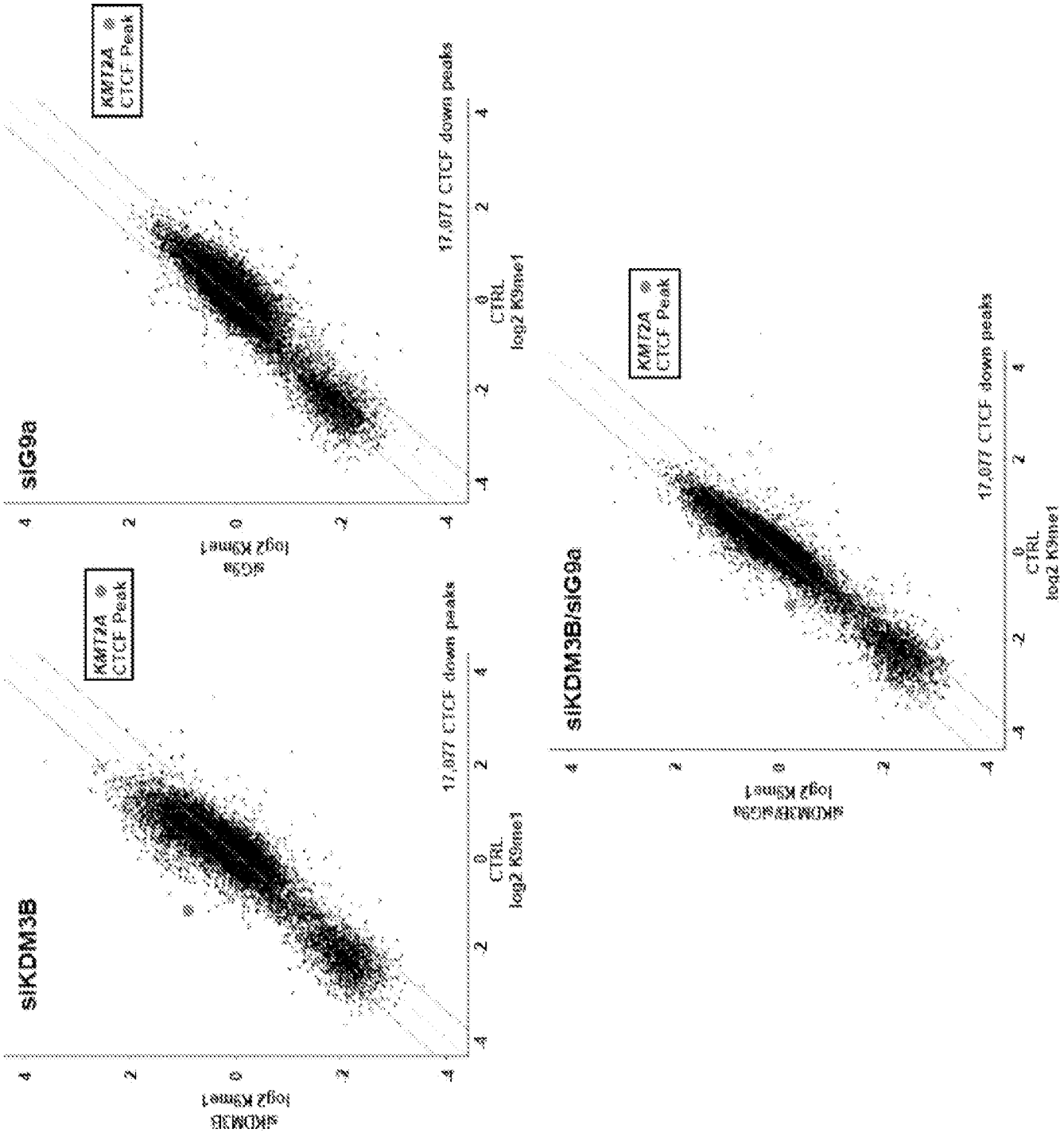
Rescue of H3K9me1 increase at CTCF peaks
siKDM3B
siG9a
siKDM3B/siG9a
KMT2A @ CTCF Peak
17,077 CTCF down peaks
siKDM3B log2 K9me1
siG9a log2 K9me1
siKDM3B/siG9a log2 K9me1
CTRL log2 K9me1

FIG. 5I

FIG. 5J

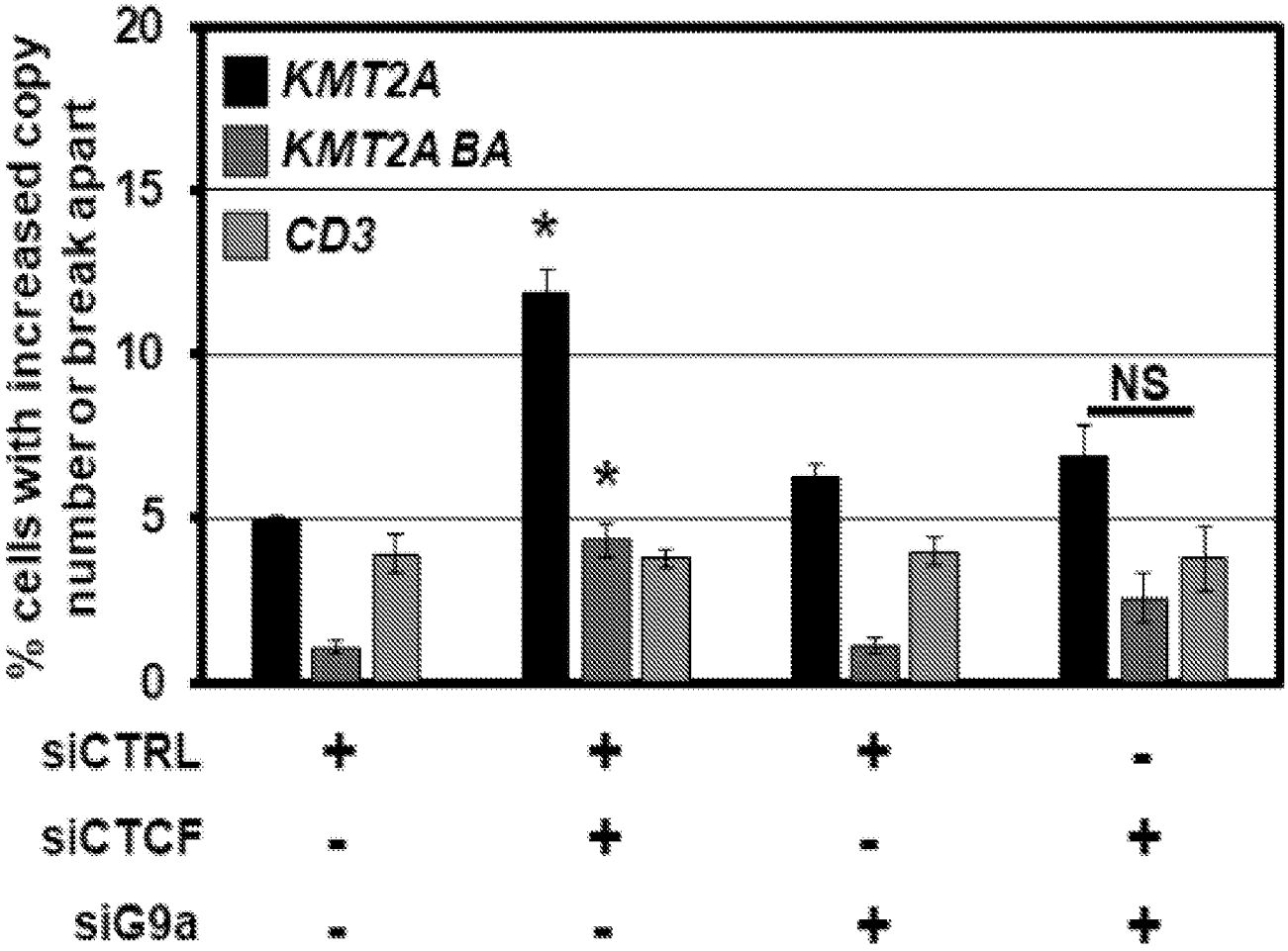
% cells with increased copy number or break apart
20
15
10
5
0
KMT2A
KMT2A BA
CD3
*
*
NS
siCTRL + + + -
siCTCF - + - +
siG9a - - + +

FIG. 5K

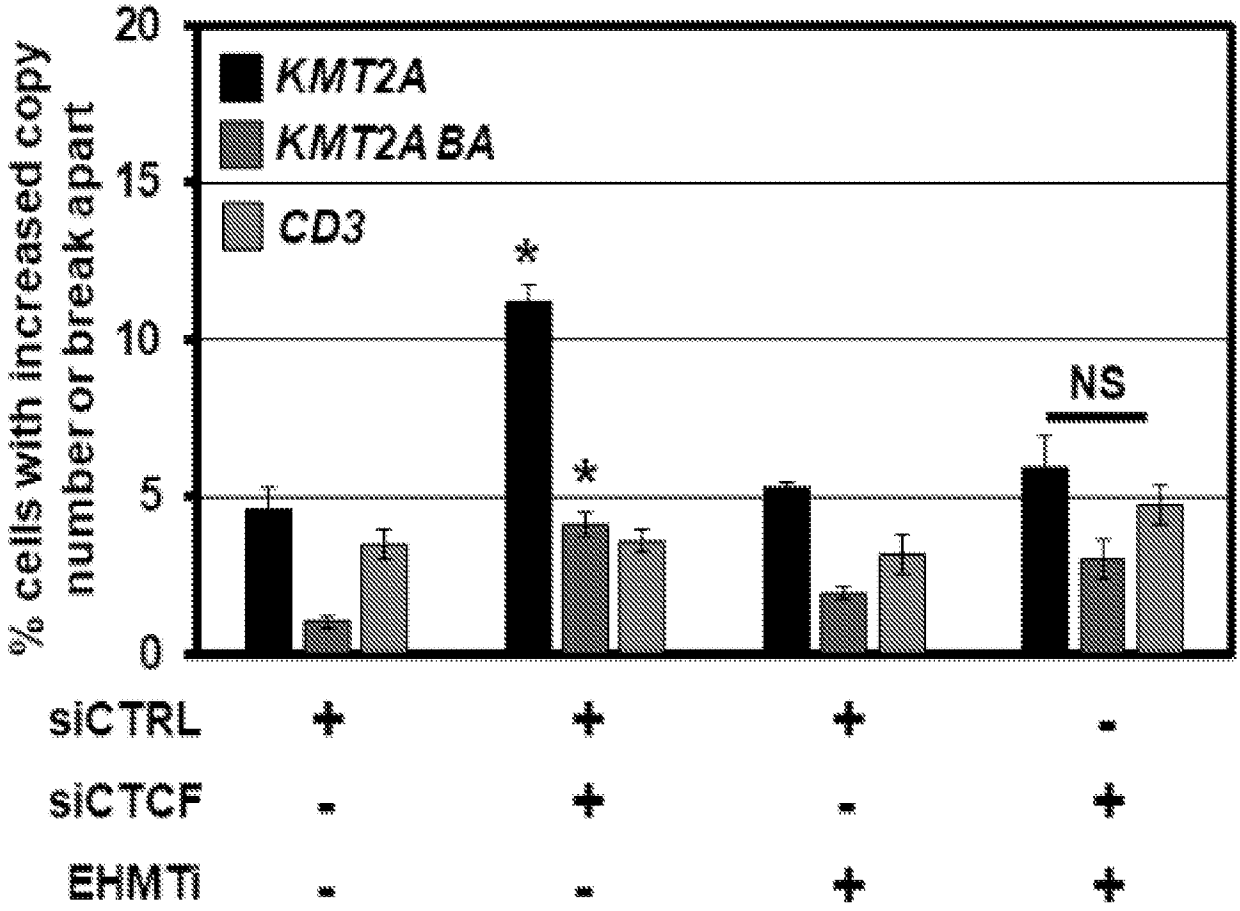
% cells with increased copy number or break apart
20
15
10
5
0
KMT2A
KMT2A BA
CD3
*
*
NS
siCTRL + + + -
siCTCF - + - +
EHMTi - - + +

FIG. 5L

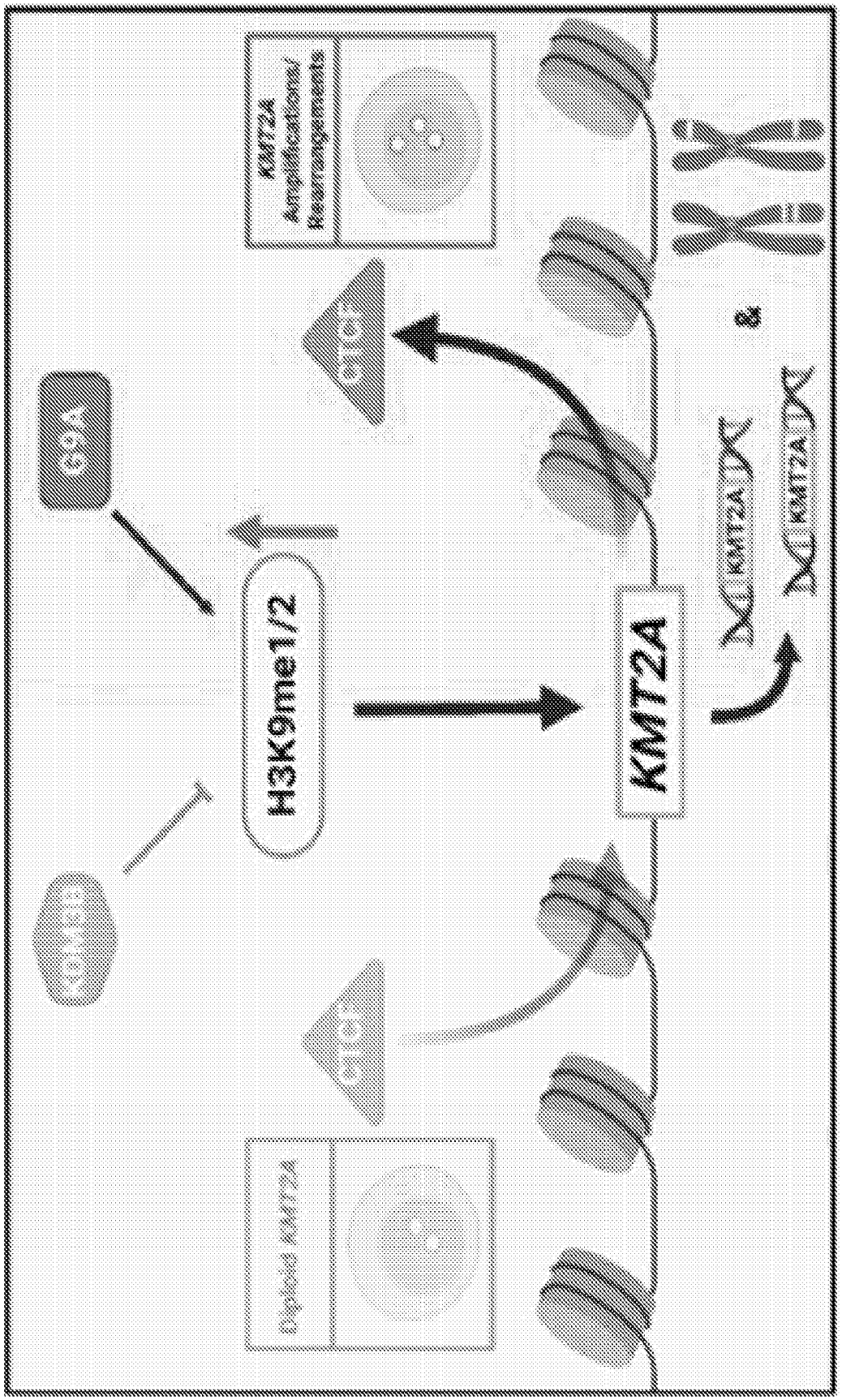
KMT2A Amplifications/ Rearrangements
Duplicated KMT2A
G9A
H3K9me1/2
KMT2A
&
KMT2A
KMT2A

FIG. 6A

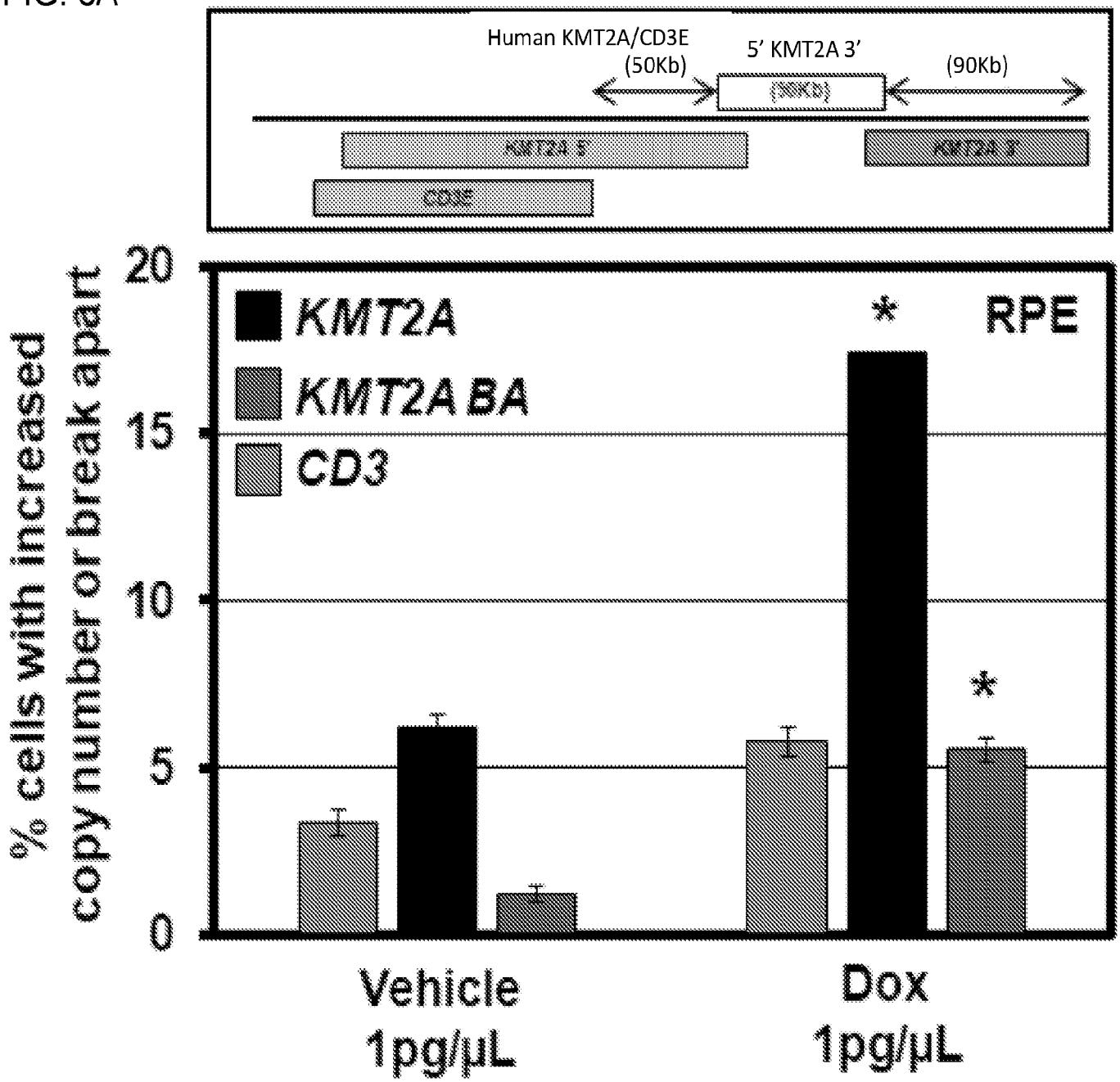
Human KMT2A/CD3E
(50Kb)
5' KMT2A 3'
(90Kb)
(90Kb)
KMT2A 5'
KMT2A 3'
CD3E
% cells with increased copy number or break apart
20
15
10
5
0
KMT2A
KMT2A BA
CD3
*
RPE
*
Vehicle 1pg/µL
Dox 1pg/µL

FIG. 6B

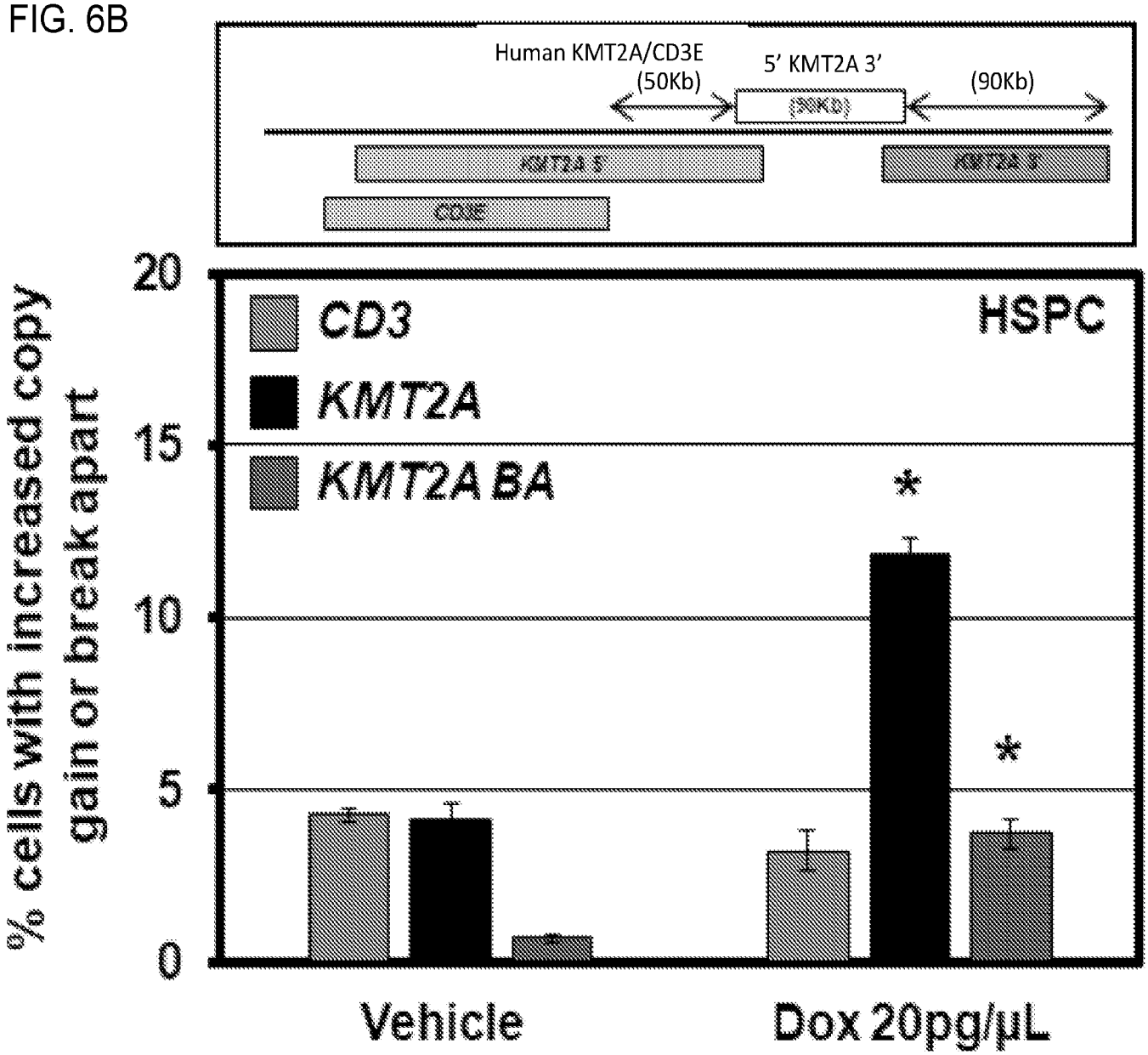
Human KMT2A/CD3E
(50Kb)
5' KMT2A 3'
(90Kb)
KMT2A 5'
KMT2A 3'
CD3E
% cells with increased copy gain or breakapart
20
15
10
5
0
CD3
KMT2A
KMT2A BA
HSPC
*
*
Vehicle
Dox 20pg/µL

FIG. 6C

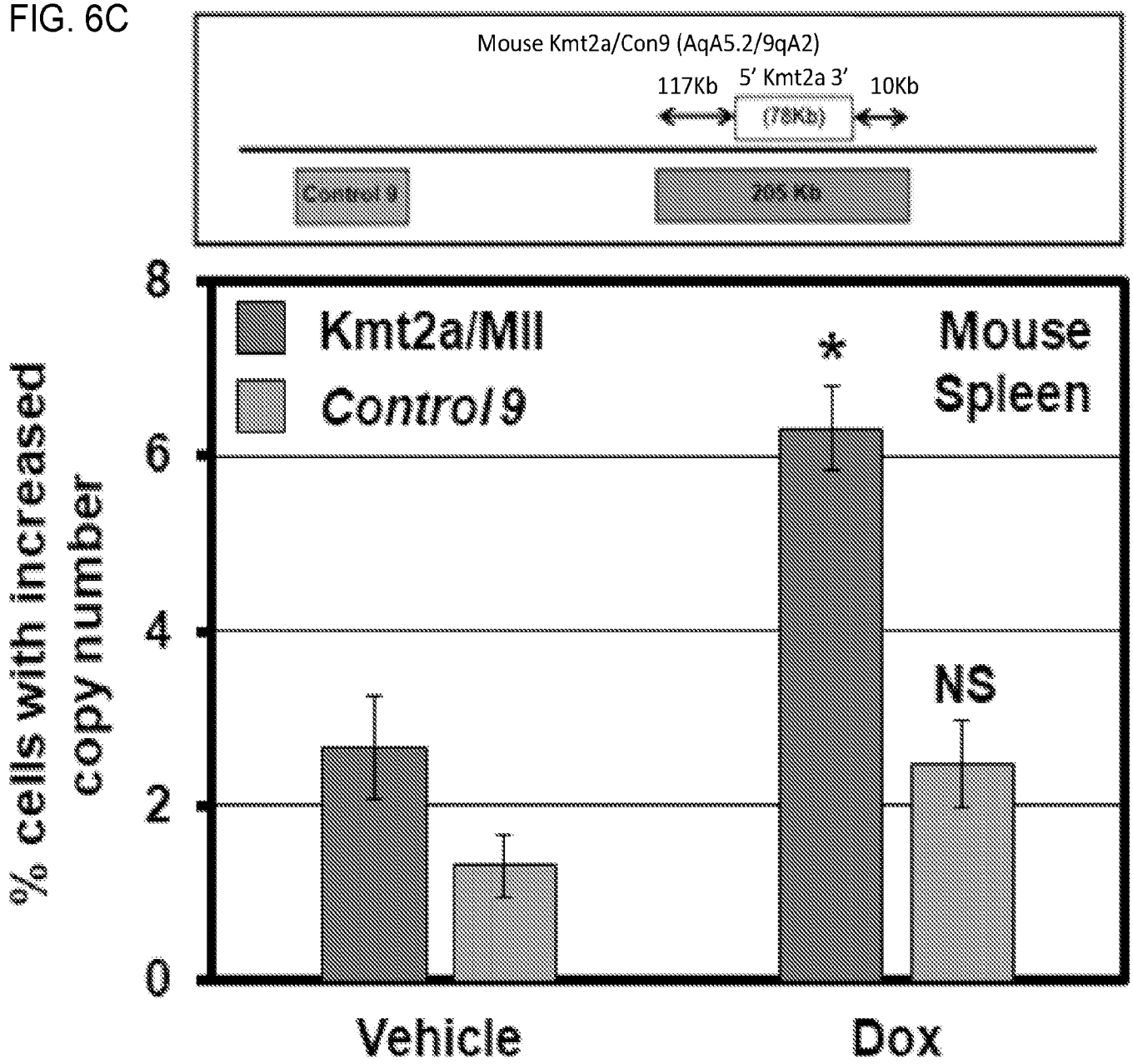
Mouse Kmt2a/Con9 (AqA5.2/9qA2)
117Kb
5' Kmt2a 3'
10Kb
(78Kb)
Control 9
205 Kb
% cells with increased copy number
8
6
4
2
0
Kmt2a/MII
Control 9
*
Mouse Spleen
NS
Vehicle
Dox

FIG. 6D

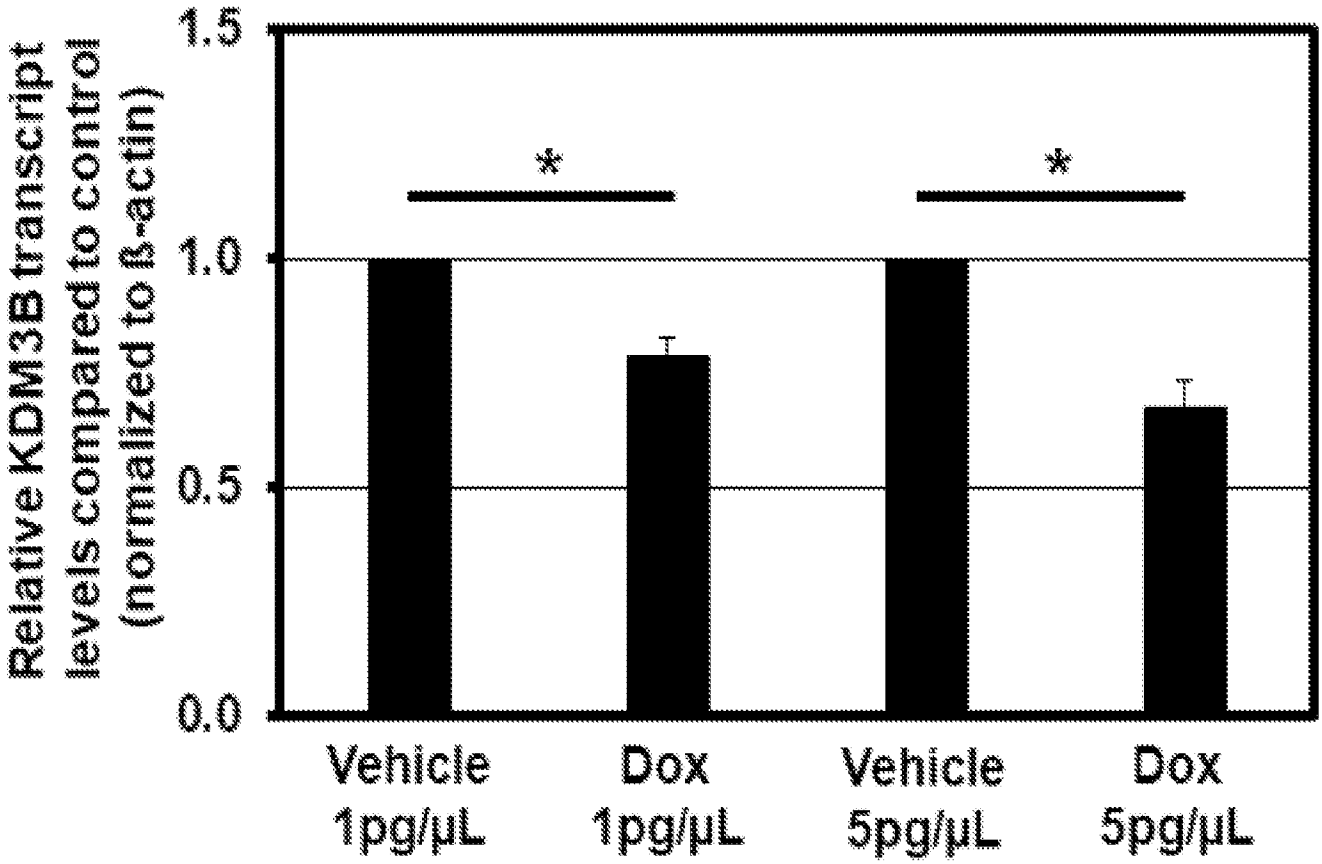
Relative KDM3B transcript levels compared to control (normalized to ß-actin)
1.5
1.0
0.5
0.0
*
*
Vehicle 1pg/µL
Dox 1pg/µL
Vehicle 5pg/µL
Dox 5pg/µL

FIG. 6E

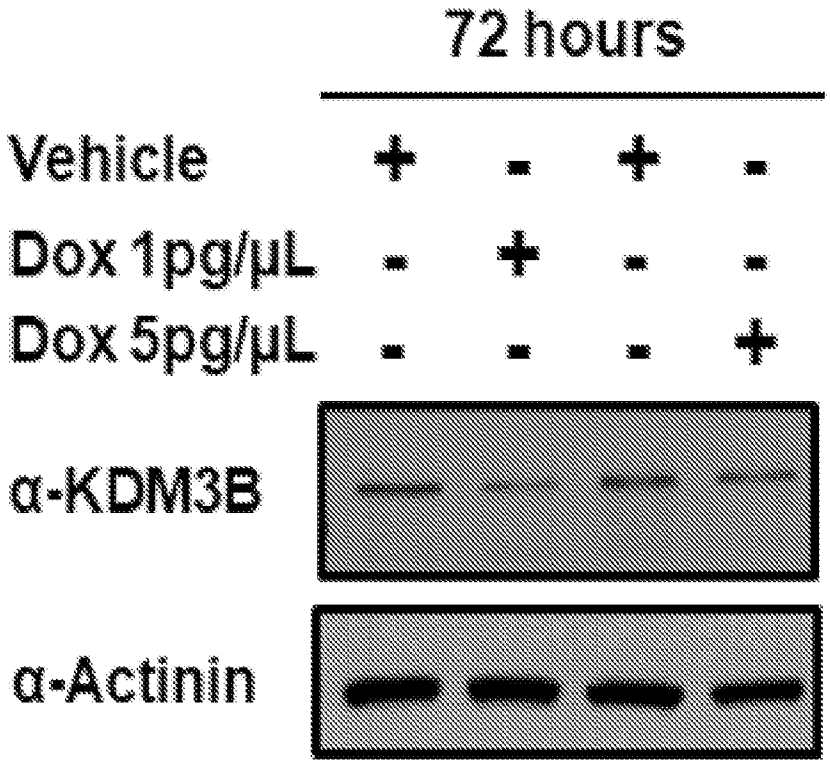
72 hours
Vehicle + - + -
Dox 1pg/µL - + - -
Dox 5pg/µL - - - +
α-KDM3B
α-Actinin

FIG. 6F

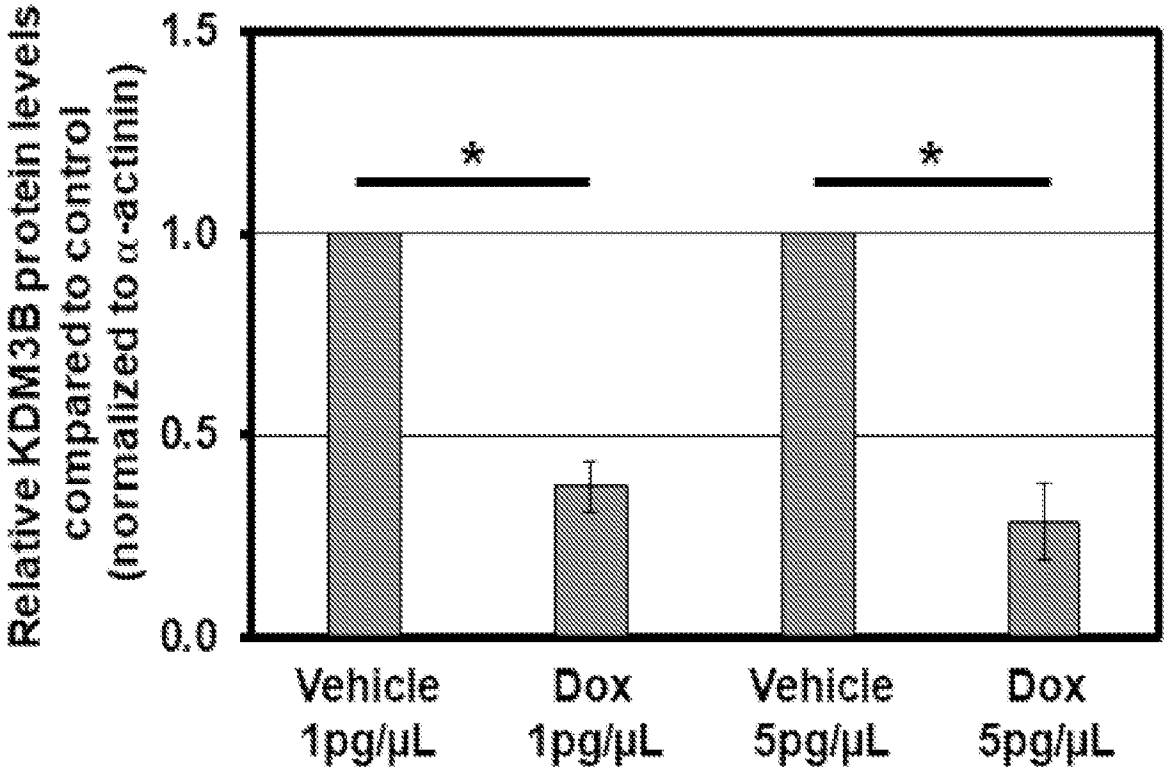
Relative KDM3B protein levels compared to control (normalized to α-actinin)
1.5
1.0
0.5
0.0
*
*
Vehicle 1pg/μL
Dox 1pg/μL
Vehicle 5pg/μL
Dox 5pg/μL

FIG. 6G

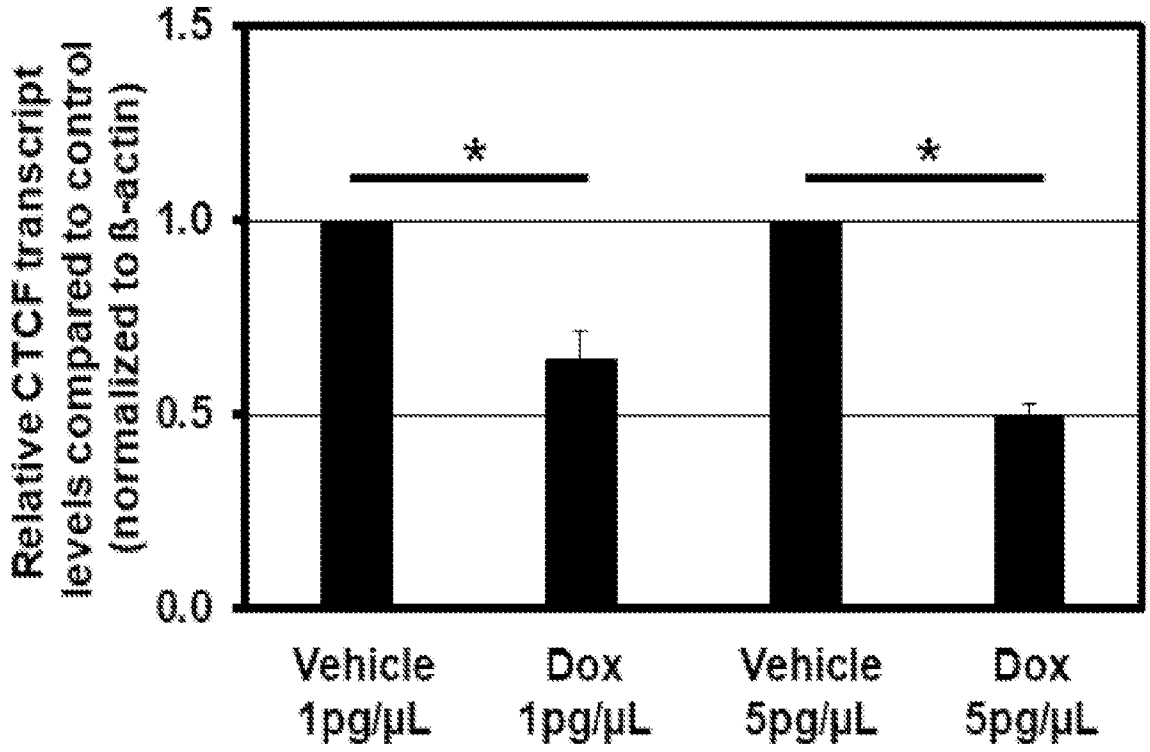
Relative CTCF transcript levels compared to control (normalized to ß-actin)
1.5
1.0
0.5
0.0
*
*
Vehicle 1pg/μL
Dox 1pg/μL
Vehicle 5pg/μL
Dox 5pg/μL

FIG. 6H

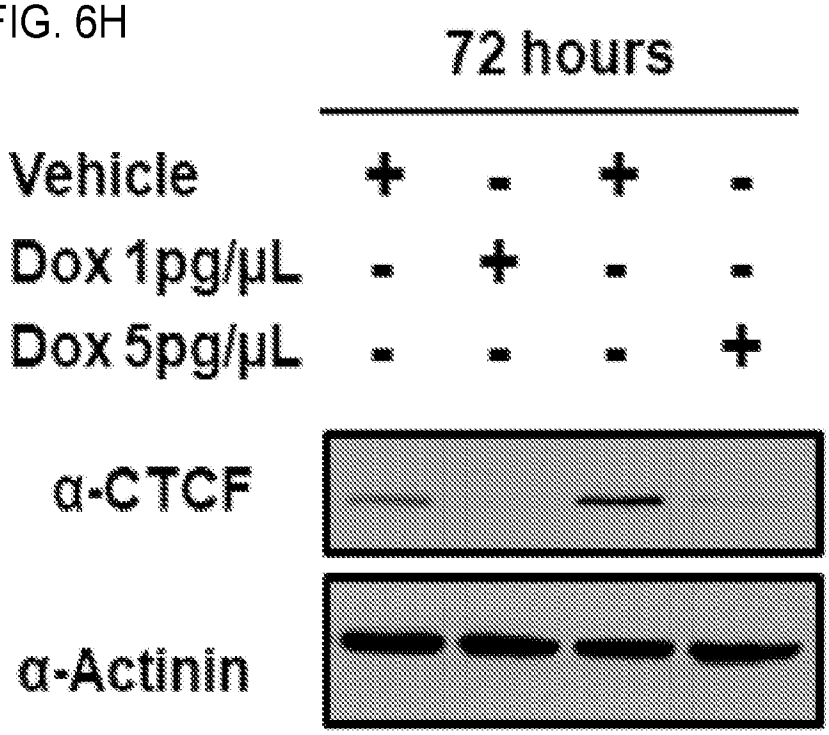
72 hours
Vehicle + - + -
Dox 1pg/μL - + - -
Dox 5pg/μL - - - +
α-CTCF
α-Actinin

FIG. 6I

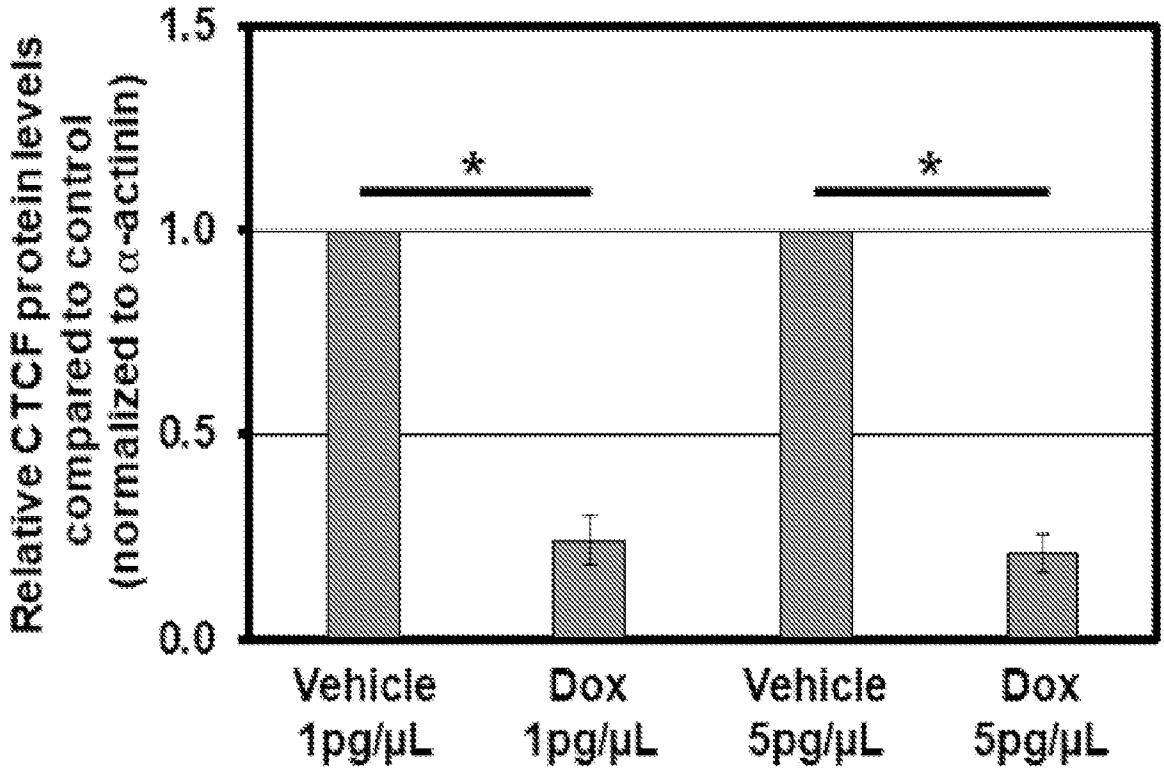
Relative CTCF protein levels compared to control (normalized to α-actinin)
1.5
1.0
0.5
0.0
*
*
Vehicle 1pg/μL
Dox 1pg/μL
Vehicle 5pg/μL
Dox 5pg/μL

FIG. 6J

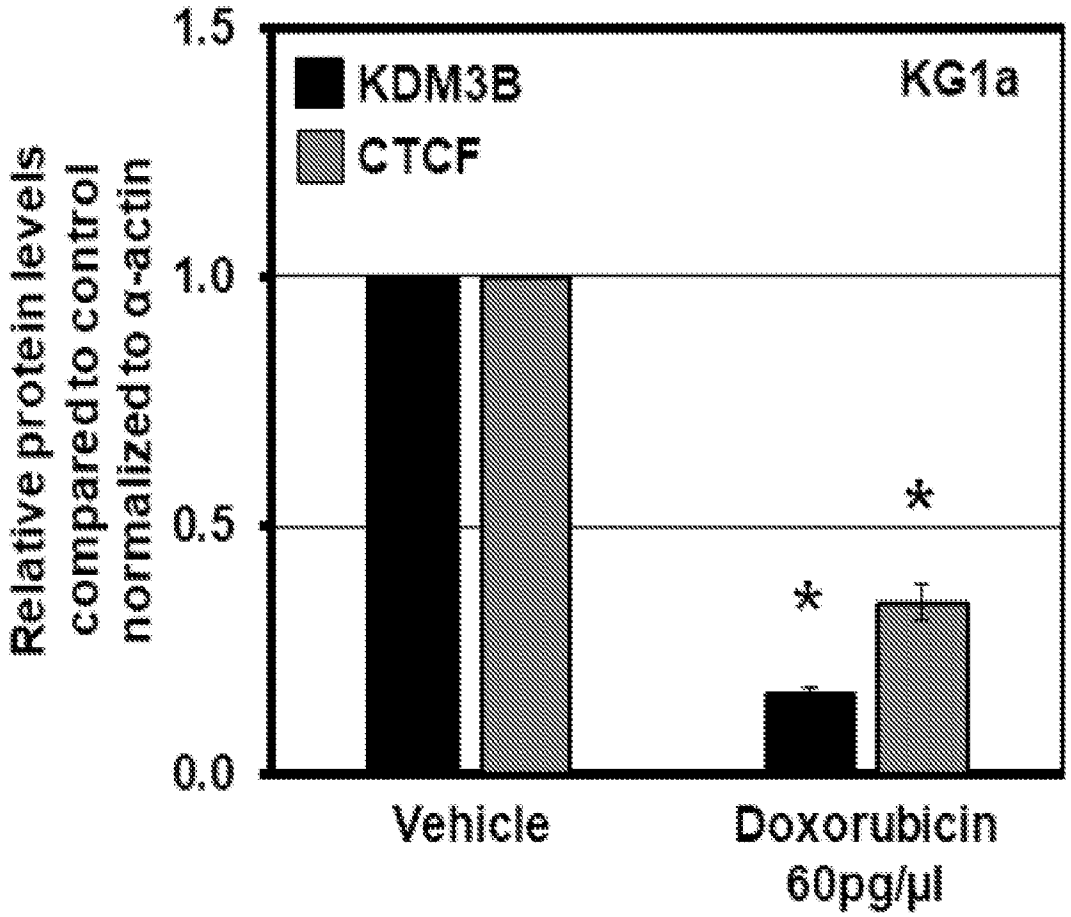
KDM3B
CTCF
KG1a
Relative protein levels compared to control normalized to α-actin
1.5
1.0
0.5
0.0
*
*
Vehicle
Doxorubicin 60pg/μl

FIG. 6K

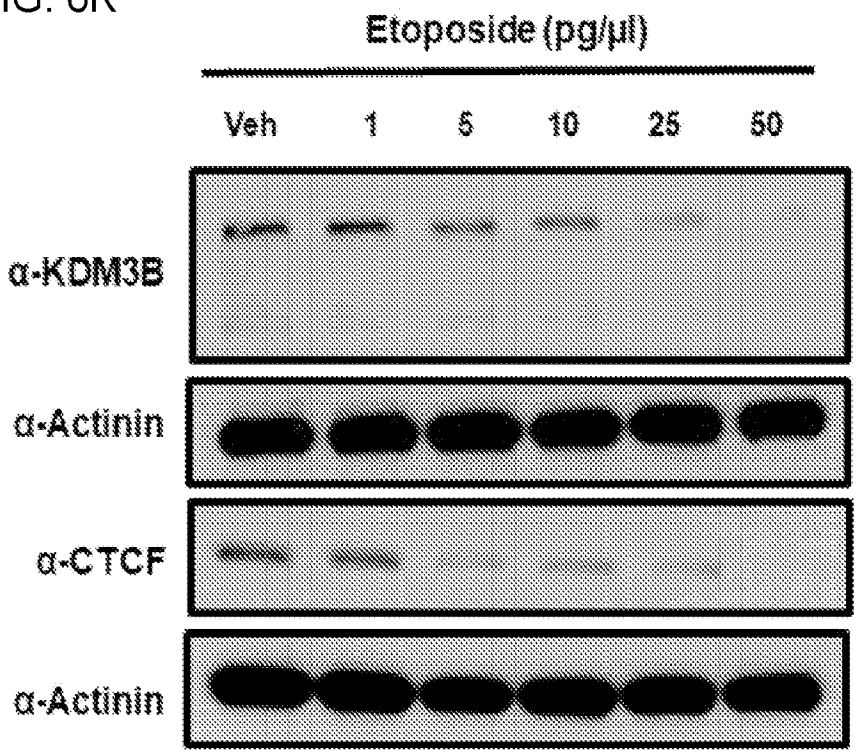
Etoposide (pg/μl)
Veh
1
5
10
25
50
α-KDM3B
α-Actinin
α-CTCF
α-Actinin

FIG. 6L

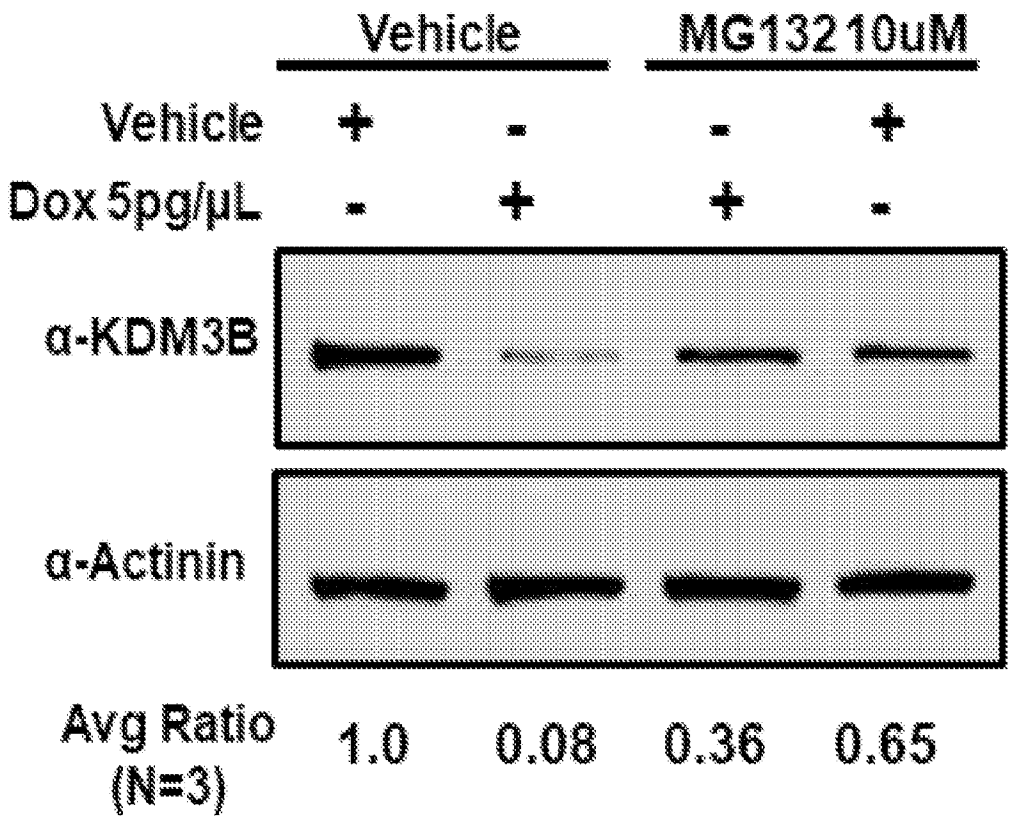
Vehicle
MG13210uM
Vehicle + - - +
Dox 5pg/μL - + + -
α-KDM3B
α-Actinin
Avg Ratio (N=3) 1.0 0.08 0.36 0.65

FIG. 6M

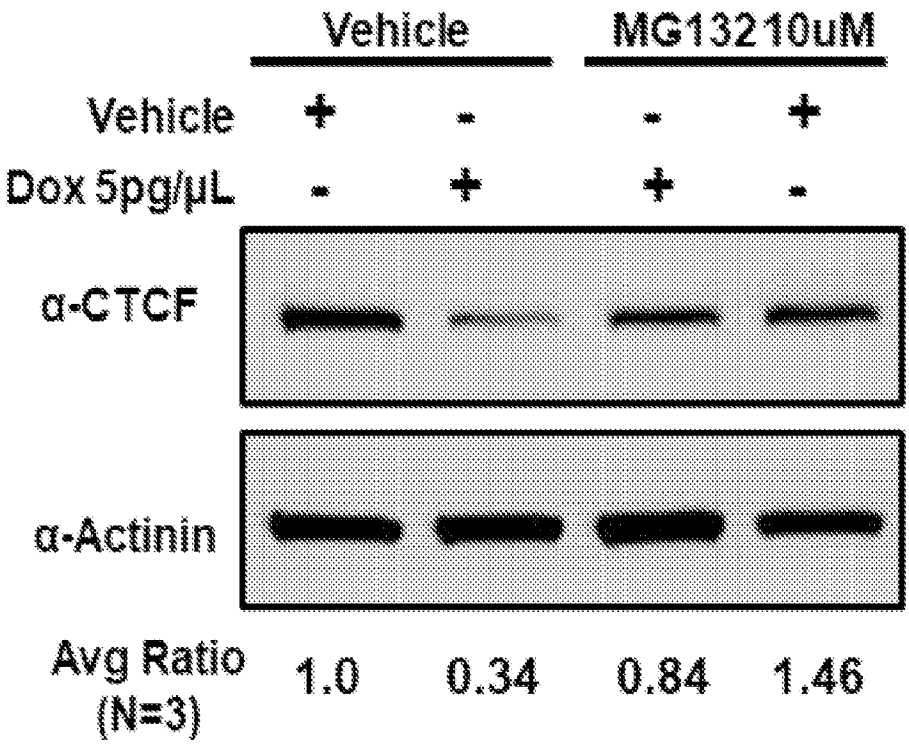
Vehicle
MG13210uM
Vehicle + - - +
Dox 5pg/μL - + + -
α-CTCF
α-Actinin
Avg Ratio (N=3) 1.0 0.34 0.84 1.46

FIG. 7A

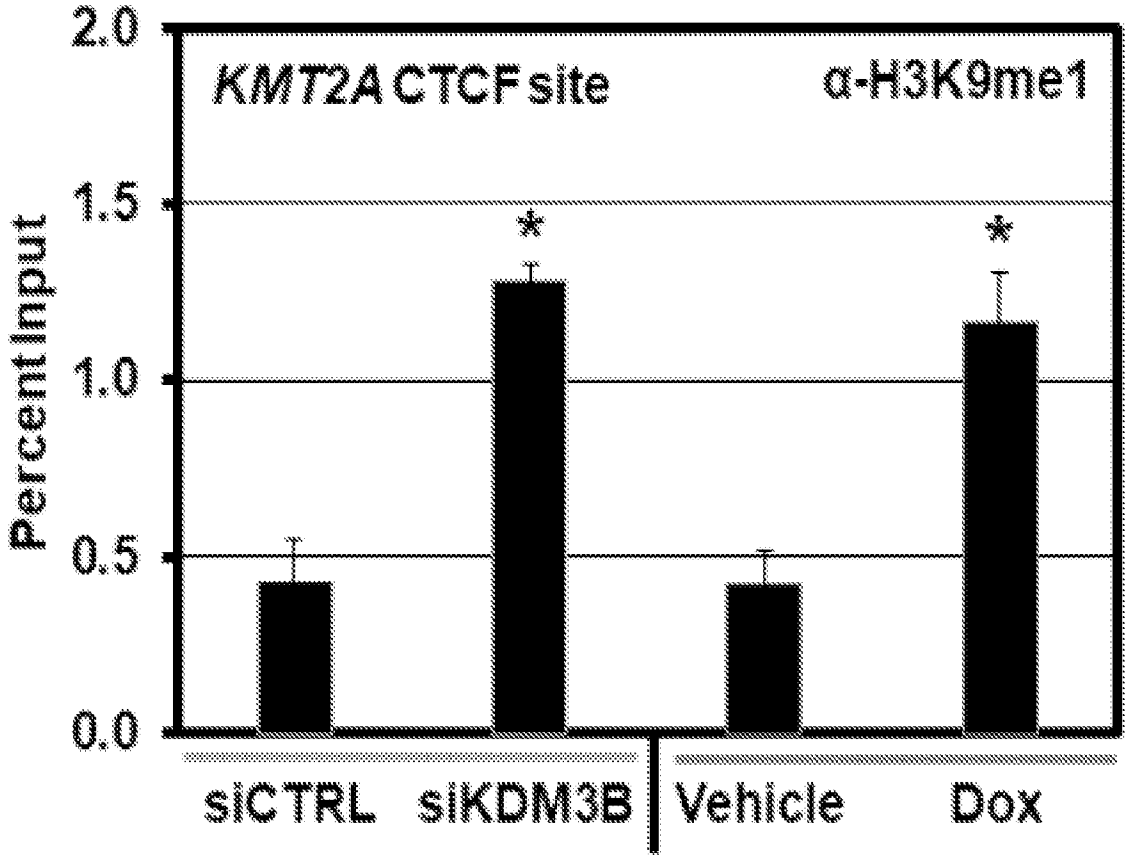
KMT2A CTCF site
α-H3K9me1
Percent Input
2.0
1.5
1.0
0.5
0.0
*
*
siCTRL
siKDM3B
Vehicle
Dox

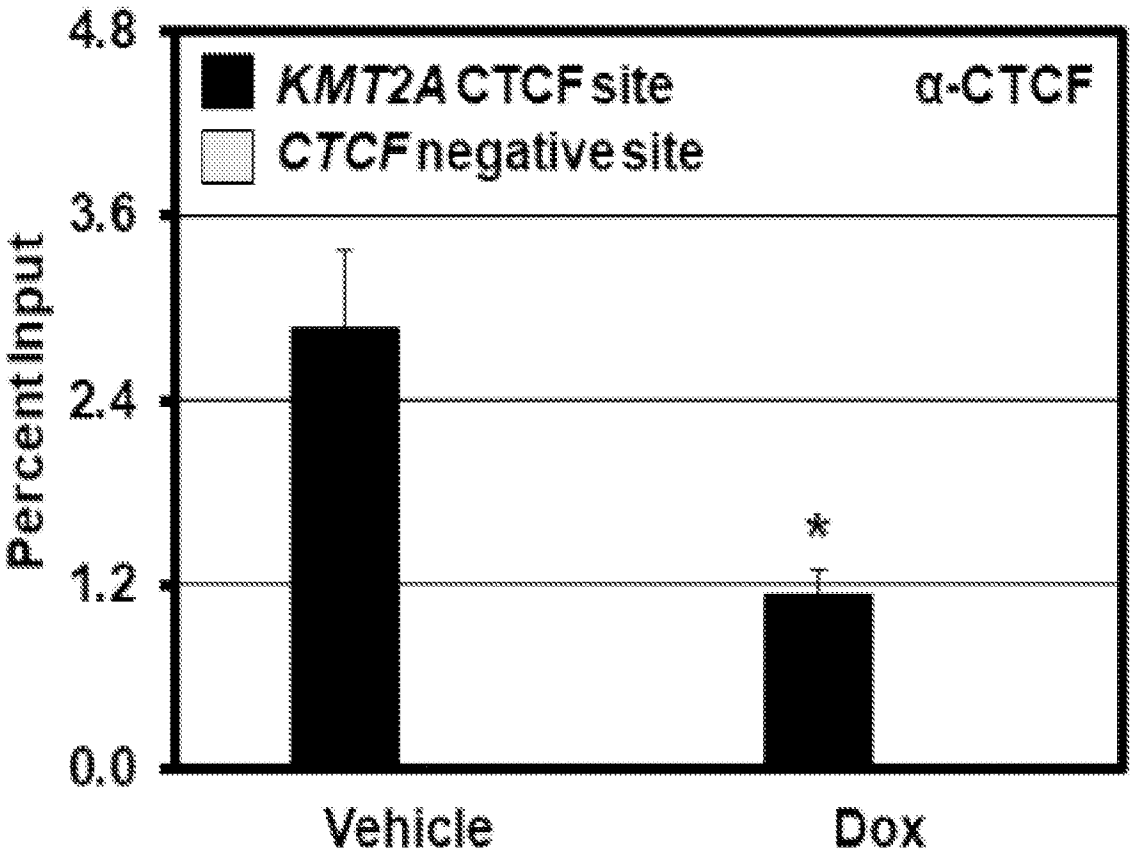
KMT2A CTCF site
CTCF negative site
α-CTCF
Percent Input
4.8
3.6
2.4
1.2
0.0
*
Vehicle
Dox

FIG. 7B

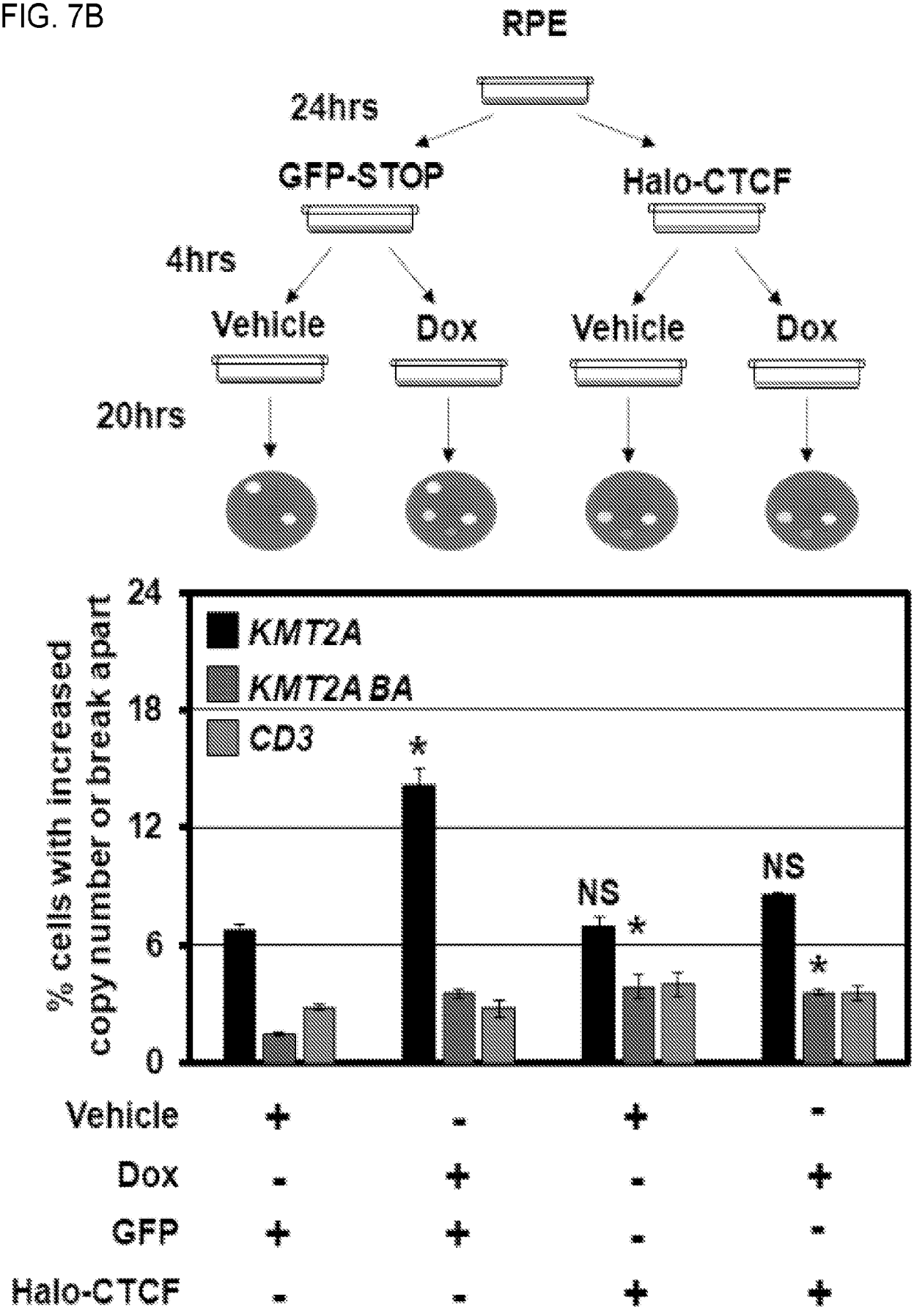
RPE
24hrs
GFP-STOP
Halo-CTCF
4hrs
Vehicle
Dox
Vehicle
Dox
20hrs
% cells with increased copy number or break apart
24
18
12
6
0
KMT2A
KMT2A BA
CD3
*
NS
*
NS
*
Vehicle + - + -
Dox - + - +
GFP + + - -
Halo-CTCF - - + +

FIG. 7C

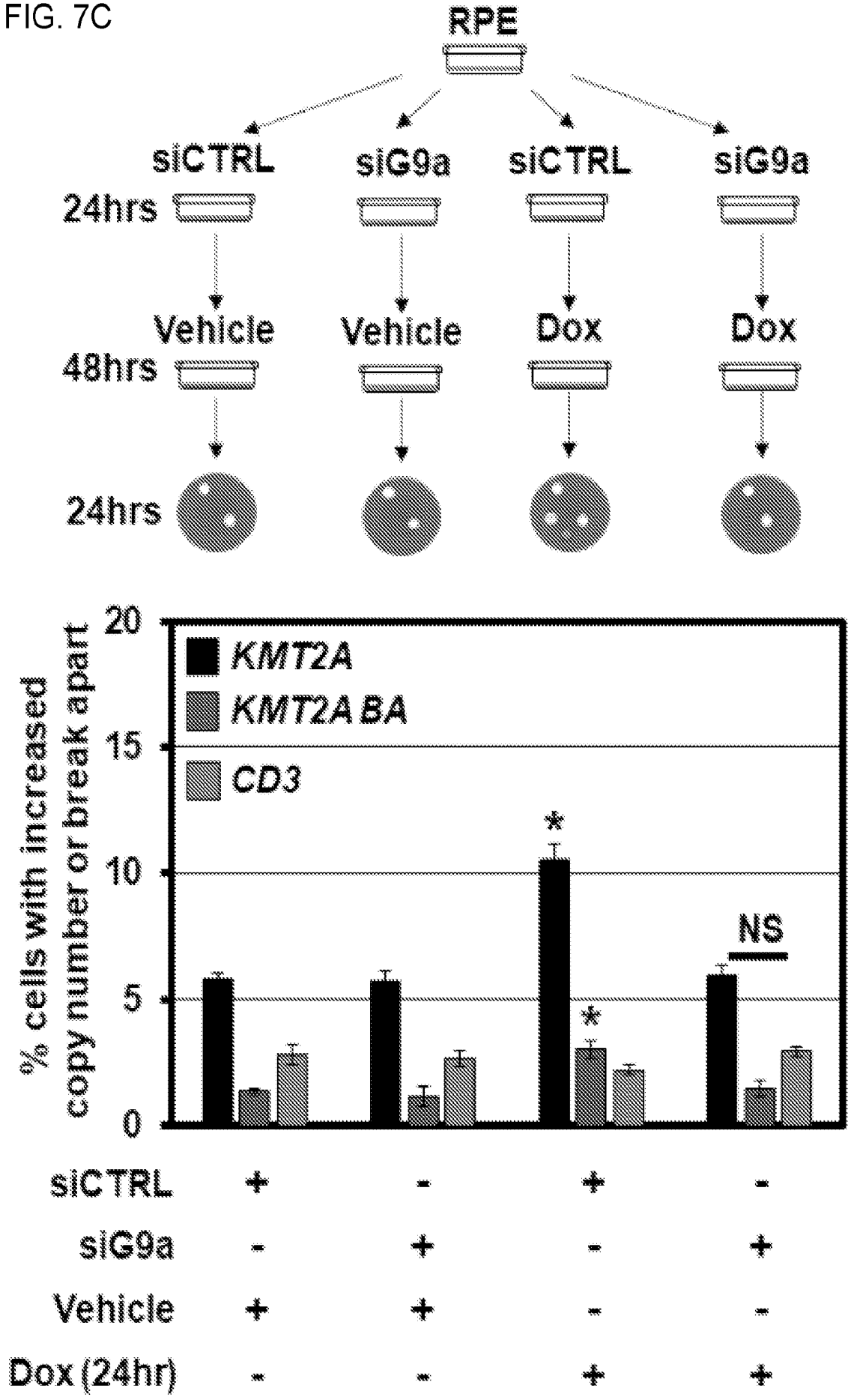
RPE
siCTRL
siG9a
siCTRL
siG9a
24hrs
Vehicle
Vehicle
Dox
Dox
48hrs
24hrs
% cells with increased copy number or break apart
KMT2A
KMT2A BA
CD3
20
15
10
5
0
*
*
NS
siCTRL + - + -
siG9a - + - +
Vehicle + + - -
Dox (24hr) - - + +

FIG. 7D

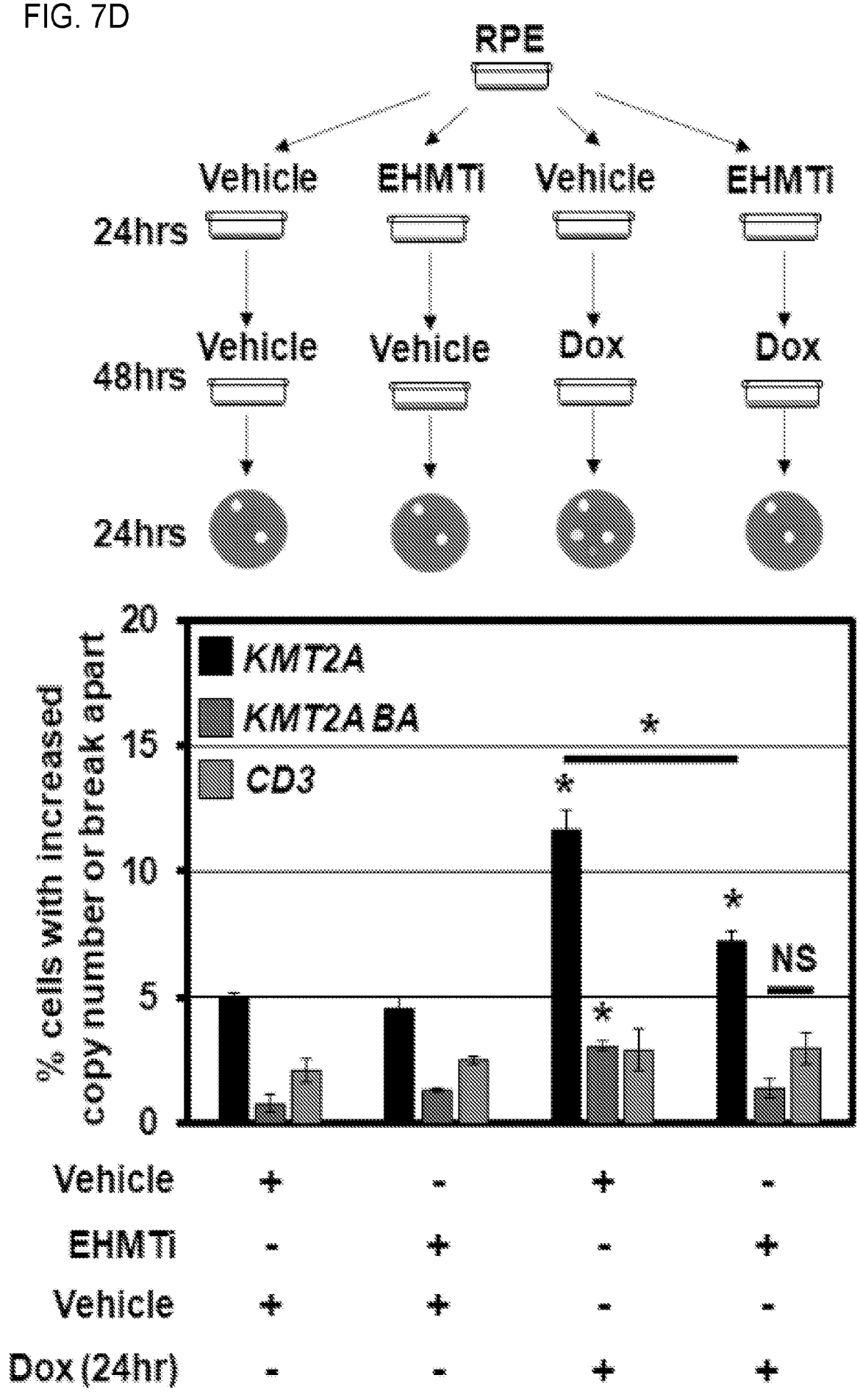
RPE
Vehicle
EHMTi
Vehicle
EHMTi
24hrs
Vehicle
Vehicle
Dox
Dox
48hrs
24hrs
% cells with increased copy number or break apart
20
15
10
5
0
KMT2A
KMT2A BA
CD3
*
*
*
*
NS
Vehicle + - + -
EHMTi - + - +
Vehicle + + - -
Dox (24hr) - - + +

FIG. 7E

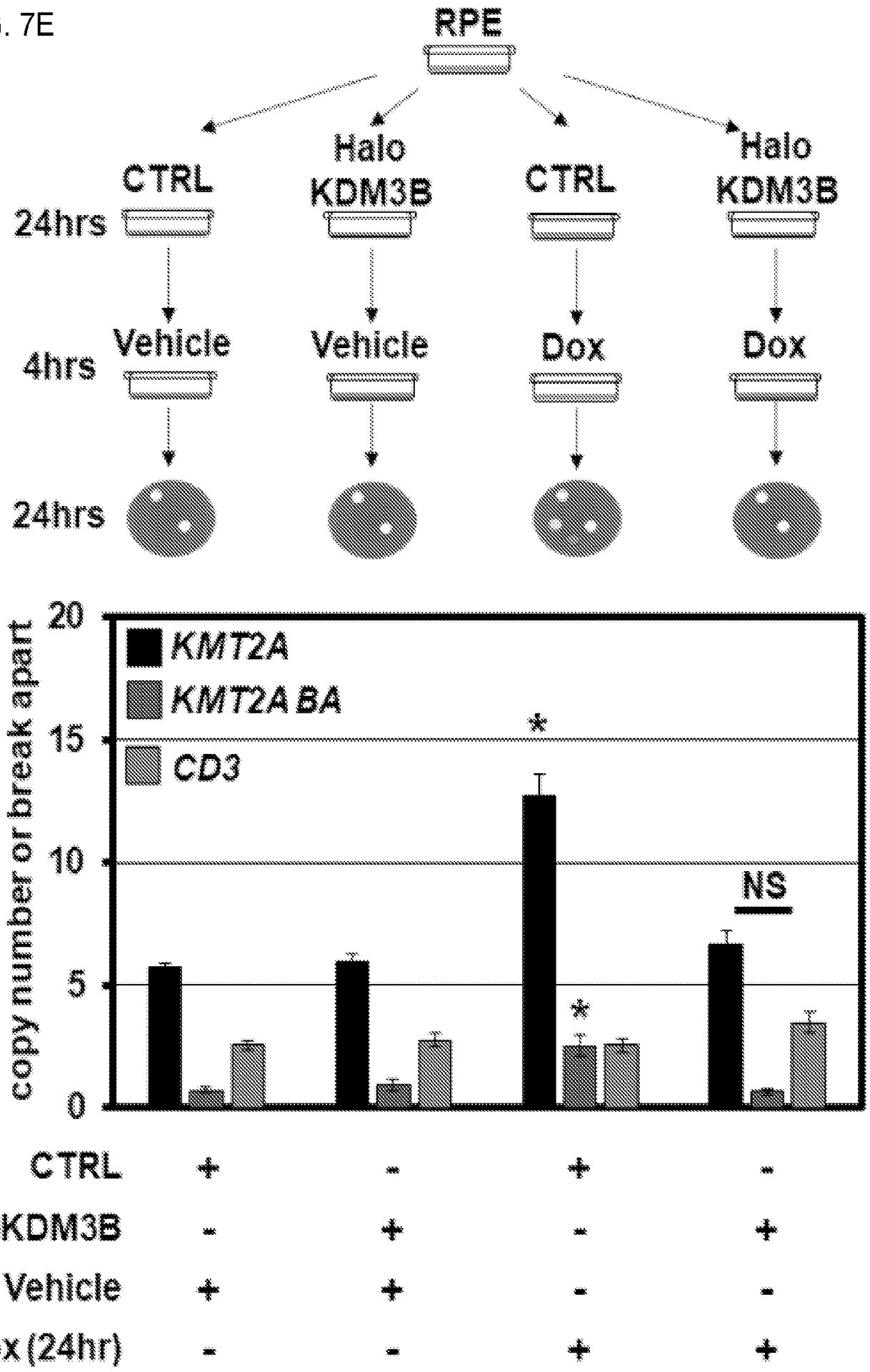
RPE
CTRL
Halo KDM3B
CTRL
Halo KDM3B
24hrs
Vehicle
Vehicle
Dox
Dox
4hrs
24hrs
% cells with increased copy number or break apart
KMT2A
KMT2A BA
CD3
20
15
10
5
0
*
*
NS
CTRL + - + -
Halo-KDM3B - + - +
Vehicle + + - -
Dox (24hr) - - + +

FIG. 7F

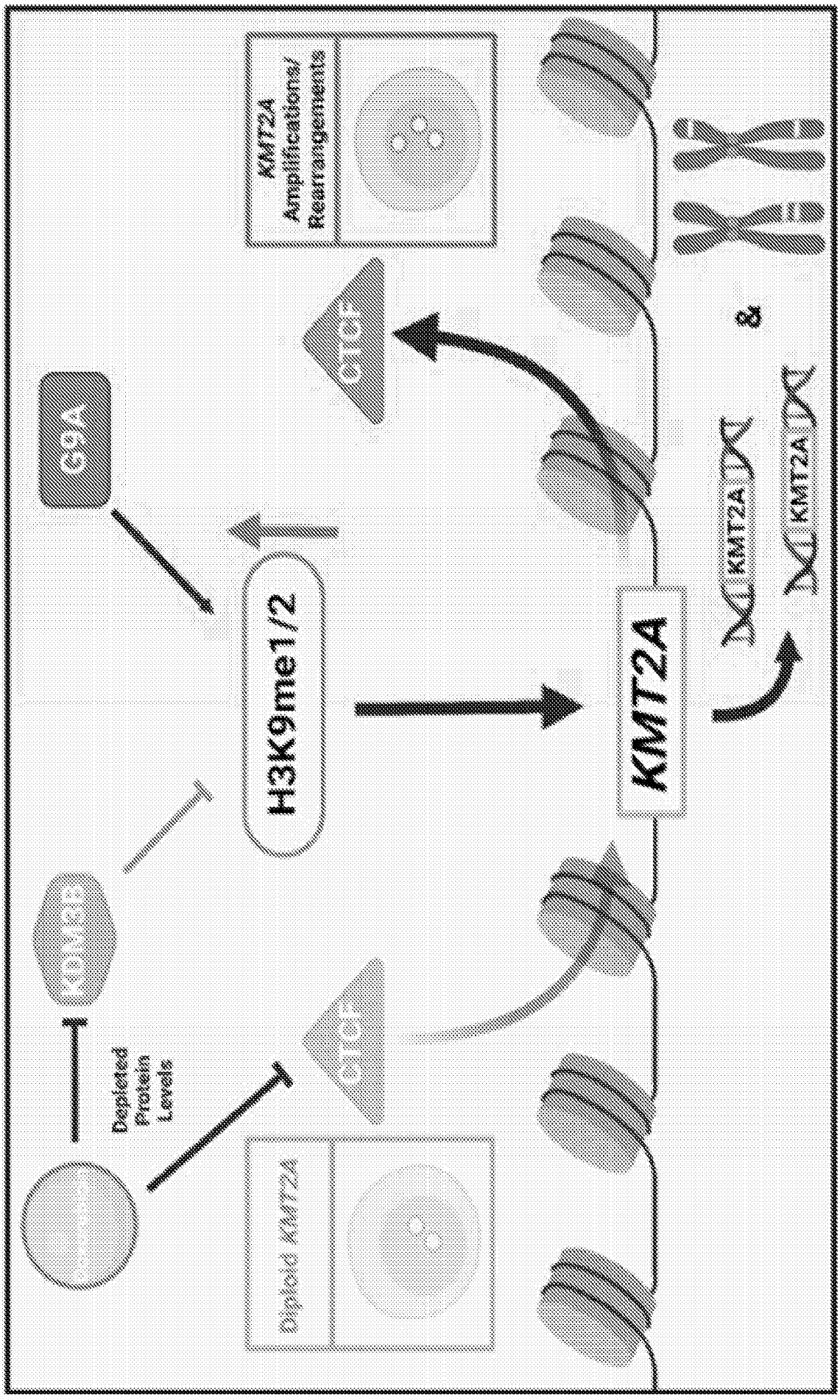
KMT2A Amplifications/ Rearrangements
G9A
Depleted Protein Levels
H3K9me1/2
KMT2A
Diploid KMT2A
&

FIG. 7G

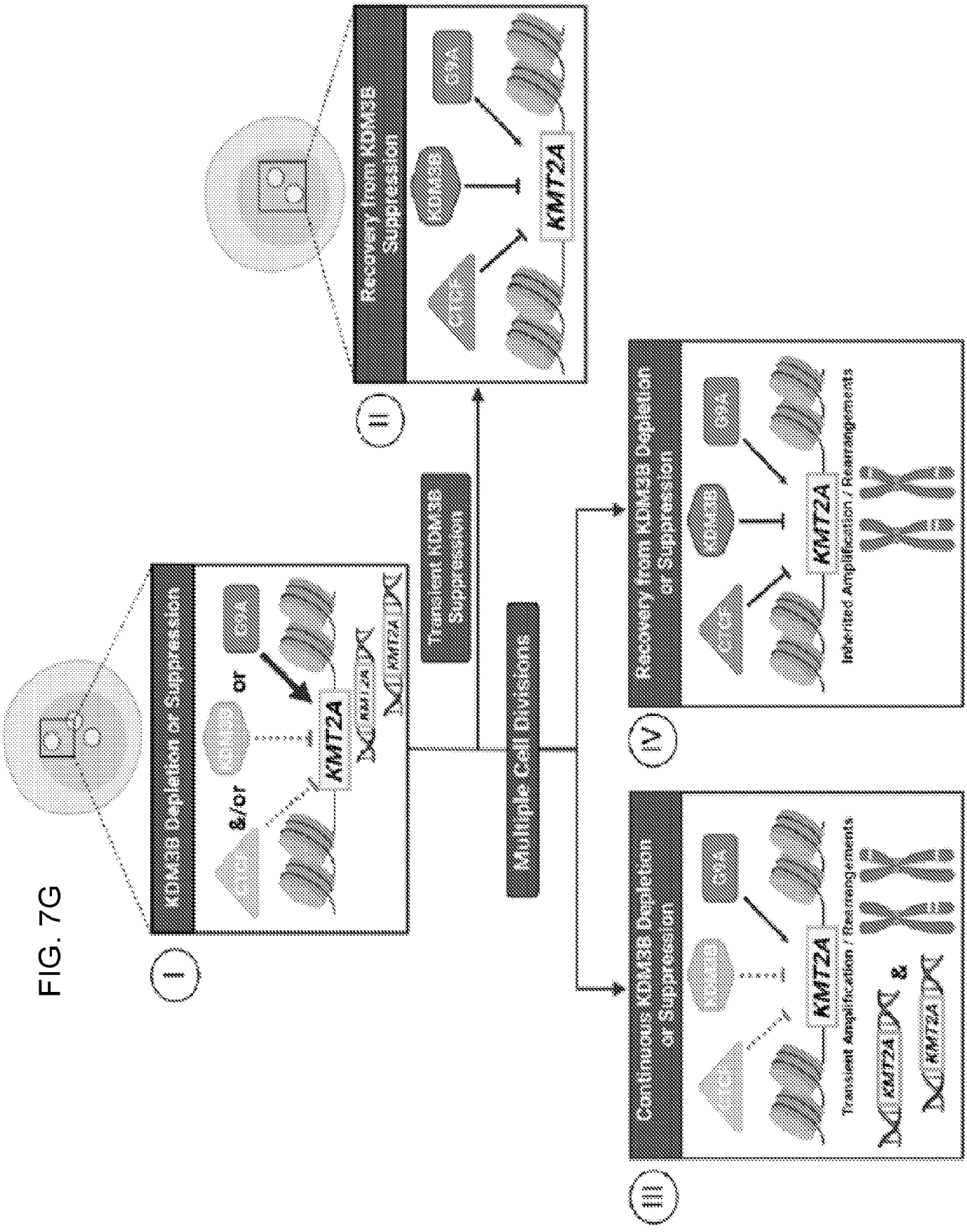
KMT2A Depletion or Suppression
&/or
or
KMT2A
Transient KMT2A Suppression
Multiple Cell Divisions
II
Recovery from KMT2A Suppression
Deletion
DNA
KMT2A
III
Continuous KMT2A Depletion or Suppression
Transient Amplification / Rearrangements
&
IV
Recovery from KMT2A Depletion or Suppression
Inherited Amplification / Rearrangements

Domains and regions structure of KDM3B

Region	253-346	Disordered (Automatic Annotation)
Compositional bias	273-312	Basic and acidic residues (Automatic Annotation)
Region	370-394	Disordered (Automatic Annotation)
Region	436-496	Disordered (Automatic Annotation)
Compositional bias	449-496	Polar residues (Automatic Annotation)
Region	572-603	Disordered (Automatic Annotation)
Region	714-762	Disordered (Automatic Annotation)
Region	805-828	Disordered (Automatic Annotation)
Compositional bias	808-828	Polar residues (Automatic Annotation)
Zinc finger	1031-1056	C6-type (Sequence Analysis)
Compositional bias	1142-1166	Polar residues (Automatic Annotation)
Region	1142-1220	Disordered (Automatic Annotation)
Compositional bias	1178-1192	Basic and acidic residues (Automatic Annotation)
Motif	1293-1297	[redacted] motif
Domain	1498-1721	JmjC (PROSITE-ProRule Annotation)

FIG. 8

INTERNATIONAL SEARCH REPORT

International application No.
PCT/US2023/025793

A. CLASSIFICATION OF SUBJECT MATTER

IPC(8) - INV. - A61P 35/02; A61K 38/46, 47/69; C12N 15/113, 15/52 (2023.01)
ADD. - A61K 31/7115; C12N 15/85 (2023.01)

CPC - INV. - A61P 35/02; A61K 38/46, 47/6911; C12N 15/1137, 15/52 (2023.08)

ADD. - A61K 2121/00, 31/7115; C12N 15/85, 2310/14 (2023.08)

According to International Patent Classification (IPC) or to both national classification and IPC

B. FIELDS SEARCHED

Minimum documentation searched (classification system followed by classification symbols)
See Search History document

Documentation searched other than minimum documentation to the extent that such documents are included in the fields searched
See Search History document

Electronic database consulted during the international search (name of database and, where practicable, search terms used)
See Search History document

C. DOCUMENTS CONSIDERED TO BE RELEVANT

Category*	Citation of document, with indication, where appropriate, of the relevant passages	Relevant to claim No.
X	US 2014/0161785 A1 (LIU et al.) 12 June 2014 (12.06.2014) entire document	21, 38-40
---		---
Y		1-4, 18, 19, 22-24
Y	WO 2018/102736 A1 (THE GENERAL HOSPITAL CORPORATION) 07 June 2018 (07.06.2018) entire document	1-4, 18, 19, 23
Y	CN 110680816 A (WEIFANG MEDICAL UNIVERSITY) 14 January 2020 (14.01.2020) machine translation	2, 19, 22
Y	LIBURA et al., Therapy-related acute myeloid leukemia–like MLL rearrangements are induced by etoposide in primary human CD34+ cells and remain stable after clonal expansion, Blood, Vol. 105, No. 5, 04 November 2004, Pgs. 2124-2131. entire document	3, 4, 18, 19, 23, 24
A	US 2018/0045727 A1 (CARIS MPI INC) 15 February 2018 (15.02.2018) entire document	1-4, 18, 19, 21-24, 38-40
A	US 2019/0211036 A1 (JANSSEN PHARMACEUTICA NV) 11 July 2019 (11.07.2019) entire document	1-4, 18, 19, 21-24, 38-40

☐ Further documents are listed in the continuation of Box C. ☐ See patent family annex.

* Special categories of cited documents:
"A" document defining the general state of the art which is not considered to be of particular relevance
"D" document cited by the applicant in the international application
"E" earlier application or patent but published on or after the international filing date
"L" document which may throw doubts on priority claim(s) or which is cited to establish the publication date of another citation or other special reason (as specified)
"O" document referring to an oral disclosure, use, exhibition or other means
"P" document published prior to the international filing date but later than the priority date claimed
"T" later document published after the international filing date or priority date and not in conflict with the application but cited to understand the principle or theory underlying the invention
"X" document of particular relevance; the claimed invention cannot be considered novel or cannot be considered to involve an inventive step when the document is taken alone
"Y" document of particular relevance; the claimed invention cannot be considered to involve an inventive step when the document is combined with one or more other such documents, such combination being obvious to a person skilled in the art
"&" document member of the same patent family

Date of the actual completion of the international search	Date of mailing of the international search report
18 September 2023	OCT 27 2023
Name and mailing address of the ISA/ Mail Stop PCT, Attn: ISA/US, Commissioner for Patents P.O. Box 1450, Alexandria, VA 22313-1450 Facsimile No. 571-273-8300	Authorized officer Taina Matos Telephone No. PCT Helpdesk: 571-272-4300

INTERNATIONAL SEARCH REPORT

International application No.
PCT/US2023/025793

Box No. I Nucleotide and/or amino acid sequence(s) (Continuation of item 1.c of the first sheet)

1. With regard to any nucleotide and/or amino acid sequence disclosed in the international application, the international search was carried out on the basis of a sequence listing:

   a. ☐ forming part of the international application as filed.

   b. ☒ furnished subsequent to the international filing date for the purposes of international search (Rule 13*ter*.1(a)),

      ☒ accompanied by a statement to the effect that the sequence listing does not go beyond the disclosure in the international application as filed.

2. ☐ With regard to any nucleotide and/or amino acid sequence disclosed in the international application, this report has been established to the extent that a meaningful search could be carried out without a WIPO Standard ST.26 compliant sequence listing.

3. Additional comments:

INTERNATIONAL SEARCH REPORT

International application No.
PCT/US2023/025793

Box No. II Observations where certain claims were found unsearchable (Continuation of item 2 of first sheet)

This international search report has not been established in respect of certain claims under Article 17(2)(a) for the following reasons:

1. ☐ Claims Nos.:
because they relate to subject matter not required to be searched by this Authority, namely:

2. ☐ Claims Nos.:
because they relate to parts of the international application that do not comply with the prescribed requirements to such an extent that no meaningful international search can be carried out, specifically:

3. ☒ Claims Nos.: 5-17, 20, 25-37, 41, 42
because they are dependent claims and are not drafted in accordance with the second and third sentences of Rule 6.4(a).

Box No. III Observations where unity of invention is lacking (Continuation of item 3 of first sheet)

This International Searching Authority found multiple inventions in this international application, as follows:

1. ☐ As all required additional search fees were timely paid by the applicant, this international search report covers all searchable claims.

2. ☐ As all searchable claims could be searched without effort justifying additional fees, this Authority did not invite payment of additional fees.

3. ☐ As only some of the required additional search fees were timely paid by the applicant, this international search report covers only those claims for which fees were paid, specifically claims Nos.:

4. ☐ No required additional search fees were timely paid by the applicant. Consequently, this international search report is restricted to the invention first mentioned in the claims; it is covered by claims Nos.:

Remark on Protest

☐ The additional search fees were accompanied by the applicant's protest and, where applicable, the payment of a protest fee.

☐ The additional search fees were accompanied by the applicant's protest but the applicable protest fee was not paid within the time limit specified in the invitation.

☐ No protest accompanied the payment of additional search fees.